# Hydrolytic vs. nonhydrolytic sol-gel routes to prepare mixed oxide catalysts for ethylene oligomerization

Atheer Hasan Yas Al Khudhair

# THÈSE POUR OBTENIR LE GRADE DE DOCTEUR DE L'UNIVERSITÉ DE MONTPELLIER

**En Chimie et Physico-Chimie des Matériaux**

**École doctorale ED 459 Sciences Chimiques Balard**

**Unité de recherche UMR 5253 - Institut Charles Gerhardt de Montpellier,**
**Département 3 :Matériaux Poreux et Hybrides**

# Hydrolytic *vs.* nonhydrolytic sol-gel routs to prepare mixed oxide catalysts for ethylene oligomerization

**Présentée par Atheer Hasan Yas AL KHUDHAIR**
**Le jeudi 09 décembre 2021**

**Sous la direction d'Ahmad MEHDI**
**et Karim BOUCHMELLA**

**Devant le jury composé de**

| | |
|---|---|
| M. Richard VILLANNEAU, Maître de Conférences, HDR, UPMC-Paris | Rapporteur |
| M. Éric BESSON, Maître de Conférences, HDR, AMU-Marseille | Rapporteur |
| Mme. Corine GERARDIN, DR CNRS, ICGM-Montpellier | Présidente |
| M. Ahmad MEHDI, Professeur, Université Montpellier | Directeur de thèse |
| M. Karim BOUCHMELLA, IE CNRS, ICGM-Montpellier | Co-Directeur de thèse |

UNIVERSITÉ DE MONTPELLIER

# Remerciements:

Cette thèse a été réalisée au sein de l'Institut Charles Gerhardt de Montpellier (ICGM) dans le Département Matériaux Poreux et Hybrides (D3) en collaboration avec l'Ecole Nationale supérieure de Chimie de Montpellier(ENSCM). Je tiens à remercier Jean-Jacques Vasseur, directeur de l'école doctorale et Éric Clot, directeur de l'ICGM d'avoir permis la réalisation de cette thèse, ainsi qu'au MOHESR Irakienne pour la bourse qui a financé mes études en France.

Je remercie vivement les membres du jury d'avoir accepté la lecture de ce manuscrit de thèse, pour leur évaluation et leurs commentaires enrichissants lors de la soutenance. Je remercie plus particulièrement M. Richard VILLANNEAU, Maître de conférences à l' UPMC de Paris et M. Eric BESSON, Maître de Conférences à la Institut de Chimie Radicalaire, Aix-Marseille Université qui m'ont fait l'honneur d'être rapporteurs de ce travail, ainsi qu'à Mme Corine GERARDIN, Directrice de Recherche à l´ICGM de Montpellier qui a présidé ce jury.

Je tiens à remercier Ahmad Mehdi, directeur de cette thèse ; Karim Bouchmella, co-directeur et Vasile Hulea pour la collaboration que nous avons développée. Merci à vous tous pour votre temps, vos conseils et les discussions que nous avons eues ; le travail ensemble de ce groupe hétérogène a enrichi le produit final présenté dans ce manuscrit. Travailler avec vous a été un grand plaisir et votre expérience m'a permis de grandir et d'améliorer mes compétences scientifiques.

Hubert Mutin, un grand merci pour ton aide et support. Tu m'as appris beaucoup de choses côté NHSG et c'était toujours un plaisir d'aller discuter les résultats avec toi. Je remercie profondément ton aide tout au long de la thèse.

Je remercie aussi tout le personnel du plateau technique de l'ICGM, de l'UM et l'IEM qui m'ont aidé avec la réalisation de certains analyses et caractérisations. Julien Fullenwarth, Bernard Fraisse de l'équipe AIME pour la formation et discussions par rapport à la diffraction aux rayons X ; Philippe Gaveau pour la réalisation des spectres RMN solide ; Fréderic Fernandez pour les images SEM et analyses EDX et Radu Andria de l'équipe MACS pour le test de catalyseur. Je tiens à remercier Valérie Flaud pour la test XPS ; Nicolas Donzel et Christine Biolley pour les caractérisations $NH_3$-TPD et TPR.

Je tiens à remercier aussi au personnel administratif et technique de l'équipe CMOS Serge, Christian, Xavier, Fatima, Magali, Nicolas, Tzvetelina, Sylvain, vous avez été toujours là que ce soit pour une commande de produit, des soucis avec le software ou les appareils. Merci à tous.

Il est important de noter que ces trois années ne seraient pas les mêmes sans la compagnie de mes chers collègues thésards et post-docs : Hussein Awada, Kassem Amro, Aurélien, Rosa, Eduardo, Sandrine, Mohammad Wehbi, et Angel Escamilla, sans oublier le team Sikémia, Guillaume et Adeline. Je voudrais surtout remercier ma famille. Ma femme, m'a énormément soutenue tout au long de ce processus et a fait d'innombrables sacrifices pour m'aider à y arriver. Mes enfants, Shams, Yousif ont continuellement fourni les pauses nécessaires à la philosophie et à la motivation pour terminer mon diplôme. Sans une telle équipe derrière moi, je doute que je serais à cet endroit aujourd'hui.

MERCI À VOUS TOUS !!!

*La vie n'est pas facile pour aucun d'entre nous. Mais que dire de qui ? Nous devons persévérer et surtout avoir confiance en nous-mêmes. Nous devons croire que nous sommes doués pour quelque chose et que nous devons l'atteindre.*

***Marie Curie***

# Abbreviations:

**ALD,** Atomic layer deposition

**ASA,** acid sites and silica-alumina

**Acac,** Acetylacetonate

**BET,** Brunauer, Emett, Teller

**BJH,** Barrett, Joyner, Halenda

**C3+,** propane and heavier hydrocarbons

**C2, C3, 1C4, 2C4**, Ethylene, propylene, 1-butene, 2-butene

**DMAP,** 4-Dimethylaminopyridine

**DMF,** Dimethylformamide

**DMSO,** Dimethylsulfoxide

**Dp,** Pore diameter

**Ea,** activation energy

**EDX**, Energy Dispersive X-ray

**E-R,** Eley-Rideal mechanism

**Et,** Ethyl group

**EtOH,** Ethanol

**HDMS,** highly dispersed metallic sites

**HRTEM,** High-resolution transmission electron microscopy

**HSG,** Hydrolytic Sol-Gel

**IUPAC,** International union of pure and applied chemistry

**iC4, *c*-2C4, *t*-2C4,** Isobutene, *cis*-2-butene, *trans*-2-butene

**$^{i}Pr_2O$,** Diisopropyl ether

**L-H,** Langmuir Hinshelwood mechanism

**MAO,** Methylaluminoxane

**Me,** Methyl group

**MHSV,** mass hourly space velocity

**NH,** Non-hydrolytic

**NHSG**, Non-Hydrolytic Sol-Gel

**NMR,** Nuclear magnetic resonance

**NPs,** Nano particles

**PE**, Poly Ethylene

**PP**, Polypropylene

**SBA**, Santa Barbara Amorphous

**SEM,** Scanning electron microscop

**SHOP,** Shell higher olefin process

**SMSI,** strong metal-support interaction

**SN,** nucleophilic substitution

**SS,** Specific surface area

**$^t$BuOH,** Tertiary butanol

**TEM,** transmission electron microscopy

**TEOS,** tetraethyl orthosilicate

**TMA,** Tetramethylammonium

**TMOS,** Tetramethyl orthosilicate

**Tf,** melting temperature in Kelvin

**TOF,** Turn Over Frequency

**Tos,** Time on stream

**TPD-$NH_3$**, Thermo Programmed Desorption of ammonia

**TPR-$H_2$**, Thermo Programmed Reduction with hydrogen

**Triglyme,** Triethylene glycol dimethyl ether

**Vp,** Pore volume

**WHSV**, Weight-hourly space velocity

**XPS,** X-ray Photoelectron Spectroscopy

**XRD,** X-Ray diffraction

# Table of contents

# Figures

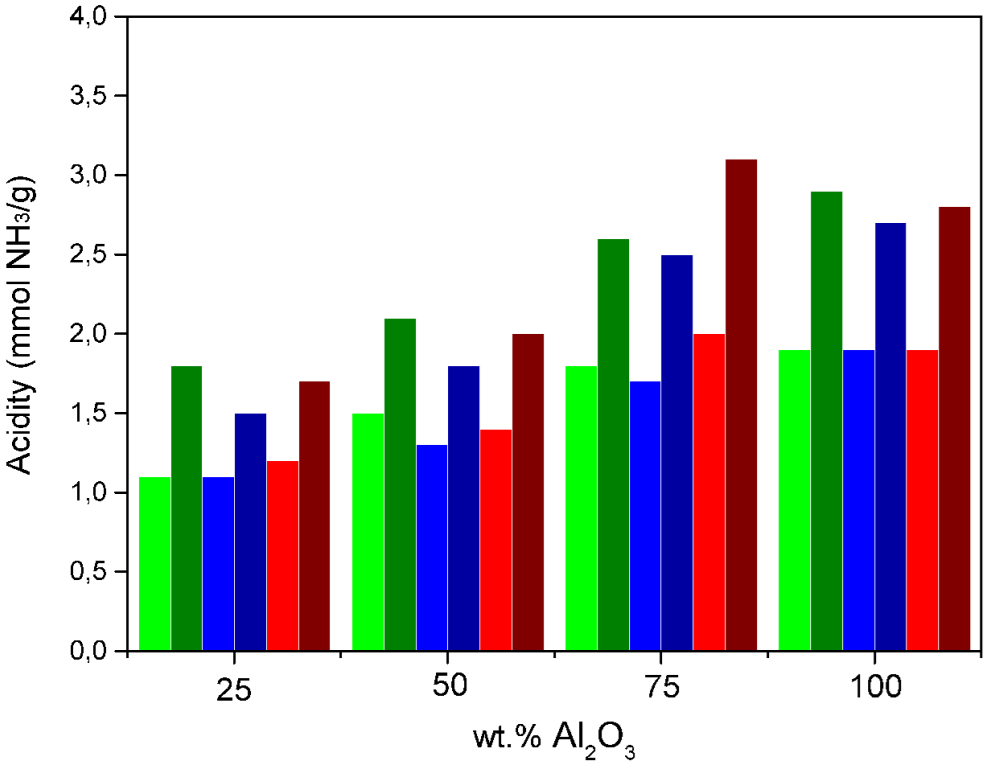


Figure 36: Influence of $Al_2O_3$ loading on acidity of $Si_x$-$Al_y$ samples where (brown): total acid sites with EtOH, (red): strong acid sites with EtOH, (dark blue): total acid sites with tBuOH, (light blue): strong acid sites with tBuOH, (green): total acid sites with ether,(light green): strong acid sites with ether. ..... 95

# Tables

# Schemes

# General introduction

The goal of research in the field of heterogeneous catalysis is to design and prepare improved catalysts and better understanding how they work. To reach this purpose, a series of catalysts are often made by varying the structure and composition through controlled alteration of the relevant variables of the preparation; activity and selectivity are then evaluated. It exists wide range of catalysts applications of heterogeneous catalysis dealing in particular with metal oxide-based catalysts. In the chemical industry, processes are including oligomerization, alkylation, metathesis and esterification, as well as environmental applications.

Oxides and mixed oxides are of interest in heterogeneous catalysis, serving as catalysts due to their redox or acid-base properties or as supports for active species due to their textural properties. The performance of a catalyst depends on its composition, texture, structure and surface properties, which must be controlled and adapted for each reaction involved. The texture of the catalyst is an extremely important parameter. In fact, the higher specific surface area, more active sites can accommodate and therefore higher specific activity of the catalyst. The size of the pores must be sufficient to allow both access of the reagents to the active sites but also the diffusion of the products. The structure of the catalyst and in particular the structure of the active sites governs the activity and the selectivity of the catalyst. Among the targeted surface properties, acidic and / or basic sites for example, which are a determining standard for certain applications. Finally, the performance of a catalyst depends on its mechanical strength, its thermal stability and on the synthesis process.

This thesis focuses on the synthesis and characterization of heterogeneous mixed oxide catalysts prepared by hydrolytic and non-hydrolytic sol-gel processes (HSG, NHSG). The development of NHSG technique started in the early 1990's. It has been widely used for the production of oxides, mixed oxides and organic-inorganic hybrids materials. It proved to be particularly successful for the synthesis of nanoparticles, bringing the advantages of better control over size, shape and crystallinity, and for the preparation of mesoporous oxides in one-step, avoiding the use of templates. The group Chimie Moléculaire et Organisation du Solide (CMOS) of the Institut Charles Gerhardt Montpellier (ICGM) is a pioneer in the NHSG field. The laboratory has more than 25 years of experience with this synthetic methodology, notably for the production of catalytic materials.

Exploiting the expertise of the CMOS group in NHSG, this PhD thesis deals with the synthesis of heterogeneous catalysts for ethylene oligomerization. The synthesis of $SiO_2$-$Al_2O_3$-NiO materials with various Ni-loading content is fully described. The prepared materials were characterized and their catalytic activity in ethylene oligomerization was studied.

This work was done in collaboration with Pr.Vasile Hulea (Ecole National Supérieure de Chimie) where the catalysts were tested in ethylene oligomerization.

# Chapter I:
# STATE OF ART

# I.1. Heterogeneous catalysis

## I.1.1 Introduction

The catalysis discovery is almost 200 years old, and goes back to the Swedish scientist Jöns Jakob Berzelius who in 1835 systemized previous work done by a number of researchers such as Faraday and Döbereiner.[1] Berzelius found that a number of reactions only took place if a certain substance, a catalyst, was present to initialize the process. However, catalysis has been used for thousands of years in the production of ethanol using yeast long before the concept of catalysis was discovered and rationalized. A catalyst can be defined as a substance that increases the rate of a reaction without modifying the overall standard Gibbs energy change in the reaction; the process is called catalysis. [2] Catalysis is often subdivided in classes such as heterogeneous, homogeneous and enzymatic.[3] The present work is focused on heterogeneous catalysis, which is characterized by the catalyst, reactants, and products forming at least two phases. A catalytic reaction is generally more complex than the non-catalytic reaction and involves more steps. Figure 1 gives a hypothetical potential energy diagram where these two processes are compared.

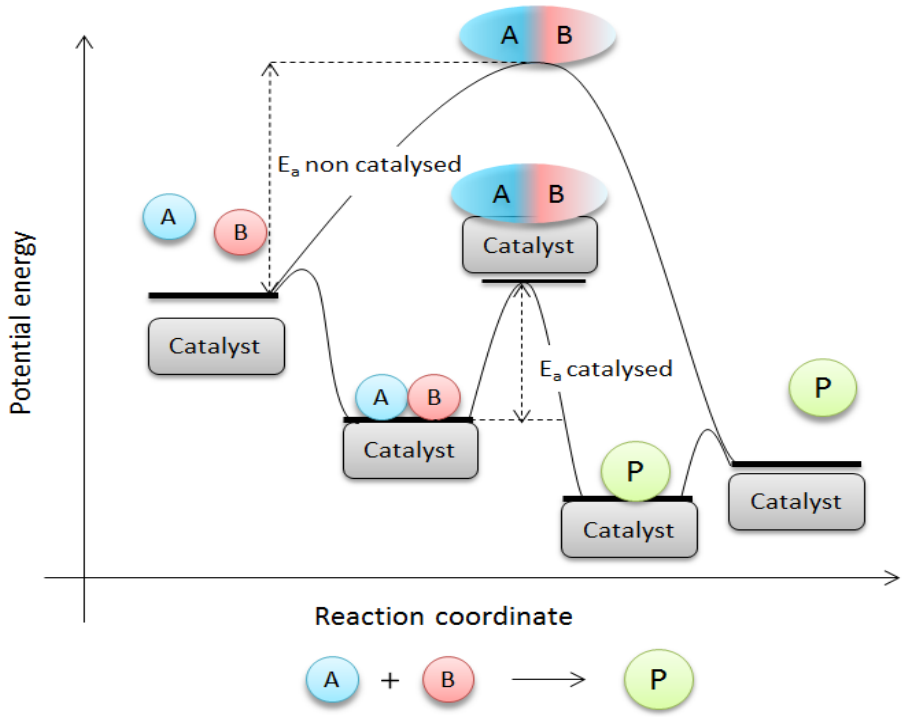


Figure 1: The potential energy diagram of the catalytic and non-catalytic reaction of A+B →P is compared. The activation energy (Ea) of a catalytic reaction is lower than the activation energy of a non-catalytic reaction, which leads to an increase in the rate.[4]

Heterogeneous catalysts usually exist in a solid state, while the reactants and products exist in a gaseous or liquid state. Gas-solid heterogeneous catalysis is usually employed in the refinery and in the bulk chemical industries, while liquid-solid heterogeneous catalysis is widespread in the fine chemical industry.[5] Heterogeneous catalysis plays a big role in our daily life; not just for economic part, but also for providing the essential infrastructure for overall well-being of society, many materials and foodstuffs could not be produced without efficient heterogeneous catalysis.[6] Heterogeneous catalysis is one of the main technologies for green chemical methods, therefore in many situations; it is preferred over other catalytic methods accessible to industry.[7] In heterogeneous catalysis, molecules can only react on the solid catalyst's surface. As a result, one objective could be to increase the catalytic surface area by using small catalyst particles for example (the specific surface area is proportional to the particle diameter).[8] Table 1 summarizes the advantages and disadvantages of heterogeneous catalysts against homogeneous ones.

Table 1: Comparison between Heterogeneous and Homogeneous Catalysis.

| Properties | Heterogeneous catalysis | Homogeneous catalysis |
|---|---|---|
| Cost of catalyst losses | Low | High |
| Selectivity | Low | High |
| Active centers | Only surface atoms | All atoms |
| Applications | Wide | Limited |
| Catalyst Separation | Cheap (easy) | Expensive (extraction or distillation) |
| Mass Transfer Limitations | Can be severe | Very rare |

## I.1.2 Support and active phase in heterogeneous catalyst

In supported catalysts, active phase-support interactions occur when the active phase (metal, oxide, sulphide or organic groups) interacts with the support phase (Figure 2) .[9]

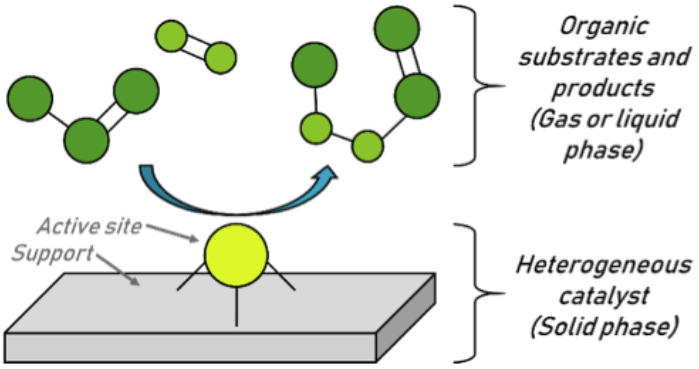


Figure 2: Support and active site in heterogeneous catalyst.

.

The surface of the support and active phase materials, as well as the interfacial between them, play a big role in determining this interaction.[10] In heterogeneous catalysis, silica and alumina, often used as supports for active phases, or as systems for acid-base catalysis.[11] Materials for heterogeneous catalysis often have a large specific surface area because, as catalytic phases, they must expose a large number of active sites and as supports, and should be able to disperse the active phase. Stability is important as well, it should be verified that the oxides are thermally stable in the temperature range of the catalytic reaction, or while regeneration of the catalyst.[12] Because of the reduced metal surface area, deactivation occurs,[13] thermal treatment in an oxidized environment is generally used to regenerate active metals. The high degree of metal dispersion can be restored by subsequent reduction under suitably mild circumstances.[14] The metal precursor should be well distributed after support impregnation.[15] Low temperature calcination produces fine dispersed oxide over layers, whereas direct low temperature reduction produces highly dispersed metal particles.[16, 17] Low temperature reduction of the distributed oxide precursor can also lead to this state, which is reversible by low-temperature re-oxidation.[18] At high calcination temperatures, a solid state reaction between the active metal precursor and the support can also produce.[19] When cohesive forces are dominating during reduction at high temperatures, particle agglomeration may occur, and referred to pill-box morphologies when the adhesive forces are the most powerful.[20] Metal must be movable in both instances. On the other hand, when the support

is movable, the area (cohesive forces). Otherwise, encapsulation (SMSI effect) may occur if adhesive forces are most powerful.[21]

In previous works, it was found that when the Tammann temperature of the active phase was sufficiently low (as in the case of $V_2O_5$, $MoO_3$ and $Re_2O_7$), calcination led to the migration of the active phase toward the surface (Figure 3).[22] The Tammann temperature is the temperature at which ionic diffusion becomes significant in a given material; this temperature roughly corresponds to 0.5 Tf, where Tf is the melting temperature in Kelvin.[23]

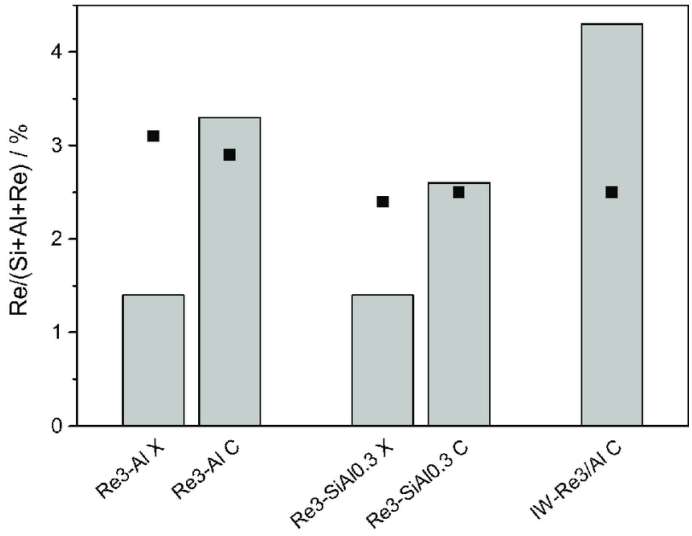


Figure 3: Surface Re/(Si + Al + Re) atomic ratios (XPS, gray bars) and bulk Re/(Si + Al + Re) atomic ratios (EDX, black squares) for xerogels and calcined catalysts. Reproduced with permission from.[24]

## I.1.3 Structure

Heterogeneous catalysis is a method for improving chemical processes by increasing conversion and selectivity, highly dependent on the structural design and surface characteristics of the catalyst material.[25] Understanding the chemistry that occurs in catalysis requires an understanding of catalyst structure. Despite of the active sites are generally found on the solid surface in heterogeneous catalysis, the bulk structure is very important, because many of catalyst properties depend on it.[26] The principal approach for studying bulk structure is X-ray diffraction. Other techniques, such as solid state NMR may be used to investigate the local environment of a specific element in a structure, while X-ray Photoelectron Spectroscopy may be used to investigate the surface structure.[27] The active phase and its surface can be affected by the structure of the catalyst bulk, in addition to reactions of the catalyst bulk during preparation and activation.[28] The

nucleophilic oxygen adsorbed into the reactant by metal oxide catalysts for partial oxidation processes, for example, may come from the catalyst bulk. Investigations of the connections between the structure and the reactivity of a heterogeneous catalyst must be carried out in-situ (*i.e.* under real reaction conditions) with the catalyst structure and gas phase composition are both being monitored at the same time.[29]

## I.1.4 Acidity

Acidity could be defined in terms of Brønsted or Lewis acid sites The number and strength of these sites as well as the morphology of the supports can lead to high product selectivity.[30] In industrial operations, solid acid catalysts are commonly used.[31] The number of operations that use such materials is expected to rise as more environmentally friendly chemicals replace mineral acids. Amorphous mixed oxides are commonly demonstrate evidence of Brønsted (surface -OH groups) and Lewis (unsaturated cationic sites), acid sites and silica-alumina (ASA) also demonstrate evidence of Lewis basic sites relatively weak.[32] These materials are usually used as both catalysts and supports for active phases.[33] Compared to pure alumina, silica-alumina is more stable[33, 34] and its catalytic activity is usually ascribed to the surface acidity.[34] The quantity and strength of these sites depend on the amount of alumina.[35] It is expected that the strength of acid sites would be distributed over the surface resulting in short-range interaction on silica-alumina surface. The structure of acid centers on silica-alumina has been studied in detail by many researchers.[36] Although there is still a debate on the origin of the acidity and why the property of the sites differ from those seen in crystalline zeolites.[37] The formation of these acid centers is considered to be owing, at least in part, to the isomorphous replacement of $Si^{4+}$ by $Al^{3+}$ in the silica lattice.[38] This process may be caused by aluminium diffusion into the silica network during high temperature calcination.[39] A net unit negative charge is generated when a typically six-coordinated Al atom is put in a four-coordinated structure, which can be balanced by adding a proton.[40] As a result Brønsted acid sites are formed, and when partially dehydroxylated, Lewis acidity (electron acceptor), in the form of unsaturated cationic sites, is produced by remove -OH groups.[32]

### I.1.5 Dispersion of metal

It is widely established that the specific activity per metal atom increases as the size of the metal particle decreases because such low-coordinated metal atoms frequently function as the catalytically active center.[41] It is an old and difficult problem that heterogeneous catalysis, even at nano and subnano scale, are less effective and dependable than in enzymology or homogeneous catalysis. Lopez *et al.* proposed the catalytically active single-atom site.[42] Since then, many types of novel, well-defined, and widely dispersed metallic catalysts have appeared.[43] Highly dispersed metallic sites (HDMS) are active centers that are energetically uniform, spatially isolated from one another and well distributed on the surface of supports. HDMS are similar to single sites in homogeneous molecular catalysts and are also called as analogues of soluble catalysts.

### I.1.6 Applications

Catalysts are applied in a wide range of chemical processes, from medicines to polymers to petroleum refining. Catalysis is used in about 90% of all industrial processes.[44] The widespread use of catalytic processes in industry is due to the economic and environmental benefits that catalysis provides.[45] The heterogeneous catalysis dealing in particular with metal oxide-based catalysts is the most significant route. In the chemical industry, we found processes including alkylation[46], metathesis[47], and esterification[48], as well as environmental applications. Among them, many studies are related to the oxidation of volatile organic compounds and reduction of NOx that produce harmful health and environmental consequences .[49]

## I.2. Acid catalyzed esterification

### I.2.1 Introduction

Esterification is an essential reaction for alcohols and carboxylic acids.[50] Esters are a family of functional groups that are widely found in a high range of useful chemicals, including fibers, plasticizers, solvents, lubricants, fragrances, surfactants, pharmaceuticals, food additives, etc.[51] Because of their importance, esterification processes should hold a prominent position to integrate safe and sustainable chemical technologies into various industrial operations. Esterification have traditionally been carried out in the presence of homogeneous acid catalysts such as HCl, $H_2SO_4$,

$H_3PO_4$, $AlCl_3$ and HF.[52] However, because of their toxicity, corrosivity and non-recyclability, these homogeneous catalysts are no more suitable. Polluted environment and difficulties in separation and purification products are further disadvantages of these systems. As a result, development of novel heterogeneous catalytic systems with good catalytic performance and high recoverability is a major challenge in this field.[53] Esterification of acetic acid with n-butyl alcohol to give n-butyl acetate, is highly used in industry as a raw material of flavoring extract, artificial perfume, photographic films, safety glass and plastics.[54] While the demand for n-butyl acetate has been grown from 40 thousand tons in 1990 to 1030 thousand tons in 2013[55], the industrial production of n-butyl acetate mostly used the classic concentrated sulfuric acid-catalyzed esterification technique.[56] Through time, this method has been completely exploited due to their environmental damages.[54] Many heterogeneous catalysts have been reported to be active in the esterification process in the literature like zeolites[57], ion exchange resins[58], H-ZSM-5[59], sulphated oxides[60], amorphous catalysts (silica-alumina) and mesoporous hexagonally structured materials such as SBA-15 and MCM-41.[61]

## I.2.2 Mechanism

While the mechanism of esterification reaction in homogeneous phase is well understood. The majority of scientists agree on a protonated carboxylic acid intermediate.[62] Langmuir-Hinshelwood and Eley-Rideal are two main reaction mechanisms suggusted in heterogeneous catalysis. The two reacting species are chemisorbed on the catalyst surface before the reaction takes place in the Langmuir-Hinshelwood mechanism, while one species reacts directly with the chemisorbed species in Eley-Rideal mechanism, as shown in (Figure 4).[63]

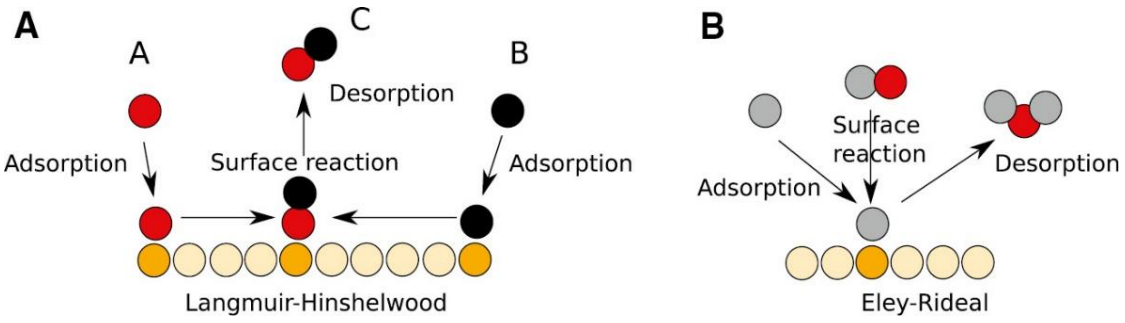


Figure 4: (A) Simple adsorption and desorption (L-H mechanism). (B) Dissociative adsorption and associative desorption (E-R mechanism).[64]

These two mechanisms are competitive depending on the compositions of the catalysts and the activation of adsorbates on them.[65]The Langmuir-Hinshelwood mechanism has been regarded as the dominant mechanism for the great majority of surface catalytic reactions, while Eley-Rideal mechanism is used in a few reactions.[63]Gas-phase esterification reactions for example, have been investigated on many of solid acids, like silica-supported sulfonic acids[66], metal oxides [67], ion-exchange resins [67, 68], heteropolyacids [69] and zeolites.[68] A variety of alcohols, including methanol[70], ethanol[71], isopropanol[72] and butanol[68], were employed as the esterifying agent and acids like acetic acid[72], lactic acid[71] and benzoic acid[73] were employed as acylating agent. Chu *et al.* investigated the gas-phase esterification of acetic acid with butanol and ethanol over carbon-supported heteropolyacids.[69] They postulated that esterification of acetic acid with ethanol followed two-site (Langmuir-Hinshelwood) mechanism, while esterification of acetic acid with butanol, followed an Eley-Rideal mechanism.[69] Koster *et al*. studied the gas-phase esterification of acetic acid with ethanol over MCM-41 as catalyst, and found that it proceeds through a protonated acetic acid intermediate and follows a Langmuir-Hinshelwood mechanism.[74] Altiokka and Citak investigated the esterification of acetic acid with isobutanol in the liquid phase in the presence of a highly acidic ion-exchange resin, as catalyst.[75] They founded that the reaction between an adsorbed alcohol and acid molecules takes place in the bulk phase following a single-site Eley-Rideal mechanism. Teo and Saha investigated the kinetics of acetic acid esterification with isoamyl alcohol in the presence of a cation-exchange resin Purolite CT-175 at temperatures 60-85 °C.[76] They reported that reaction following a modified Langmuir-Hinshelwood mechanism, in which acetic acid adsorbed on one active site, interacts with isoamyl alcohol adsorbed on the next active site to produce isoamyl acetate and water. Liu and Tan, in their experiments on liquid phase esterification of propionic acid with n-butanol, have founded that esterification occurs via an Eley-Rideal mechanism over Amberlyst as catalyst.[77] S.R. Kirumakki *et al*. studied the kinetic of liquid phase esterification of benzyl alcohol with acetic acid and found it follows an Eley-Rideal, mechanism.[78] From the above literature, it was concluded that the mechanism of esterification is influenced by the reactants and catalysts. It is also possible that the mechanism differs for activities in the gaseous and liquid phases.[72]

## I.2.3 Silica-alumina solids

Silica-alumina is an essential industrial material for variety of applications.[79] It is a mixed oxide network of linked silica and alumina tetrahedral that has both Brønsted and Lewis acid sites. The quantity of aluminum determines the strength, distribution, and number of these sites.[79, 80] Several silica-alumina catalysts have been shown to be active in the esterification reaction, such as Hb, HY and HZSM5 zeolites[62], MCM-41[81], SBA-15.[82] Zeolites are microporous crystalline aluminosilicates generally composed of silicon, aluminum and oxygen. They are effective esterification catalysts[83] due to their high Brønsted acidity and ability to change physical and chemical properties by changing their Si/Al ratio (Figure 5).[84]

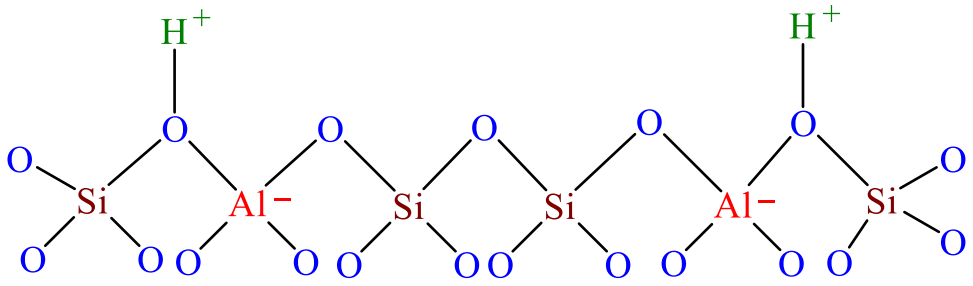


Figure 5: Brønsted acid sites in zeolites.[85]

Currently, a number of methods are available to synthesis hierarchical porous zeolites in the form of composites[86], nanosized crystals[87], and mesoporous crystals.[88] Acidity is an essential parameter which comes from the charge unbalance between alumina and silica units. This property makes zeolites effective catalysts for a variety of organic reactions.[89] Another mesoporous molecular sieves, MCM-41 have drawn great interest for their excellent characteristics like high specific area, volume and pore size which enable them to be used as adsorbents, catalytic supports, and heterogeneous catalysts in a variety of chemical reactions, including esterification.[90] In addition to their well-ordered distribution of mesopores, MCM-41 solids offer the possibility of incorporating metals into their structures. This tuning increases their hydrothermal stability and generates active sites and thus expanding their application range.[91] It has been reported that the acidity of mesoporous silica was found to improve when Al was grafted into MCM-41 silica framework.[92] It is well known that acidity increases as Al incorporated into the structural lattice

of MCM-41 as shown by studies on the influence of the Si/Al ratio of Al-MCM-41 on the esterification reaction of alkyl acids with various alcohols.[93] Another ordered mesoporous molecular sieves, SBA-15, have been studied due to its excellent structural properties, such as tunable pore size, high surface area and pore volume. SBA-15 silica has high structural stability and appears as a promising catalyst support candidate.[94] This mesoporous material can host a wide range of catalytically active functional groups by drafting or by direct synthesis.[95] Al-SBA-15[96] is widely studied due to Al substitution in silicate structures generate Bronsted acidity and these acid sites have wide range industrial reactions such as esterification reaction.[97]The general simple procedure for preparation SBA-15 is showeh in (Figure 6).[98]

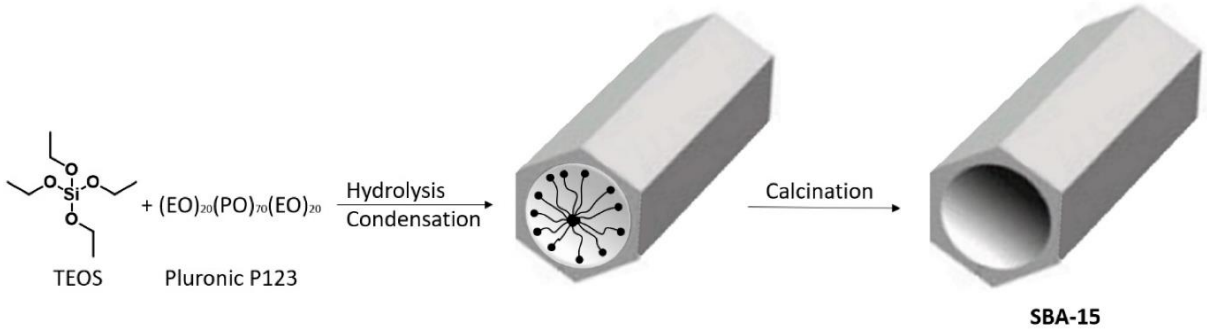


Figure 6: General procedure for the Santa Barbara Amorphous (SBA)-15 preparation. [98]

# I.3. Ethylene oligomerization

## I.3.1. Heterogeneous catalysts for ethylene oligomerization

The oligomerization of ethylene can be efficiently catalyzed by heterogeneous catalysts.[99] The type of catalyst and operating conditions have a high effect on product selectivity. In the petrochemical industry, ethylene is produced via steam thermal cracking of gaseous or liquid saturated hydrocarbons.[100] Alternative strategies involving other sources like natural gas, coal and biomass are imagined. For instance, methanol (which is easily produced from all these sources via syngas) can be effectively converted into ethylene by a zeolite-catalyzed method.[101] The conversion of bioethanol to ethylene is also a very promising application (Figure 7).[102] Because ethylene oligomerization is one of the major processes to produce linear and branched higher

olefins, it took high interest in both industrial and academic fields, which are components of plastics, plasticizers, lubricants and surfactants.

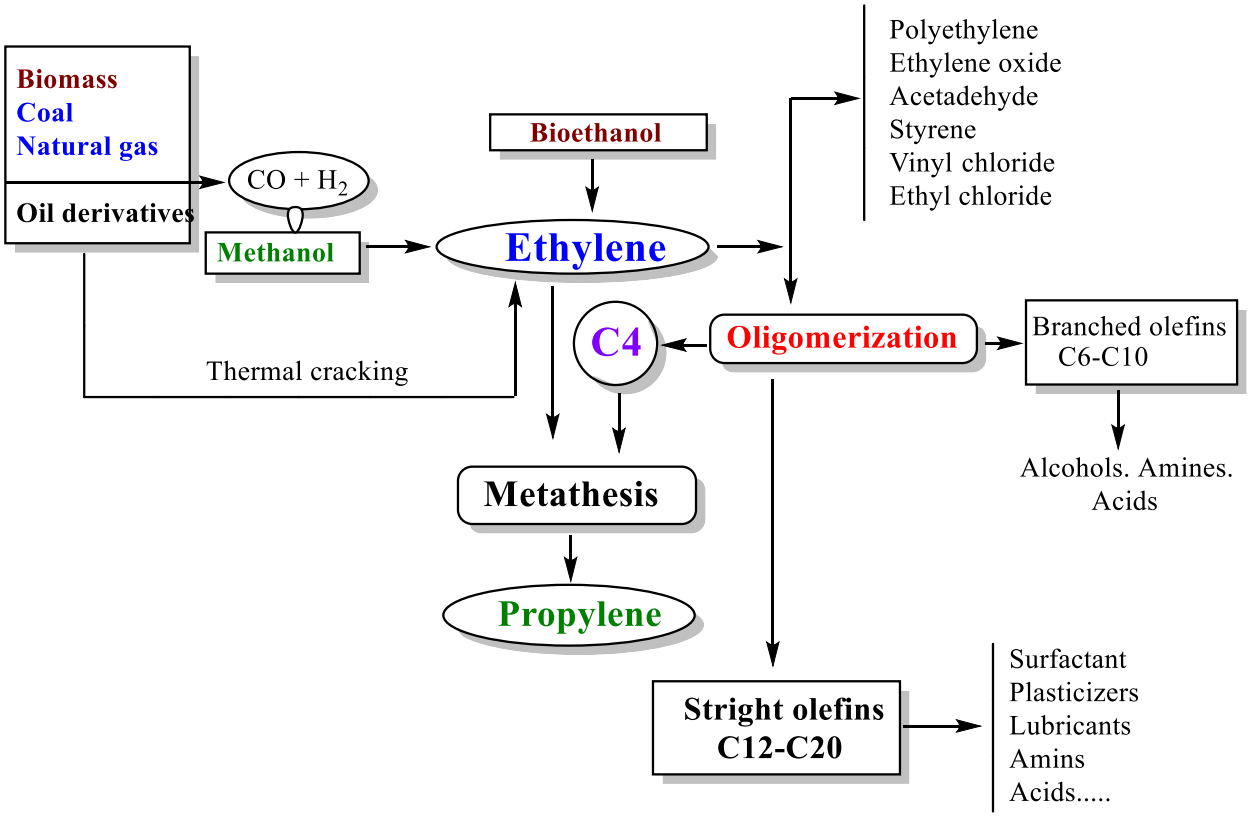


Figure 7: Ethylene feedstock and major derivatives.[102]

The ethylene oligomers can be also considered as starting materials for other essential chemicals, including propylene, alcohols, amines and acids. This oligomerization process can be carried out in the presence of heterogeneous catalysts. The industrial procedures for producing higher olefins from ethylene oligomerization use organic solvents and homogeneous catalysts, such as trialkylaluminium (Chevron and Ethyl) and nickel complexes (Shell).[103] In the previous decades new homogeneous catalysts such as complexes of nickel, titanium, zirconium, iron, chromium and cobalt have been developed.[104] Heterogeneous catalysis can be considered as environmentally friendly compared to the traditional methods. As a result, considerable research efforts have been focused on the development of heterogeneous ethylene oligomerization methods. Solid catalysts can be classified into three main types: solid acids, nickel complexes immobilized on polymers and oxides, and nickel supported on inorganic porous materials.[102] Acid catalysts, including

supported phosphoric acid, zeolites, silica-alumina, and macroporous sulfonic resins demonstrated great potential for oligomerization of C3+ olefins. Unfortunately, the oligomerization rate of ethylene is significantly lower than that of other olefins when using acid catalysts at mild temperatures.[102] In general, ethylene oligomerization occurs at higher temperatures, and zeolites are the best acid catalysts.[105] Besides oligomerization, processes including isomerization, aromatization, disproportionation and cracking, take place at these conditions, resulting a wide range of products and large amount of cokes. The Ni-based heterogeneous catalysts included nickel oxide supported on silica, are commonly used for ethylene oligomerization.[106] Morikawa *et al.* first detailed that NiO supported on Kieselguhr can catalyze the dimerization of ethylene even at room temperature.[107] Bailey and Reid from Phillips Petroleum Company reported that NiO supported on silica gel demonstrated catalytic activity at temperatures ranging from 0 to 150 °C.[108] They mentioned that the presence of alumina in the support seems to be required to make sure of the catalyst properties. In addition, only catalysts initiated by heating in an oxidizing atmosphere at 400-500 °C can catalyze ethylene oligomerization. Ozaki and Shiba reported that $NiO/SiO_2$ is a good catalyst for the dimerization of ethylene at room temperature. [109] After a series of studies, it has been demonstrated that the support has a major role in ethylene oligomerization with NiO. Therefore, Matsuda *et al*. found that only NiO supported on acidic silica and/or alumina showed ethylene dimerization activity.[110] It was discovered that silica-alumina oxide is an effective NiO support. Silica-alumina oxide was found to be an excellent support for NiO. Furthermore, the amount of alumina in the support seemed to affect the catalyst's behavior.[102]

## I.3.2. Parameters effects on ethylene oligomerization

Ethylene oligomerization is a simple chemical process to produce linear alpha olefins. In order to make a better transition from homogeneous catalytic systems to heterogeneous catalysts, it is necessary to characterize and study the parameters of the overall reaction. The operational parameters, which range from reaction temperature to reaction pressure, must be examined for their influence on the reaction. Other appropriate parameters helpful for reactor configuration include the weighted hourly space velocity, which dictates the ratio of the reactant ethylene mass flow rate with the amount of catalyst used. Furthermore, specific features relating to the design of the catalyst

must also be investigated, since the catalyst is the essential vehicle for the reaction. Parameters such as pore size, acid site concentration, and active metal concentration must be accounted on their overall influence on ethylene oligomerization.

### I.3.2.1. Effect of Pore Size

The pore size has been shown to be one of the most important characteristics for ethylene oligomerization reactions. In general, the catalyst pore size plays an important role in catalytic reactions that occur over heterogeneous catalysts. For heterogeneous catalysts, the modes of transport are dictated by the simplicity of diffusion of the reactant molecules to the actives sites of the catalyst. The steps involved in carrying out a chemical reaction in the presence of a heterogeneous catalyst are described as follows: [111]

1. Diffusion of the reactant from the bulk stream to the gas-solid interface.
2. Diffusion of the reactant through the interior pores of the catalyst.
3. Adsorption of the reactant species to the chemical active site.
4. Reaction of the adsorbed reactant with other adsorbents into products.
5. Desorption of the products from the active site.
6. Diffusion of the product from the active site through the interior pores of the catalyst.
7. Diffusion of the product from the catalyst surface into the bulk stream.

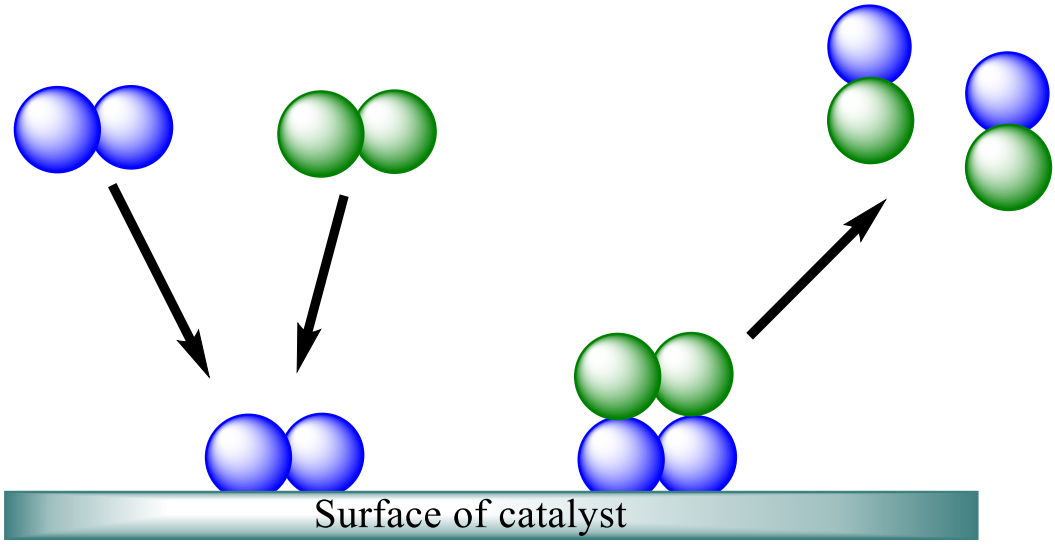


Figure 8: Main steps of catalysis reaction.

In steps, 1, 2, 6, and 7, diffusion is the primary mode of transport that simplify the delivery of the reactant to the catalyst, thus starting the reaction. Therefore, the pore size is one of the major factors to consider for the design of a catalyst, as the pore size plays analogously as a "gatekeeper" for the reactant molecules before any chemical reaction can occur. The differentiation between materials and their pore sizes can be portrayed into two dominant classes: microporous and mesoporous materials. Microporous materials have pore sizes on the span of less than 2 nm in diameter.[112] Some zeolites, such as ZSM-5, can be ordered as microporous materials. Industrial applications can exploit of the unique and narrow pore size to force isomerization reactions, for example, of o- and m-xylene to the more valuable p-xylene isomer.[113] However, in the ethylene oligomerization case, the activity of the catalyst improves drastically as the pore sizes increase as shown in (Figure 9). Lallemand *et al* synthesized Ni-MCM-22, a zeolite comprising of micropores, and observed rapid deactivation and negligible catalyst activity due to pore blocking and heavy oligomeric accumulation. [114]

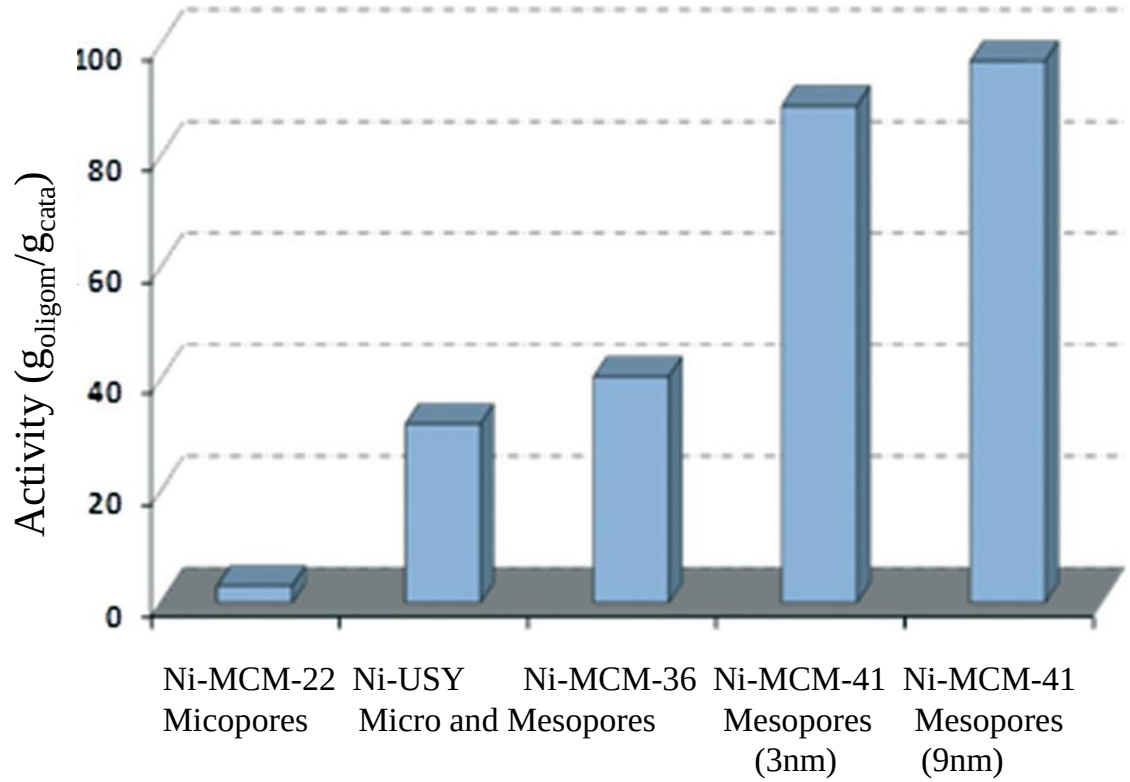


Figure 9: Activity as a function of pore size, observed through several microporous and mesoporous materials.[102]

The catalyst activity significantly expanded for Ni-USY and Ni-MCM-36 materials, both are composed of a combination of micropores and mesopores. The reasoning behind this was because of the presence of the mesopores.[114] Having mesopores in the framework of the catalyst allowed for the diffusion of larger oligomers. The authors theorized that the larger oligomers that gathered in the microporous material could diffuse more productively through mesoporous material, thus allowing for higher overall catalyst activity and turnover. Accordingly, a purely mesoporous material, Ni-MCM-41, performed the best, having the highest activity.[115]

### I.3.2.2. Effect of Acid Site Concentration

The action of the acid sites in nickel-based silica alumina catalysts for ethylene oligomerization has been a highly disputed topic. While it is comprehended throughout the research that nickel sites are basic for ethylene oligomerization, the part of the acid sites is still unclear. Several authors claimed that the acid sites are necessary for ethylene oligomerization. The activity of the nickel exchanged silica-alumina was found to be proportional to the acid strength of the surface.[102] Lapidus *et al*. suggested that, for silica-alumina materials prepared by ionic exchange of $Ni^{+2}$ , that catalytic activity is also dependent on the number of acid sites as a function of the aluminum content.[116] They found that the combinatorial effect of having nickel and acid sites to be beneficial for facilitating ethylene oligomerization reactions. Another author, Sohn *et al.*, directed ethylene oligomerization with sulfated nickel catalysts and found a relationship between catalyst activity and acid strength with NiO and $NiSO_4$ supported on various substrates, such as $TiO_2$, $ZrO_2$, and the predominant $SiO_2$-$Al_2O_3$ seen in most of the literature.[117] Davydov *et al.* suggested that the role of the proton was used to simplify a nickel reduction reaction of divalent nickel to monovalent nickel ($Ni^{+2}$ to $Ni^{+}$).[118] Lallemand *et al.* show that there are two types of mechanisms which contribute to the oligomerization process on zeolite-based catalysts: one is based on nickel site coordination chemistry and the other is based on the acid catalysis (Figure10).[114]

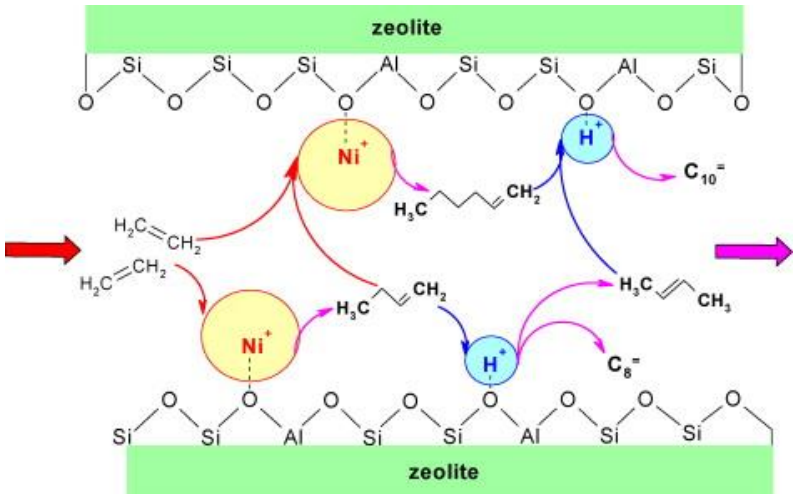


Figure 10: Main reaction pathways of the reaction of ethylene over Ni-exchanged molecular sieves. [114]

From the results, the authors suggested that the $Ni^+$ species is the active form of the catalyst due to this reduction. Ng and Creaser also proposed that the $Ni^+$ and $H^+$ coupling played a major role in carrying out oligomerization. The variety of the interpretation of the results assumes that the role of the acid site is still in the area of high interest for this process. Oligomerization studies performed under mild reaction conditions, in a slurry batch reactor, in the presence of Ni-AlMCM-41,[115] Ni-Y,[119] and Ni-MWW.[114] Finiels et *al.* found that both nickel and acid sites are necessary for the activation of this reaction. Furthermore, the balance between the acid and nickel site densities is a key factor that influences the activity, selectivity, and stability of the catalyst (Table 2). However, the influence of having too high of a concentration of acid sites on a support was observed to be negative for the oligomerization reaction and the resulting catalyst activity.[102] For Ni-based zeolites, a very high density of acid sites may be detrimental to the activity by promoting the formation of long chain oligomers, responsible for pore blocking and catalyst deactivation sources.[119] In the case of Ni-containing mesoporous materials, Hulea *et al*. found that the amount of oligomers strongly increased when the acidic site concentration decreased from 0.72 to 0.3 mmol/g.[115] Moreover, a very low acidity is detrimental for the catalytic activity. A high acid/nickel ion site ratio results in quick surface deactivation of Ni-containing materials due to acid-catalyzed reactions, which are in charge of the formation of strong adsorbed long-chain oligomers.[115] Consequently, just a carefully selected acid site density has a beneficial effect on the stability of Ni-based catalysts and implicitly on the oligomerization activity.

Table 2: Main reaction pathways of the reaction of ethylene over Ni-exchanged molecular sieves.[102]

| Catalyst | Si/Al(mol.mol$^{-1}$) | Acidity[c] (mmol. g$^{-1}$) | Ni/acid site (mol.mol$^{-1}$) | Average activity[d] (g.g$^{-1}$.h$^{-1}$) |
|---|---|---|---|---|
| Ni-Y[a] | 6 | 1.02 | 0.25 | 15 |
| | 15 | 0.58 | 0.29 | 20 |
| | 30 | 0.35 | 0.29 | 30 |
| Ni-MCM-41[b] | 10 | 0.72 | 0.14 | 21 |
| | 18 | 0.59 | 0.14 | 25 |
| | 26 | 0.45 | 0.19 | 41 |
| | 49 | 0.34 | 0.21 | 46 |

Oligomerization conditions: [a] 50 °C, 40 bar. [b] 150°C, 35 bar. [c] From ammonia TPD, [d] $g_{oligom}$ $g_{cata.}^{-1}h^{-1}$.

## I.3.2.3. Effect of Nickel Loading

The catalytic activity of nickel was observed to be critical for carrying out ethylene oligomerization reactions for a few substrates. For nickel loadings of 5 wt.% and 10 wt.% for $NiO/SiO_2$-$Al_2O_3$ catalysts, the ethylene conversion was found to be at 30.4% and 23.8%, respectively at 275 ºC.[116] A. Lapidus *et.al* additionally tested Ni-Y catalysts at similar loadings and observed that the conversion followed a similar trend, with 39.2% conversion at 4.7 wt. % and 29.4% conversion at 8.1 wt.% nickel loading.[120] Nicolaides *et al* observed that the ethylene conversion expanded steadily until a nickel loading of 1.5 wt.%, after which a sharp decrease in ethylene conversion was observed.[121] The research group concluded that this result was because of higher activity per nickel site at lower nickel loadings compared to higher nickel loadings, which resulted in lower activity at the latter. In contrast, higher loadings up to 5 wt. % had a marked lighter product and lower conversion, which is consistent with the results discussed earlier. To better comprehend the rationale behind this behavior, Heveling *et al.* attributed the lower activity at higher nickel loadings to a selective growth reaction that was dictated by Schulz-Flory statistics.[122] The authors determined that the high nickel content positively affected the growth factor, $\alpha$. Thus, high nickel loadings were better theorized to be better attributed to the formation of diesel-range olefins. However, in spite of this high activity, the overall deactivation and lower conversion of the catalyst was generally attributed to the development of long oligomers that prevented further reaction. As such, having too high of a nickel loading, while theoretically useful for growing larger oligomers,

is limited by having too low of a conversion and catalyst activity. The localized state of the nickel species on catalyst support was found to play a key role in the oligomerization of ethylene. For further investigation, several studies were conducted using ionic-exchange and impregnation synthesis routes to introduce nickel onto a catalytic substrate. Several authors observed that ionic-exchanging the nickel to the substrate resulted in higher catalytic activity, with 2 wt. % being a local maximum. After 2 wt. % of nickel, the activity strongly drops off. The authors of this study justified that the reason behind this is because the nickel ions more than 2 wt.% are most likely present on the material as solid NiO species.[123] NiO is inactive for ethylene oligomerization and are detrimental to the reaction due to partial blocking of the catalyst pores. This behavior was verified utilizing temperature programmed reduction (TPR), with the results showing that, above a certain threshold, nickel just appears as NiO. The thinking behind a preliminary ion exchange is because the charge imbalances presented in the material because of framework aluminum. The presence of silicon in the framework (+4 charge) neutralizes the charges of the surrounding oxygen atoms. If the aluminum (+3 charge) replaces the silicon, an unbalanced negative charge is formed in the silica-alumina framework. This negative charge must be repaid with an accompanying cation, for example ionic forms of nickel and acidic protons. Therefore, the aluminum content is in charge of the number of cations the material can theoretically be ion-exchanged with. Martinez *et al*. observed that the increase in the Ni loading up to 2.7 wt.%, will increase the activity of Ni-Beta catalyst. The activity plateaued at nickel loadings past 2.7 wt.% until a constant conversion of 85% was achieved at 5 wt.%.[124] This result was corroborated by Heveling *et al*., as they observed that a Ni-exchanged silica-alumina with 0.73 wt.% nickel had noticeably higher conversion and catalyst activity compared to a catalyst with a higher nickel loading (3.84 wt.%).[125] The major findings from these articles indicates that a lower weight percentage is effective, for ethylene oligomerization. However, the difficulty with these catalytic systems understands the specific nature of the active nickel species on the catalyst. In spite of the authors did not specify the characteristics of the active nickel species, the results demonstrate that lower nickel loadings ion-exchanged with the material was far more active for ethylene oligomerization.[102]This behavior is reported in (Figure 11).

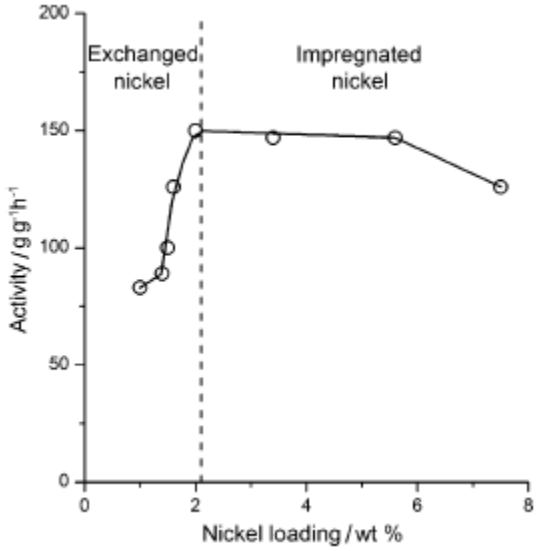


Figure 11: Oligomerization activity as a function of nickel loading.[123]

## I.3.2.4. Effect of Temperature

The reaction temperature plays a critical role in determining the overall stability of a catalyst as the reaction progresses. In turn, the stability of the catalyst will also affect the reaction pathways as well as the types of products generated. For ethylene oligomerization, the reaction temperature has been observed to have a large number of consequences on the reaction. For slurry semi-batch systems, researchers have observed that the reaction rate tends to decrease with an increase in the reaction temperature.[102] This behavior has been credited to a decrease in ethylene solubility in the heptane solvent commonly utilized as the reaction medium for these systems. However, this decrease in the reaction rate was not because of the catalyst not being active for reaction, but more so attributed to the heat and mass transfer limitations of the reactor design. In contrast, these mass transfer limitations are removed in fixed bed reactors as there is no longer a solvent that the ethylene needs to be dissolved into. To further investigate the implementation of nickel oligomerization catalysts in fixed bed reactors, several authors conducted low temperature studies over a fixed bed reactor over a variety of silica-alumina substrates. Ng and Creaser ran ethylene oligomerization with Ni-HY catalyst in the range of 50 ºC to 70 ºC in a packed bed reactor. They observed that butenes were the most favorable and selective product at lower reaction temperatures.[126] With a

slight uptick in the reaction temperature to 70 ºC, they observed that the selectivity towards hexenes increased, proposing that a small increase in temperature was sufficient to more facilitate oligomerization of butene with ethylene to form hexenes. In conjunction to this behavior, the activity of the catalyst was additionally found to increase in this narrow range, from 6.04 mmol $g^{-1}$ $h^{-1}$ to 13.19 mmol $g^{-1}$ $h^{-1}$ at 50 ºC and 70 ºC, respectively. Heveling *et al*. also tested Ni-HY and Ni-$SiO_2$-$Al_2O_3$ catalysts over a range of temperatures spanning 40-360 ºC.[125] They observed two distinct temperature regimes that had high conversion and activity near 120 ºC and at temperatures above 300 ºC. Hulea *et al*. were also observed this volcano-type of curves for activity with Ni-Y and Ni-MCM-41 in batch systems, with maxima for conversion and activity at 50 ºC and 150 ºC, respectively.[119] As such, some researchers performed further studies that examined the effect of higher reaction temperatures on ethylene oligomerization.[125] The product distribution for a number of systems was observed to shift with temperature. At low temperatures, the major oligomerization product observed for most systems was primarily butene. However, as the reaction temperature increased, the product distribution shifted to that of a Schulz-Flory distribution, with C4>C6>C8>C10>…> C (2n). The effect of high temperature indicated that there a bimodal or potentially polymodal distribution of activity. The rationale that the authors provided behind this behavior is that the nickel species at higher temperatures become far more unstable and tended to facilitate other secondary reactions. These reactions could include, especially in the presence of materials with acid sites, secondary oligomerization, cracking, alkylation, disproportionation, and isomerization reactions which would result in the formation of saturated and unsaturated hydrocarbons.[127]

## I.3.2.5. Effect of Pressure

Ethylene oligomerization is a chemical reaction that is strongly depends on the reaction pressure. For chemical reactor systems involving semi-batch processing, the ethylene pressure plays a big role in determining its solubility in the solvent containing the catalyst. This, however, is an inherent diffusional limitation of this three-phase system, as the rate of ethylene oligomerization is emphatically reliant on the selected solvent as well as the solubility of ethylene in that given solvent. Not surprisingly, the rate of reaction expanded relatively with ethylene pressure for semi-batch systems using Ni-MCM-41 catalysts.[128] The literature detailing the role of pressure in flow systems, however, is restricted. Ng and Creaser assessed the effect of pressure on Ni-HY

catalysts. They observed that the activity of the catalyst increased with pressure; however, the justification behind this behavior was unclear. Reaction kinetics manage that, for gas-phase reactions, the rate of reaction should increase as the partial pressure of the gaseous reactant (ethylene) increases. Moreover, the number of ethylene molecules increases with the increases of pressure, which would take into consideration higher degrees of collision with the catalytic active sites. As such, the reaction pressure for flow system is beneficial for both higher ethylene conversion and catalyst activity.

## I.3.3. Catalyst deactivation in oligomerization reaction

The catalyst deactivation (which is a major disadvantage in heterogeneous processes) has been assessed in a various investigations on ethylene oligomerization. The deactivation resulted generally from strong adsorption of products on active sites and pore blocking with heavy molecules. Thus, the catalyst lifetime is principally represented by the pore size and reaction conditions. The microporous Ni-exchanged zeolites (Ni-Y, Ni-MCM-22) encountered very fast deactivation.[126] For instance, NiY has lost about 50% of the initial activity after 2-3 h time-on-stream (tos) at reaction temperatures between 50 and 70 °C. An exception was the Ni-Beta nanocrystalline zeolite with a high external surface.[124] This catalyst showed no indications of deactivation under reaction conditions (120 °C and 35 bar). In contrast, catalysts with mesopores, such as Ni-amorphous silica-alumina, Ni-mesostructured silica-alumina, and Ni/sulphated alumina, exhibted very high stability against deactivation. Thus, utilizing a Ni-exchanged silica-alumina catalyst in a fixed-bed micro reactor at relatively low temperature (100-120 °C), high pressure (35 bar) and MHSV= 2. Heveling *et al*. reported very good catalyst stability over 144 days of tos.[125] In order to compare the deactivation rates of a Ni-exchanged silica-alumina catalyst at various reaction conditions, Espinoza *et al.* observed the ethylene oligomerization at temperatures ranging from 240 and 380 °C and pressure from 1.7 to 26 bar in a fixed-bed microreactor.[129] The deactivation of the catalyst (between 50 and 70% over 100 h time on stream) was independent of the space velocity; however, its rate increased with pressure and with temperature. The execution of Ni-mesoporous materials has been also assessed in pilot plants equipped with continuous stirred tank reactors. Zhang *et al*. discovered that Ni/sulphated alumina showed great oligomerization activity with no apparent deactivation at low temperatures (5-25 °C) during 34 h tos.[130] According to Heydenrych *et al*., under more severe conditions (35 bar, 120-180 °C) Ni-exchanged

silica-alumina showed just a slight deactivation during experimental runs of 900 h tos.[131] Lallemand *et al*. reported that during catalytic tests performed at 30 °C and 35 bar, over 170 h on stream, the Ni-MCM-41 catalyst was exceptionally active (ethylene conversion > 95%) and very stable to deactivation.[132]

# I.4. Heterogeneous catalysts prepared by sol-gel route

This part is to show an overview of the sol-gel route and its application in the synthesis of heterogeneous mixed oxides catalysts. The point here is to present this simple, cheap and original hydrolytic and non-hydrolytic sol-gel processes as an alternative for the synthesis of materials for catalysis when the impregnation of preformed supports are lacking.

## I.4.1. Hydrolytic sol-gel route (HSG)

### I.4.1.1. Principles of sol-gel route

The term "hydrogel" involve a wide range of materials, both natural and synthetic. Sol-gel attracted great interest of chemists for a period between the late nineteenth century and the early twentieth century. The first article on sol-gel was published by the French chemist Eblemen[133] (1846) who described that under acidic conditions, $Si(OEt)_4$ (tetraethyl orthosilicate, TEOS) underwent hydrolysis, yielding silica in the form of a glass-like material. prepared the first silica gels.[134] Cossa (1870) synthesized the first alumina gels by electrolytic method.[135] In the l930's Geffcken and Dislich of Schott Company searched an economic way of covering industrial glass with a thin oxide layer, who prepared single oxide coatings.[136] After that, D. Roy and R. Roy proposed a method to prepare more homogenous metals and glasses by sol-gel route.[137] In the early 1960s, H. Schroeder deposited transparent coatings on glass surfaces in order to correct the refractive index using titanium butoxide.[138] Dislich and Hinz elaborated the chemical basis for preparation of multicomponent oxides.[139] Independently and simultaneously, a similar but not identical route was taken by Levene and Thomas and was likewise patented.[140] The sol-gel process has continued to grow in interest and versatility thereafter. In fact, obtaining materials in different forms (Scheme 1), such as dense film, nanopowders or fibers are today possible, but it is in the production of functional thin-film deposits that it finds its main application.[141] Sol-gel process can be defined as the conversion of a precursor solution into an inorganic solid through water-

induced inorganic polymerization reactions.[142] This polymerization can be carried out under simple experimental conditions, such as neutral pH, in water, and low temperatures. This is why it was given the name "Chimie Douce".[143] Metal oxides with the general formula $M(OR)_n$ (M = Si, Al, Ti, etc. and R being an alkyl group such as Me, Et, $^{i}$Pr, etc.) and metal halides ($MX_n$) can be used as starting materials. Silicon is the most studied metal, and silicon alkoxides are the preferred molecular precursors for the sol-gel process. There are two distinct states of inorganic polymerization.

A sol can be defined as a stable suspension of colloidal solid particles within liquid (Hiemenz 1977),[144] which is formed after hydrolysis of the precursors followed by polycondensation to form an oxide gel. After more drying and heat treatment, the 'gel' converted into oxide.[145] Within several days after water added, gelation occurs, the rate of hydrolysis and condensation by acid or base catalysis must be increased.[146]

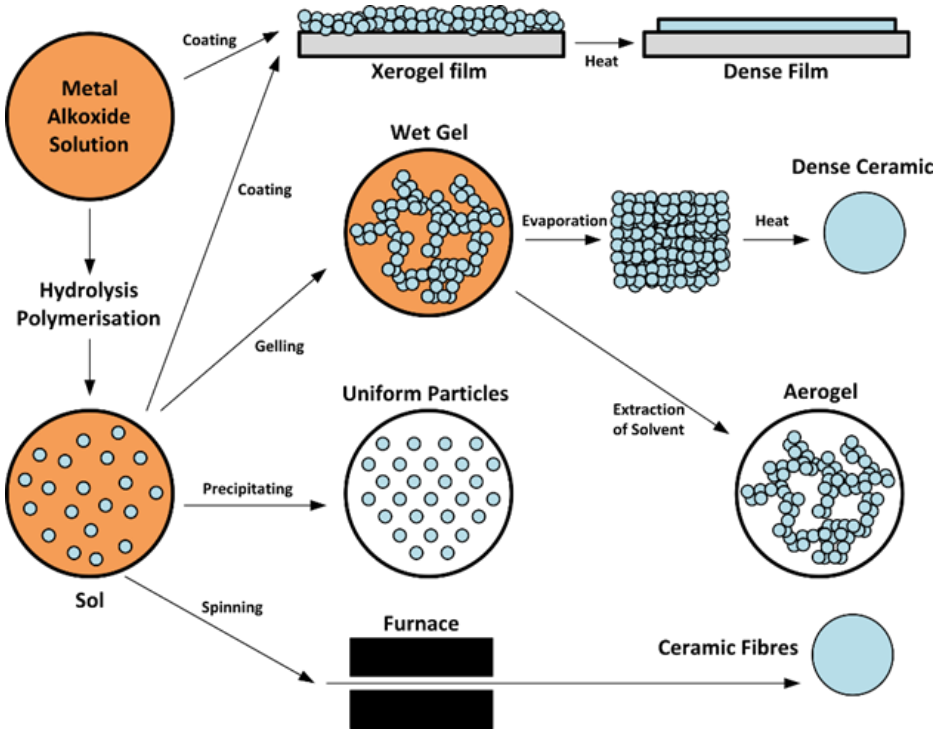


Scheme 1: Represents the various phases and methods of Sol-Gel technology. [147]

The sol-gel route has many advantages over other synthesis routes, such as lower processing temperature, homogeneity, purity, stoichiometric power, easy preparation.[148] These conditions present the possibility of combining organic and inorganic species to form new classes of organic-

inorganic hybrid compounds, with new properties that have never seen before compared to normal routes. Furthermore, the homogeneity and purity of the solution at the molecular or nanometric scale could be maintained in the final material. [149] Because of their mesoporous structures, oxides and mixed oxides are important in a variety of industrial processes, including catalysts[150], gas sensors[151] and photocatalysts.[152] Among the mixed oxides, silica-alumina is one of the most widely used solid acid catalysts.[153]

### I.4.1.2 Mechanism of Sol-Gel Synthesis

The last two decades have witnessed a rapid development of organic-inorganic materials prepared by sol-gel routes.[154] In a conventional sol-gel process, a metal alkoxide is used as the starting material.[155] This work will be limited to use tetraethoxysilane (TEOS). Hydrolysis and polycondensation are the first two steps in the process, both need the use of a catalyst and resulting the formation of the -Si-O-Si- bond, which is the fundamental unit of an inorganic material. There are three types of catalysts used: acidic ($H^+$), basic ($OH^-$) or nucleophilic ($F^-$, DMF, DMAP, etc.). Hydrolysis is the first step in the inorganic polymerization process, silanol group -Si-OH is primarily result of this process (Equation1). Condensation begins with the formation of the first silanol entity, and the two reactions happen at the same time. Condensation occurs in two different ways. The term oxolation is used when two hydroxysilyl groups react together (Equation 2). When a hydroxysilyl group reacts with an alkoxysilyl group, alkoxolation occurs, as shown in (Equation 3).

$$(RO)_3\text{-Si-OR} + H_2O \xrightarrow[\text{-R-OH}]{\text{hydrolysis}} (RO)_3\text{-Si-OH} \quad (1)$$

$$(RO)_3\text{-Si-OH} + (RO)_3\text{-Si-OH} \xrightarrow[\text{-}H_2O]{\text{oxolation}} (RO)_3\text{-Si-O-Si-}(OR)_3 \quad (2)$$

$$(RO)_3\text{-Si-OH} + (RO)_3\text{-Si-OR} \xrightarrow[\text{-R-OH}]{\text{alkoxolation}} (RO)_3\text{-Si-O-Si-}(OR)_3 \quad (3)$$

Successive condensations produce siloxane units (Si-O-Si bonds) and polymeric chains that expand linearly. Furthermore, the silicon atom's tetravalence enables three to four separate partners to be

linked together. These covalent bonds form a three-dimensional network that is stable. As a result, the sol-gel process enables bottom-up network creation by combining relatively small molecular blocks to create a supramolecular matrix. Hydrolysis and condensation reactions take a long time at neutral pH. The hydrolysis and condensation rates as a function of pH were described by Brinker *et al*. (Figure12).[145] Hydrolysis is preferable at both acidic and basic pH levels, while condensation occurs quickly at very low pH, drops sharply at pH 1.5 - 2, and then steadily rises to pH 11-12. The rate of hydrolysis is much faster than condensation under basic conditions (pH more than 12). Depolymerisation occurs and the network collapses.

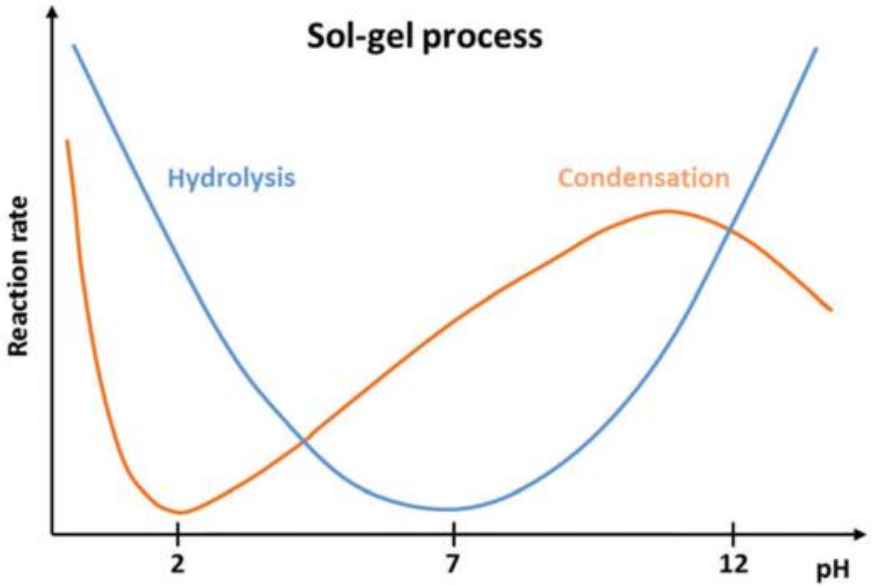


Figure 12: As a function of pH, reaction rates of tetraethyl orthosilicate hydrolysis (blue curve) and condensation (orange curve).[145]

**I.4.1.2.1 Mechanism of hydrolysis**

The sol-gel reaction involves hydrolysis of the metal alkoxide followed by condensation. However, depending on the amount of water and the catalyst present, the hydrolysis may go to complete or stop while it is only partially hydrolyzed. It is also worth noting that silicon alkoxides are less reactive than the corresponding transition metal alkoxides and hence acids or bases are often used as catalysts for promoting the hydrolysis and the subsequent condensation (polymerization) reactions.[145] In the past, various mechanisms for the hydrolysis of Si(OR)4 have been proposed [145, 156] For both acid and base-catalysed reactions (Equations. 4 and 5), a backside

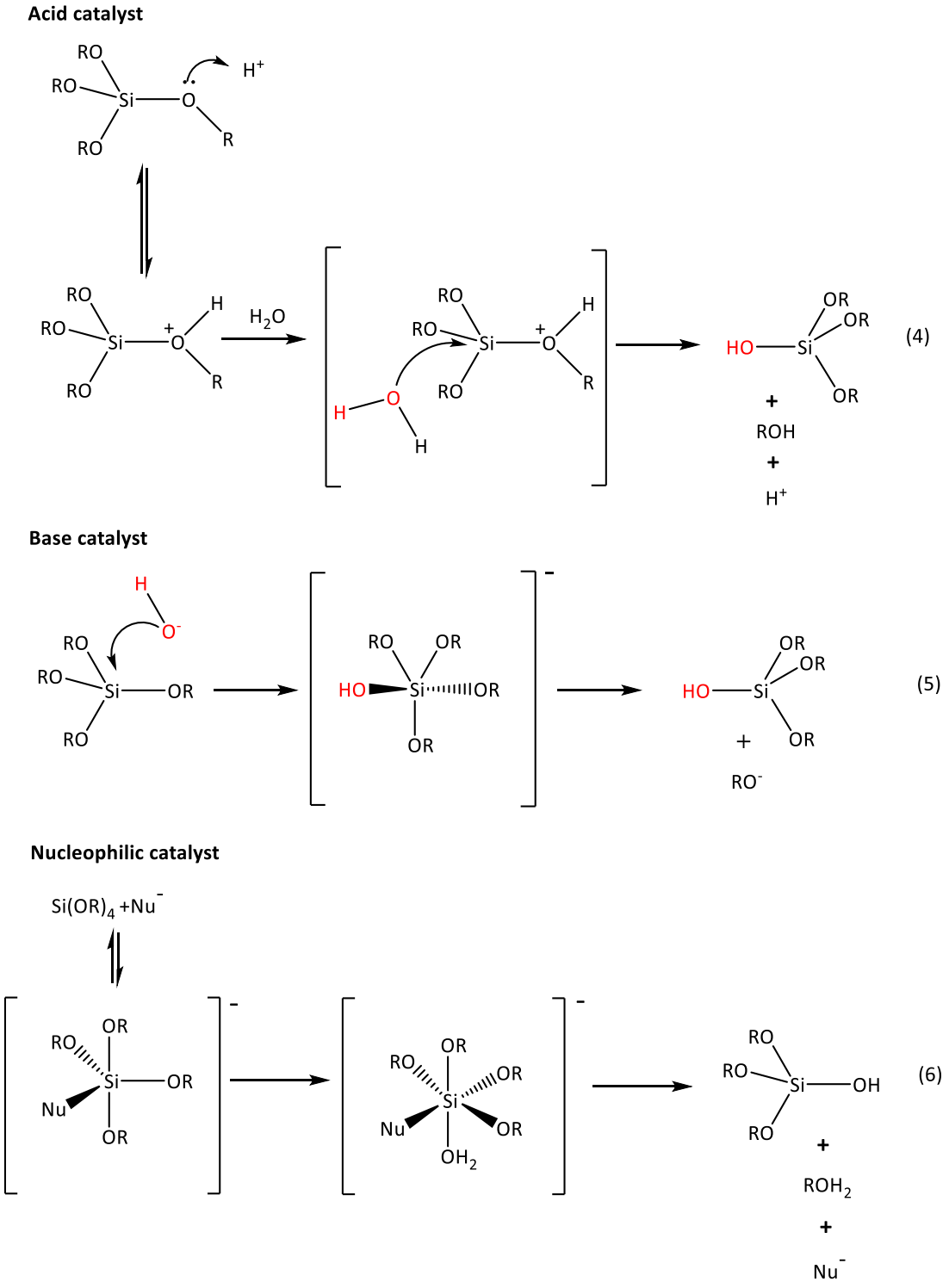


Scheme 2: Mechanism of the acid, basic and nucleophilic hydrolysis of an alkoxysilane.

displacement (with inversion) direction of the form $SN_2$ was suggested.[145] However, under basic conditions, a $SN_2$ mechanism involving a stable pentacoordinate intermediate with two traditional states has been suggested.[157] The following is the suggested mechanism for hydrolysis: In an

acid catalyzed medium, the reaction takes place on the alkoxysilane conjugated acid (Equation 4) while basic catalysts provide better nucleophilic $OH^-$ groups for hydrolysis while deprotonated silanol groups $SiO^-$ enhance condensation rates (Equation 5). Hydrolysis is favoured by acid catalysis so that $Si(OH)_4$ species can be obtained when an excess of water is added [146]. Hydrolysis of alkoxides occurs through a nucleophilic substitution (SN) reaction. When a nucleophile, such as water is introduced to silicon alkoxide a rapid exothermic reaction proceeds. Meanwhile, a nucleophilic catalyst works by extending coordination on the silicon atom, then attacking the penta-coordinated complex with $H_2O$ (Equation 6).[158]

**I.4.1.2.2. Mechanism of condensation**

The sol-gel process is completed by condensation reactions. In an acid catalysed medium, the Si-OH oxygen reacts with either the conjugated acid of an alkoxysilane (heterocondensation) or the conjugated acid of a silanol (homocondensation) (Scheme 3).

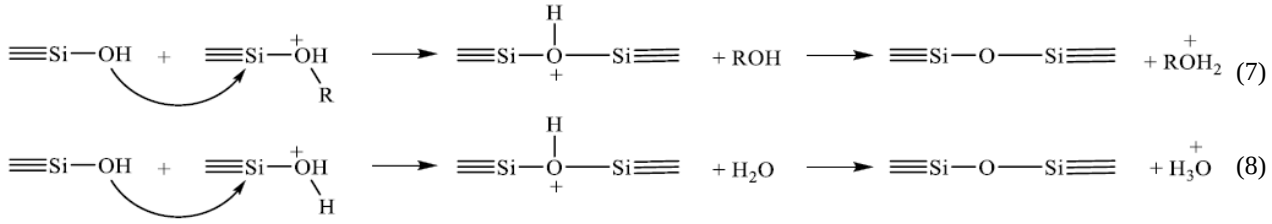


Scheme 3: Mechanism of the acid polycondensation reactions. Equation 7: heterocondensation. Equation 8: homocondensation.

On other hand, in a basic catalyzed medium, a silanolate shaped in (Equation 5) can attack either an alkoxysilane molecule (heterocondensation) or a silanol molecule (homocondensation) to form the bridged siloxanes (Scheme 4).

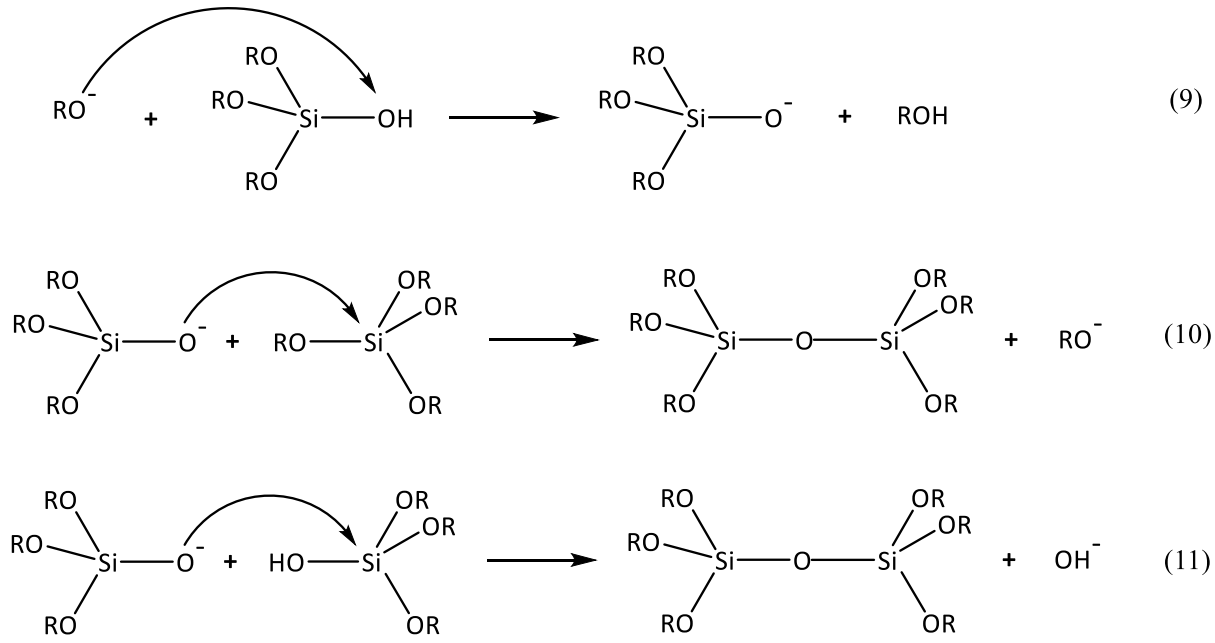


Scheme 4: Mechanism of the basic polycondensation reactions. Equation 10: heterocondensation. Equation 11: homocondensation.

## I.4.1.3. Parameters influence on sol-gel route

The sol-gel route includes various parameters with high effect on the structural and textural properties of the synthesized material. The route is affected by the initial reaction conditions, such as precursors, solvent composition, pH, temperature (drying and aging) and water amount.

### I.4.1.3.1 Type of precursors

Many metals exist as precursors for sol-gel. In general, there are two requirements needed for sol -gel precursors. First, a good solubility in the reaction media is necessary and second reactive enough to participate in the gel formation. Groups like salts, oxides, hydroxides, alkoxides, and acrylates are consist of the most common precursors that can be used.[159] Among these, alkoxides are the most widely used. Metal alkoxides of aluminium, titanium or zirconium are much more reactive towards water than alkoxysilanes due to the lower electronegativity and higher Lewis acidity[160]. The reaction between water and alkoxysilanes is very gentle, preventing phase separation and leading to strong homogeneity. The most common alkoxysilane precursors for sol-gel route are TEOS and TMOS.[160] The concentration and form of silicon alcoxides affect both hydrolysis and condensation levels, thus creating reactive monomers at various rates.[148]

#### I.4.1.3.2 Type of solvent

In the sol-gel route, the solvent plays a significant role. It is used as a reaction medium to dissolve reactive species due to the immiscibility of water and alkoxysilanes. The bulk density of the gels is simply adjusted by altering the precursor concentration in the stock solution. The nature of the solvent used has a strong effect on the kinetics of reactions. It affects the formation reactions of particles and the network by because of its viscosity and its polarity. Polarity describes the potential of polar and nonpolar species to be dissolved, and it can be described using the dipole moment of the molecule. In general, polar solvents such as alcohols are used to dissolve tetrafunctional silicates. [145] Protic solvents with at least one hydrogen atom bonded to an oxygen or nitrogen atom and thus have an acidic character. Furthermore, they facilitate alcoholysis, esterification, and hydrolysis reactions by releasing a proton. An aprotic solvent does not give a proton. It solves the cations very strongly and produces very crowded, reactive anions. While the worst solvents are the non-polar aprotic which do not stabilize the reaction intermediates which poorly solvate the catalysts.

#### I.4.1.3.3 Catalysts and pH

As the kinetics of the reactions of hydrolysis and condensation at room temperature are slow, a catalyst, acidic or basic, is usually added to the solution. The form and proportion of the catalysts significantly affect the structural properties of the gel (Table 3).

Table 3: Influence of the nature of the catalyst on the gel time.[161]

| No. | Catalyst | Initial pH | Gelation time (h) |
|---|---|---|---|
| 1 | HF | 1.90 | 12 |
| 2 | HCl | 0.01<<0.05 | 92 |
| 3 | $HNO_3$ | 0.01<<0.05 | 100 |
| 4 | $H_2SO_4$ | 0.01<<0.05 | 106 |
| 5 | $CH_3COOH$ | 3.70 | 72 |
| 6 | $NH_4OH$ | 9.95 | 107 |
| 7 | No Catalyst | 5.00 | 1000 |

They function on the kinetics of gelation, and thus on the gel texture.[135] They enforce the pH and provide a counter-ion that activates the silicon more or less. The hydrolysis solution's pH helps facilitate either hydrolysis or condensation.

The mechanisms and kinetics of chemical reactions depend on the pH and the nature of the species (organic or inorganic) in solution. Its role is twofold: to control reaction kinetics and increase soil stability and thus control the architecture of the final material. In basic catalysis, the hydrolysis reactions are very rapid. Much more reactive, the hydroxide ion replaces water as the nucleophilic agent.[145] The hydrolysis of the precursor molecules is therefore complete even before the polycondensation reactions start. The species are then ordered into colloidal particles. In acid catalysis, an alcoholate group is easily protonated. The electron density of the center metallic is reduced which makes it more electrophilic. The protonation thus increases the nucleofuge character of the leaving group. The proton transfer between the incoming group and the leaving group is no longer necessary and therefore the reaction occurs more easily. Hydrolysis of the first precursor molecule is faster than the following ones. Thus, polycondensation will gradually work until a linear branched molecular structure is obtained. Catalysts independent of pH by nucleophilic attack, for example using $F^-$ ions, are possible.[145] The reaction rates are higher in basic medium than in an acidic medium, which increases the kinetics of the sol-gel transition .[145] The average pores of the gels obtained in this basic route are generally larger than in an acidic medium, the materials obtained in acid path will then be denser. In conclusion, the type of gel (polymeric or colloidal) and the porosity of the final material are essentially governed by the pH of the solution. During soil deposition, acid catalysis can produce dense coatings which will be so especially since the branching chains line up. Soils in basic catalysis form networks of particles which generally produce thicker coatings but also more porous. In addition, a combination of acid (cluster-cluster) and basic (monomer cluster) catalysis promotes the formation of random cross-linked aggregates, which tend to form very porous coatings when the sol is deposited on a substrate.[145]

#### I.4.1.3.4. Effect of temperature

Hydrolysis and condensation reactions are also influenced by temperature.[162] At all stages of gelation, raising the temperature accelerates these reactions, from soil preparation to drying. As a result, by altering a physical parameter (temperature), it is possible to slow down or speed up the forming of the gel and not to use chemical devices slowing or speed up the setting of the gel.

#### I.2.2.3.5. Effect of water

The kinetics and final structure of the gels obtained are also influenced by the addition of water to the organic solvent. Depending on how acidic or basic the medium is, water plays various functions.[163] The mechanisms of first-order hydrolysis reactions are affected by the water concentration in acidic conditions, while in a basic medium, water does not participate in the mechanisms, and the rate of reaction is of zero order. Studies have confirmed that kinetics of the sol-gel phase under acid catalysis are affected by the water concentration.[164] They also confirmed that the structures changed based on the amount of water present. Thus, low water concentrations ($H_2O$/TEOS < 2) favour the formation of a linear network structure, while high concentrations ($H_2O$/TEOS > 2) rather favour the formation of branched and cross-linked structure.[146] Brunet investigated the formation of different species during hydrolysis and condensation using high-resolution $^{29}$Si NMR, in particular by varying the w= $H_2O$/Si ratio at constant pH.[165] So, at pH = 3, he demonstrated that hydrolysis was extremely difficult for w = 0.5, and no entirely hydrolysed species could be seen, while start to appear when w > 1 is used. He also showed that in the presence of excess water (w = 8) hydrolysis is fast and complete, while condensation, is a slower and more difficult process.

## I.4.2. Non-hydrolytic sol-gel route (NHSG)

A process of sol-gel is called non-hydrolytic (NH) if the oxygen donor used is not water and if no water is produced during synthesis. Many NHSG routes involving different precursors (chlorides, alkoxides, acetylacetonates, etc.) with different oxygen donors (alkoxides, ethers, alcohol, acetate, aldehydes , ketones, etc.) have been identified over the last 2 decades.[149, 166] It is possible to distinguish NHSG routes according to either the existence of the oxygen donor (ether, alcohol, alcohol, etc.), the metal precursor (alkoxide, halide, acetylacetonate, etc.) or the removed dominant molecule (alkyl halide, ether, ester, etc.). There was high interest in the preparation of catalytic materials in either the ether and alkoxide routes based on the reaction of chloride precursors to ether or alkoxide. The main reactions involved in the NHSG ether and alkoxide routes, which are most widely used for mixed oxide catalyst synthesis, are shown in (Figure 13).

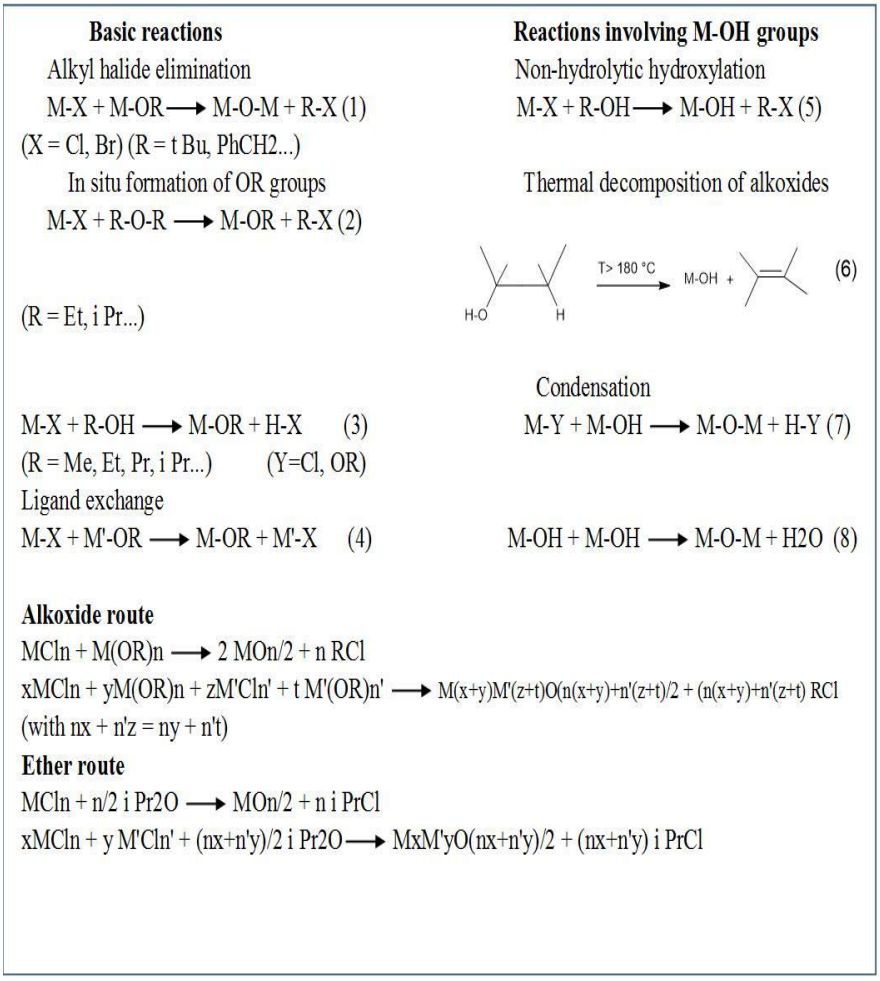


Figure 13: Main reactions involved in the NHSG process based on the reaction of halide precursors with alkoxide, ether or alcohol oxygen donors, and overall ideal reaction schemes for the synthesis of oxides and mixed oxides by the alkoxide and ether sol-gel routes.[167]

These routes are based on condensation with the removal of an alkyl chloride between a metal chloride and a metal alkoxide (Figure 13, reaction 1). It was highlighted in 1951 by Gerrard *et.al* [168] and generalized for the first time by the French group headed by Corriu, Vioux and Mutin in sol-gel in the early 1990s.[169] For metals and transition metals, this reaction takes place between 80 and 150 °C even with simple primary or secondary R groups. In the case of silicone, the reactivity is very limited, so it is important to use tert-butyl or benzyl R groups [169] or to add a Lewis acid catalyst ($AlCl_3$, $FeCl_3$).[170] In all cases, the first reaction that occurs when precursors of chloride and alkoxide are combined is the exchange (or redistribution) of ligands Cl and OR (Figure 13, reaction 4),[171] leading to a mixture of chloroalkoxides $M(OR)_xCl_y$, which are therefore the true precursors of these NHSG routes. The formation of M-O-M bonds results from a nucleophilic attack on the alpha-carbon of the oxygen atom of an alkoxide group by a chlorine

atom. Alkyl chloride removal and formation of the oxo bridge resulting from the C-O break (Scheme 5). Thus, the condensation reactions are encouraged by all the effects that favor the formation or stabilization of the R+ carbocation and the attack of chlorine on the carbon.

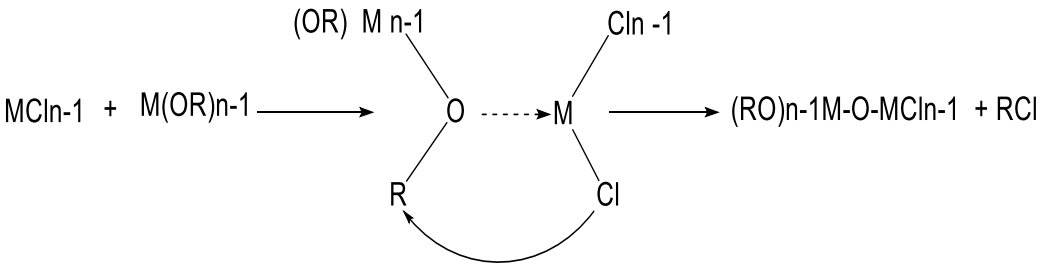


Scheme 5: Condensation reaction of both ether and alkoxide routes.

## I.4.2.1 Main reactions

### I.4.2.1.1. Alkyl halide elimination

NHSG method is a reaction between metal chloride and metal alkoxide (Equation 1). Condensation and formation of the M-O-M bond leads to inorganic oxides, while volatile alkylchlorides are released as organic reaction products. The elimination of alkyl halide is a significant one-step process that gives us highly porous (mixed) metal oxides. Usually, the homogeneity of mixing at the atomic level is very high. The homogeneity of mixing at the atomic level is usually very high. Through metal chloride reaction with ether (Equation 2) or primary / secondary alcohols (equation 3), the metal alkoxide group can be formed in situ. In this way, there are three subtypes of alkyl halide elimination reactions recognized by the oxygen donor used: alkoxide, ether or alcohol.[149]

$$M\text{-}Cl + R\text{-}O\text{-}M \longrightarrow M\text{-}O\text{-}M + RCl \qquad (1)$$

$$M\text{-}Cl + R\text{-}O\text{-}R \longrightarrow M\text{-}O\text{-}R + RCl \qquad (2)$$

$$M\text{-}Cl + ROH \longrightarrow M\text{-}O\text{-}R + HCl \qquad (3)$$

Reactions of chlorosilanes with dimethylsulfoxide (DMSO) display a small branch of alkyl halide elimination. DMSO plays here as an oxygen source. The reaction between DMSO and metal chlorides is very slow can therefore be well regulated, and offers interesting products such as cage

siloxanes.[172] The reactivity of tertiary alcohols and benzyl alcohol toward the metal chlorides contrasts from primary and secondary alcohols. This reaction prompts to the formation of M-OH groups and benzyl chloride (Equation 4). Therefore, hydroxyl groups condense with M-Cl groups (Equation 5) and form inorganic oxides. In this situation, reactions of metal chlorides with benzyl alcohol at temperatures between 180 and 250 °C have been shown to give nanoparticles of crystalline metal oxide (compared with amorphous and porous products in the previous case). This process developed rapidly into the well-known method of benzyl alcohol, and other compounds (alkoxides, acetylacetonates, and acetates) were soon distinguished as acceptable metal oxide precursors. It provides monodisperse nanoparticles without any added surfactant. Benzyl alcohol acts efficiently as a solvent, source of oxygen and capping agent.[173]

$$M\text{-}Cl + C_6H_5CH_2OH \longrightarrow M\text{-}OH + C_6H_5CH_2Cl \qquad (4)$$

$$M\text{-}OH + Cl\text{-}M \longrightarrow M\text{-}O\text{-}M + HCl \qquad (5)$$

**I.4.2.1.2. Thermal decomposition**

In the previous NH method (alkoxide, ether or alcohols), the complexity of the reaction pathways increases with the reaction temperature. It is not surprising that precursors, intermediate compounds and oxide products can play a role as catalysts in various reactions, such as polymerization, oxidation, or thermal decomposition of the precursors. For example, alkoxide precursors usually break down over 250-300 °C by alkene elimination and formation of hydroxyl groups, which at that point condense with other alkoxide groups to form oxo-bridges with the elimination of alcohol. The hydroxyl groups can condense with each other as well, leading to water formation; however, as long as kinetics have prevented M-OH self-condensation, these thermal decomposition reactions can be regarded as NH. Along these lines, a few NH routes based on the rapid thermal decomposition of different precursors (alkoxides, acetates, acetylacetonates, chlorides, etc.) at relatively high temperatures have been proposed, especially for the preparation of nanoparticles. These reactions are usually carried out in hot surfactant solutions (trioctylphosphine oxide, oleic acid, oleylamine, etc.), providing nanoparticles with size and shape

control.[174] The tri(tert-butoxy siloxy) derivative $M(OR)n(OSi(OtBu)_3)n'$ decomposes at relatively mild temperatures (100-180 °C) and has been used to prepare mixed metal oxides by thermolysis.[175] They have also been utilized for grafting isolated catalytic species at the surface of silica supports.[176]

**I.4.2.1.3. Ester elimination**

The condensation between metal carboxylates $M(OCOR)_x$ and metal alkoxides $M(OR^1)_y$ (Equation 6) leads directly to the formation of oxo bridges in nonpolar, aprotic solvents and has been proposed as a general sol-gel route to (mixed) metal oxides.[177]

$$M\text{-}OCOR^2 + M\text{-}OR^1 \longrightarrow M\text{-}O\text{-}M + R^2COOR^1 \qquad (6)$$

Alkoxide precursor reactions with carboxylic acids are not completely NH, as water is most likely generated in situ by reaction of the acid with alcohol formed in a first step by the exchange of carboxylate and alkoxy groups (Equations 7 and 8).

$$M(OR^1)n + R^2COOH \longrightarrow M(OR^1)_{n-1}(OCOR^2) + R^1OH \qquad (7)$$

$$R^1OH + R^2COOH \longrightarrow R^1OCOR^2 + H_2O \qquad (8)$$

Nevertheless, formic acid[178] or acetic acid[179] was effectively utilized for the synthesis of silica or hybrid materials. Hyeon *et al.* used the reaction between titanium tetraisopropoxide and oleic acid at 270 °C to produce $TiO_2$ nanorods in multi-gram amounts.[180] For sol-gel synthesis in uncommon media, the reaction of alkoxide precursors with carboxylic acids is particularly important, for example, perfluoro solvents,[178] ionic liquids,[181] or supercritical CO ($scCO_2$).[182] In comparision, the reaction of metal or silicon alkoxides with an acid anhydride (Equation 9) leads to the in situ formation of carboxylate groups, which can then condense with alkoxide groups (Equation 6), providing a completely NH (and hydroxyl-free) sol-gel route.

$$M(OR^1)_n + (R^2CO)_2O \longrightarrow M(OR^1)_{n\_1}(OCOR^2) + R^2COOR^1 \qquad (9)$$

This anhydride route was successfully used to prepare titania (in the presence of $TiCl_4$ catalyst),[183] silica-titania mixed oxides[184] and titania photocatalysts.[185]

## I.4.3. Characteristics of NHSG method

NHSG routes illustrate entirely different reactions and reaction conditions compared to classical hydrolytic sol-gel routes, which greatly affect the surface chemistry, homogeneity and texture of the resulting oxide materials.

### I.4.3.1. Chemistry of surface

Because of alkoxide, ether and anhydride routes do not include the formation of hydroxyl groups. Therefore, in the absence of secondary reactions and before calcination or exposure to ambient air, the residual surface groups are chloride, alkoxide or acetoxy groups but not hydroxyl groups. For instance, silica-based and metal oxide nanoparticles terminated by chloride and isopropoxide groups were obtained recently utilizing the ether route; their surface chemistry makes these nanoparticles organically soluble in the absence of surfactants and reactive toward water, alcohols or hydroxylated surfaces.[186] The hydroxyl content is much lower even in the alcohol route than in traditional sol-gel.[187] The surface of the nanoparticles in the benzyl alcohol route tends to be capped by adsorbed benzyl alcohol molecules that avoid the agglomeration of the particles and make them organosoluble.[188]

### I.4.3.2. The medium of reaction

The first characteristic of NHSG routes is that they occur in a non-water medium, ideally anhydrous. NHSG syntheses can be performed either in an organic solvent or in the oxygen donor itself (e.g. benzyl alcohol), and in some cases without of solvent (e.g. when the precursors are liquids as in the case of silicon and titanium alkoxides and chlorides).

### I.4.3.3. Kinetic of reaction

As a rule, non-hydrolytic reactions include effectively controllable kinetics. Thus, there is no need to use reactivity modifiers or elaborated procedures to avoid the formation of precipitates even in the case of metal oxides. The reaction rates around various metal precursors seem significantly less sensitive to the nature of the metal, which encourages the preparation of homogeneous mixed metal

oxide systems[189] and metastable phases.[190] Although the reactions around silicon have a tendency to be too slow, their rate can be simply increased using a Lewis acid catalyst. This is particularly important in the preparation of silicates $SiO_2$-$MO_n$ (M= Al, Ti, Zr, etc.). In this situation, the metal species efficiently catalyze the reactions around silicon, leading to a leveling of the reaction rates of silicon and metal precursors. Therefore, NH condensation routes are especially interesting for the preparation of homogeneous silicates $SiO_2$-$MO_n$. Microwave heating offers interesting perspectives for the control of NH reactions kinetics, especially for the preparation of nanoparticles. Microwave chemistry is broadly used in organic synthesis.[191] Despite the fact that there are significantly fewer examples in materials synthesis, the use of microwaves in the synthesis of materials is gaining importance and a wide variety of materials and nanomaterials were prepared using microwave heating, including carbides, nitrides, oxides, chalcogenides, phosphates and metals.[192] Microwave-assisted synthesis is generally considered much faster, cleaner, and more economical than the conventional methods.[193] Recently, Niederberger *et al.* have applied microwave heating to the NH synthesis of highly crystalline NP using benzyl alcohol route.[194] Microwave irradiation significantly accelerates nanoparticle production, by increasing the rate constants for the condensation rate and the crystal growth.

# I.5. Control of structure and morphology

One important result of the moderate reaction rates in NH syntheses is the formation of well-crystallized metal oxides at temperatures lower than that used in aqueous or solvothermal methods. Moreover, the versatility of NHSG offers a few possibilities for controlling the crystal structure. For example, in the preparation of titania at 110 °C from $TiCl_4$ and different oxygen donors, Arnal *et al*. reported that the crystalline form depended on the nature of the oxygen donor. Whereas $Ti(O^iPr)_4$, $^iPr_2O$, or $^i$PrOH led at 110 °C (and after calcination at 500 °C) exclusively to the formation of anatase, EtOH led to the formation of rutile, and $^t$BuOH led to a mixture of brookite and rutile.[183] The high, molecular scale, homogeneity in NH mixed oxides permits the formation at low temperature of metastable phases on annealing, as shown in the case of b-$Al_2TiO_5$,[195] trigonal $ZrW_2O_8$,[196] and monoclinic $Ga_2Mo_3O_{12}$.[197]

Portehault *et al.* recently reported the first NHSG example of lamellar titanates intercalated by (TMA) ions.[198] The synthesis is based on the reaction at 220 °C of $TiCl_4$ with (triglyme) as an oxygen donor, in the presence of $Me_3N$-$BH_3$ (or $Me_2NH$-$BH_3$) complex. $BH_3$ is Lewis acid and

acts as an amine-sequester, avoiding the formation of a $TiCl_4$-amine adduct. The formation of the titanium-oxo species, as well as the in situ formation of the TMA was rationalized based on the analysis of the organic byproducts. The texture of the final material probably tuned by the addition of bulkier trialkylamines, which were not intercalated but apparently stabilized the basal (0 1 0) faces. In the case of nanocrystals, both the structure and morphology of the particles strongly depend on the synthesis parameters. The adsorption of organic species to the surface plays a major part. These organic species can either be surfactants added in the synthesis[174] or, in surfactant-free routes, the organic solvent and/or the oxygen donor (or species formed during the reaction).[199] As a result, crystalline nanoparticles with an impressive variety of sizes and shapes (platelets, spheres, rods, multipods) were prepared by NH routes, as detailed in former review articles.[200]

# I.6. Classification of (NHSG) routes

## I.6.1. Ether and alkoxide routes

In ether route, the formation of oxo bridges requires, in a first step, the formation in situ of alkoxide groups (Figure 12, reaction 2), by reaction of chloride groups with an organic ether (usually diisopropyl ether $^{i}Pr_2O$), which reacts in a second step with the chloride groups. The alkoxide and ether routes based on the removal of an alkyl chloride are recognized as being particularly effective for the synthesis of mesoporous mixed oxides, with a control of homogeneity and texture.[201, 202] The benefit of the ether route is that it requires only chlorides as metallic precursors, as compared with metal alkoxides for instance. The main disadvantage of some solid metal chlorides is their low solubility in the organic medium. However, depending on the case, soluble intermediate $M(OR)_xCl_y$ species may be formed at room temperature or during heating of the mixture of the chloride precursors and the oxygen donor. For example, $AlCl_3$ is insoluble in $CH_2Cl_2$ but after addition of $^{i}Pr_2O$ there is a very rapid formation of soluble $Al(O^{i}Pr)_{3-x}Cl_x$ species. The structure of the trimeric $Al_3Cl_5(O^{i}Pr)_4$ chloroalkoxide species is shown in (Figure 14).[203]

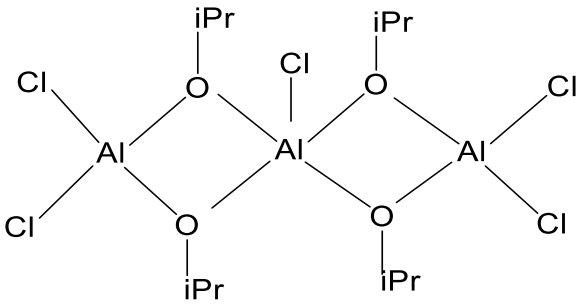


Figure 14: Structure of an aluminum chloroisopropoxide with a pentacoordinated Al atom.[203]

The use of various reactions and synthesis media (compared to the HSG) has an extensive impact on the structure, texture and surface properties of oxides obtained by NHSG. For metal precursors, the rate of the reactions 1 and 2 (Figure 13) are moderate and can be effectively controlled by shifting the temperature. To achieve maximum condensation, it is important to have an equal number of Cl and R groups (from M(OR)n or ROR) as shown in equations corresponding to the synthesis of oxides and mixed oxides by the alkoxide and ether (Figure 13). The main characteristic of the NHSG is that the syntheses are carried out in an anhydrous medium. The syntheses are carried out with or without an organic solvent, (e.g. when chloride precursors or alkoxides are liquids). In the case of the alkoxide and ether routes, the reactions do not lead to the formation of hydroxyl groups. Thus, in the absence of secondary reactions and before calcination or presentation to surrounding air, the residual surface groups are chlorides and alkoxides. The reaction rates around the various metal precursors seem less sensitive to the nature of the metal, which facilitates the preparation of homogeneous mixed metal oxides [204] and metastable phases.[197] The reactions around the silicon are much slower, but their speed can be expanded by the addition of a Lewis acid catalyst. In the case of the preparation of mixed oxides $SiO_2$ -$MO_n$ (M = Ti, Zr, Al, etc.), the metal species catalyze the reaction around the silicon, prompting a leveling of the reaction rates around the silicon precursors and the metallic precursors. Hence, NH condensations make it possible to synthesize very homogeneous silicates $SiO_2$-$MO_n$. The NH syntheses have the benefit of having moderate reaction rates, which makes it conceivable to get well-crystallized metal oxides at lower temperatures than those utilized in aqueous or solvothermal methods. By changing the oxygen donor, it is possible to obtain different crystal structures of the oxides. For example, Arnal *et al*.[205] demonstrated that the reaction of $TiCl_4$ with different oxygen donors led to anatase formation after calcination at 500 °C when the oxygen donors were Ti $(OiPr)_4$, $^{i}Pr_2O$ or $^{i}PrOH$,

rutile with EtOH or a mixture of brookite and rutile with $^{t}$BuOH. As mentioned in the introduction, the problem in HSG is the collapse of the network when the gel is dried by evaporation. The NHSG helps to solve this problem and leads to materials with large specific surfaces, high porous volumes with disordered pores in the absence of structuring agents and without supercritical drying. This characteristic is ascribed to the high degree of condensation leading to a high mechanical strength of the NH gels, and also to the reduction of the capillary forces due to: (1) weak interactions between the surface (terminated by chlorides or alkoxide groups) and the liquid phase ($CH_2Cl_2$, $^{i}$PrCl) and to (2) the low surface tension of the liquid phase compared to the water used in HSG. Some groups have also prepared materials with ordered mesopores using surfactants.[206] As in HSG, the first template is the liquid phase composed of the solvent and the reaction products caught in the gel. The pores come from the elimination of this liquid phase. The porosity of xerogels prepared by NHSG depends on the synthetic parameters.[207] For example, the porosity of amorphous $SiO_2$-$TiO_2$ xerogels synthesized by the ether or alkoxide route depends on the volume of the liquid phase and the degree of condensation of the gel, allowing texture control simply by changing solvent volume, time or the reaction temperature (Figure 16).[208]

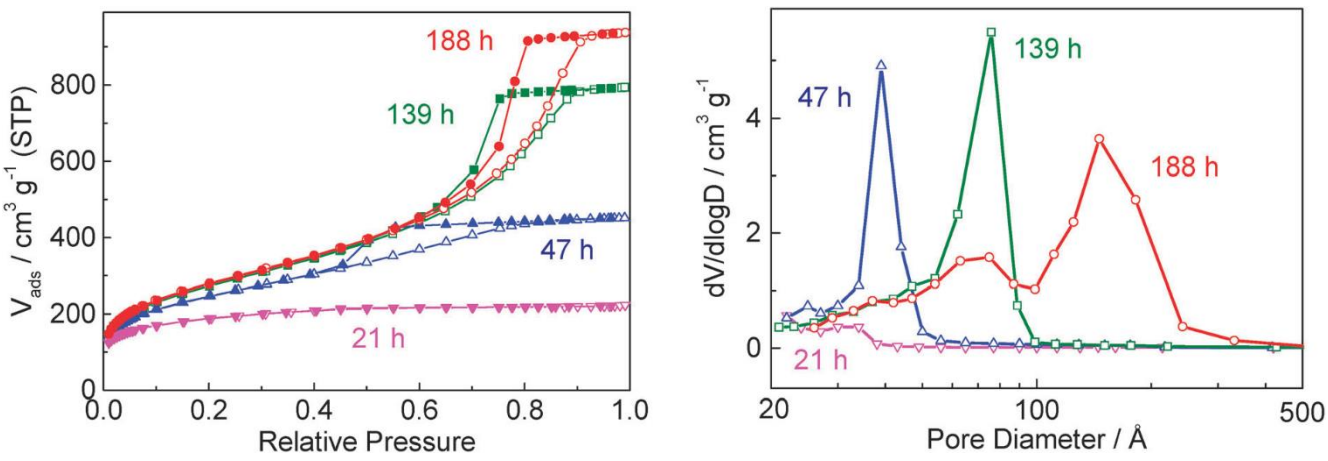


Figure 15: $N_2$ physisorption isotherms at -196 °C (left) and corresponding pore size distributions (right) of Si-Ti xerogels (Si/Ti = 10) prepared *via* the ether route at 110 °C with different reaction times.[208]

During the aging step, the specific surface area increases, indicating that dissolution-precipitation phenomena remain marginal in NHSG, in contrast to HSG, where aging of silica gels at high temperatures leads to an increase in pore size and a decrease in the specific surface area.[209] After these promising results, Cojocariu *et al.*[210] described the ether synthesis of $TiO_2$-$SiO_2$ catalysts

with remarkable textures. The gel was obtained by reacting $SiCl_4$, $TiCl_4$ and $^iPr_2O$ in the presence of $CH_2Cl_2$ in teflon autoclaves at 150 °C for 4 days. After drying by evaporation and calcination at 500 °C for 5 hours, the specific surface area and the pore volume (1215 $m^2\ g^{-1}$ and 2.4 $cm^3\ g^{-1}$) are much greater than those reported for calcined $TiO_2$-$SiO_2$ aerogels.[211] As long as the chloride precursors are soluble in the reaction mixture, the ether route gives a simple, one-step method to prepare mesoporous mixed oxide xerogels with interesting textures, beginning from cheap chloride precursors and avoiding utilization of any reactivity modifier, templating agent or supercritical drying step. Else, when the chloride precursors are not soluble in the reaction mixture, the alkoxide route may be helpful.[212] The influence of calcination on the surface composition of the mixed oxides is related to the value of Tammann temperature to the active metal oxide.[213] When the Tammann temperature of active metal oxide component is low (e.g. VOx, MoOx, ReOx, WOx, AgOx), suitable thermal treatments can bring about the migration of active species toward the surface, leading to an increase of their surface concentration. For example, mesoporous $ReO_3$-$SiO_2$-$Al_2O_3$ catalysts obtained by the ether route.[214] Migration of rhenium oxide species toward the surface occurred during calcination at 500 °C, as evidenced by XPS and ToF-SIMS. The resulting high concentration of well-dispersed $ReO_x$ surface species together with the high specific surface area and the acidity of the catalysts accounted for their excellent performances in the metathesis of ethene and butene to propene. Recently, the ether route was shown to be suitable for the synthesis of amorphous silica-based nanoparticles ($SiO_2$, $SiO_2$-$TiO_2$)[149] as well as crystalline metal oxide nanoparticles ($TiO_2$, $SnO_2$).[215] The syntheses were performed in dilute $CH_2Cl_2$ solutions, using a stoichiometric amount of $^iPr_2O$, at mild temperatures (80-150 °C) and in the absence of any surfactant or coordinating solvent. The ether alkoxide routes have been utilized for the preparation of a wide assortment of metal oxides. They have demonstrated especially helpful for the synthesis of mixed oxides with an amazing control over their homogeneity and their texture.[216] They also gave basic and powerful syntheses of oxide nanoparticles, with or without capping agents.[217]

## I.6.2. Alcohol route

The reaction between a chloride precursor and an alcohol oxygen donor is related to the ether and alkoxide routes. Primary and secondary alcohols lead to the in situ formation of alkoxide groups

(equation10), which can condense in a second step with chloride groups according to (Equation11) as in the ether and alkoxide routes.

$$M\text{-}Cl + R\text{-}OH \longrightarrow M\text{-}OR + H\text{-}Cl \quad (10)$$

$$M\text{-}Cl + M\text{-}OR \longrightarrow M\text{-}OM + R\text{-}Cl \quad (11)$$

However, tertiary and benzylic alcohols can lead to the in situ formation of hydroxyl groups (Equation12), which react in the second step with chloride groups as indicated by (Equation13).[169]

$$M\text{-}Cl + R\text{-}OH \longrightarrow M\text{-}OH + R\text{-}Cl \quad (12)$$

$$M\text{-}Cl + M\text{-}OH \longrightarrow M\text{-}OM + H\text{-}Cl \quad (13)$$

The alcohol route for the preparation of oxides and mixed oxides has been much less examined than the alkoxide and the ether routes. Orsini *et al*.[213] showed that it was possible to modify the texture of tungsten oxides (phases α-$WO_3$ and β-$W_{20}O_{58}$) obtained by reaction of $WCl_6$ and an alcohol by acting on the 1-butanol / *tert*-butanol ratio and on the calcination temperature. The benzyl alcohol route which includes the reaction of chloride precursors at 40-175 °C with benzyl alcohol which is used as a solvent, oxygen donor and capping agent at the same time , has shown highly successful for the synthesis of crystalline oxide nanoparticles.[199] The benzyl alcohol route has been later extended to other precursors, such as metal alkoxides or acetylacetonates. Higher temperatures (between 200 and 250 °C) are then required. The reactions involved depend on the nature of the precursor and can involve the elimination of dibenzylether or complicated C-C bond formation reactions with the elimination of 4-phenyl-2-butanol or 1,2-diphenylethanol for example.[218]

## I.6.3. Benzyl alcohol route

The benzyl alcohol route developed by Niederberger *et al.* represents a versatile surfactant-free NH reaction system giving rise to numerous metal oxide nanoparticles and oxide-based inorganic-

organic nanohybrids.[173, 219] Metal precursors like chlorides, alkoxides or acetylacetonates readily react with benzyl alcohol and subsequently produce the corresponding oxide or mixed oxide nanoparticles. Depending on the precursor utilized, the reaction mechanism is proposed as an alkyl halide or ether elimination. Recently, it was appeared for the preparation of $GeO_2$ NPs that hydrolysis must be considered as a potential pathway as well because water could be formed in situ.[220] The reaction parameters include solvothermal treatment (e.g., 180-250 °C in the case of metal alkoxides). If the reactions are carried out in the presence of alkaline species, metal alkoxides react with benzyl alcohol by means of a C-C coupling mechanism.[221] This mechanism was described in the case of the non-aqueous formation of $BaTiO_3$ and $SrTiO_3$. Benzyl alcohol, the organic solvent, also acts as a surfactant and provides the control of the nanoparticle shape, morphology and size distribution. In any case, the nature of precursor is important as well. For instance, the reaction of niobium ethoxide in benzyl alcohol gives orthorhombic $Nb_2O_5$ particles with platelet-like morphologies and sizes ranging from (50 to 80 nm) while the reaction of $NbCl_5$ in benzyl alcohol led to small, slightly agglomerated crystallites of just a few nanometers.[222] An interesting reaction was reported when yttrium isopropoxide was used as a precursor. The reaction with benzyl alcohol leads to a lamellar nanohybrid consisting of crystalline yttrium oxide layers with intercalated benzoate molecules.[223] Thus, it was shown in numerous studies on the benzyl alcohol route that by choosing the appropriate reaction system, it is possible to gain control over the nanocrystal parameters. Based on the development of new reaction techniques, the benzyl alcohol route was stretched out with the utilization of microwave reactor, which decreased the reaction times significantly and enabled scale-up of the syntheses to multi-gram quantities.[224] An interesting study announced by Bilecka *et al*. concentrated on the microwave helped synthesis and kinetic analyses of ZnO nanoparticles from zinc acetate in benzyl alcohol. Contrasted with conventional heating, the microwave-assisted route highly accelerated the formation of nanoparticles by: (1) simplifying the dissolution of a precursor in the solvent; (2) increasing the rate of the esterification reaction, resulting in faster production of monomer and consequently earlier nucleation; and (3) increasing the rate of crystal growth from 3.9 $nm^3.min^{-1}$ (conventional heating) to 15.4 $nm^3.min^{-1}$ (microwave heating) (Figure 16).

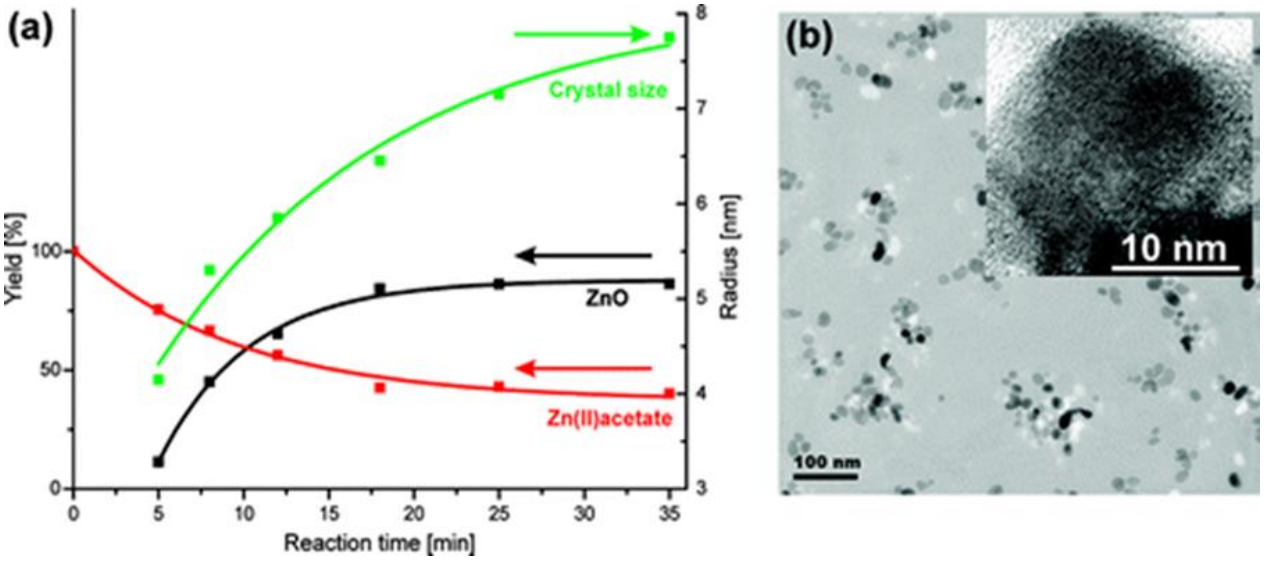


Figure 16: (a) Time-dependent evolution of the crystal size (green curve), yield of ZnO powder (black curve), and zinc acetate concentration (red curve) at 120 °C, (b) TEM overview image of ZnO nanoparticles obtained at 120 °C after 3 min (inset: (HRTEM) image of one particle).[225]

A mechanism of ZnO nanoparticle formation was proposed based on the results of the work. The esterification reaction produces monomers most probably in the form of Zn-hydroxo species. Once the monomer concentration achieves supersaturation, ZnO clusters form. The microwave helped benzyl alcohol route has additionally been utilized for the preparation of ZnO doped with an assortment of metals, such as Ni, Co, Fe, Mn, and V.[226] ZnO-based magnetic semiconductor nanocrystals with high concentrations of dopants were synthesized by this strategy. For instance, homogeneous distributions of Cobalt in $Co_xZn_{1-x}O$ were achieved up to x = 0.2. Higher loadings of cobalt resulted in the separation of $Co_3O_4$ phase. Room temperature ferromagnetic behavior was seen in the case of Fe doped ZnO. Other interesting work from the Niederberger group describes benzyl alcohol based microwave helped synthesis of monodispersed Sb-doped $SnO_2$ nanocrystals and their application as transparent electrodes in thin film optoelectronic devices.[227] Microwave helped synthesis in benzyl alcohol was additionally observed to be an efficient method for the preparation of metallophosphates. Bilecka *et al*.[228] got highly crystalline, well defined $LiFePO_4$ and $LiMnPO_4$ mesocrystals with sizes of (50 and 200 nm), respectively. The precursor solution for $LiFePO_4$ was synthesized by the addition of $H_3PO_4$ to a mixture of lithium chloride and iron (II) acetate in benzyl alcohol. For $LiMnPO_4$ preparation, $H_3PO_4$ was combined with a solution of manganese (II) acetylacetonate and lithium ethoxide. The reactions were done at 180 °C for 3 min with the microwave reactor frequency operating at 2.45 GHz. This work was followed by a study concentrated on the doping $LiFePO_4$ with Ni, Mn, Zn, Al, and Ti.[229] The incorporation of various

dopants in the $LiFePO_4$ lattice in different concentrations allowed modification of the specific charge capacities and achieved the desired characteristics for application in Li-ion batteries. In comparison to undoped $LiFePO_4$ prepared by the same synthetic approach, the doped powders showed significantly better electrochemical performance.

The polyol microwave helped synthesis of $TiO_2$ under NH conditions was developed in the group of Morselli due to its similarity to benzyl alcohol route (polyethylene glycol is utilized as a high-boiling solvent, surfactant, and oxygen source).[230] This innovative approach uses $TiCl_4$ as a precursor. The reactions were performed in sealed tubes and heated at 170 °C for 25 min under microwave irradiation. According to XRD analysis, all samples are composed of pure anatase NPs and are well dispersed due to the residual PEG chains bonded to the nanoparticle surface, which prevent them from aggregating. Oleyl alcohol works similar to benzyl alcohol and polyethylene glycol and has also been used for the preparation of metal oxide nanoparticles.[231]

## I.6.4. Carboxylic acid route

The carboxylic acid route was first announced by Sharp in 1994.[232] He prepared silica gels from tetramethoxysilane and formic acid. In recent days, this non-aqueous method has been applied to sol-gel processing in ionic liquids.[233] It has been found to be more suitable to produce crack-free ionogel monoliths from silicon alkoxide precursors and ionic liquids containing the bis(tri-fluoromethylsulfonyl)-imide anion than the classical hydrolytic route.[217] These ionogels are utilized as temperature-resistant electrolytes in electrochemical gadgets for their generally low viscosity and attendant high ionic mobility (Figure 17).

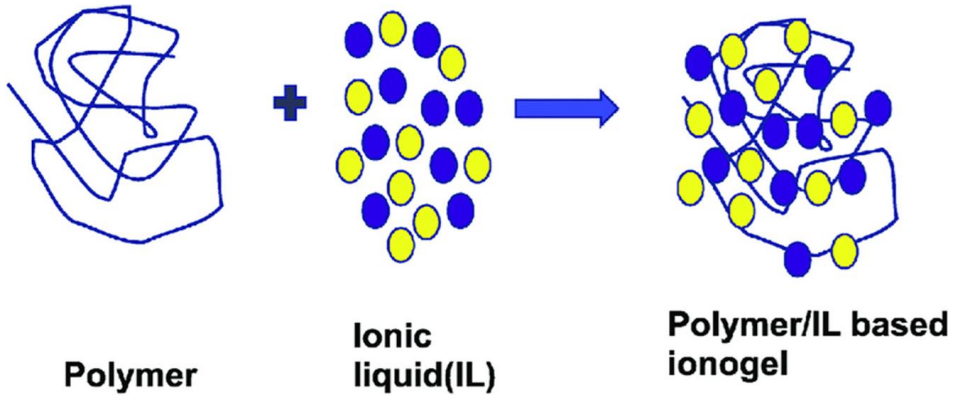


Figure 17: Polymer based ionogels.[234]

By using formulations with higher ionic liquid contents, “wet solid-like” ionogels were obtained, which showed superior ionic conductivity and double-layer capacitance.[199] Their insignificant volume loss and compliant mechanical character (flexible modulus of ca. 5 KPa) make them appropriate for the in situ manufacture of devices with flexible energy storage, including thin film electrochemical double layer capacitors. The surface reaction of metal alkoxide precursors and carboxylic acids (as oxygen donors) has been applied to the synthesis of metal oxide thin films by atomic layer deposition (ALD).[218] The condensation between metal carboxylates M(OCOR)x and metal alkoxides M (OR)y (equation 14) in nonpolar, aprotic solvents directly leads to the formation of oxo bridges and has been proposed as a general sol-gel route to (mixed) metal oxides.[235]

$$M{-}OR_1 \;+\; M{-}OCOR_2 \longrightarrow M{-}O{-}M \;+\; R_2COOR_1 \qquad (14)$$

The reaction of carboxylic acids with alkoxide precursors offers an alternative sol-gel method in non-aqueous solvents. The initial step of the process is the liberation of alcohol molecules by the exchange of carboxylate and alkoxy groups on the silicon or metal atom (Equation 15).[236]

$$M(OR_1)n \;+\; R_2COOH \longrightarrow M(OR_1)n\text{-}1\ (OCOR_2) \;+\; R_1OH \qquad (15)$$

Although direct aprotic condensation (Equation.14) cannot be excluded, the NH hydroxylation of carboxylate derivatives (e.g., acetoxysilane) by the nascent alcohol (Equation 16)[236] is destined to happen, as well as the esterification of carboxylic acid (Equation 17) with the formation of water in situ.[237]

$$M(OR_1)n\text{-}1\ (OCOR_2) \;+\; R_1OH \longrightarrow M(OR_1)n\text{-}1\ (OH) \;+\; R_2COOR_1 \qquad (16)$$

$$R_1OH \;+\; R_2COOH \longrightarrow R_2COOR_1 \;+\; H_2O \qquad (17)$$

This method is thus not strictly NH, at least in solution. On the other hand, this reaction has been used as of late for the vapor phase deposition of metal oxides.[238] On the basis of kinetic considerations, pathway involving mainly acetoxylation (Equation 6) followed by aprotic condensation (Equation 14) is involved. In this case, the alcohol formed in the first step is likely removed in the vapor phase and cannot react on the surface with the carboxylic acid to form ester and water (Equation 17).

# I.7. Mixed oxides catalysts prepared by NHSG

Metal oxides and mixed oxides have application as catalysts of chemical reactions due to their acidic, basic and/or redox properties. Some oxides can either be used as supports or as active phases dispersed on the support surface. The support gives the textural properties of the last material and advances the dispersion of the active phase; but controlling the dispersion of the active phase and stabilizing its active form stays challenging. A main feature of sol-gel processes is its ability to prepare such catalysts in a single step. In this case, however, the sol-gel approaches suffer from a serious problem compared to other approaches such as impregnation represented by dispersion of active phase on the surface of a pre-formed support. In fact, in one-step sol-gel approaches there is a risk of losing a significant part of the active species on the bulk of the material (e.g. on pore walls), where they are not accessible to the reactants. Luckily, the proportion of accessible surface species increases when the specific surface area increases. Moreover, when the Tammann temperature of the active species is sufficiently low (e.g. $VO_x$, $MoO_x$, $AgO_x$), suitable thermal treatments can lead to the migration of active species toward the surface, successfully increasing the proportion of accessible sites. NHSG routes have led to promising results in both cases.[22] The first example of mixed oxide catalysts prepared by NHSG was postponed in 2000 by Barbieri *et al*.[239], they synthesized catalysts based on Nb-V and Nb-V-Si for the oxidative dehydrogenation of propane. After a thermal treatment of the xerogels at 550 °C. Since then, NHSG has been used to prepare catalysts used in many chemical reactions, involving mild and total oxidation, photodegrdation, alkene metathesis, etc.

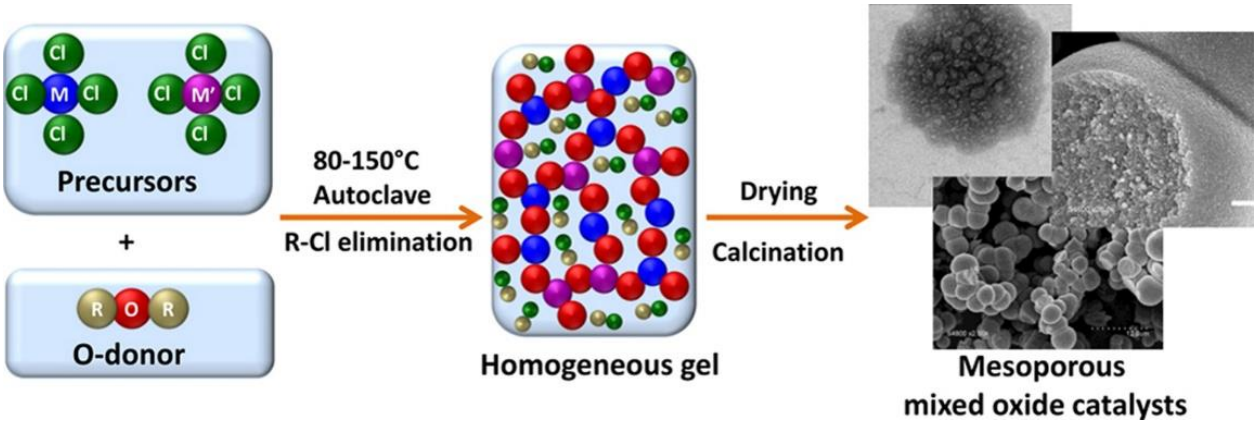


Figure 18: The preparation of mixed oxides with good homogeneity and texture is a challenge.[240]

In the last years, a developing interest has been focused on tuning material properties and particular highlights toward new application possibilities. This motivation has led to syntheses of new oxidic materials with special compositions. Few examples of newly mixed oxides prepared by NH chemistry were published recently. Bouchmella *et al.* detailed preparation of mesoporous Re-O-Al, Re-O-Si and Re-O-Si-O-Al mixed oxides through a one-step NHSG route with the goal of tuning the acidic properties of these solids and thus influence their catalytic performance. [241] The authors used the alkyl halide elimination, "ether route", including the reaction of chloride precursors with diisopropylether at 110 °C. The Re content dictated by a nominal Re/ (Re + Si + Al) atomic ratio was around 0.03. The textural properties in terms of a specific surface area and pore volume depended on the Si/Al ratio, where minima were observed for Si/Al ~0.3. The addition of Re caused a decrease in pore volume.

XPS and EDX investigations of xerogels demonstrated interesting results on surface and bulk Re/ (Re + Si + Al) atomic ratios. While, the Re species in as-prepared samples are homogeneously dispersed in the bulk, the calcined xerogels exhibit an increase of the surface Re/ (Re + Si + Al) atomic proportion comparing to the migration of Re to the surface upon thermal treatment. The same behavior was previously reported for vanadium, molybdenum, and tungsten in Ti-O-V, Ti-O-V-O-W, Ti-O-V-O-Mo and Si-O-Al-O-Mo mixed oxide catalysts prepared by NHSG and was clarified by a low Tammann temperature of the respective metal oxides allowing for their migration at increased temperatures.[242]

Si-O-Al-O-Mo mixed oxides were synthesized through the same NH alkyl halide elimination reaction and with the same aim tuning the acidity for better catalytic performance.[243] In this study, two reaction parameters were varied efficiently: the alumina content (the Si/Al ratio) and the $MoO_3$ content. Si/Al ratio of 17 provided materials with high specific surface areas and pore volumes (ca. 500 $m^2.g^{-1}$ and from 0.9 to 1.6 $cm^3.g^{-1}$, respectively). $MoO_3$ content ranging from 5 to 20 wt. % was analyzed and no significant effect on texture was observed. However, the catalytic properties depended strongly on the $MoO_3$ content. Oxide materials with the composition $V_2O_5$-$MoO_3$-$TiO_2$ or $V_2O_5$-$WO_3$-$TiO_2$ were prepared from chloride precursors by the same group.[244] Surface areas of the resulting samples ranged from 53 to 109 $m^2.g^{-1}$ with the pore diameters of about 10 nm. SEM micrographs showed spherical micrograins of about (2-5 μm) formed by an agglomeration of small elementary nanoparticles in the range of (10-25 nm). Another group of novel mixed oxides prepared by NHSG is represented by $WO_3$-$SiO_2$-$Al_2O_3$ materials. [245] $WO_3$

contents were established at 10 and 20 wt. %, while the amount of $Al_2O_3$ ranged from 5 to 20 wt. %. These mixed oxides prepared by alkyl halide elimination exhibited surface areas up to 740 $m^2.g^{-1}$, pore volumes of 1.7 $cm^3.g^{-1}$, and pore diameters of 9.9 nm. The materials discussed above illustrate that the NHSG approach based on alkyl halide elimination allows for excellent control of composition.

# I.8. Applications of NHSG route

Materials prepared by NHSG chemistry have discovered useful application in numerous fields. Two main areas of recent interest are identified in the context below: heterogeneous catalysts and catalyst supports. These two applications will be briefly discussed, recent works related to NH syntheses of mixed oxides and their applications are listed in (Table 4).

Table 4: Examples of application of materials prepared by NHSG.[246]

| **Mixed oxides** | **Non-hydrolytic synthetic route** | **Application** |
|---|---|---|
| Al-Si | acetamide elimination | aminolysis catalyst |
| Zr-Si | acetamide elimination, alkyl halide elimination | aminolysis, MPV, Friedel-Crafts catalysts |
| Sn-Si | acetamide elimination, twin polymerization | aminolysis catalyst |
| Ti-Si | acetamide elimination, alkyl halide elimination | mild oxidation, epoxidation catalysts |
| Fe-Al | alkyl halide elimination (ether route) | mild oxidation catalyst |
| Co-Al-Si | alkyl halide elimination (ether route) | mild oxidation catalyst |
| Re-Al-Si | alkyl halide elimination (ether route) | olefin metathesis catalyst |
| Mo-Al-Si | alkyl halide elimination (ether route) | olefin metathesis catalyst |
| Mo-Ti-V | alkyl halide elimination (ether route) | total oxidation catalysts |
| W-Ti-V | alkyl halide elimination (ether route) | total oxidation catalysts |
| Nb-V-Si | alkyl halide elimination | oxidative dehydrogenation catalyst |
| Ga-Si | thermal decompositon of Ga[OSi(OtBu)3]3_THF | Lewis acid catalyst |
| Si-P | ester elimination | Brønsted acid catalyst |
| $BiVO_4$ | microwave assisted twin polymerization | photocatalyst |
| $TiO_2$ | ether elimination (chitosan templated) | photocatalyst |
| $TiO_2$ | alkyl halide elimination (alkoxide route) | photocatalyst, S, N doped |

| | | |
|---|---|---|
| Y-V | alkyl halide elimination | luminescent materials, Ln3+ doped |
| Y-Al | alkyl halide elimination | luminescent materials, Ln3+ doped |
| Gd-Ca-Al | alkyl halide elimination | luminescent materials, Ln3+ doped |
| Gd-Al | alkyl halide elimination | luminescent materials, Ln3+ doped |
| Ln-P | benzyl alcohol route, microwave assisted | luminescent materials, Ln3+ doped |
| Ti-V | alkyl halide elimination (ether route) | Li-ion batteries |
| $Li4Ti_5O_{12}$ | benzyl alcohol route | Li-ion batteries |
| $LiFePO_4$ | benzyl alcohol route, microwave assisted | Li-ion batteries |
| $LiMnPO_4$ | benzyl alcohol route, microwave assisted | Li-ion batteries |
| $SnO_2$ | benzyl alcohol route, microwave assisted | optoelectonic devices, Sb doped |
| Si-P | ester elimination | catalyst support |

## I.8.1. Heterogeneous catalysts

The particular properties and highlights of mixed oxides open a large area of the application possibilities in heterogeneous catalysis. Imaginative thoughts of catalysts applications and their design require specific catalytic sites with a high activity, stability, and recyclability. The chemistry of NHSG offers a promising pathway for the targeted preparation of heterogeneous catalysts with control of structure, texture, and composition. Aluminosilicates represent a group of materials with both Lewis and Brønsted acidity. They can be utilized as catalysts or as supports for other active species. The essential condition for catalytic activity is the presence of tetracoordinated and pentacoordinated Al atoms. These species can be examined by the $^{27}$Al MAS NMR spectroscopy. Recently, mesoporous aluminosilicate catalysts (up to 627 $m^2.g^{-1}$) synthesized by templated acetamide elimination were reported.[247] The products were utilized in aminolysis reactions, where high catalytic activities were observed. The catalytic activity of $SnO_2$-$SiO_2$ mesoporous xerogels in aminolysis of styrene oxide has additionally been explored. For this situation the conversion of styrene oxide was reasonably high and reached 50% after 1h.[247] The total oxidation of volatile organic compounds (VOCs) which are released in some industrial processes is currently a subject frequently discussed. Decomposition of these pollutants, represented mostly by chlorinated aromatics, can be catalyzed by so-called total oxidation catalysts. These catalysts were prepared by Debecker *et al.* and were based on $WO_3$-$V_2O_5$-$TiO_2$ and $MoO_3$ oxides.[242] The authors reported high conversions of benzene and chlorobenzene especially in the case of samples

with 10 wt. % $V_2O_5$ loadings. The incorporation of Mo and W into catalysts displayed promoting effects and increased their efficiency. For instance, the total oxidation of chlorobenzene reached 93 % conversion after 150 min at 300 °C. NHSG derived VOC total oxidation catalysts showed by Debecker and coworkers[242] show a similar activity to the catalysts prepared by impregnation method on $TiO_2$ supports [248]. Another class of materials examined by the same group were catalysts for olefin metathesis. They prepared mesoporous mixed oxide based catalysts with the compositions of Mo-O-Si-O-Al [243] and Re-O-Si-O-Al.[241] All samples catalyzed the conversion of propene to ethene and butene with more than 99 % selectivity. In the case of Mo-O-Si-O-Al samples, the best catalysts contained only 5 wt. % $Al_2O_3$ and their activity increased with higher $MoO_3$ loading. The Re-O-Si-O-Al catalysts exhibited a comparable catalytic activity to the Mo-O-Si-O-Al catalysts. The best catalytic performance was accomplished with a sample $Re_3$-$SiAl_{0.3}$ (ca. 10 wt. % $Re_2O_7$) which produced propene at a specific activity of 45 mmol $.g^{-1}.h^{-1}$. It is important to use a Si-O-Al mixed oxide as a support because Al atoms significantly increase the acidity of the catalysts according to $NH_3$-TPD.

## I.8.2. Catalyst Supports

It is imperative that NHSG materials have diverse groups on the surface than silica prepared by conventional methods (e.g., Si-Cl, Si-OAc, Si-OEt, etc. vs. Si-OH) and in this manner their reactivities differ significantly. Silica-based materials containing catalytic centers, such as metallocenes or (MAO), were studied by the group of Dos Santos.[249] The preparation of their silica supports is based on the reaction between $SiCl_4$ and $Si(OEt)_4$ in toluene with the addition of a catalytic amount of $FeCl_3$. MAO is then added into the silica precursor mixture. Unfortunately, resulting materials exhibit low surface areas and poor catalytic activities. This conduct might be caused by some side reactions of MAO with silica. Additionally, access to the active centers encapsulated inside an almost non-porous silica support is strongly hindered. An increase in catalytic activity was achieved by increasing metallocene concentration in these materials.[250] The same group also described alizarin incorporated silica materials with potential application as pH sensors.[251] The surface reactivity of silicophosphates and their hybrid derivatives prepared by ester elimination was recently investigated. It was possible to graft highly acidic P-OH groups and pure tetrahedral Al atoms onto the surface. Potential application of these materials was

demonstrated in α-methylstyrene dimerization where they were used as acidic heterogeneous catalysts.[252] Recently Kejik *et al*. reported the preparation of microporous and mesoporous organosilicates.[253] These materials, prepared through a novel NHSG method from Si $(OAc)_4$ and polyphenols, show high surface areas and their porosity can be controlled by the type of linker utilized. An interesting area of future investigation is the combination of NHSG method and click chemistry. Click chemistry is already widely used for the surface grafting. Click reactions often need anhydrous conditions.[254] Moreover, the introduction and homogeneous dispersion of organic groups in metal oxides by NHSG were reported to be successful in many cases thus providing ideal conditions for surface grafting by click chemistry.

# Goals of the thesis

The objective of the thesis was to study sol-gel processes, hydrolitic sol-gel and non-hydrolytic sol-gel as a simple and powerful route to prepare based-mixed oxides catalysts.

The focus was done in the preparation, characterization and application in the ethylene oligomerization of Si-Al-Ni ternary mixed oxides.

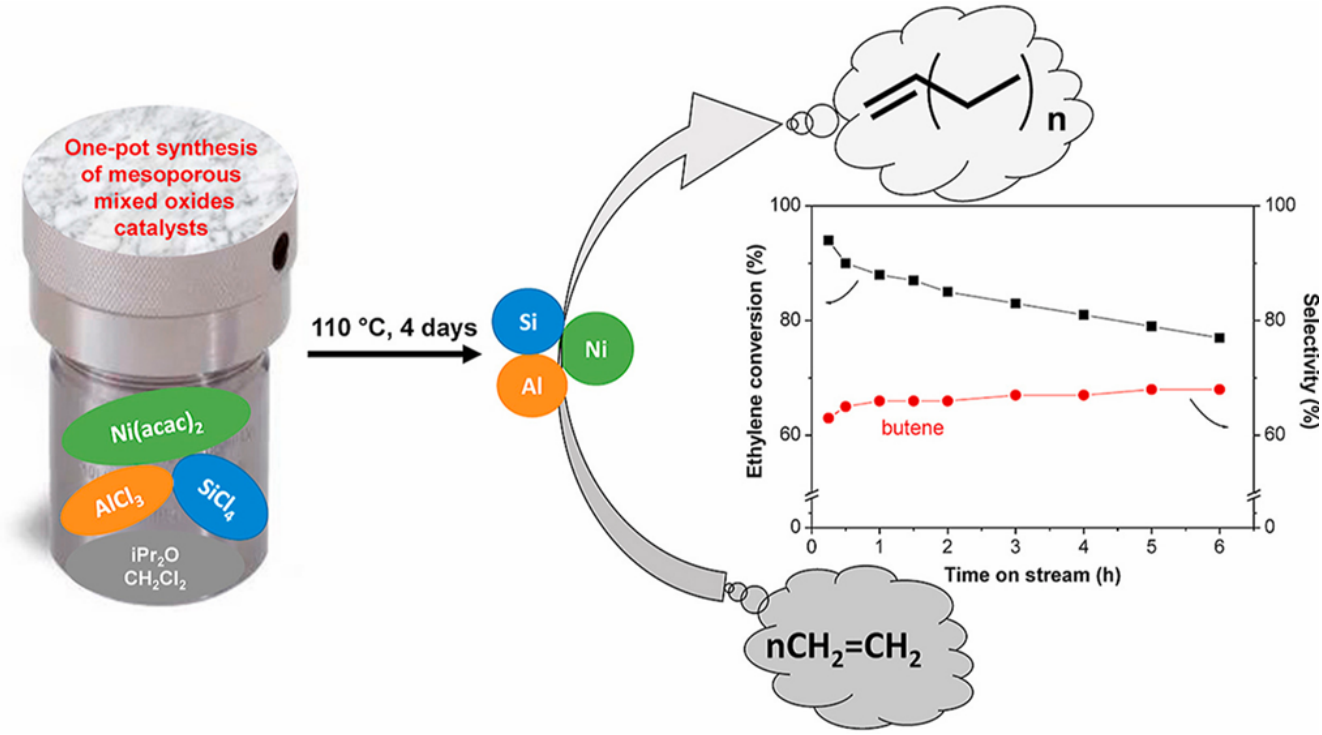


Figure 19: $SiO_2$-$Al_2O_3$-NiO catalysts prepared by NHSG for ethylene oligomerization.

# Chapter: II

# Silica-alumina: hydrolytic sol-gel synthesis, characterizations and application in esterification reaction

# II.1. Introduction

Esterification of carboxylic acids is one of the major reactions in organic synthesis.[255, 256] In addition to this, esterification of acetic acid with n-butyl alcohol is commercially significant cause the product n-butyl acetate is widely consumed in the manufacture of artificial perfumes, photographic films, plastics, safety glasses,[257] food additive, extractant, as solvent for coating resin, and pharmaceutical intermediate. In recent years, consumer demand for n-butyl acetate has grown, resulting in higher prices and profit margins. Therefore, esterification reactions have been carried out on a large scale using heterogeneous catalysts.[258, 259] Indeed, mesoporous metal oxides and mixed oxides with acidic, basic and/or redox properties are highly used as catalysts in heterogeneous catalysis, including environmental catalysis. Among these mixed oxides, $SiO_2$-$Al_2O_3$ have been extensively used in the esterification reactions because of their high surface area and high thermal stability.[72, 240, 260] The sol-gel process based on the formation of inorganic matrices by hydrolysis and polycondensation of molecular precursors (usually silicon or metal alkoxides) has been extensively used to prepare mixed oxide catalysts with high surface area and ordered mesoporosity.[145, 261] This process can be defined as the conversion of a precursor solution into an inorganic solid through water-induced inorganic polymerization reactions which, can be carried out under simple experimental conditions, such as low temperatures.[142, 262] It is one of the most popular to produce oxide materials with high control over their textural and surface properties, as well as high purity and homogeneity.[145, 263, 264] In the nineteenth century, pioneering experiments in sol-gel by Ebelmen [133, 265] and Graham[266], described that $Si(OEt)_4$ (tetraethyl orthosilicate, TEOS) hydrolyzed under acidic conditions, yielding silica in the form of a glass-like material. However, this process has faced a very important development, which started to be used in a various academic and industrial domains, notably for production of hybrid materials.[267] As the sol-gel reactions (hydrolysis and condensation) are slow at room temperature, a catalyst, acidic, basic or nucleophilic, is usually added to the solution.[268, 269] Accordingly, the pH is one of the important factors influencing the properties of mixed oxides prepared by sol-gel process. It is affects the hydrolysis and condensation behaviour during gel formation, and hence the morphology of mixed oxides.[262, 270, 271] For example, Li *et al*. found that the solution conditions affect the particle size of ZnO.[272] P.R. Aravind *et al*. claimed that pH of hydrolysis and gelation is a significant factor in determining the final composition of the

substances.[273] J. Livage *et al*. reported that gelation time of TEOS has been stated to vary depending on the acid used. As a result, the gelation time could be reduced.[274]

In this study, we applied pH adjustment and Si/Al ratio to the preparation of various $SiO_2$-$Al_2O_3$ catalysts. The effects of the pH and Si/Al ratio are discussed in relation to their catalytic activities in the esterification of carboxylic acid and alcohol.

# II.2. Results and discussion

## II.2.1. Synthesis and characterization

To investigate the effect of the composition of $SiO_2$-$Al_2O_3$ mixed oxides on the physico-chemical properties and on the catalytic activity, $SiO_2$-$Al_2O_3$ mixed oxides with different Si/Al ratios (0, 0.1, 0.3, 1, 2.9, 8.7 and ∞) were synthesized. Tetraethylorthosilicate TEOS ($Si(OC_2H_5)_4$), 98% from Sigma Aldrich, aluminium isopropoxide $Al(O\text{-}i\text{-}Pr)_3$, 98% from Sigma Aldrich (Table 19, Experimental Part) and aluminium nitrate $Al(NO_3)_3$, 95% from Sigma Aldrich were used as molecular precursors (Table 20, Experimental Part).

$Al(NO_3)_3$ was used instead of $Al(O\text{-}i\text{-}Pr)_3$ in the basic medium because of its better solubility in the experimental conditions. Ethanol absolute and distilled water were used as a solvent and reactant. In acid medium, starting from TEOS, ethanol and water (which was adjusted to a pH of 1.5 with HCl), a good colloidal $SiO_2$ sol was prepared using the volume ratios 1:1:2. After that, the initial solution was stirred for 1 hour using a magnetic stirrer at room temperature to get a transparent sol. Following Yoldas' method, an $Al_2O_3$ sol was prepared.[275, 276] Aluminum isopropoxide $Al(OC_3H_7)_3$ was dissolved in distilled water (pH 1.5) that had been preheated to about 90 °C. In addition, the solution was stirred for 1h to obtain homogenous sol. By mixing and stirring the $SiO_2$ and $Al_2O_3$ sols, the $SiO_2$-$Al_2O_3$ sol was prepared. The sol was heated to 50 °C for 3 days (aging), the gel was washed under air atmosphere with ethanol, acetone and diethyl ether respectively and dried at 25 °C under vacuum (10 Pa) for 1 h and then for 4 h at 120 °C. The resulting xerogel was crushed in a mortar and calcined in air at 500 °C for 5h (heating rate 10 °C $min^{-1}$). The samples are labeled $Si_xAl_y$ where x and y represent the nominal $SiO_2$, and $Al_2O_3$ weight loadings, respectively.

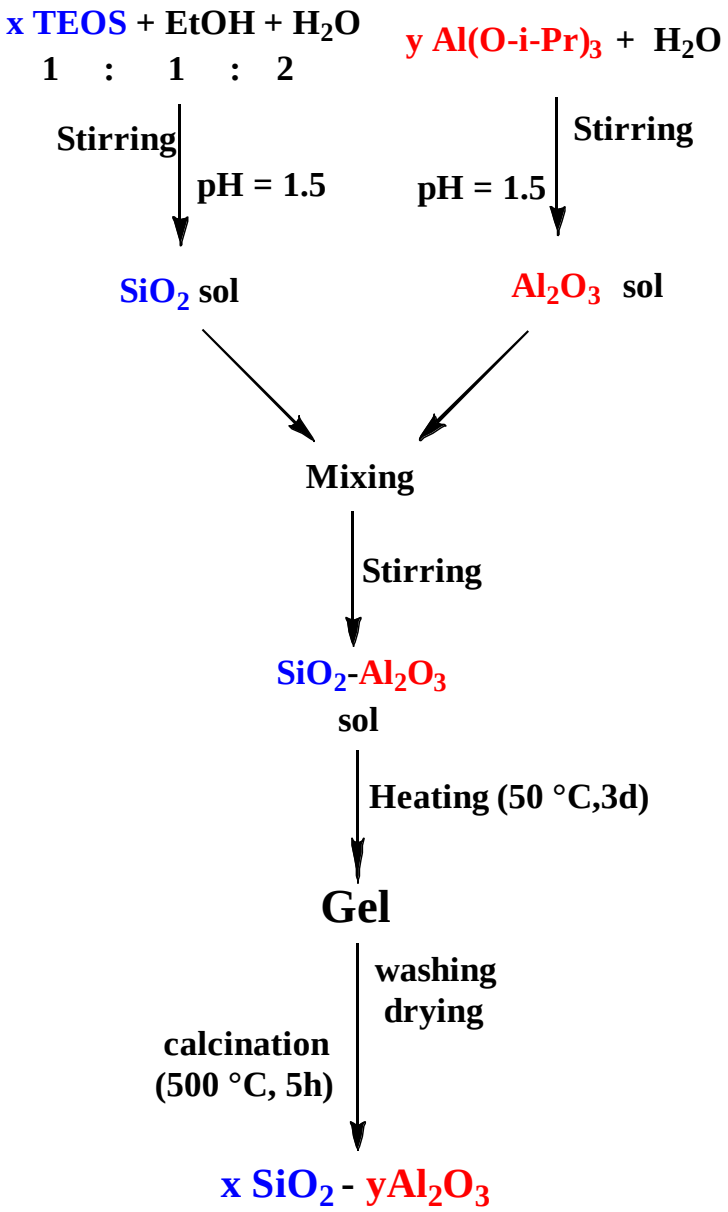


Scheme 6: HSG process in acidic medium for the preparation of silica-alumina mixed oxides.

In Basic medium, $SiO_2$-$A1_2O_3$ were prepared by using a sequential route at a constant pH of 8.5.[277] The $SiO_2$ sol was prepared by mixing one part (by volume) of TEOS with two parts of distilled water, which was adjusted to a pH of 1.6 with nitric acid. The TEOS was then allowed to hydrolyze overnight at room temperature under continuous agitation to give a homogeneous sol. Next, saturated aluminum nitrate, the quantity depend on the desired amount of $Al_2O_3$, was added. Mixing was continued for 1 h. Finally, ammonium hydroxide solution (2 M) was added drop wisely to form a hydrogel at a pH of 8.5. The gel was washed with distilled water and vacuum filtered

three times to remove the ammonium nitrate from the gel. In the final washing and filtering step, ethanol was used in same proportion. A final washing with ethanol is believed to allow the pore structure to expand [277] Dried at 25 °C under vacuum (10 Pa) for 1 h and then for 4 h at 120 °C. The resulting xerogel was crushed in a mortar and calcined in air at 500 °C for 5h (heating rate 10 °C $min^{-1}$). The samples are labeled $Si_xAl_y$ where x and y represent the nominal $SiO_2$ and $Al_2O_3$ weight loadings, respectively.

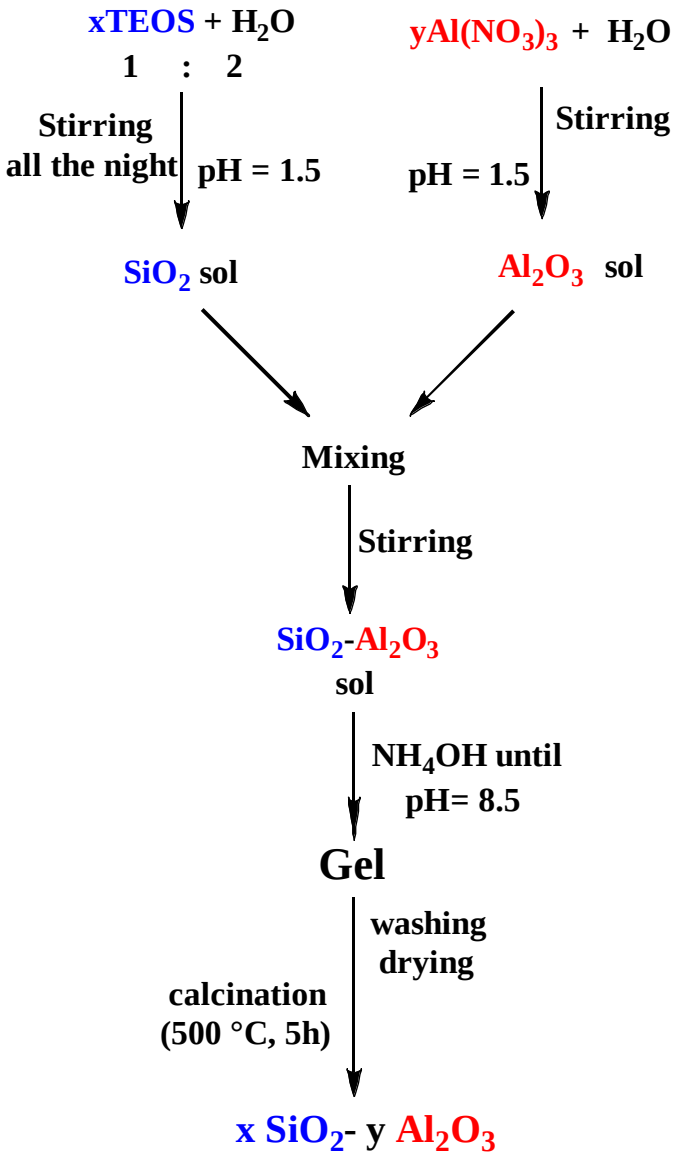


Scheme 7: HSG process in acidic medium for the preparation of silica-alumina mixed oxides.

## II.2.2. Composition:

### II.2.2.1. Scanning electron microscopy (SEM)

SEM images were performed to study the structure and morphology of the prepared materials. A clear dependence of the structure on Si/Al ratio and medium of reaction (acidic or basic) was observed in SEM images (Figure 20).

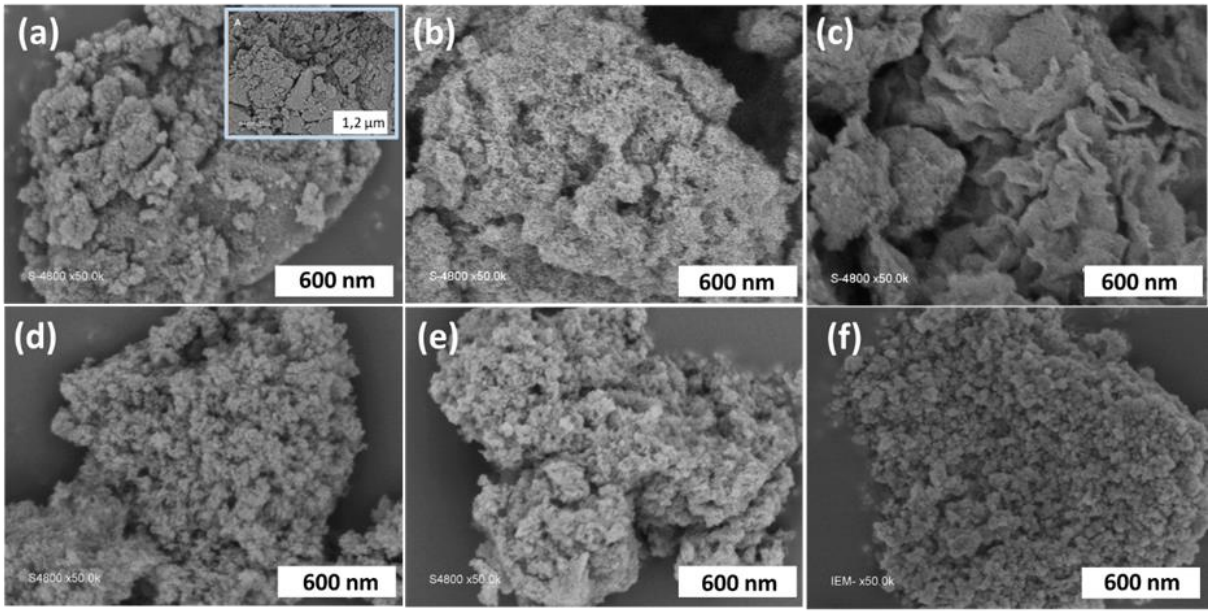


Figure 20: SEM images of samples with different compositions and prepared in different media: acidic medium (a) $Si_{75}Al_{25}$, (b) $Si_{25}Al_{75}$, (c) $Si_0Al_{100}$ and basic medium (d) $Si_{75}Al_{25}$, (e) $Si_{25}Al_{75,}$ (f) $Si_0Al_{100}$.

The SEM images show the Al atoms are distributed in the silica frameworks, they does not show any regular particles, which suggests that the synthesized materials are amorphous. There is a noticeable difference in morphologies between the compounds prepared in acidic and basic medium. In basic medium, compounds are more porous and regular (Figures1d, 1e and 1f). In the case of different (Si/Al), the difference is more clear in acidc medium than in basic. Aluminum-rich compound is more porous while the silicon-rich one appears as agglomerates, (Figures 1a and 1c).[278] These results indicates that the sol-gel route was functional at controlling the homogeneity in the mixed oxide.

### II.2.2.2. Energy Dispersive X-ray Analysis (EDX)

EDX analysis was used to determine the experimental composition of the samples. As shown in (Table 5) experimental weight percentages were close to the nominal ones, based on the amounts of reactants, indicating that all of the Si and Al atoms were included in the final oxide. Li. *et al*. showed the same behavior when they have been synthesized amorphous silica-alumina via sol-gel process. EDX was used on various portions of oxides to analyse the element distribution, and as expected, similar results were obtained.[279] This finding showed that oxides were chemically homogeneous. The experimental Si/Al ratio in the oxide was similar to the nominal one.

Table 5: Composition by EDX measurements.

| Sample | Experimental / (nominal) composition (wt%) [a] | | | | |
|---|---|---|---|---|---|
| | Acid | | Base | | |
| | $SiO_2$ | $Al_2O_3$ | $SiO_2$ | $Al_2O_3$ | Si/Al [b] |
| $Si_{100}Al_0$ | 99.6 / (100) | 0.4 / (0) | 99.3 / (100) | 0.7 / (0) | - |
| $Si_{90}Al_{10}$ | 89.5 / (89.7) | 10.5 / (10.3) | 95.4 / (89.8) | 4.6 / (10.2) | 8.7 |
| $Si_{75}Al_{25}$ | 74.9 / (74.7) | 25.1 / (25.3) | 82.2 / (74.6) | 17.8 / (25.4) | 2.9 |
| $Si_{50}Al_{50}$ | 47.5 / (50.6) | 52.5 / (49.4) | 53.4 / (49.4) | 46.6 / (50.6) | 1.0 |
| $Si_{25}Al_{75}$ | 28.8 / (24.7) | 71.2 /( 75.3) | 29.1 / (24.6) | 70.9 /( 75.4) | 0.3 |
| $Si_{10}Al_{90}$ | 11.5 / (10.2) | 88.5 /( 89.8) | 13.5 / (10.1) | 86.5 /( 89.9) | 0.1 |
| $Si_0Al_{100}$ | 0.26 / (0.0) | 99.74 /( 100) | 0.3 / (0.0) | 99.7 /( 100) | 0.0 |

[a] Experimental and nominal weight percentages (in brackets). Weight loadings are calculated from EDX results assuming that all Si and Al atoms are in the form of $SiO_2$ and $Al_2O_3$ respectively.[b] Experimental atomic Si/Al ratio (EDX).

## II.2.3. Structure

### II.2.3.1. X-ray Diffraction Analysis (XRD)

The X-ray diffractograms of the silica-alumina mixed oxides prepared *via* HSG in acidic and basic media and calcined under air at 500 °C are shown in Figure 21.

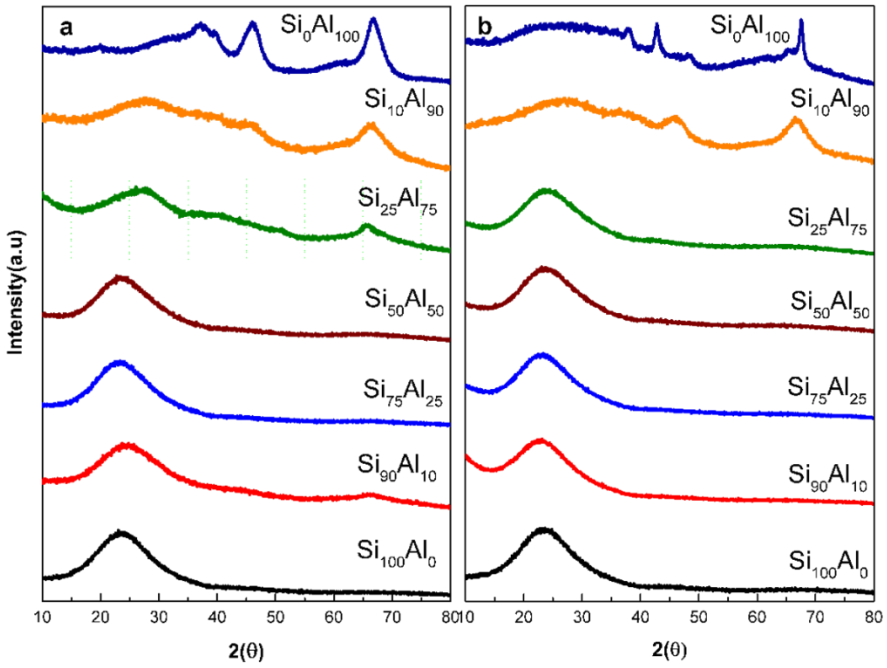


Figure 21: Powder XRD patterns of $Si_xAl_y$ samples prepared in (a) acidic medium and (b) basic medium.

Independently of the medium synthesis, all samples showed broad peaks at 2θ = 23° attributed to amorphous silica.[277] Samples with high silica loading showed only peaks of amorphous silica. Decreasing silica loading leads to a decrease of the intensity of this peak. Other phases like alumina, zeolite, and layered structures were not detected in samples containing high silica loading .[280] Broad reflections typical of bulk γ-alumina (2θ = 37.3°, 43° and 67°) were detected for the samples with high alumina loading.[275, 281] These alumina peaks are broader in acid medium than those of samples with the same composition but prepared in basic medium. The broadness of the diffraction indicates that the alumina crystallites would have low crystallinity or small size.[280]

## II.2.3.2. Nuclear Magnetic Resonance (NMR):

$^{29}$Si and $^{27}$Al solid-state NMR gives information on the structure of the alumino-silicate network. The $^{29}$Si CP-MAS NMR spectra of Si-containing mixed oxides (Figure 22) showed broad resonances, typical of amorphous materials.[282]

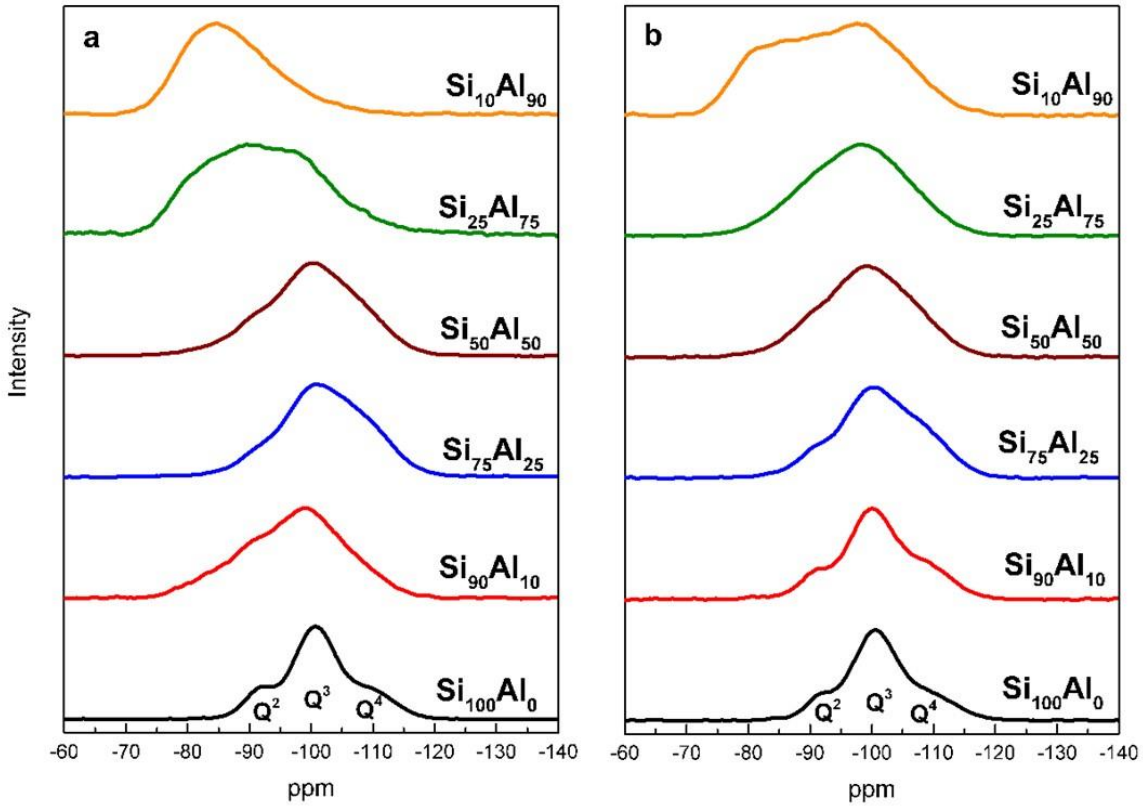


Figure 22: $^{29}$Si CP-MAS NMR spectra of $Si_xAl_y$ samples in (a) acidic medium and (b) basic medium.

The chemical shift of the Si atoms in amorphous silica-alumina depends on the nature of the second neighbors. In amorphous silicas or alumino silicates, each replacement of a (OSi) group in $Si(OSi)_4$ tetrahedra by an (OAl) or an (OH) group leads to a downfield shift of about 5 to 10 ppm.[283] The spectrum of $Si_{100}Al_0$ show 3 broad signal at ≈ -110, -101 and -93 ppm attributed to $Si(OSi)_4$ ($Q^4$), $Si(OSi)_3(OH)$ ($Q^3$), and $Si(OSi)_2(OH)_2$ ($Q^2$) sites, respectively. [153, 284] Similar $^{29}$Si CP-MAS NMR spectra with a major $Q^3$ resonance have been reported for mesoporous silicas or silica-alumina with a low Al content. [285, 286] The incorporation of large amount of aluminum in the silica network led to a significant low-field shift of the resonances indicating extensive formation

of Si-O-Al bridges in $Si(OSi)_{4-x}(OAl)_x$(Q4xAl) sites or $Si(OSi)_{3-x}(OH)(OAl)_x$(Q3xAl) sites .[282, 283] Substitution of Si with Al in $Si(OSi)_4$ results in a shift in resonance of the 5 ppm per Al.

The $^{27}$Al solid-state MAS NMR spectra (Figure 23), exhibited broad resonances around 70 ppm, 35 ppm and 5 ppm, ascribed to tetra-coordinated ($Al^{IV}$), penta-coordinated ($Al^{V}$) and hexa-coordinated ($Al^{VI}$) aluminum sites. [283, 287, 288]

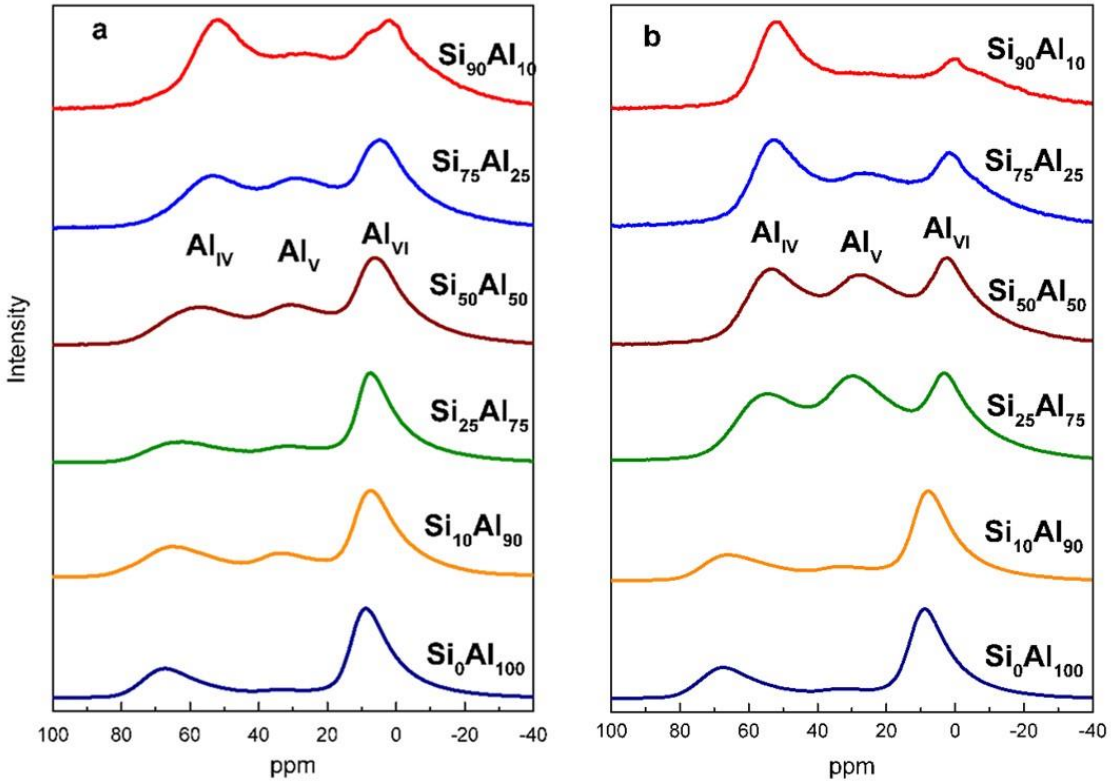


Figure 23: $^{27}$Al MAS NMR spectra of $Si_xAl_y$ samples in (a) acidic medium (b) basic medium.

The $Al^{IV}$ peak increased as the Si content increased, suggesting that the insertion of $AlO_4$ tetrahedral in the silica network is favored at high Si/Al, in acidic and basic medium, respectively.[282] As shown in Figure 24 , the spectra of all samples prepared by SG route exhibit clearly three peaks at ca 70, 35, and 5 ppm, assigned to $Al^{IV}$, $Al^{V}$ and $Al^{VI}$, respectively.[288] For the samples prepared in both acidic and basic medium, the spectrum of the rich alumina samples shows same major resonances arising from $Al^{VI}$ sites, and when the Si content increases the proportion of $Al^{V}$ and $Al^{IV}$ sites increases at the expense of $Al^{VI}$ sites. $Al^{V}$ spectrum is well

recognized in basic medium than in acidic. Leonardo et *al* .[289] and Hensen et *al* [35] observe a similar behavior in the case of amorphous aluminosilicates.

The signal corresponding to $Al^{IV}$ sites shifted upfield when the $SiO_2$ loading increased from 0 to 90%; this effect has been previously ascribed to the decreased concentration of aluminum atoms around Al sites.[35, 289, 290].

## II.2.3.3. Fourier transform infrared (FTIR)

FTIR spectroscopy is a rapid and non-destructive analytical technique that identify local changes and provide information on the functional groups of a mixed oxides structure. We have recorded the FTIR spectra of the materials (Figure 24).

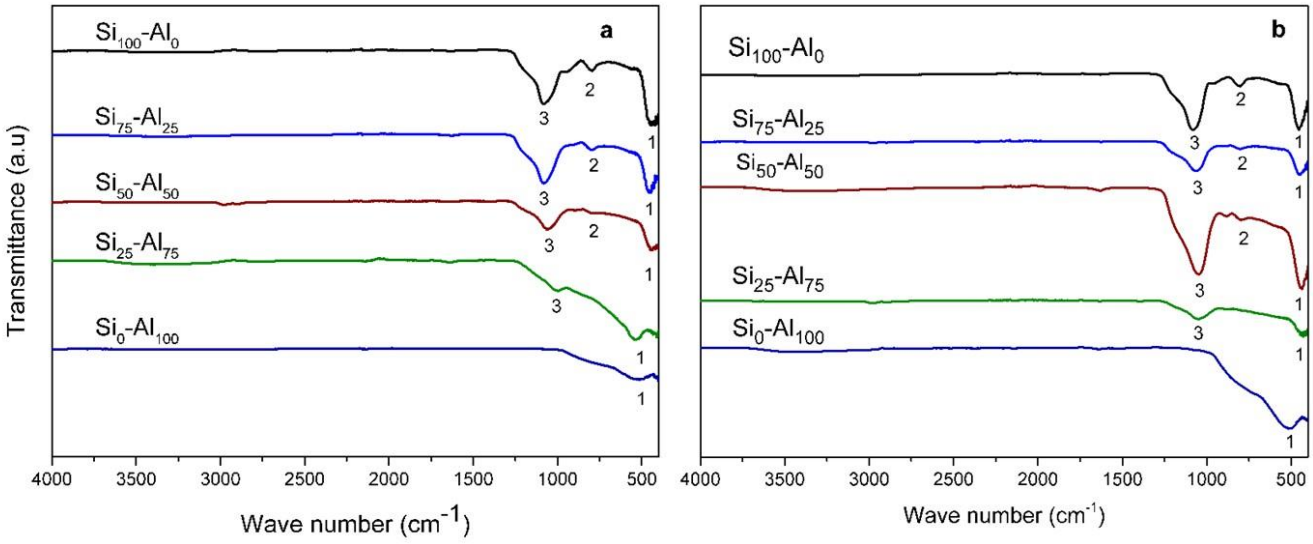


Figure 24: FTIR spectra of $Si_xAl_y$ samples in acidic medium  basic medium.

The peak related to Si-OH was absent at 950 $cm^{-1}$. A peak near 450 $cm^{-1}$ (labeled 1) is assigned to a rocking mode or rocking motion that proves the silicate's three-dimensional network There is a vibrational mode of Si-O-Si group that are mostly seen in the range 400-1300 $cm^{-1}$. A significant peak around 1150 $cm^{-1}$ (labeled 3) is attributed to the Si-O-Si asymmetric stretching mode in which the bridging oxygen atoms migrate horizontally into the Si-O-Si plane.[291-294] Furthermore, the intensity of this peak increases with the increase of silica.

## II.2.4. Texture

The specific surface areas, pores volume, and pores size distribution data derived from nitrogen adsorption are shown in Table 6. The pores diameter data range between 1.8 and 11.1 nm revealing a mesoporous structure of $Si_xAl_y$. The texture of the samples depends on the Si/Al ratio. For the sample made of pure silica, a specific surface area is 477 $m^2.g^{-1}$ in basic medium and 377 $m^2.g^{-1}$ in acidic one. It was increased as the amount of Al increases up to 75%. A further increase in the Al leads to a decrease in the specific surface area.

Table 6: Textural Properties of the samples (obtained from $N_2$-physisorption).

| Sample | SSA ($m^2/g$) [a] | | Vp ($cm^3/g$) [b] | | Dp (nm) [c] | | Si/Al [d] |
|---|---|---|---|---|---|---|---|
| | Acid | Base | Acid | Base | Acid | Base | |
| $Si_{100}Al_0$ | 377 | 477 | 0.2 | 1.0 | 1.9 | 8.7 | - |
| $Si_{90}Al_{10}$ | 437 | 613 | 0.7 | 1.7 | 6.2 | 10.9 | 9 |
| $Si_{75}Al_{25}$ | 237 | 547 | 0.1 | 1.1 | 1.8 | 8.0 | 3 |
| $Si_{50}Al_{50}$ | 311 | 448 | 0.4 | 1.2 | 5.4 | 11.0 | 1 |
| $Si_{25}Al_{75}$ | 513 | 482 | 1.4 | 0.9 | 11.1 | 7.7 | 0.3 |
| $Si_{10}Al_{90}$ | 286 | 400 | 0.3 | 0.4 | 4.4 | 3.6 | 0.1 |
| $Si_0Al_{100}$ | 375 | 340 | 0.4 | 0.4 | 4.8 | 4.0 | 0 |

[a]Specific surface area determined by the BET method.
[b] Total pore volume at P/P0.
[c] Average pore diameter Vp / $S_{BET}$.

The specific surface area and pore diameter of samples prepared in basic media are higher than those ones prepared in acidic medium. The same observation was given by Agliullin, M.R., *et al.* when they prepared porous aluminosilicates by sol-gel in different pH values.[295] The alumina and silica rich samples ($Si_{25}Al_{75}$ and $Si_{90}Al_{10}$) showed high specific surface area (513 and 437 $m^2$ $g^{-1}$) and pore volume (1.4 and 0.7 $cm^3g^{-1}$). While the other samples showed moderate specific surface area (between 237 and 377 $m^2$ $g^{-1}$). The average pore diameter (Dp) ranged between 1.8 and 11.1 nm. For the samples prepared n basic medium, most of the specific surface areas are

higher than the corresponding samples (same composition) prepared in acidic medium. Silica-rich samples ($Si_{90}Al_{10}$ and $Si_{75}A_{25}$) exhibited high specific surface areas (613 and 547 $m^2\ g^{-1}$) and pore volumes (1.7 and 1.1 $cm^3\ g^{-1}$). The average pore diameter (Dp) ranged between 3.6 and 11 nm. These results show clearly the dependence of specific surface area, pore volume, and average pore diameter on contents/Al ratio and on the synthesis medium.

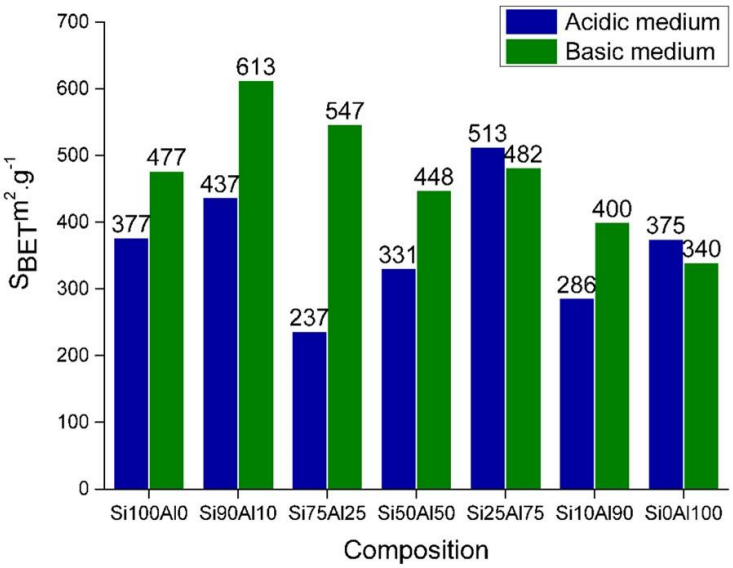


Figure 25: Comparison between specific surface area for samples prepared by sol-gel rout in acidic and basic medium.

The adsorption and desorption isotherms of nitrogen for the samples prepared in acidic and basic medium are presented in Figure 25. The nitrogen adsorption isotherms of the samples were of type IV which is characteristic of mesoporous materials.[296] At the adsorption branch, the adsorbed amount increased gradually with an increase in relative pressure by multilayer adsorption. A sudden uptake of the adsorbed amount was observed over a range of relative pressure ($P/P_0$) between 0.4 and 1.0. This phenomena caused by capillary condensation of nitrogen in the pores. The desorption branch of the isotherm coincides with the adsorption branch.

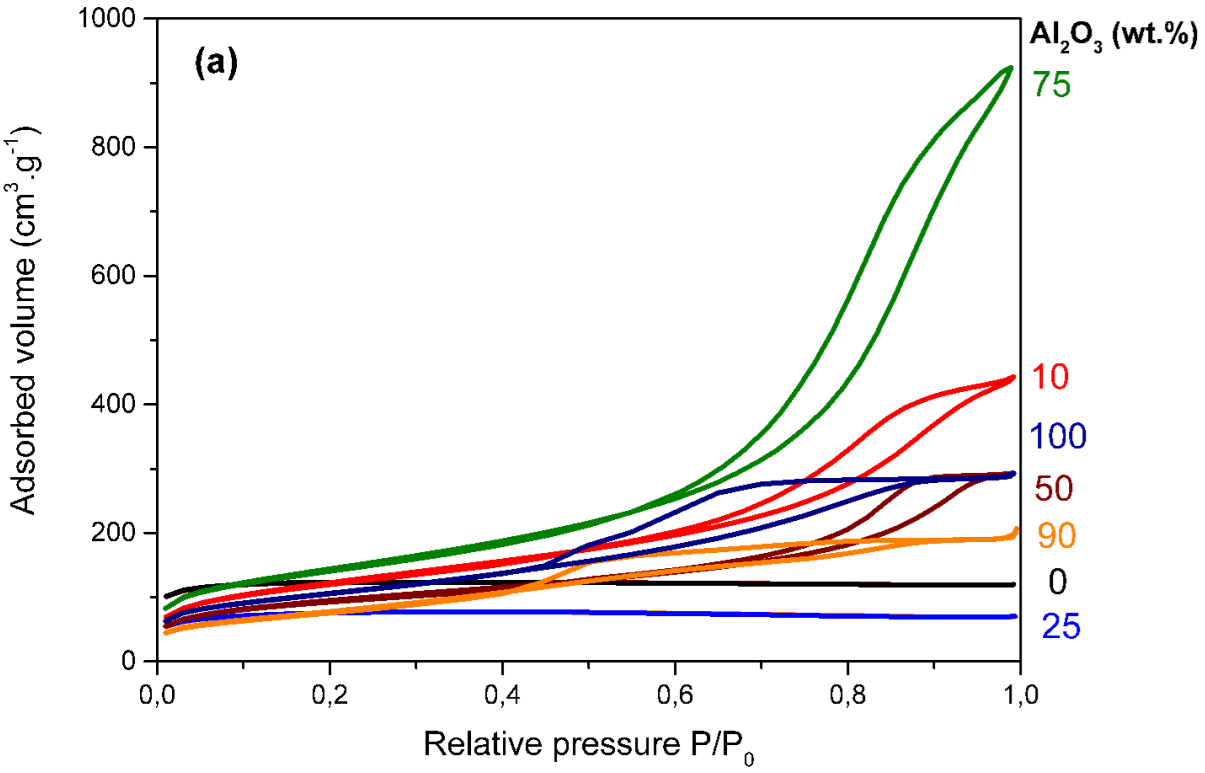
(a)
Adsorbed volume (cm$^3$.g$^{-1}$)
Relative pressure P/P$_0$
0
200
400
600
800
1000
0,0
0,2
0,4
0,6
0,8
1,0
Al$_2$O$_3$ (wt.%)
75
10
100
50
90
0
25

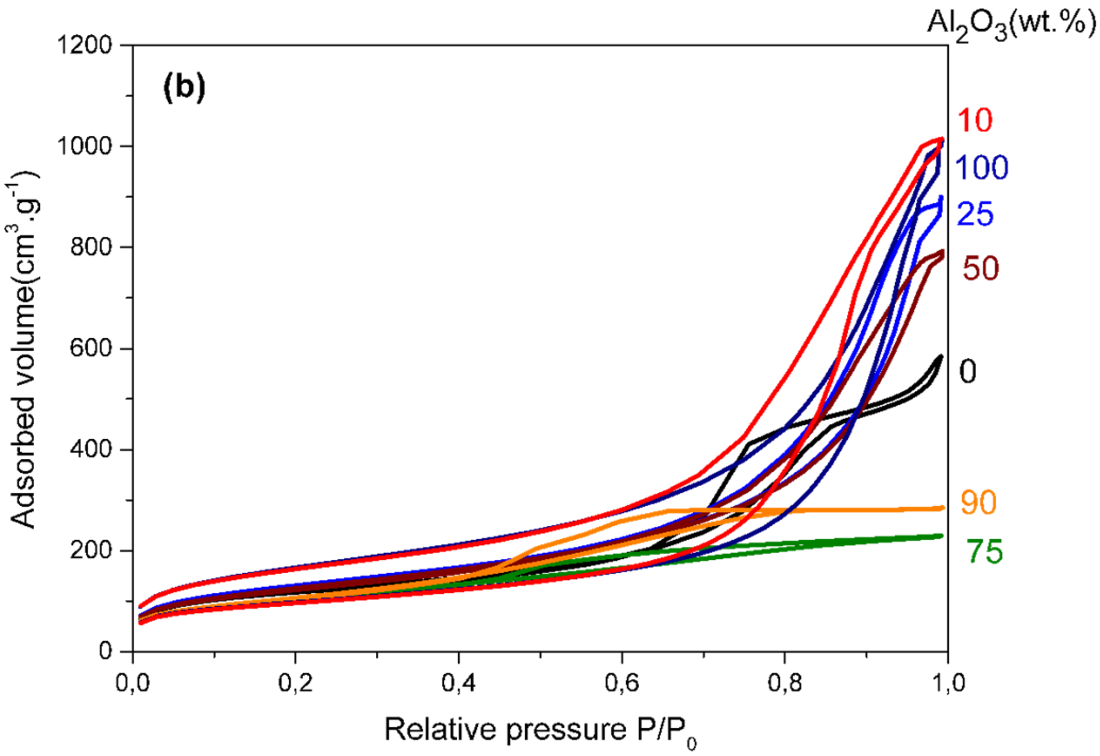


Figure 26: $N_2$ adsorption–desorption isotherms of SixAly samples prepared in (a) acidic medium, (b) basic medium.

## II.2.5. Acidity:

The acid properties of the samples prepared by HSG route in acidic and basic medium were investigated by ($NH_3$-TPD). As expected, the acid sites increase as Al content increases. (Table 7).

Table 7: Acidity measured by NH3-TPD.

| Sample | Total acidity (mmol $g^{-1}$) | | Weak acidity (mmol $g^{-1}$) | | Medium-strong acidity (mmol $g^{-1}$) | |
|---|---|---|---|---|---|---|
| | Acid | (Base) | Acid | (Base) | Acid | (Base) |
| $Si_{100}Al_0$ | 0.4 | (1.0) | 0.1 | (0.1) | 0.3 | (0.9) |
| $Si_{90}Al_{10}$ | 0.6 | (0.6) | 0.1 | (0.1) | 0.5 | (0.6) |
| $Si_{75}Al_{25}$ | 1.0 | (0.9) | 0.1 | (0.1) | 0.9 | (0.7) |

| | | | |
|---|---|---|---|
| $Si_{50}Al_{50}$ | 1.2 (1.3) | 0.2 (0.2) | 1.0 (1.1) |
| $Si_{25}Al_{75}$ | 1.4 (1.4) | 0.2 (0.2) | 1.1 (1.2) |
| $Si_{10}Al_{90}$ | 1.3 (1.4) | 0.1 (0.1) | 1.2 (1.2) |
| $Si_{0}Al_{100}$ | 1.0 (0.9) | 0.1 (0.1) | 0.9 (0.8) |

Ammonia-TPD profiles of $Si_xAl_y$ samples with different Si/Al ratios and prepared by different routes are plotted in Figures 27 a and b. The presence of medium or strong acidic sites seems related to the presence of Al. The thermogram obtained for $Si_{100}Al_0$ prepared in acidic medium showed a broad desorption profile indicating the presence of medium or strong acidic sites only. Conversely, the thermograms of all Al-containing samples showed that ammonia desorbed peak at ≈180 °C attributed to weak acid sites. Another peak at about 300-400 °C attributed to medium or strong acid sites. The acidity seems to be intermediate between the highly acidic sites found in zeolites and the weakly acidic sites of silica. [297]

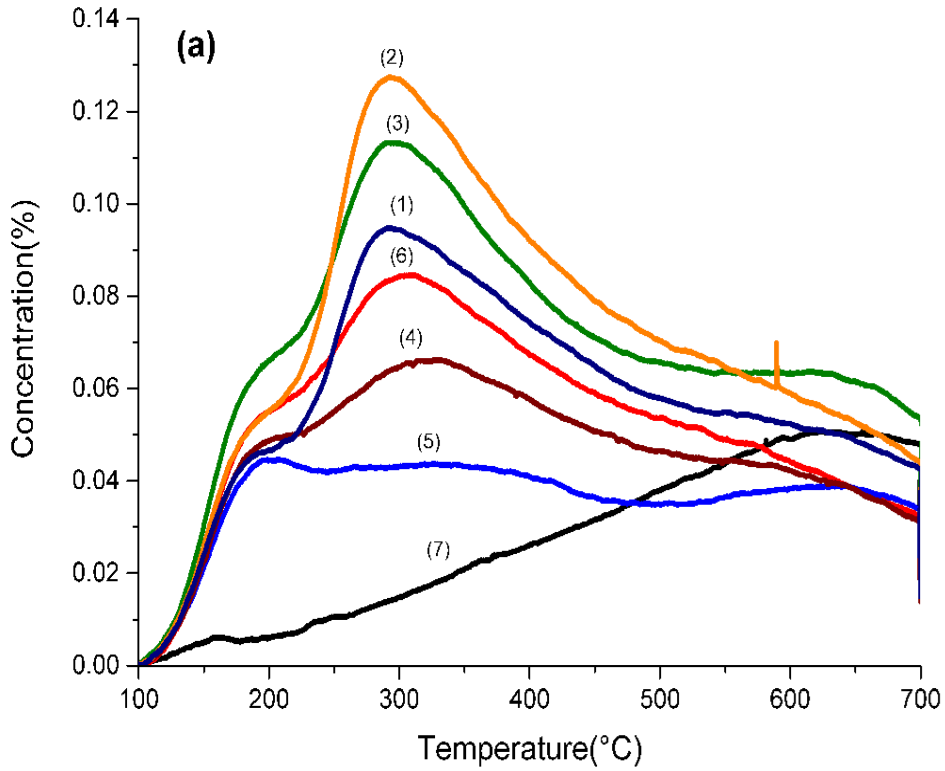

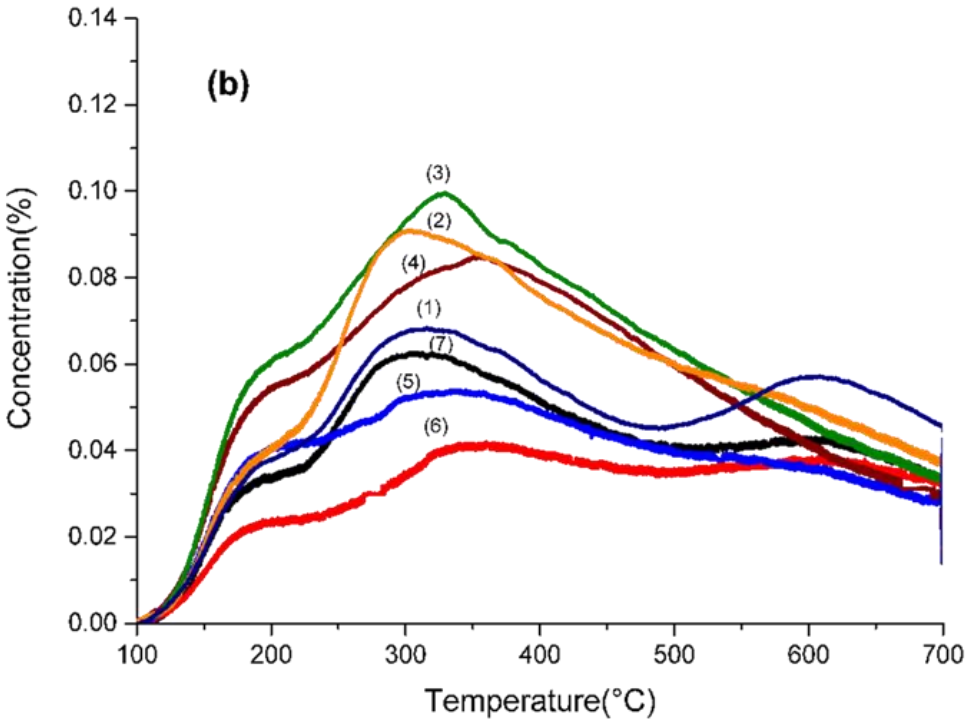


Figure 25: $NH_3$-TPD thermograms of: (1) $Si_0Al_{100}$, (2) $Si_{10}Al_{90}$, (3) $Si_{25}Al_{75}$, (4) $Si_{50}Al_{50}$, (5) $Si_{75}Al_{25}$, (6) $Si_{90}Al_{10}$ and (7) $Si_{100}Al_0$ prepared in (a) acidic medium and (b) basic medium .

The relative amounts of weak and medium-strong sites was estimated using the method of Katada *et al.* [298] A Gaussian function centered at 180 °C was fitted to the peak and attributed to weak acidic sites. The rest of the peak was attributed to medium and strong acidic sites. The total amount of ammonia desorbed from each sample, the values of total acidity for samples prepared in acidic and basic medium are approach are given in Table 7. The density of acidic sites increased with the alumina content up to and then tended to decrease for higher alumina contents. The same observation can be made concerning the acidity strength.

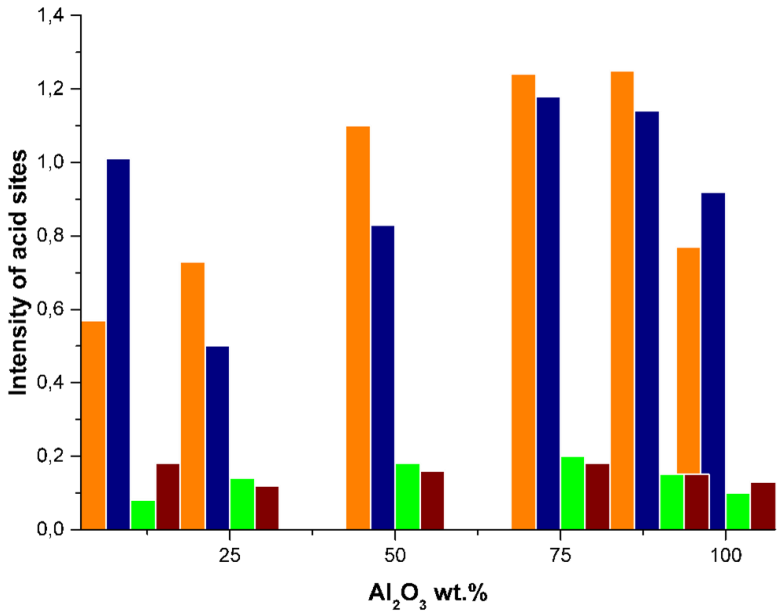


Figure 26: Comparison between acidity values obtained in acidic and basic medium, where (orange) and (blue) columns present strong acid sites in basic and acetic media respectively, while (green) and (brown) present weak acid sites in basic and acetic media respectively.

## II.4.Conclusions

In this part, we showed that hydrolytic sol-gel HSG route was successfully used to prepare ($Si_xAl_y$) mixed oxides from non-expensive precursors. The oxides were prepared in acidic and basic medium. The Si/Al ratio can be easily controlled, knowing that it plays an important role in the structure, texture, acidity of the samples. Calcination in air largely eliminates carbon from essentially non-condensed groups and the solvent. The composition of all samples prepared by HSG route show good control on composition. The $N_2$-physisorption measurements showed that the samples are mesoporous and texture strongly depends on the composition and pH. The $N_2$-adsorption desorption showed that samples prepared in basic medium show higher specific surface area and pore volume than samples prepared in acidic medium. The structure of all samples were studied by XRD and NMR, the results showed that all the mixed oxides are amorphous. Broad reflections typical of bulk γ-alumina were detected for the samples with high alumina loading. However, the study of the structure showed that there is not significant difference considering the synthesis conditions. The acidity was also studied; the presence of strong, medium or weak acid sites appeared related to the presence of alumina. As Al is introduced in silica-rich formulations, the density of both weak and medium/strong acidic sites increases and reaches a maximum for alumina contents of 75-90 wt.%.

# Chapter III

# Silica-alumina: non-hydrolytic sol-gel synthesis, characterizations and application in esterification reaction

# III.1. Introduction

A novel non-hydrolytic sol-gel (NHSG) synthesis of mesoporous aluminosilicate is presented by the action of alcohols on halides. Bourget *et al* reported the synthesis of silica by alcohol route, [299] using solvent-free non-hydrolytic condensation reaction between silicon tetrachloride with benzyl alcohol as oxygen donor. The reactions involved in the alcohol route, depend on the nature of the alcohol (primary, secondary or tertiary alcohol). In the case of silicon, tetraalkoxysilanes are formed by reaction of silicon tetrachloride with primary and secondary alcohol [189] whereas the reaction with tertiary and benzylic alcohols leads to silica and the corresponding alkyl halide.[300] Independently of the starting alcohol, initially the reaction involve the coordination of a lone pair of electrons of an alcoholic oxygen atom to the silicon center, followed by the cleavage of either the hydroxyl or alkoxyl group (Scheme 8).[189]

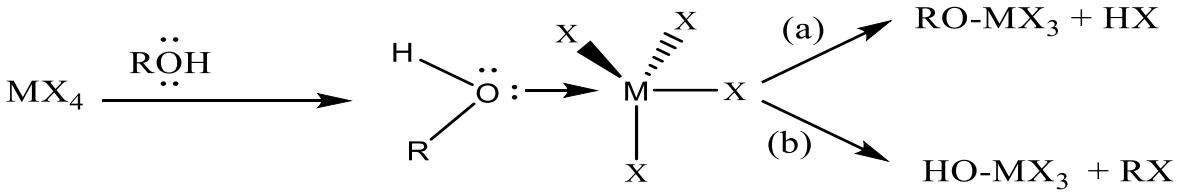


Scheme 8: Production of hydroxyl groups through a cyclic elimination mechanism.[189]

Arnal *et al*. reported the formation of monolithic gels leading to mesoporous anatase by reaction of $TiCl_4$ with isopropyl alcohol.[301] In addition, Niederberger et *al.* reported NHSG routes for the reaction between $TiCl_4$ and benzyl alcohol to synthesize a highly crystalline titania nanoparticles.[302] They found that benzyl alcohol and titanium chloride provide exceptionally versatile reaction system for the synthesis of spherical titania nanoparticles. The NHSG process gives excellent control of the size, phase and crystallinity. Later, they extended this route to different metal organic precursors like metal alkoxides, or acetylacetonates.[303] The reaction is typically performed in a temperature range of 50-250°C. The so-called benzyl alcohol route, in which various metal oxide precursors are reacted with benzyl alcohol used as a solvent and an oxygen donor provides a particularly versatile reaction system that gave access to a large number of metal oxide nanoparticles and oxide-based inorganic-organic nanohybrids.[304] Furthermore,

J.M.Szeifert *et al*.reported the synthesis of ultra-small (≈ 3 nm size) and highly soluble anatase nanoparticles by the reaction of $TiCl_4$ with tert-butyl alcohol under microwave heating, with reaction times of less than (1h) at temperatures as low as 50°C.[305] More recently, Nassar, *et al* reported the synthesis of lanthanide-doped alumina by reaction of $AlCl_3$ and $YCl_3$ precursors with ethanol.[306]

In this chapter, we present the synthesis of silica-alumina mixed oxides using two NHSG routes (alcohol and ether). Aluminosilicate have a uniform molecular pore size, high surface acidity, and large number of active sites. These features gave these materials potential candidates for various scientific as well as industrial applications, such as an ion exchangers, molecular sieves, and solid acid catalysts since the last century.[307] The effect of the synthetic route and the composition of $SiO_2$-$Al_2O_3$ on structure, texture and acidity was investigated.

# III.2. Results and discussion

## III.2.1.Synthesis and characterization

$SiO_2$-$Al_2O_3$ mixed oxides with various Si/Al ratio were prepared by alcohol route using two alcohols: a primary alcohol (ethanol) and a tertiary alcohol (tert-butanol) (Tables 21,22, Experimental Part). The same compositions were synthesized via ether route (Table 23, Experimental Part) in order to compare and study the effect of the oxygen donor on the physico-chemical properties. The $SiO_2$-$Al_2O_3$ mixed oxides with different Si/Al ratios (0, 0.1, 1, 8, ∞) were synthesized using silicon tetrachloride ($SiCl_4$, Alfa Aesar, 99.98%), aluminum trichloride ($AlCl_3$, Alfa Aesar, 99.98%).

In alcohol route, all $SiO_2$-$Al_2O_3$ samples were synthesized by NHSG process through using two different types of alcohols (ethanol and tertiary butanol) which play as a solvent and oxygen donor in the same time (Scheme 9). The mixed oxides were synthesized by adding precursors ($SiCl_4$, $AlCl_3$) in a Schlenk tube under argon atmosphere inside the glove box (non-aqueous medium).

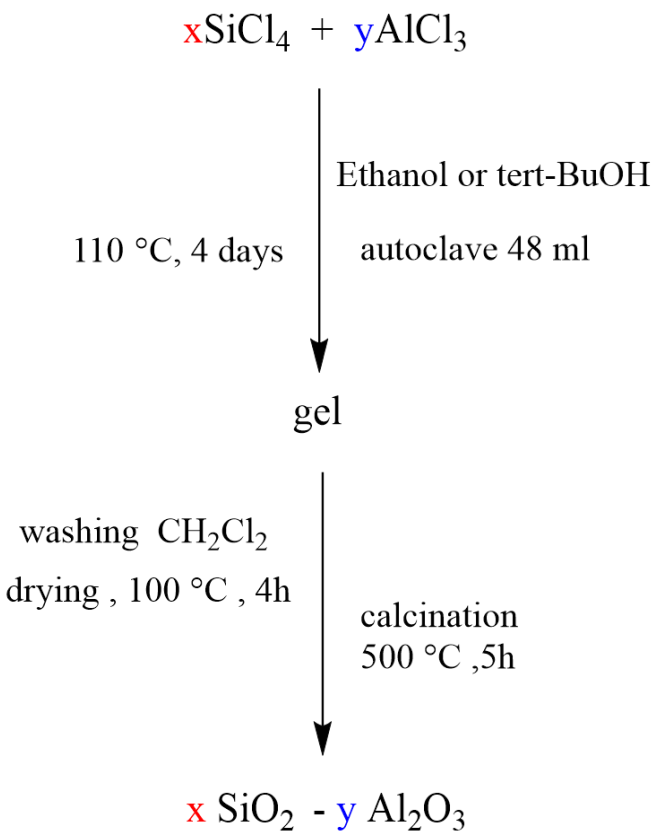


Scheme 9: NHSG process using alcohols as oxygen donors for the preparation of silica-alumina mixed oxides.

An excess amount of alcohol (25 ml) of EtOH or $^{t}$BuOH were added into the schlenk (outside the glove box) by using the syringe technique, the reason for this being that reaction is accompanied with releasing HCl. Next, the reactant were transferred into an autoclave under Argon. The reaction takes place at 110 °C under autogenous pressure for 4 days, after being cooled to room temperature, light or clear gel were produced. The product was isolated by filtration and purified by successive washing with $CH_2Cl_2$ to remove unreacted species and bi-products. Powders were manually grinded by using mortar after drying 1h at room temperature and 4h at 100 °C. Finally, the samples were calcined under air at 500 °C for 5h. The powders color ranging from white to gray depending on the Al content. The samples were labeled as $Si_xAl_y$ where x and y are the expected weight percentage of $SiO_2$ and $Al_2O_3$, respectively. The $SiO_2$ and $Al_2O_3$ content varies from 0 to 100 wt. %.

In ether route (Scheme 10), the mixed oxides with formula $SiO_2$-$Al_2O_3$ were synthesized under argon atmosphere inside the glove box (non-aqueous medium), by using dried $SiCl_4$, $AlCl_3$ as

silicon and aluminum precursors. Dry di-isopropyl ether (< 4 ppm $H_2O$) was used as oxygen donor and all the reactants were dissolved in 10 ml of dry $CH_2Cl_2$ (< 6 ppm $H_2O$) inside the autoclave under stirring. The reaction was performed at 110 °C under autogenous pressure for 4 days. Colorless or white gel products were obtained. The gels were isolated by filtration and purified by washing with $CH_2Cl_2$ to remove unreacted species and bi-products. The final products were dried at 25 °C for 1h and then dried at 100 °C for 4h. Powders were grinded manually by using mortar to obtain fine powders

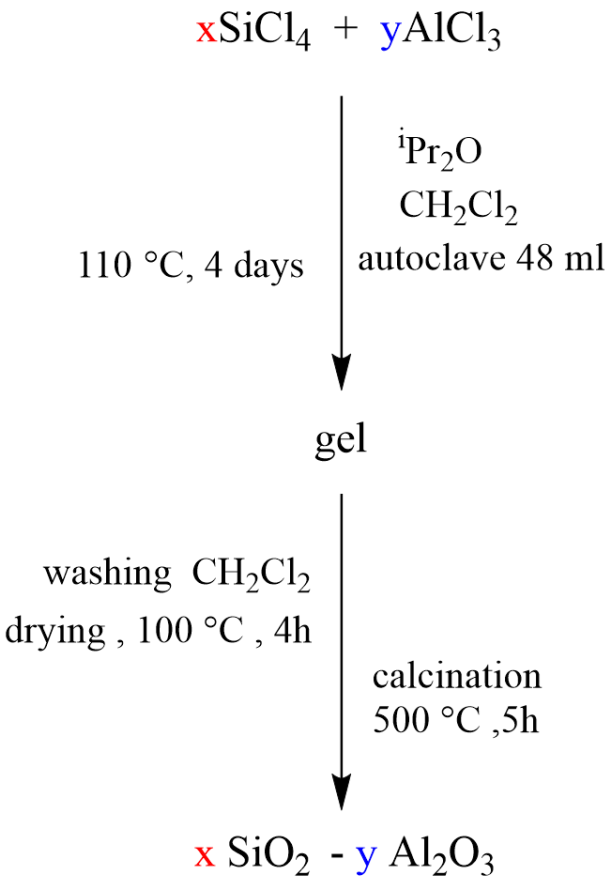


Scheme 10: NHSG process using $^{i}Pr_2O$ as oxygen donors for the preparation of silica-alumina mixed oxides.

## III.2.2. Composition

### III.2.2.1. Scanning electron microscopy (SEM)

SEM images were performed to study the structure and morphology of the prepared samples. Silica-alumina were prepared with different compositions and different oxygen donors were tested. First, on the SEM images of the silica-alumina prepared *via* EtOH and $^{i}Pr_2O$ routes, the solids are hard and compact (Figures 29 a, b, e and f ). However a powder is obtained by using tBuOH route (Figures 31 c and d). The size of the mixed oxides range from micrometer to millimeter scale.

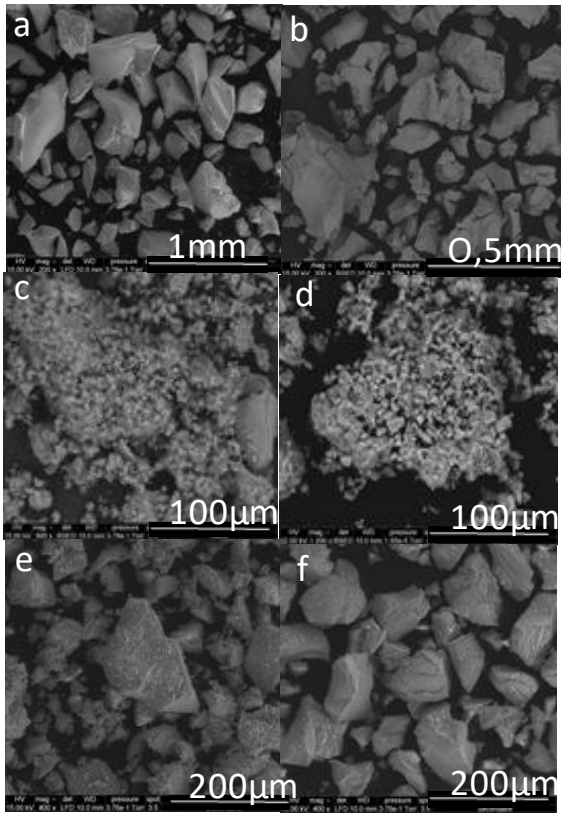


Figure 27: SEM images for samples with different compositions and different oxygen donors : with EtOH (a) $Si_{75}Al_{25}$, (b) $Si_{25}Al_{75}$ , with $^{t}BuOH$ (c) $Si_{75}Al_{25}$, (d) $Si_{25}Al_{75}$, with $^{i}Pr_2O$ (e) $Si_{75}Al_{25}$, (f) $Si_{25}Al_{75}$.

### III.2.2.2. Energy dispersive X-ray analysis (EDX)

Composition analyzed by EDX spectroscopy (Table 8) shows that there is a relatively good accordance between experimental weight content and nominal ones. These results show that the NHSG provide good control on the composition of the final mixed oxide. EDX analysis shows that

samples prepared by alcohol route are homogeneous at the micrometric scale by taking three measurements for each sample. The solids are hard and compact when Al is a minority and in the form of fine powder when Al is the majority.

Table 8: Compositions (atomic %) by EDX measurements for $SiO_2$-$Al_2O_3$ prepared with EtOH, $^t$BuOH and $^i Pr_2O$.

| Samples | Nominal | | | Experimental | | | Oxygen donor |
|---|---|---|---|---|---|---|---|
| | Si/(Si+Al) | Al/ (Si+Al) | Si/Al | Si/(Si+Al) | Al/ (Si+Al) | Si/Al | |
| $Si_{100}Al_0$ * | 100 | 0.0 | ∞ | 100 | 0.0 | ∞ | EtOH |
| $Si_{100}Al_0$ | 100 | 0.0 | ∞ | 100 | 0.0 | ∞ | $^t$BuOH |
| $Si_{100}Al_0$ | 100 | 0.0 | ∞ | 100 | 0.0 | ∞ | $^i Pr_2O$ |
| $Si_{90}Al_{10}$ | 93.6 | 6.4 | 14.6 | 95.2±1.2 | 4.8±0.04 | 19.8 | EtOH |
| $Si_{90}Al_{10}$ | 93.6 | 6.4 | 14.6 | 94.7±0.9 | 5.3±0.07 | 17.9 | $^t$BuOH |
| $Si_{90}Al_{10}$ | 93.6 | 6.4 | 14.6 | 95.8±0.6 | 4.2±0.1 | 22.8 | $^i Pr_2O$ |
| $Si_{75}Al_{25}$ | 71.8 | 28.2 | 2.5 | 68.1±0.8 | 31.9±0.06 | 2.1 | EtOH |
| $Si_{75}Al_{25}$ | 71.8 | 28.2 | 2.5 | 78.4±0.2 | 21.6±0.07 | 3.6 | $^t$BuOH |
| $Si_{75}Al_{25}$ | 71.8 | 28.2 | 2.5 | 69.5±0.5 | 30.5±0.3 | 2.3 | $^i Pr_2O$ |
| $Si_{50}Al_{50}$ | 51.4 | 48.6 | 1.06 | 43.5±1.3 | 56.5±0.1 | 0.7 | EtOH |
| $Si_{50}Al_{50}$ | 51.4 | 48.6 | 1.06 | 47.7±0.9 | 52.3±0.4 | 0.9 | $^t$BuOH |
| $Si_{50}Al_{50}$ | 51.4 | 48.6 | 1.06 | 44.4±0.1 | 55.6±0.05 | 0.8 | $^i Pr_2O$ |
| $Si_{25}Al_{75}$ | 22.1 | 77.9 | 0.28 | 28.0±1.3 | 72.0±0.08 | 0.4 | EtOH |
| $Si_{25}Al_{75}$ | 22.1 | 77.9 | 0.28 | 23.2±0.7 | 76.8±0.2 | 0.3 | $^t$BuOH |
| $Si_{25}Al_{75}$ | 22.1 | 77.9 | 0.28 | 24.1±1.2 | 75.9±0.06 | 0.3 | $^i Pr_2O$ |
| $Si_{10}Al_{90}$ | 15.8 | 84.2 | 0.19 | 17.1±0.6 | 82.9±0.04 | 0.2 | EtOH |
| $Si_{10}Al_{90}$ | 15.8 | 84.2 | 0.19 | 18.3±1.3 | 81.7±0.08 | 0.2 | $^t$BuOH |
| $Si_{10}Al_{90}$ | 15.8 | 84.2 | 0.19 | 16.6±0.3 | 83.4±1.1 | 0.19 | $^i Pr_2O$ |
| $Si_0Al_{100}$ | 0.0 | 100 | 0.0 | 0.0 | 100 | 0.0 | EtOH |
| $Si_0Al_{100}$ | 0.0 | 100 | 0.0 | 0.0 | 100 | 0.0 | $^t$BuOH |
| $Si_0Al_{100}$ | 0.0 | 100 | 0.0 | 0.0 | 100 | 0.0 | $^i Pr_2O$ |

∗ 1mol% $AlCl_3$ added as catalyst.

## III.2.3. Structure

### III.2.3.1. X-Ray diffraction (XRD)

The X-ray diffractograms of the silica-alumina mixed oxides prepared *via* NHSG with different synthetic routes (EtOH, $^{t}$BuOH and $^{i}Pr_2O$) and calcined under air at 500 °C. For the samples containing a high concentration of aluminium oxide (samples without silica) even with different oxygen donor, the characteristic peaks of the gamma-alumina phase at 2Θ = 44° for (222) reflection and 2Θ = 66° for (440) reflection were detected. In the presence of silica content ($Si_{25}Al_{75}$), broad peaks at (2Θ = 23°) of amorphous silica were started to appear and the intensity of characteristic peaks of gamma-alumina were observed to decrease which is an indication of aluminium incorporation (Figure 30).

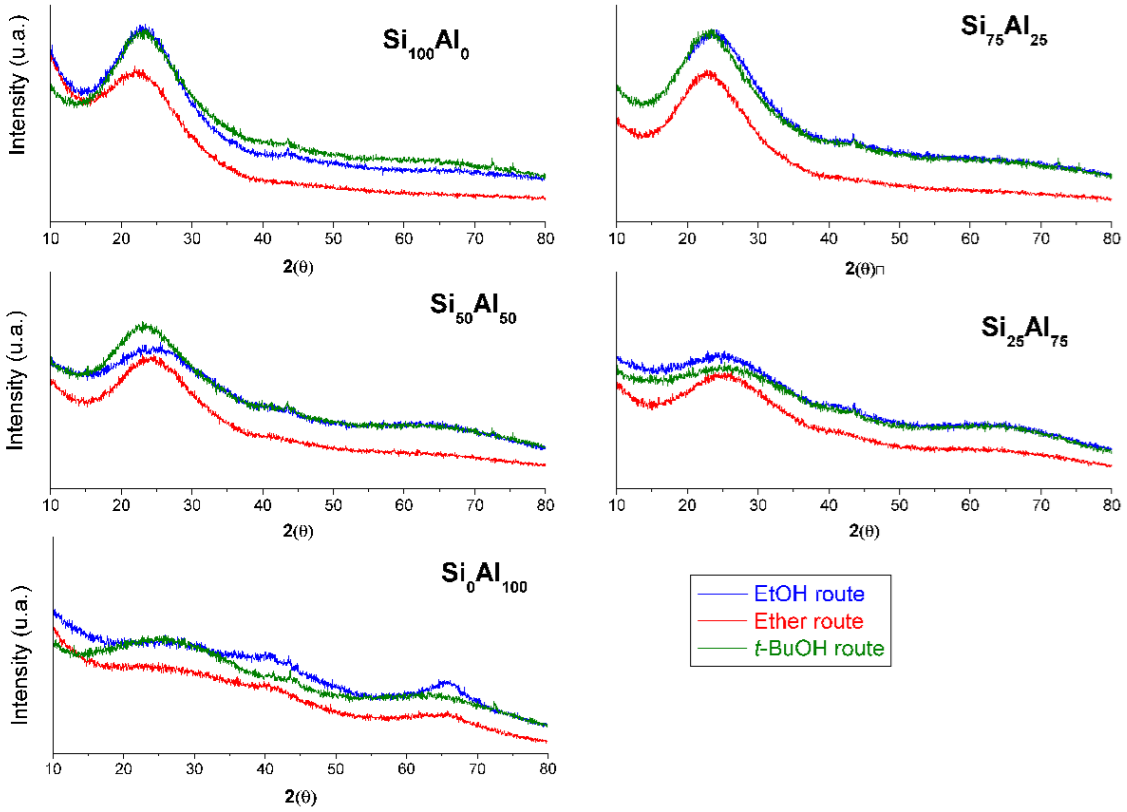


Figure 28: Diffractograms of $Si_xAl_y$ samples prepared with (a) EtOH (b) $^{t}$BuOH and (c) $^{i}Pr_2O$ and (d) X-ray diffraction patterns of the prepared silica-containing alumina with different $Al_2O_3/SiO_2$ M ratios.[308]

Increasing Si content from 0 to 100 is accompanied with decrease of Al content from 100 to 0 leads to increase the intensity of the peak at ($2\Theta = 23°$) and decrease the intensity of peaks at $2\Theta = 44°$, 66° until disappeared revealing presence of silica and absence of alumina. As conclusion, oxygen donor did not influence on the structure of the mixed oxides. It is then concluded that amorphous character of the obtained silica-alumina systems generally indicates a well-mixed two-component oxide. The obtained results are in agreement with previous studies reported by V. La Porla *et al*, J.G.Checmanowski *et al.* and O.Saber *et al.* for silica-alumina mixed oxides prepared by sol-gel process and calcined at 500 °C.[308-310]

## III.2.3.2. Nuclear magnetic resonance (NMR)

Solid $^{29}Si$ and $^{27}Al$ NMR, in rotation at the magic angle (MAS-NMR) have been used to study the environment of the Si and Al atoms. In $^{29}Si$ NMR, the chemical shift of the Si atoms in an aluminosilicate network depends on the nature of the second neighbors, Si, H, or Al. Each replacement of a silicon second neighbor by an H or an Al leads to a downfield shift. For instance, in silicas, $[Si(OSi)_4]$ ($Q^4$), $[Si(OSi)_3(OH)]$ ($Q^3$) and $[Si(OSi)_2(OH)_2]$ ($Q^2$) sites are found at about -110 ppm, -100, and -92 respectively. In aluminosilicates, $[Si(OSi)_3(OAl)]$, ($Q^{3Al}$), $[Si(OSi)_2(OAl)_2]$ ($Q^{2Al}$), $[Si(OSi)(OAl)_3]$ ($Q^{3Al}$), and $[Si(OAl)_4]$ ($Q^{4Al}$) sites are found at about -102 ppm, -96, -90, and -86, respectively. Figure 31 shows the $^{29}Si$ MAS NMR spectra of $Si_xAl_y$ samples prepared by $^{i}Pr_2O$ and EtOH routes respectively. For the samples prepared with EtOH, the spectrum of $Si_{100}Al_0$ shows a main peak centered at -110 ppm assigned to $Q^4$ $[Si(OSi)_4]$ and smaller peaks at (-100 and -93 ppm) assigned to $Q^3$ $[Si(OSi)_3(OH)]$ and $Q^2$ $[Si(OSi)_2(OH)_2]$ respectively.[247] When the percentage of alumina increases, the signal broadens and shifts, due to the formation of Si-O-Al bonds. The spectrum of $Si_{25}Al_{75}$ sample shows a major resonance at -85 ppm assigned to $[Si(OAl)_4]$ ($Q^{4Al}$) or $[Si(OAl)_3(OH)]$ ($Q^{3Al,OH}$) sites. [311]

For comparison, the spectra of the samples prepared by the ether route appear closer to the spectra of the samples prepared from EtOH, with a large number of Si-O-Al bridges.

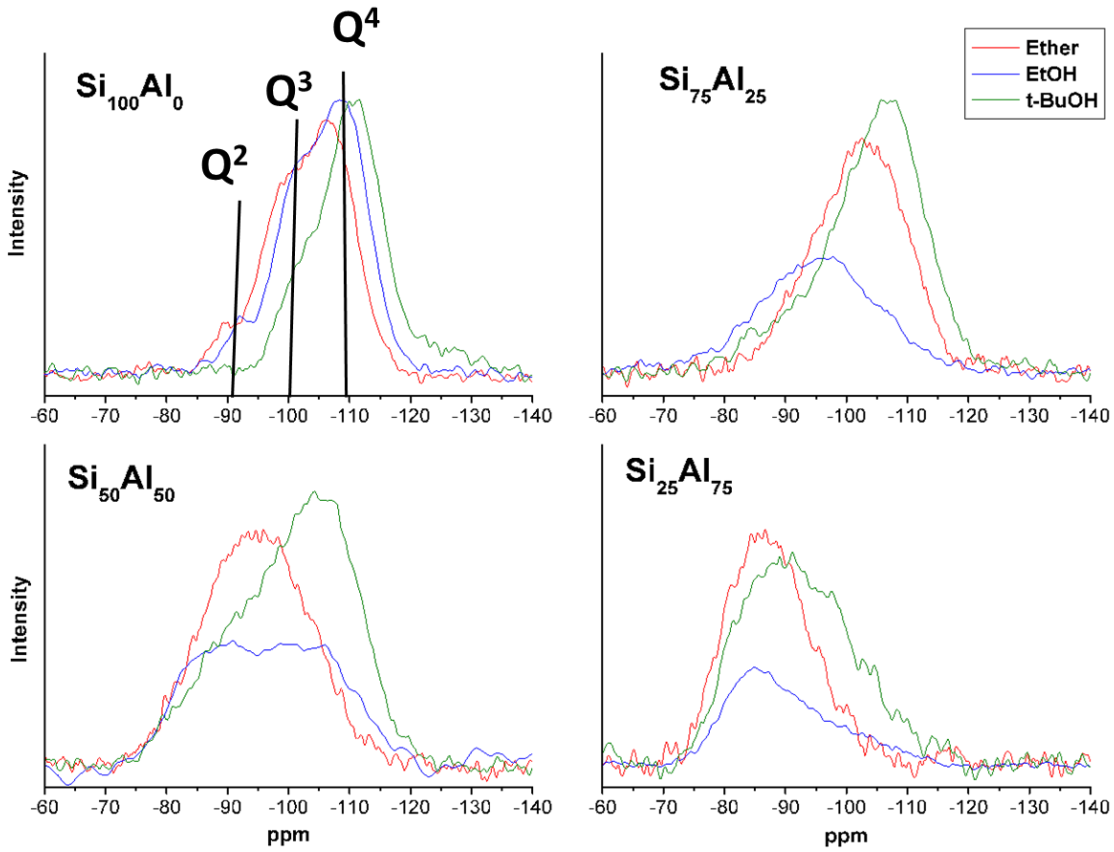


Figure 29: $^{29}$Si MAS NMR of alumina-silica mixed oxides prepared by alcohol route $^{i}Pr_2O$ route.

$^{27}$Al MAS (SP) NMR: The spectra of $Si_xAl_y$ samples using EtOH and $^{t}$BuOH and ether route are presented in Figure 32. Aluminum atoms in crystalline aluminas are usually in coordination 6 ($Al^{VI}$) in the 0-7 ppm range and coordination 4 ($Al^{IV}$) in the 50-70 ppm range).[312] In amorphous alumino-silicate, Al atoms are also observed in coordination 5 ($Al^{V}$) in the 20-40 ppm range.[313]

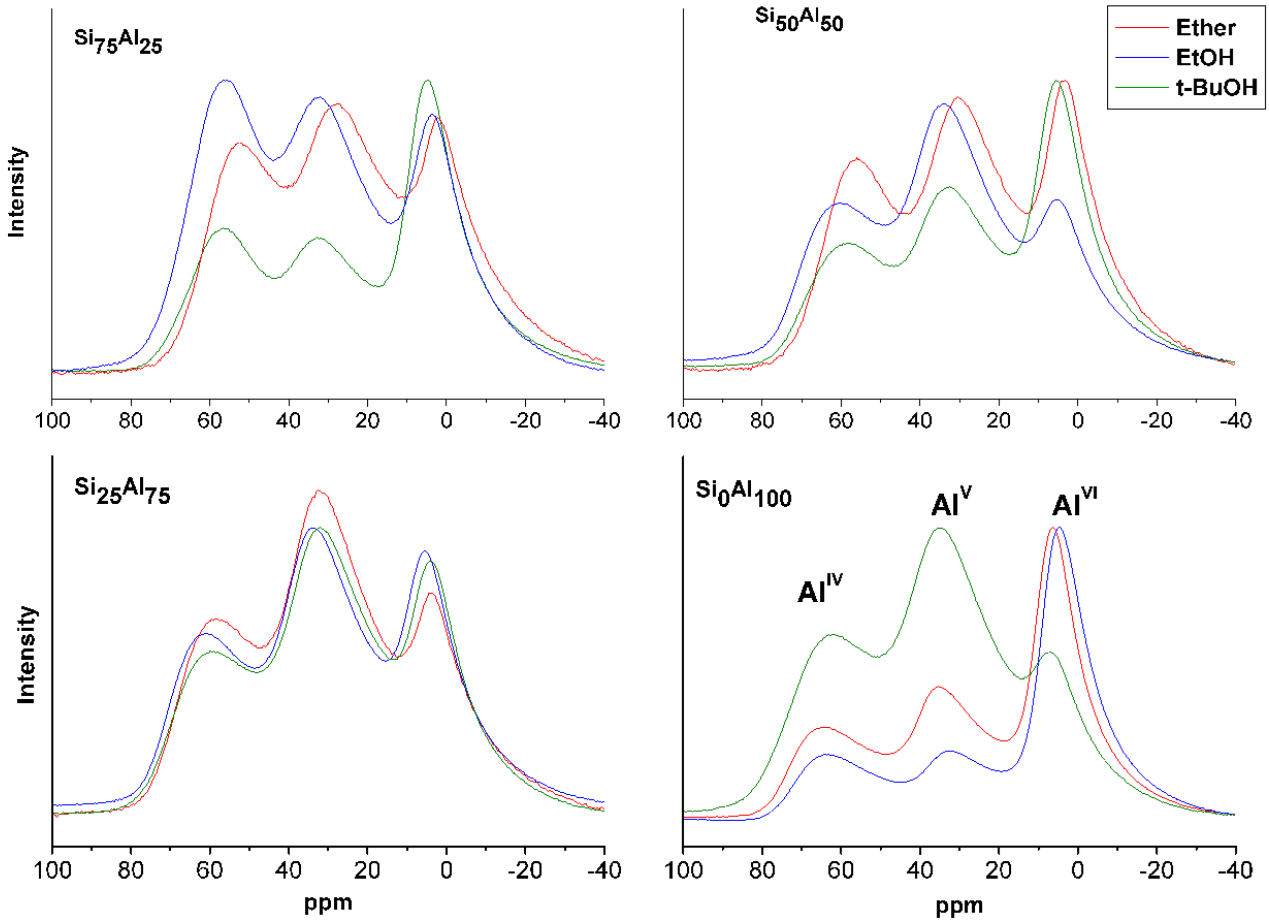


Figure 30: $^{27}$Al MAS NMR of silica-alumina mixed oxides prepared by EtOH, $^{t}$BuOH and $^{i}Pr_2O$ routes.

As shown in Figure 32, the spectra of all samples prepared by NHSG exhibit clearly three peaks at ca 65, 35, and 5 ppm, assigned to $Al^{IV}$, $Al^{V}$ and $Al^{VI}$, respectively.[288] For the samples prepared with EtOH, the spectrum of the alumina sample ($Si_0Al_{100}$) shows a major resonances arising from $Al^{VI}$ sites, and when the Si content increases the proportion of $Al^{V}$ and $Al^{IV}$ sites increases at the expense of $Al^{VI}$ sites. The spectra of samples prepared with $^{t}$BuOH show an opposite behavior: the spectrum of the alumina sample ($Si_0Al_{100}$) shows major resonances arising from $Al^{V}$ and $Al^{IV}$ sites, and when the Si content increases the relative amount of $Al^{VI}$ sites increases at the expense of increasing the proportion of $Al^{V}$ and $Al^{IV}$ sites. Leonardo et *al* .[289] and Hensen et *al* [35] observe

a similar behavior in the case of amorphous aluminosilicates. Again, the spectra of the samples prepared by the ether route appear quite similar to that of the samples prepared by the ethanol route, suggesting similar structures.

## III.2.4. Texture

The specific surface area, pore volume, and pore size distribution data derived from nitrogen adsorption are shown in Table 9. The pore diameter data range between 2 and 14 nm revealing a mesoporous structure of $Si_xAl_y$. The texture of the samples depends on the composition and the synthetic route (type of oxygen donor). For the samples made by pure silica, the highest specific surface area were obtained for EtOH (677 $m^2 g^{-1}$), $^t$BuOH (467 $m^2 g^{-1}$) and $^i$Pr$_2$O(595 $m^2 g^{-1}$). A decrease in the specific surface area was combined with the decrease in silica content. The specific surface area tends to increase again for the sample with pure alumina $Si_0Al_{100}$. For similar composition, the highest specific surface area was obtained for the samples prepared by EtOH route. To confirm the reproducibility of the synthetic procedure each experiment was performed twicely.

Table 9: Texture of $SiO_2$ $Al_2O_3$ samples measured by $N_2$- physisorption.

| Samples | Si/Al | Texture | | | Oxygen donor |
|---|---|---|---|---|---|
| | | S ($m^2 g^{-1}$) | $V_P$ ($cm^3 g^{-1}$) | $D_P$ (nm) | |
| $Si_{100}Al_0$ | ∞ | 677 | 0.4 | 2.2 | EtOH |
| $Si_{100}Al_0$ | ∞ | 370 | 0.6 | 5.1 | $^t$BuOH |
| $Si_{100}Al_0$ | ∞ | 595 | 1.9 | 13.8 | $^i$Pr$_2$O |
| $Si_{90}Al_{10}$ | 9 | 479 | 0.6 | 2.0 | EtOH |
| $Si_{90}Al_{10}$ | 9 | 421 | 0.5 | 5.3 | $^t$BuOH |
| $Si_{90}Al_{10}$ | 9 | 459 | 0.6 | 6.8 | $^i$Pr$_2$O |
| $Si_{75}Ai_{25}$ | 3 | 380 | 0.2 | 2.3 | EtOH |
| $Si_{75}Ai_{25}$ a | 3 | 340 | 0.5 | 6.1 | $^t$BuOH |
| $Si_{75}Al_{25}$ b | 3 | 355 | 0.5 | 5.7 | $^t$BuOH |
| $Si_{75}Al_{25}$ | 33 | 335 | 0.6 | 6.8 | $^i$Pr$_2$O |
| $Si_{50}Ai_{50}$ | 1 | 195 | 0.1 | 2.3 | EtOH |

| | | | | | |
|---|---|---|---|---|---|
| $Si_{50}Ai_{50}$ | 1 | 90 | 0.2 | 9.9 | $^{t}$BuOH |
| $Si_{50}Al_{50}$ | 1 | 312 | 0.6 | 8.4 | $iPr_2O$ |
| $Si_{25}Al_{75}$ | 0.33 | 170 | 0.1 | 2.8 | EtOH |
| $Si_{25}Al_{75}$ | 0.33 | 30 | 0.1 | 16.7 | $^{t}$BuOH |
| $Si_{25}Al_{75}$ | 0.33 | 200 | 0.3 | 6.8 | $^{i}Pr_2O$ |
| $Si_{10}Al_{90}$ | 0.1 | 287 | 0.3 | 5.5 | EtOH |
| $Si_{10}Al_{90}$ | 0.1 | 71 | 0.1 | 11.5 | $^{t}$BuOH |
| $Si_{10}Al_{90}$ | 0.1 | 264 | 0.2 | 8.1 | $^{i}Pr_2O$ |
| $Si_{0}Al_{100}$ | 0 | 360 | 0.2 | 3.1 | EtOH |
| $Si_{0}Al_{100}$ | 0 | 90 | 0.3 | 2.4 | $^{t}$BuOH |
| $Si_{0}Al_{100}$ | 0 | 197 | 0.2 | 5.0 | $iPr_2O$ |

All samples displayed nitrogen adsorption/desorption isotherms of type IV. The samples prepared by $^{i}Pr_2O$ route showed isotherms of type IV according to the IUPAC classification. The relationship between $S_{BET}$, Vp, Dp, composition and type of NHSG route (oxygen donor) were studied (Figure 33).

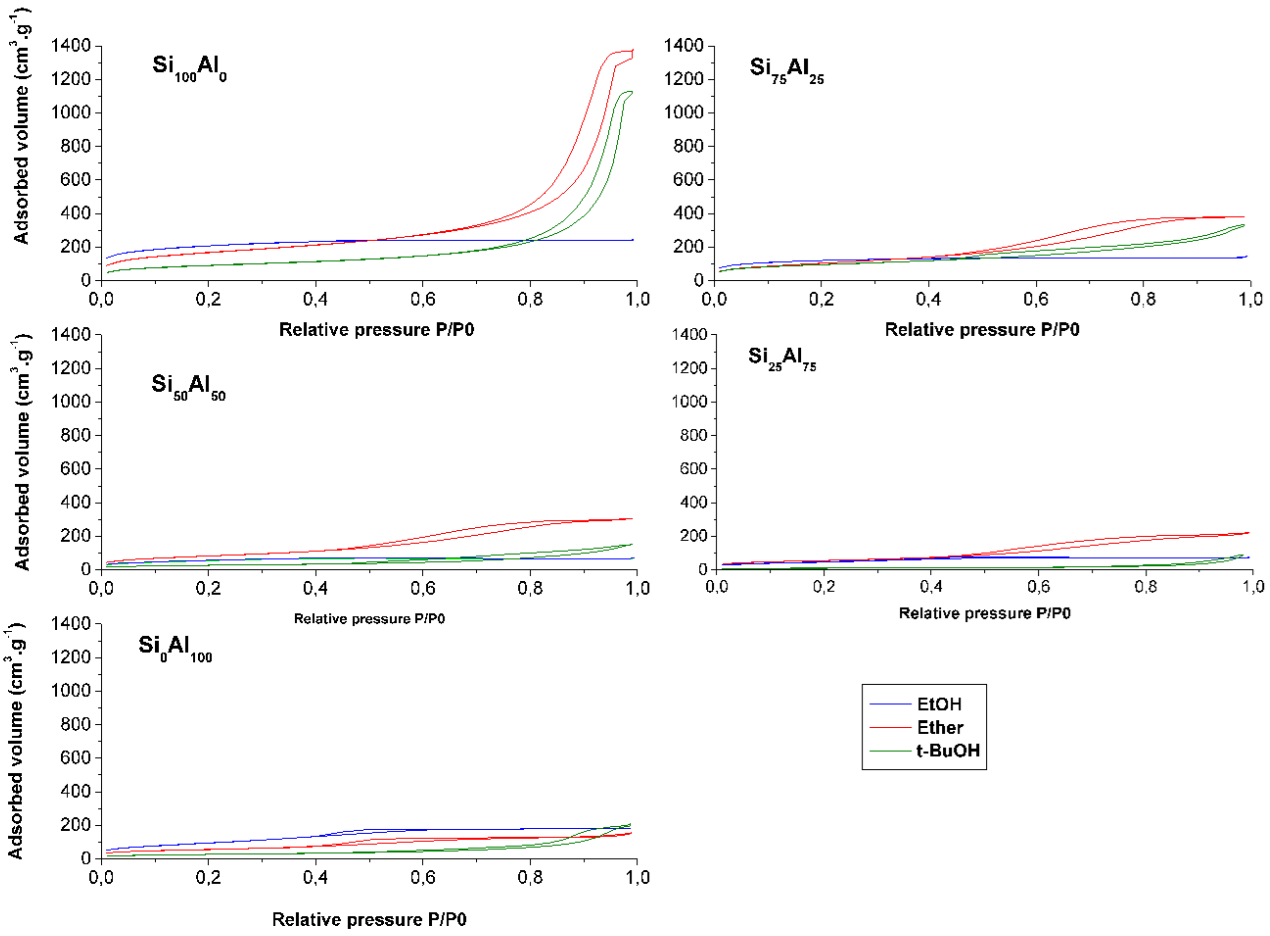


Figure 31: $N_2$ adsorption-desorption isotherm for $Si_xAl_y$ materials prepared with EtOH, $^t$BuOH and $^i Pr_2O$.

Specific surface area ($S_{BET}$) of samples prepared by different NHSG routes decreased when $Al_2O_3$ increased. While samples prepared with EtOH route presented higher $S_{BET}$ than samples prepared by $^i Pr_2O$ and $^t$BuOH routes (Figure 34 a). Pore volume (Vp) exhibited the same behavior of specific surface area ($S_{BET}$). The samples prepared by ether route have relatively higher pore volume compared to samples prepared with alcohols (Figure 34 b). The relation between pore diameter (Dp) and composition ($Al_2O_3$ wt. %) is quite complicated, while (Dp) decrease with the increase of $Al_2O_3$ for the samples prepared using $^i Pr_2O$ route, as samples prepared with EtOH and $^t$BuOH. It is clear that texture have been influenced by both composition and the route of synthesis (Figure 34 c).

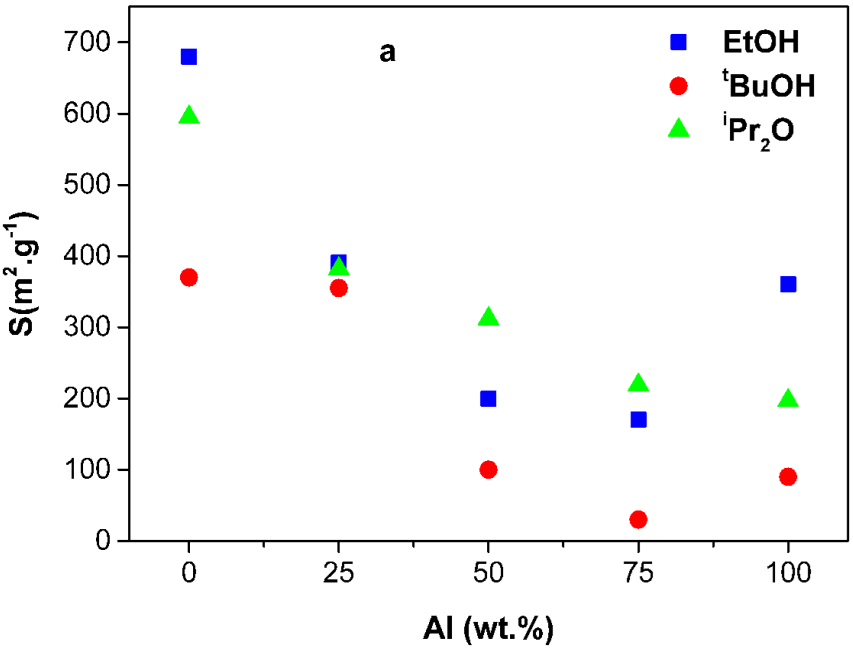
a
EtOH
tBuOH
iPr2O
S(m2.g-1)
700
600
500
400
300
200
100
0
0
25
50
75
100
Al (wt.%)

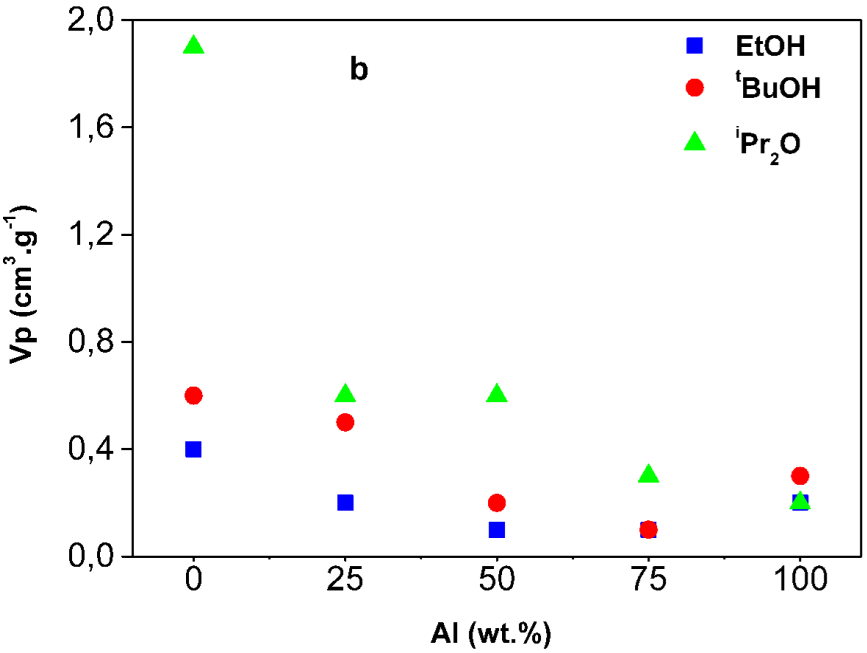
b
EtOH
tBuOH
iPr2O
Vp (cm3.g-1)
2,0
1,6
1,2
0,8
0,4
0,0
0
25
50
75
100
Al (wt.%)

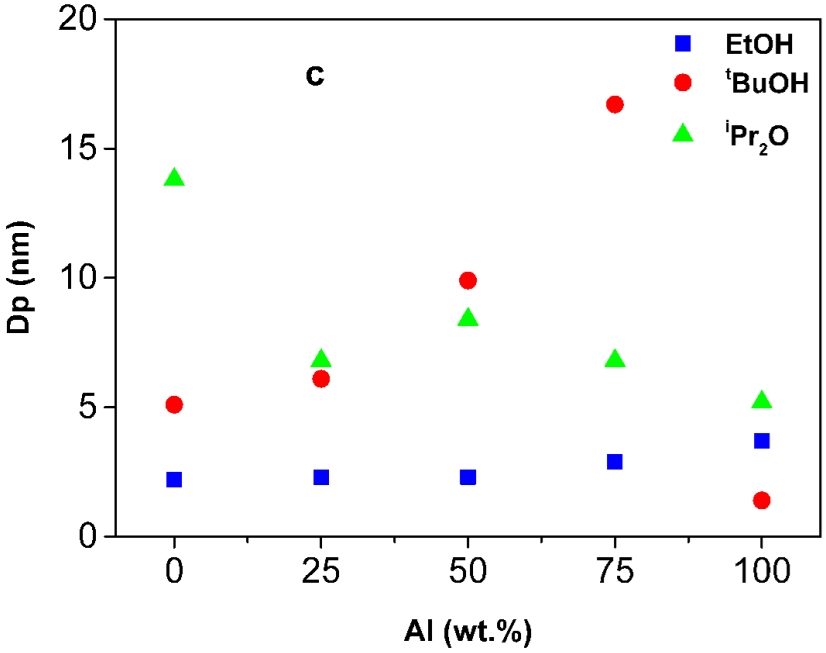


Figure 32: Relation between (a) $S_{BET}$, (b) Vp, (c) Dp and $Al_2O_3$% for mixed oxides prepared by EtOH ,$^{t}$BuOH and $^{i}Pr_2O$ route.

## III.2.5. Acidity

The acidic properties of the samples prepared by alcohol route and ether route were investigated by $NH_3$-TPD. The presence of medium or strong acidic sites appeared related to the presence of Al. As expected, the density of the accessible acid sites increase as the Si/Al ratio increases. Ammonia-TPD profiles of $Si_xAl_y$ samples with different Si/Al ratios and prepared by different routes are plotted in Figure 35.

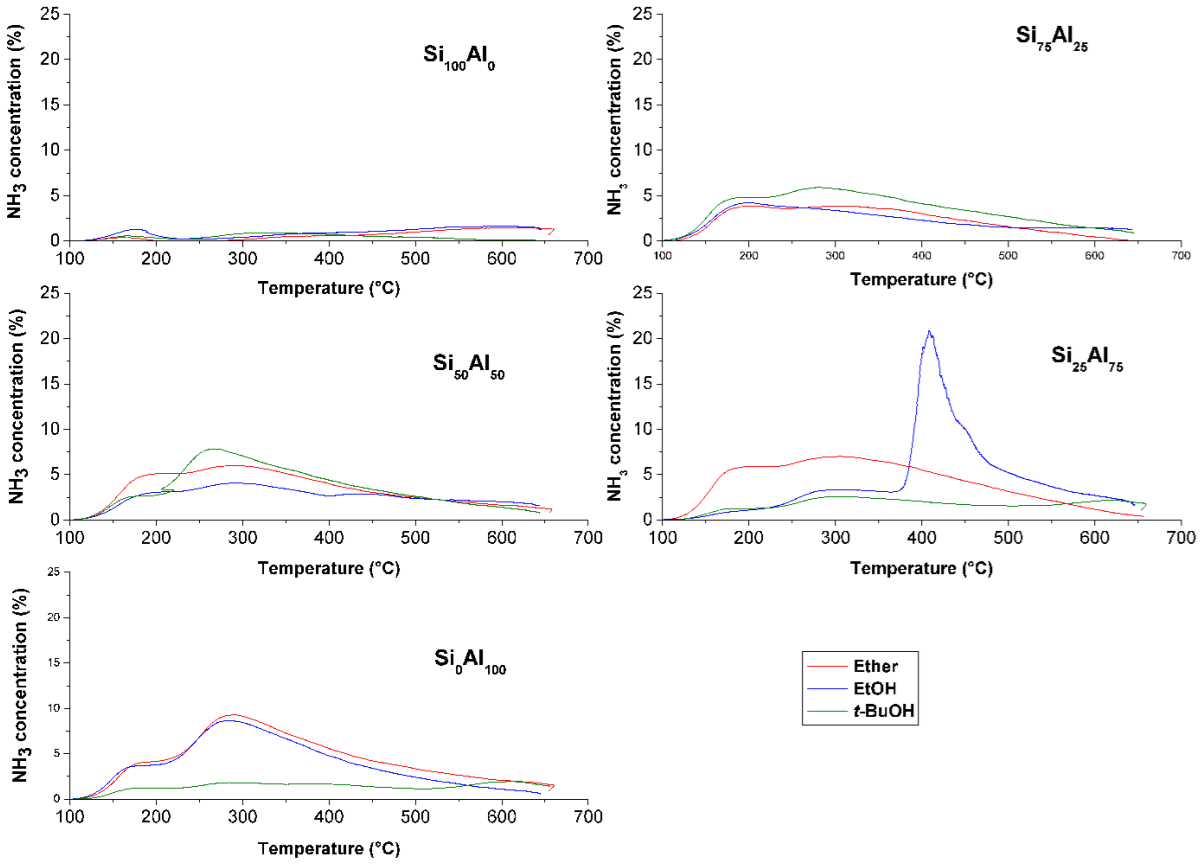


Figure 33: $NH_3$-TPD thermograms of different mixed oxides prepared with (a) EtOH,(b) $^{t}$BuOH and (c) $^{i}Pr_2O$.

The thermogram of $Si_{100}Al_0$ (0 wt.% of $Al_2O_3$) showed browed desorption profile near 200°C indicating the presence of weak acid sites [314]. The thermograms of all Al-containing samples showed that ammonia desorbed up to 500 °C, indicating the presence of higher strength acid sites.

Their acidity was intermediate between the weakly acids sites of silica and highly acidic sites found in zeolites.[297] This TPD profile suggests that $Si_xAl_y$ have mainly weak and medium acid sites. The quantitative evaluation of acidity shows this trend (Table 10), indicating that the total amount of ammonia desorbed from each sample. Following the method of Katada *et al.* [314], one Gaussian function was fitted to the peaks centered at 150 °C (attributed to weak acid sites). The signal that is not part of the Gaussian is attributed to medium and strong acid sites. The total acidity is relatively low for the silica-based samples and relatively high for all $Al_2O_3$-containing samples. The density in medium and strong acid sites increases according to the composition of the support: $Al_2O_3$> $SiO_2$-$Al_2O_3$> $SiO_2$. This order has also been observed by Handzlik.[315]

Table 10: Quantification of acidity in mmol/g obtained by $NH_3$-TPD for samples prepared with EtOH, t-BuOH and $^{i}Pr_2O$ .

| Sample | Total acidity | Weak acidity | Medium/ strong acidty | Oxygen donor |
|---|---|---|---|---|
| $Si_0Al_{100}$ | 2.8 | 0.9 | 1.9 | EtOH. |
| $Si_0Al_{100}$ | 2.7 | 0.8 | 1.9 | $^{t}$BuOH |
| $Si_0Al_{100}$ | 2.9 | 1.1 | 1.8 | $^{i}Pr_2O$ |
| $Si_{25}Al_{75}$ | 3.1 | 1.1 | 2.0 | EtOH. |
| $Si_{25}Al_{75}$ | 2.5 | 0.8 | 1.7 | $^{t}$BuOH |
| $Si_{25}Al_{75}$ | 2.6 | 0.8 | 1.8 | $^{i}Pr_2O$ |
| $Si_{50}Al_{50}$ | 2.0 | 0.6 | 1.4 | EtOH. |
| $Si_{50}Al_{50}$ | 1.8 | 0.5 | 1.3 | $^{t}$BuOH |
| $Si_{50}Al_{50}$ | 2.1 | 0.6 | 1.5 | $^{i}Pr_2O$ |
| $Si_{75}Al_{25}$ | 1.7 | 0.5 | 1.2 | EtOH. |
| $Si_{75}Al_{25}$ | 1.5 | 0.4 | 1.1 | $^{t}$BuOH |
| $Si_{75}Al_{25}$ | 1.8 | 0.7 | 1.1 | $^{i}Pr_2O$ |
| $Si_{100}Al_0$ | 0.1 | 0.1 | 0.0 | EtOH. |
| $Si_{100}Al_0$ | 0.1 | 0.1 | 0.0 | $^{t}$BuOH |
| $Si_{100}Al_0$ | 0.2 | 0.2 | 0.0 | $^{i}Pr_2O$ |

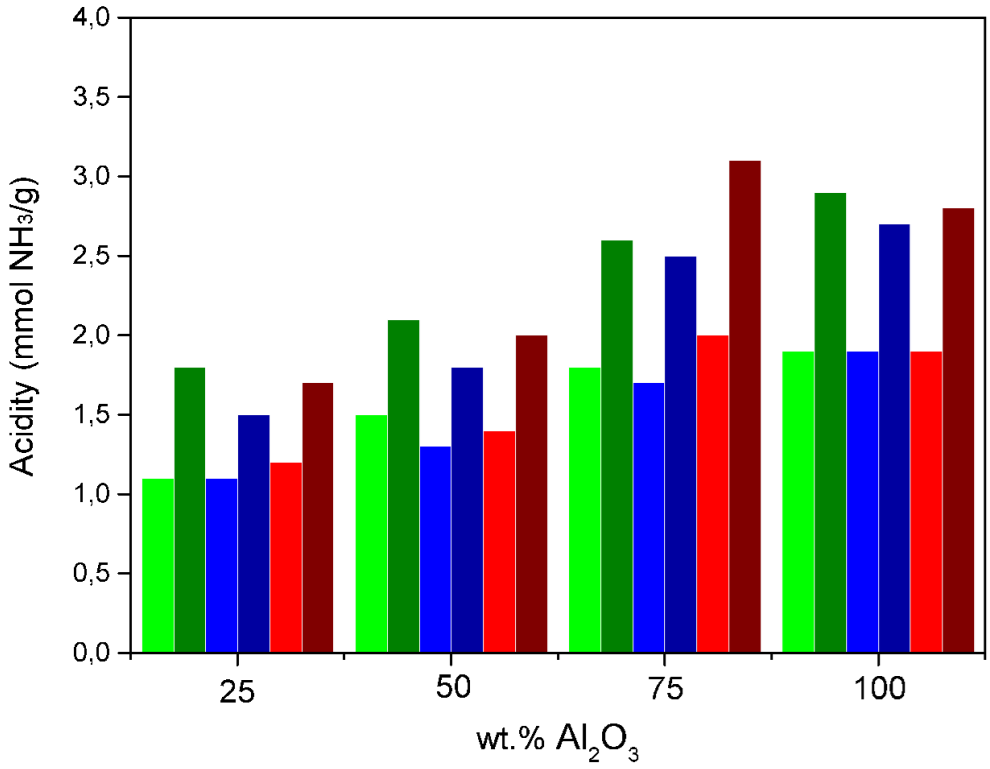


Figure 34: Influence of $Al_2O_3$ loading on acidity of $Si_x$-$Al_y$ samples where (brown): total acid sites with EtOH, (red): strong acid sites with EtOH, (dark blue): total acid sites with tBuOH, (light blue): strong acid sites with tBuOH, (green): total acid sites with ether,(light green): strong acid sites with ether.

## III.2.6. Application of Si-Al supports on esterification reaction

The silica alumina mixed oxides synthesized by sol-gel routes (HSG and NHSG) were tested in an esterification reaction used as model reaction to correlate acidity of the solids to an application in heterogeneous catalysis.

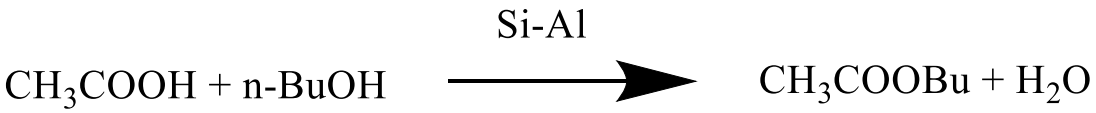


Scheme 11: Esterification reaction in toluene between acetic acid (5 mmol) and *n*-BuOH (10 mmol), catalysed by silica alumina mixed oxides, at 80 °C for 1 h.

As showed in Figure 37, the ester yields obtained by samples prepared by NHSG is much higher than those obtained by samples prepared by HSG.

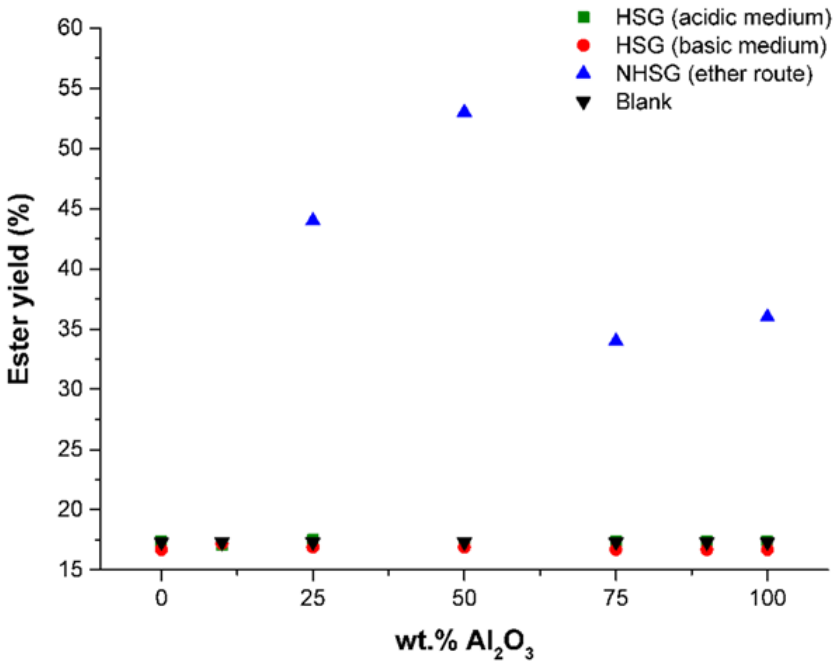


Figure 35: Ester yield using 100 mg of Si-Al supports prepared by HSG (acidic, basic medium) and NHSG routes.

The HSG samples activities not appeared to be dependent on the composition and were similar to the reference one. It suggests that HSG catalysts were not effective in the experimental conditions used in esterification reaction.

Conversely, all NHSG samples catalysed the conversion of acetic acid to *n*-butyl acetate with 100 % selectivity. The NHSG catalyst activity appeared to be highly dependent on the alumina content. The $Si_{50}Al_{50}$ and $Si_{75}Al_{25}$ catalysts shows the highest activities with a yield in ester of 53 and 44 %, respectively. These two compositions showed higher acidity, evaluated by $NH_3$-TPD, than $Si_{25}Al_{75}$ and $Si_{100}Al_0$ (Table 7). The high activity of NHSG catalysts compared to HSG ones can be clearly explained by an acid effect. The NHSG samples exhibited higher total amount of ammonia desorbed (from $NH_3$-TPD measurements) than those prepared by HSG (Tables 7 and 10). It's well known that solid catalysts which are acidic exhibited good catalytic performance in esterification reaction[316], suggesting they are more suitable for esterification reactions.[317] It is well known that when a tetracoordinated silicon atom in the zeolite framework is substituted by an aluminum atom, a cation is required to balance the negative charge; if the cation is a proton, a bridged hydroxyl group [Si-(OH)-Al] acting as a Brönsted acid site is formed.[317] Texture results

showed that catalysts prepared by NHSG showed lower $S_{BET}$ than HSG, therefore expecting higher acid density for catalysts prepared by NHSG (Tables 6 and 9). As seen in Figures 37 and 38, composition effected on catalytic activity, hence, Si/Al ratio affects the density and strength of acid sites, Si/Al ratio.[318]

To take into account the differences in Al content of the catalysts, we investigated the esterification reaction using a fixed Al mole percentage (20 mol.% of Al related to acetic acid moles). As shown in Figure 38, the HSG samples exhibited same low yield, similar to reference and confirming no activity.

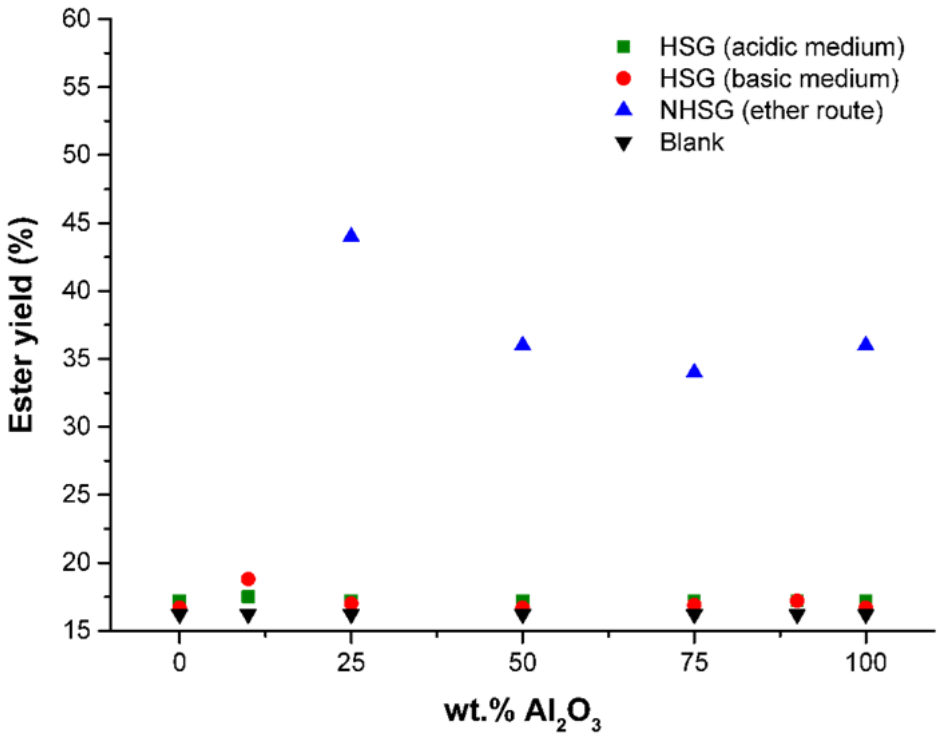


Figure 36: Ester yield using 20 mol.% of Al of Si-Al supports prepared by HSG (acidic, basic medium) and NHSG.

The $Si_{75}Al_{25}$ exhibited higher ester yield (36 and 44 %, respectively). As the specific surface area of $Si_{50}Al_{50}$ and $Si_{75}Al_{25}$ catalysts are similar (Table 9), the higher activity of the $Si_{25}Al_{75}$ catalyst can be correlated to a better surface dispersion of acid sites.[319] According to Eley-Rideal reaction mechanism, acetic acid is adsorbed first onto Brönsted acid sites, which are considered as catalytically active for esterification reactions. [320] [321]This intermediate formed by a

protonated acetic acid which is an electrophile, reacts with *n*-BuOH to form the ethyl acetate and water.

# III.3. Conclusion

Another one-step NHSG (alcohol route) were successfully used to prepare $Si_xAl_y$ mixed oxides from non-expensive precursors. Two types of alcohol, ethanol and $^t$BuOH were used as a solvent and oxygen donor in the same time. The $Si_xAl_y$ mixed oxides were also prepared by NHSG (ether route) and compared with the same composition samples prepared by alcohol route The Si/Al ratio can be easily controlled, knowing that it plays an important role in the structure, texture, acidity of the samples. Calcination in air largely eliminates chlorine and carbon from essentially non-condensed groups and the solvent. The NHSG is very good method to control the composition, the composition of all samples prepared by both alcohol and ether routes show good control on composition, while ether route provides better control on composition than alcohol route. The texture is strongly depend on the composition and on type of solvent, the $N_2$-adsorption/desorption presented that samples prepared with EtOH and ether show high specific surface area and it decrease with Si% decrease in the samples, in the same time ether route provides higher pore volume than alcohol route. The structure of all samples were studied by XRD and NMR, the results obtained showed that all the mixed oxides are amorphous, however the study of the structure showed that there is not significant different between mixed oxides prepared with different oxygen donor. The BET study of texture showed that mixed oxides are mesoporous in general and there is a different in specific surface area and pore volume for samples with same composition and prepared with different oxygen donor. The acidity of all samples was studied to show the effect of oxygen donor on the acid sites, the presence of strong, medium or weak acid sites appeared related to the presence of Al. As expected, the concentration of the accessible acid sites increase as the Al/Si ratio increases. The composition or (Si/Al ratio) has more effect on acidity than the type of the route (oxygen donor). The mixed oxides catalysts prepared by HSG and NHSG were tested their activity on esterification reaction. The esterification activity is well related to the acidity of mixed oxides. Samples prepared by NHSG were highly active in esterification of acetic acid with *n*-BuOH.

# Chapter: IV

# Mixed oxide catalysts based on Nickel prepared via non-hydrolytic sol-gel for ethylene oligomerization

# IV.1. Introduction:

Ethylene oligomerization is one of the major technologies for producing higher olefins, which are key feedstock in the synthesis of plastics, lubricants, surfactants, alcohols, etc. The current oligomerization processes use organic solvents and homogeneous catalysts.[322-324] In line with sustainable chemistry principles, significant research efforts have been directed to the development of heterogeneous catalysts and processes.[102, 324, 325] Various families of solid catalysts, including complexes immobilized on polymers and oxides, metal-organic framework and covalent organic framework materials, and nickel supported on inorganic porous materials, have been examined during the past decades.[324, 325] Among them, Ni-containing zeolites, clays and mesoporous aluminosilicates have shown very promising performances in terms of catalytic activity and selectivity.[102, 324, 326] In addition, they are the only catalysts that can function without solvents and activators/cocatalyst. These Ni-containing catalysts are actually bifunctional catalysts, containing both nickel ions and acid sites. It is generally accepted that the isolated nickel ions are involved in the formation of 1-olefins by ethylene dimerization/oligomerization, while the acid sites catalyze the double bond isomerization and the co-oligomerization of primary olefins. These reactions lead to a mixture of C4, C6, C8,… olefins, the composition of which also depends on the reaction conditions (temperature, pressure, contact time).[325, 327, 328] The performances of the oligomerization catalysts strongly depend on their textural properties. In a general manner, the activity increases when the pore size of the catalyst increases. The best performances were obtained over catalysts based on nickel-exchanged aluminated ordered mesoporous silicas, namely Ni/Al-MCM-41 [115, 123, 329], Ni/Al-SBA-15 [99], and Ni/Al-MCM-48 [330]. The mesoporosity of these catalysts facilitate the diffusion of higher product molecules inside the pore system, leading to a lower deactivation rate and a higher activity in comparison with the microporous catalysts. However, the preparation of these model catalysts is time-consuming and energy intensive. For instance, the preparation of Ni-AlSBA-15 [99], considered to be one of the most active and stable oligomerization catalyst [324], involves three successive steps (synthesis of the ordered silica in

the presence of a copolymer template, alumination with $NaAlO_2$, Ni deposition by a two-step exchange procedure), each of them followed by a calcination treatment. On the other hand, the non-hydrolytic sol-gel process based on the reaction of silicon or metal precursors with an organic oxygen donor (ether, alcohol, or alkoxide) offers straightforward one-step routes to non-ordered mesoporous oxides.[331] This process has been successfully applied to the synthesis of mixed oxide catalysts [332], including $TiO_2$-$V_2O_5$ DeNOx [333] or total oxidation catalysts [334], $SiO_2$-$TiO_2$ epoxidation catalysts[335], or $SiO_2$-$Al_2O_3$-$MO_x$ (M = Mo, Re) metathesis oxides catalysts [336, 337].

# IV.2. Results and discussion

## IV.2.1. Synthesis and characterization

The $SiO_2$-$Al_2O_3$-NiO catalysts were prepared by a one-step non-hydrolytic sol-gel route, involving the reaction at 110 °C under autogenous pressure of $SiCl_4$, $AlCl_3$, and $Ni(acac)_2$ precursors with $iPr_2O$ in $CH_2Cl_2$ (Scheme 12). It is important to note that among all the catalyst samples, catalysts with (10 wt.%) loading have been studied.

All samples were prepared by the non-hydrolytic sol-gel process (ether route). The $SiO_2$-$Al_2O_3$-NiO mixed oxides with different Si/Al ratios (0, 0.1, 1, 8, ∞) and a Ni content of (5,10, 15 and 20 wt.% were synthesized using silicon tetrachloride ($SiCl_4$, Alfa Aesar, 99.98%), aluminum trichloride ($AlCl_3$, Alfa Aesar, 99.98%) and nickel bis(acetylacetonate) ($Ni(acac)_2$, Alfa Aesar, 95%) as molecular precursors. (Table 24, Experimental Part) $Ni(acac)_2$ was used instead of $NiCl_2$ because of its better solubility in the experimental conditions. Dry diisopropyl ether ($iPr_2O$, $H_2O$ < 4 ppm) and $CH_2Cl_2$ ($H_2O$ < 6 ppm) used as oxygen donor and solvent, respectively, were purchased from Aldrich with 99% purity and were further dried by distillation over sodium wire. The water concentration was determined by the method of assaying water using Karl Fisher reagent (Metrohm KF 652 coulometric type). The catalysts were prepared in 1 g quantities in 48 mL PTFE lined autoclaves (Parr Instruments). All manipulations were performed under argon using a glovebox to avoid hydrolysis. The chloride and acetylacetonate precursors were introduced first in the autoclave, then $iPr_2O$ and $CH_2Cl_2$ (10 mL) were added. The number of moles of $iPr_2O$ was calculated so that the number of iPr groups in $iPr_2O$ was equal to the total number of Cl and acac

groups in the precursors. The sealed autoclave was heated at 110 C for 4 days under autogenous pressure. In this synthesis, the reactions around Si were catalyzed by $AlCl_3$. In the preparation of the Al-free mixed oxide (Si/Al = ∞), $FeCl_3$ (0.015 mmol) had to be used as a catalyst to obtain a gel. After cooling down to room temperature, the gel was washed (under air atmosphere) with $CH_2Cl_2$, dried at 20 °C under vacuum (10 Pa) for 1 h and then for 4 h at 120 °C. The gels obtained were dried under vacuum then calcined for 5 h at 500 °C in dry air. The samples are labeled $Si_xAl_yNi_z$, where x, y and z represent the experimental $SiO_2$, $Al_2O_3$ and NiO weight loadings, respectively. The overall oxide yield was better than 90% in all cases. The as-prepared materials appeared either as fine powders (more than 45 wt.% of $Al_2O_3$) or as coarse powders with larger particle sizes (less than 45 wt.% of $Al_2O_3$).

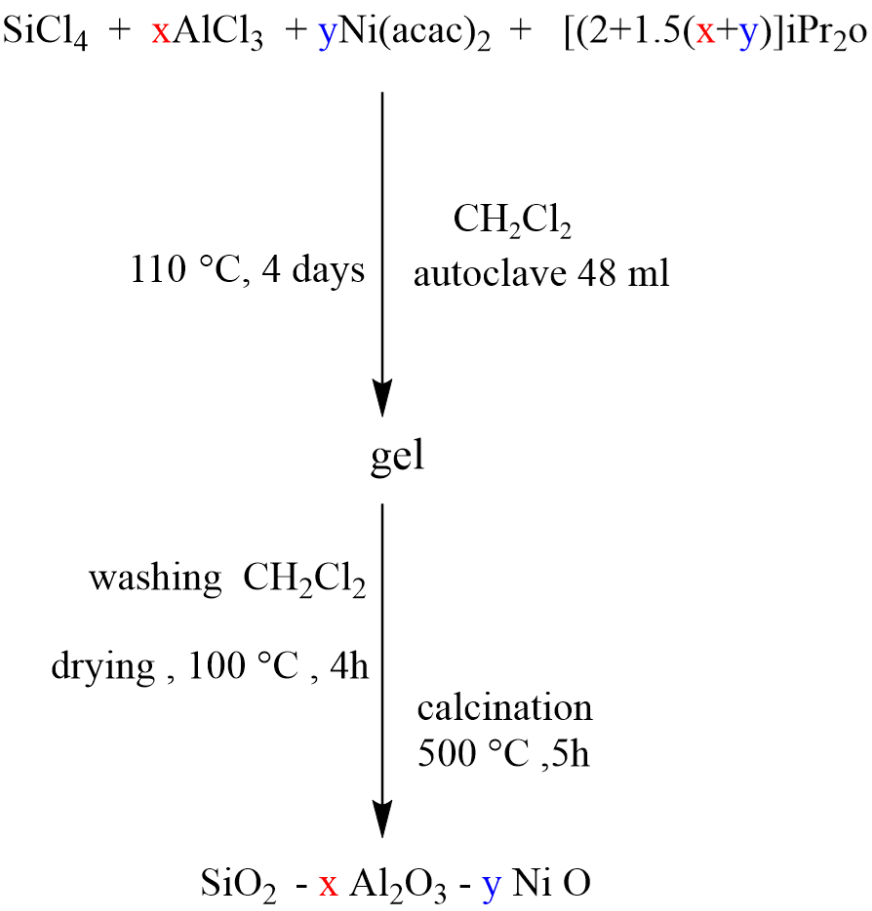


Scheme 12: Non-hydrolytic sol-gel process for mixed oxides (ether route).

The samples are identified by $Si_xAl_yNi_z$ where x is the experimental weight percentage of $SiO_2$, y the experimental-weight percentage-of $Al_2O_3$ and z the experimental weight percentage of NiO. As

shown in (Table 13), the NiO content varies from (0 to 20 wt.%). The different $Si_xAl_yNi_z$ solids were prepared at least twice to check the reproducibility of the texture (in this case the samples are named $Si_xAl_yNi_z$a and $Si_xAl_yNi_z$b).

# IV.2.2. Composition

## IV.2.2.1. Scanning electron microscopy (SEM)

After samples grinding, the grain size is heterogeneous and varies from 1 to 100 µm. The solids are composed of many very fine particles when Al loading is high and are hard and compact when Al loading is lower. In addition, as the Al loading decreased, the shape of the mixed oxides changed from spherical to pellet-like. All the samples exhibited the same topography of surface: packed elementary particles that stick together to form the overall grain (Figure 39).

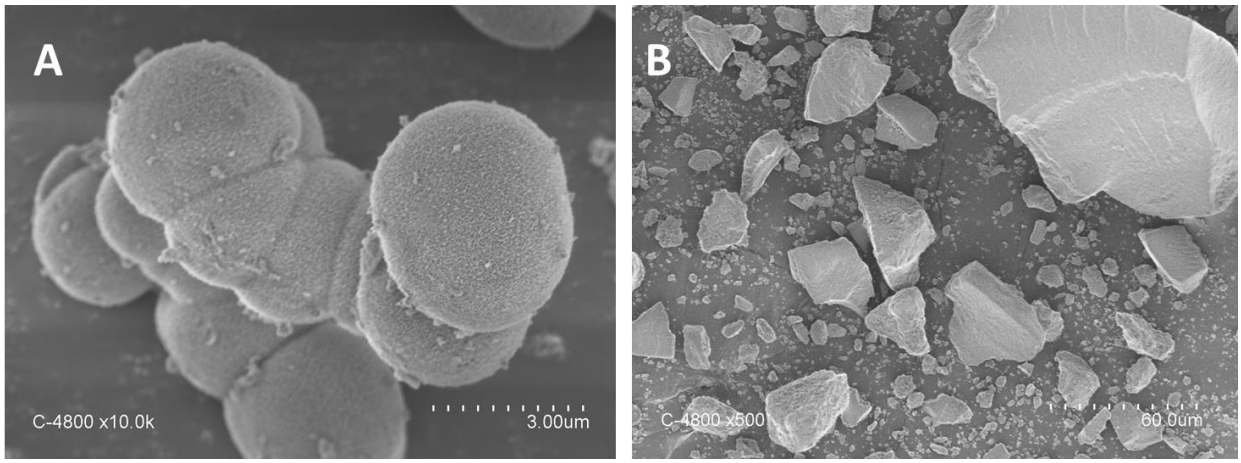


Figure 37: SEM images of (A) $Si_9Al_{84}Ni_7$ and (B) $Si_{80}Al_{12}Ni_8$.

## IV.2.2.2. Energy Dispersive X-ray Analysis (EDX)

EDX analysis was performed to probe the elements on the surface. The theoretical results were calculated and compared to the experimental values. As shown in (Table 11), for all samples the percentage of $Al_2O_3$ and $SiO_2$ varied and the percentage of NiO was changed (from 5 to 20 wt. %).

Table 11: Composition by EDX measurements.

| Sample | Experimental (nominal) composition (wt%) [a] | | | |
|---|---|---|---|---|
| | $SiO_2$ | $Al_2O_3$ | NiO | Si/Al [b] |
| $Si_0Al_{93}Ni_7$ | 0.0/(0.0) | 92.7/(92.9) | 7.3/(7.1) | 0 |
| $Si_9Al_{84}Ni_7$ | 6.3/(9.3) | 86.5/(83.6) | 7.2/(7.1) | 0.1 |
| $Si_{42}Al_{50}Ni_8$ | 40.5/(42.4) | 51.8/(50.0) | 7.7/(7.6) | 1 |
| $Si_{80}Al_{12}Ni_8$ | 81.3/(80.1) | 12.4/(12.0) | 6.3/(8.0) | 0 |
| $Si_{93}Al_0Ni_7$ | 92.2/(92.7) | 0.0/(0.0) | 7.8/(7.3) | ∞ |

[a] Experimental and nominal weight percentages (in brackets). Weight loadings are calculated from EDX results assuming that all Si, Al and Ni atoms are in the form of $SiO_2$, $Al_2O_3$ and NiO, respectively.

[b] Experimental atomic Si/Al ratio (EDX).

All Si, Al and Ni are quantitatively incorporated into the gels. The experimental composition of the samples determined by EDX analysis was close to the nominal one based on the amounts of reactants, indicating that all of the Si, Al and Ni atoms were included in the final oxide, as found previously for other mixed oxide catalysts prepared by non-hydrolytic sol-gel.[336-339] A negligible weight loss of the precursors was detected. As a result, NHSG methodology preserve the initial quantities of the starting materials.

# IV.2.3. Structure

## IV.2.3.1. X-ray Diffraction Analysis (XRD)

The prepared materials contains a constant amount of nickel (around expected 10 wt.%) with different molar ratio of Si/Al. According to X-ray diffraction (Figure 40) all samples were predominantly amorphous, but reflections at $2\theta$ = 37.3°, 43.3°, 62.9°, and 76.5° point to the presence of NiO crystallites [340, 341], with particle sizes (estimated from the width of the (200) reflection at 43.3°) of ≈25 nm for the alumina-rich samples ($Si_0Al_{93}Ni1_7$ and $Si_9Al_{84}Ni_7$) and ≈45 nm for the other samples.

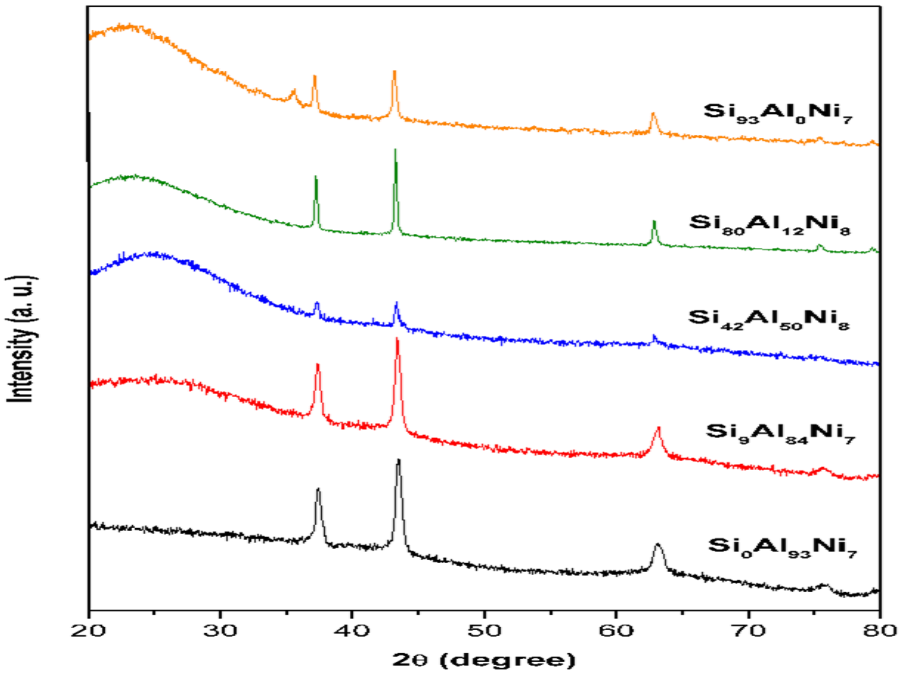


Figure 38: XRD patterns of $Si_xAl_yNi_z$ samples.

Reflections typical of nickel aluminate spinels or of γ-alumina were not detected.[342] In the case of $Si_{93}Al_0Ni_7$, a very weak reflection at ≈36° could indicate traces of a nickel phyllosilicate phase. [343]

## IV.2.3.2. Transmission electron microscopy (TEM)

Electron microscopy confirmed the formation of NiO crystallites. For instance in the case of $Si_{93}Al_0Ni_7$ TEM images (Figure 41) clearly showed the presence of aggregated, parallelepipedic NiO nanoparticles (with a relatively uniform size of ca. 10-30 nm in width and 20-50 nm in length, in agreement with the crystallite size values estimated from XRD data) dispersed in a porous silica-alumina matrix.

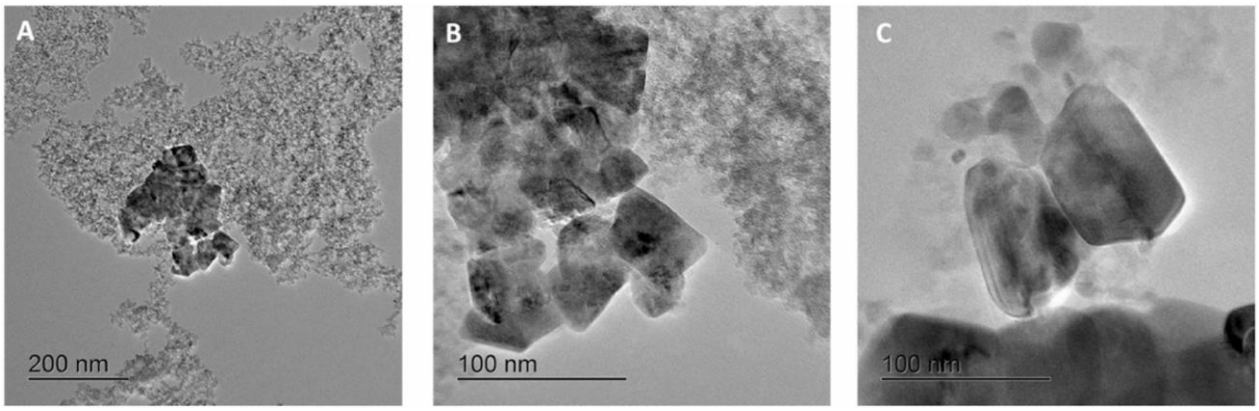


Figure 39: TEM images of $Si_{93}Al_0Ni_7$ showing the presence of aggregated NiO particles with a parallelepiped-like morphology.

## IV.2.3.3. Nuclear Magnetic Resonance (NMR)

$^{29}Si$ and $^{27}Al$ solid-state NMR gives information on the structure of the aluminosilicate network. The $^{29}Si$ CP-MAS NMR spectra of Si-containing mixed oxides (Figure 42) showed broad resonances, typical of amorphous materials. In amorphous silicas or alumino silicates, each replacement of a (OSi) group in $Si(OSi)_4$ tetrahedra by an (OAl) or an (OH) group leads to a downfield shift of about 5-10 ppm.[283] The spectrum of $Si_{90}Al_0Ni_{10}$ shows three broad resonances at ≈ -111, -101 and -91 ppm ascribed to $Si(OSi)_4$ ($Q^4$), $Si(OSi)_3(OH)$ ($Q^3$), and $Si(OSi)_2(OH)_2$ ($Q^2$) sites, respectively.[284] It must be noted that the CP-MAS sequence favors Si nuclei close to protons, thus these spectra cannot be used to quantify the concentration of each site. Similar $^{29}Si$ CP-MAS NMR spectra with a major $Q^3$ resonance have been reported for mesoporous silicas or silica-alumina with a low Al content .[285] The Ni content is too low to have a significant effect (Si/Ni = 16.5), and $Si(OSi)_3(O^-)$ sites bonded to $Ni^{2+}$ cations would lead to a resonance in the - 91 to -102 ppm range, thus overlapped by $Q^2$ and $Q^3$ resonances.[283] The incorporation of large amounts of aluminum in the silica network led to a significant low-field shift of the resonances indicating extensive formation of Si-O-Al bridges in $Si(OSi)_{4-x}(OAl)_x(Q^4_{xAl})$ sites or $Si(OSi)_{3-x}(OH)(OAl)_x$ ($Q^3_{xAl}$) sites .[283] Practically all sites from $Q^4$ sites to $Q^4_{4Al}$ or $Q^3_{3Al}$ sites are likely present in $Si_{42}Al_{50}Ni_8$, while $Q^4_{4Al}$ and/or $Q^3_{3Al}$ sites predominate in $Si_9Al_{84}Ni_7$. K. Bouchmella *et*

*al.* reported the $^{29}$Si NMR results for Si-Al-Mo mixed oxides prepared by NHSG route and these results are near to the results presented in this work.[344]

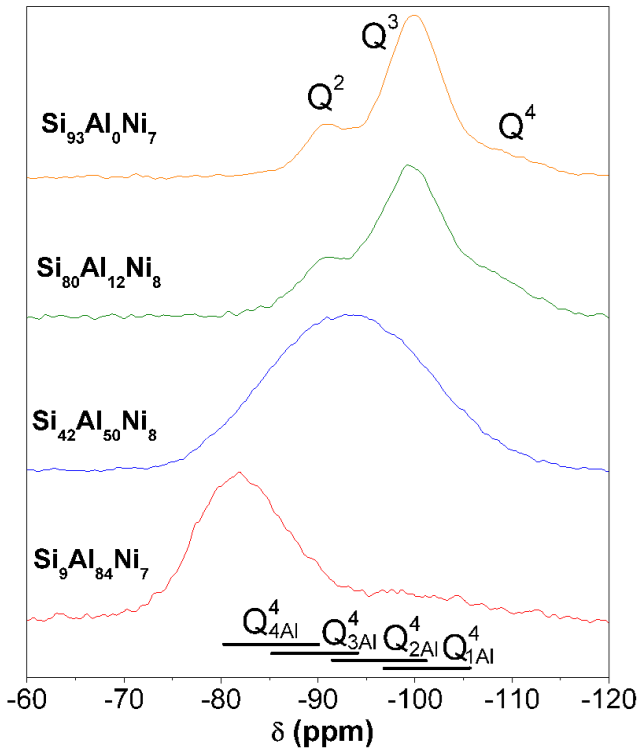


Figure 40: $^{29}$Si MAS NMR spectra of $Si_xAl_yNi_{10}$ samples.

The $^{27}$Al solid-state MAS NMR spectra (Figure 43) exhibited broad resonances around 50 ppm, 20 ppm and -10 ppm, ascribed to 4-coordinated ($Al^{IV}$), 5-coordinated ($Al^{V}$), and 6-coordinated ($Al^{VI}$) aluminum sites.[283, 287] The $Al^{IV}/Al^{VI}$ ratio increased from 0.2 to 1.71 when the Si content increased, indicating that the insertion of $AlO_4$ tetrahedra in the silica network is favored at high Si/Al. The signal corresponding to $Al^{IV}$ sites shifted up field when the $SiO_2$ loading increased from 0 to 80%; this effect has been previously ascribed to the decreased concentration of aluminum atoms around Al sites.[345]

This type of environment is commonly observed in oxides obtained by sol gel routes.[312] It can be seen that when $Al_2O_3$ increases the proportion of $Al^{V}$ sites increases at the expense of $Al^{IV}$ sites. Leonard *et al.*[289] and Hensen *et al.*[346] observe a similar behavior in the case of amorphous aluminosilicates.

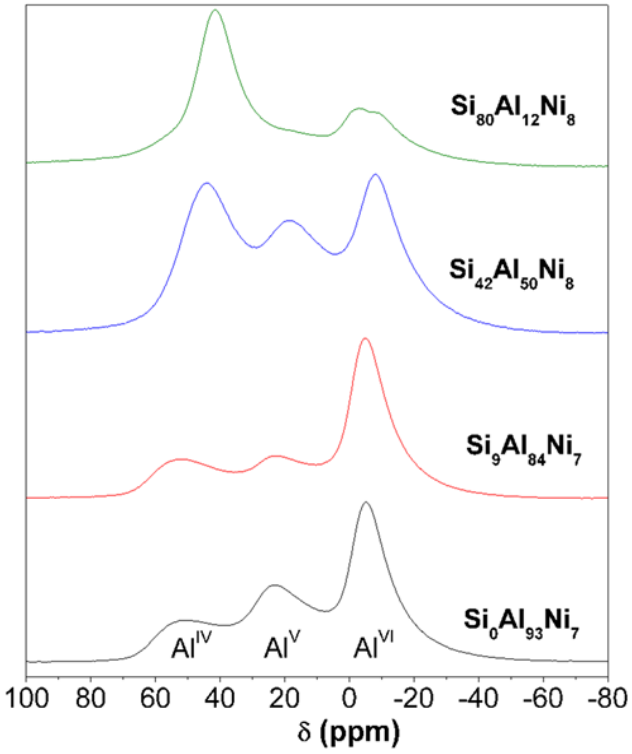


Figure 41: $^{27}$Al MAS NMR spectra of of $Si_xAl_yNi_{10}$ samples.

## IV.2.4.Texture

The specific surface area, pore volume, and pore size distribution data derived from nitrogen adsorption are shown in Table12. The silica-rich samples ($Si_{80}Al_{12}Ni_8$ and $Si_{93}Al_0Ni_7$) exhibited high specific surface areas (590 and 795 $m^2\ g^{-1}$) and pore volumes (1.5 and 2.0 $cm^3\ g^{-1}$), while the other samples displayed only moderate specific surface area (around 360 $m^2\ g^{-1}$) and significantly lower pore volumes (0.3-0.4 $cm^3\ g^{-1}$). The average pore diameter (Dp) ranged between 3.0 and 10.2 nm. *t*-Plot analysis indicated that the surface area developed by micropore walls was low, except for $Si_{42}Al_{50}Ni_8$. Samples with low $Al_2O_3$ content ($Si_0Al_{93}Ni_7$ and $Si_9Al_{84}Ni_7$), exhibited pores ranged from 2 to 30 nm whereas broader size distribution was observed for $Si_{93}Al_0Ni_7$ (Figure 62 in Annex). The pores diameter data range between 3 and 10.2 nm revealing a mesoporous structure of $Si_xAl_yNi_z$ The texture of the samples depends on the Si/Al ratio and Ni content. For the sample made of pure silica, a specific surface area of 795 $m^2\ g^{-1}$ was obtained. It is go down to 360 $m^2\ g^{-1}$ as the amount of Al increases.

Table 12: Texture of the samples measured by $N_2$-physisorption.

| Sample | Texture | | | |
|---|---|---|---|---|
| | Si/Al | S ($m^2 g^{-1}$) | Vp ($cm^3 g^{-1}$) | Dp (nm) |
| $Si_0Al_{93}Ni_7$ | 0 | 360 | 0.4 | 4.7 |
| $Si_9Al_{84}Ni_7$ | 0.13 | 365 | 0.3 | 3.7 |
| $Si_{42}Al_{50}Ni_8$ | 1 | 360 | 0.3 | 3.0 |
| $Si_{80}Al_{12}Ni_8$ | 8 | 590 | 1.5 | 10.2 |
| $Si_{93}Al_0Ni_7$ | ∞ | 795 | 2.0 | 9.9 |

The adsorption and desorption isotherms of nitrogen for the samples containing 10 wt.% of nickel are presented in Figure 44. Isotherms of the samples were of type IV, typical of mesoporous solids. It is seen that these distributions are relatively narrow and located in the 2-5 nm range for the others alumina-rich samples ($Si_{42}Al_{50}Ni_8$ and $Si_{80}Al_{12}Ni_8$).

At the adsorption branch, the adsorbed amount increased gradually with an increase in relative pressure by multilayer adsorption. A sudden uptake of the adsorbed amount was observed over a range of relative pressure ($P/P_0$) between 0.4 and 1.0. This phenomena caused by capillary condensation of nitrogen in the pores. The desorption branch of the isotherm coincides with the adsorption branch.

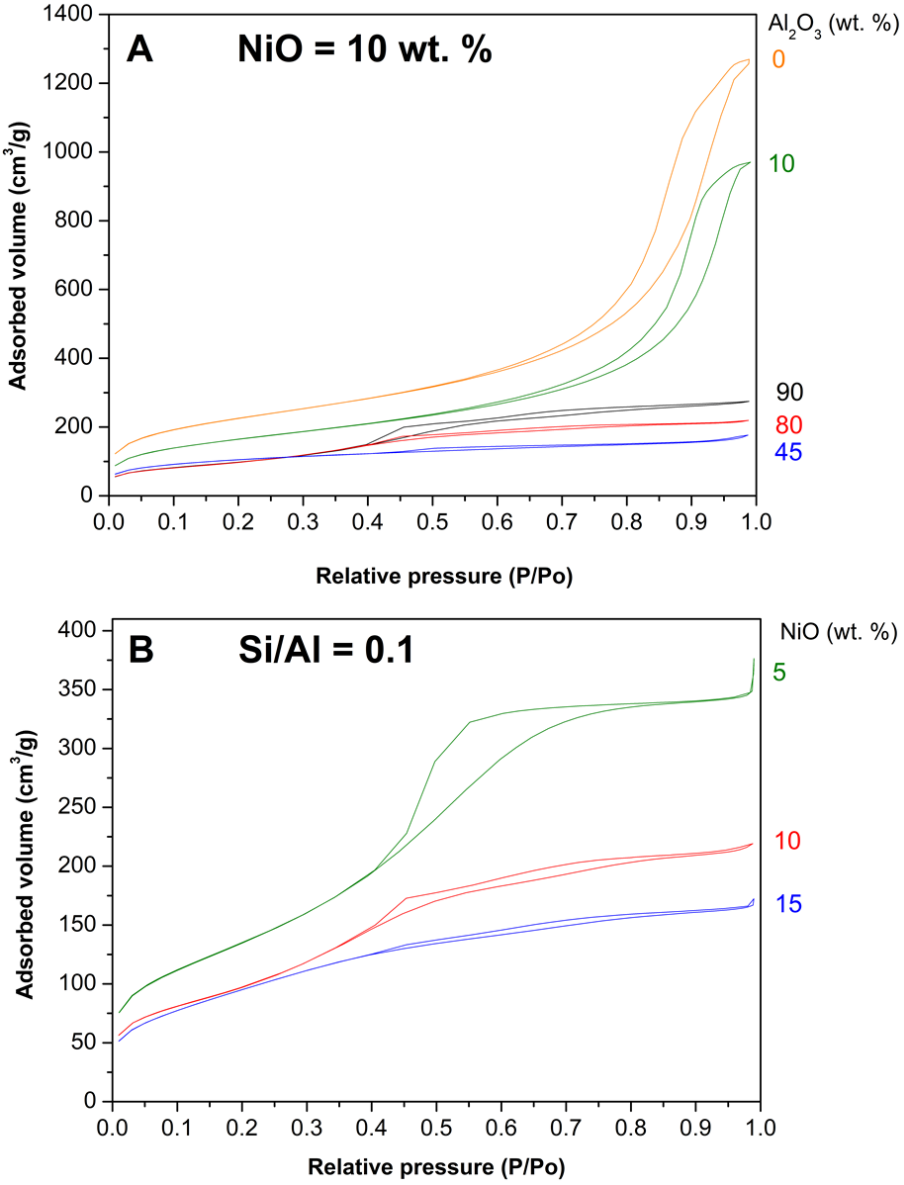


Figure 42: $N_2$-adsorption–desorption isotherms for the synthesized samples with (A) constant NiO loading (when $Al_2O_3$ is varied) and (B) constant Si/Al atomic ratio (when NiO is varied). In this figure, the samples are labelled using the expected weight percentage of each oxide.

## IV.2.4.Acidity:

Temperature programmed desorption of ammonia ($NH_3$-TPD) was used probe the acidity of the $Si_xAl_yNi_Z$ samples. All samples exhibited adsorption peak at near 180 °C (maximum temperature) ascribed to weak acid sites and another peak at 300-350 °C ascribed to medium and strong acid sites (Figure 45) . Quantitative analysis of these thermograms, shows that the amount of ammonia desorbed (in mmol $g^{-1}$) follows this trend.

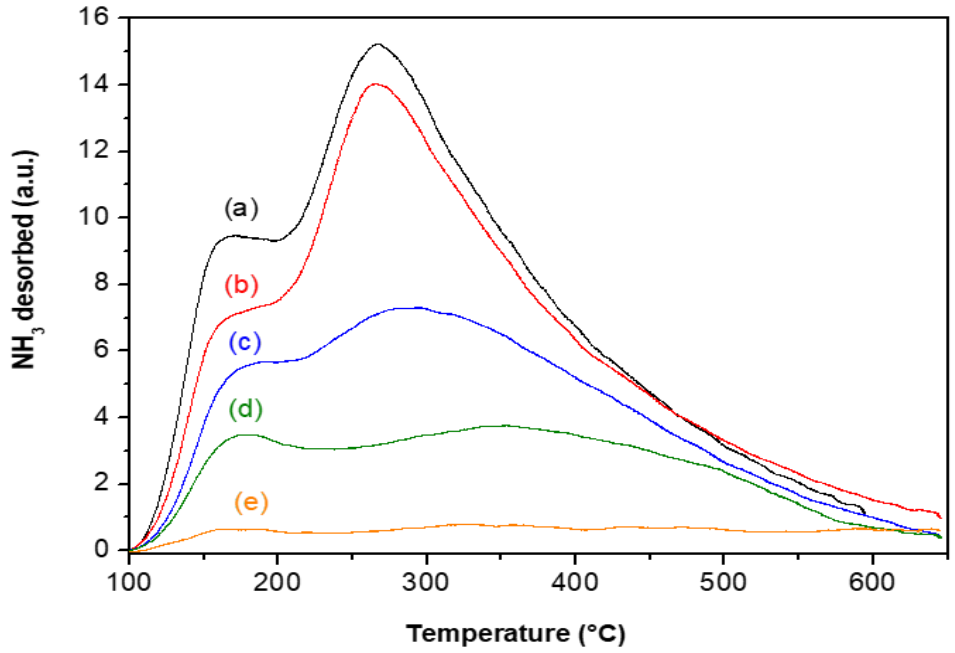


Figure 43: $NH_3$-TPD thermograms, normalized to sample weight, of: (a) $Si_0Al_{93}Ni_7$, (b) $Si_9Al_{84}Ni_7$, (c) $Si_{42}Al_{50}Ni_8$, (d) $Si_{80}Al_{12}Ni_8$ and (e) $Si_{93}Al_0Ni_7$.

As shown in Table 13, gives the total amount of ammonia desorbed from each sample. Following the method of Katada *et al.* [314], one Gaussian function was fitted to the peaks centered at 160 °C (attributed to weak acid sites). The high temperature signals that are not part of the Gaussian are attributed to medium and strong acid sites.

Table 13: Quantification of acidity (in mmol/g) obtained by $NH_3$-TPD.

| Samples | Total acidity | Weak acidity | Medium and strong acidity |
|---|---|---|---|
| $Si_0Al_{93}Ni_7$ | 4.8 | 0.8 | 4.0 |
| $Si_9Al_{84}Ni_7$ | 4.4 | 0.8 | 3.6 |
| $Si_{42}Al_{50}Ni_8$ | 3.0 | 0.7 | 2.3 |
| $Si_{80}Al_{12}Ni_8$ | 1.9 | 0.4 | 1.5 |
| $Si_{93}Al_0Ni_7$ | 0.4 | 0.4 | 0 |

The acidity in medium and strong acid sites increases according to the composition of the support: $SiO_2$> $Al_2O_3$> $SiO_2$-$Al_2O_3$. This order has also been observed by Handzlik.[315] It is well known

that mixed amorphous $SiO_2$-$Al_2O_3$ oxides prepared by sol-gel exhibit notable acidity. For example, they catalyze the dehydration of propanol to propene.[347] In contrast to spectroscopic methods (e.g. IR spectroscopy of adsorbed pyridine), $NH_3$-TPD does not distinguish between Lewis and Brönsted acid sites. Rajagopal *et al*. [348] conducted a study on the acidity of silica-alumina supports with different percentages of $Al_2O_3$ and their respective supported $MoO_3$ catalysts by FTIR spectroscopy (pyridine chemisorption) and by chemisorption of $NH_3$. They showed that with 25% $Al_2O_3$ (and 2, 4 or 12% $MoO_3$) the acidity was maximal (in mmol of $NH_3$ $g_{cata}^{-1}$) with a majority of Lewis acid sites.

The high Brönsted acidity of the silica-alumina is attributed to hydroxyl groups in the "Si-O-Al mixed phase". The debate still exists on the structure of these sites in amorphous materials (Figure 46).[349]

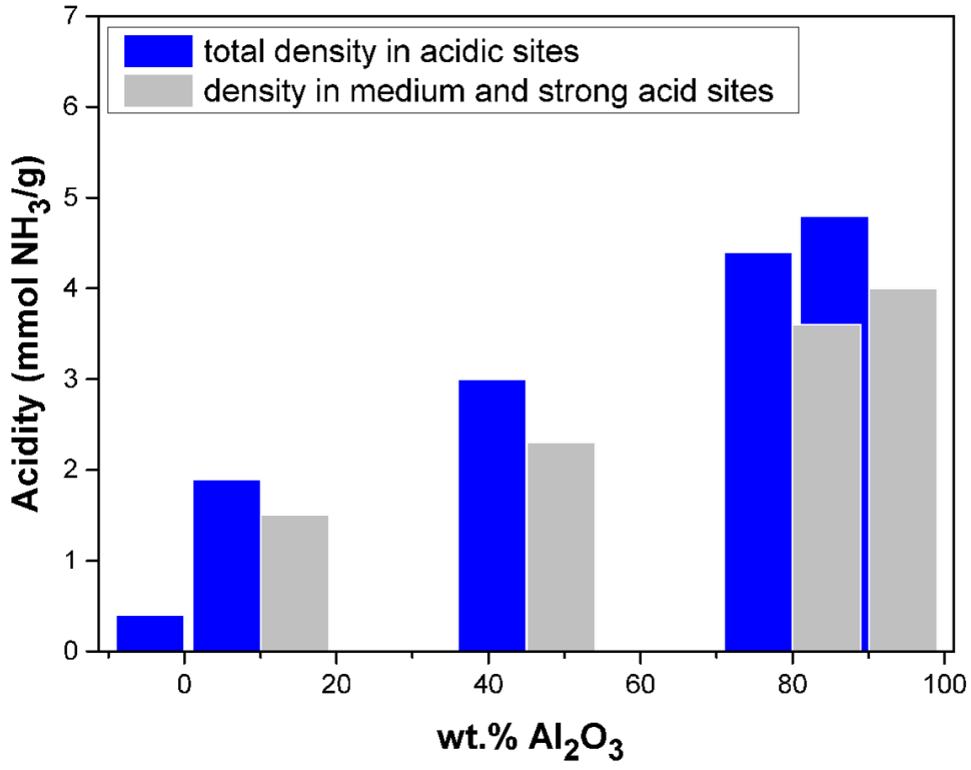


Figure 44: Influence of the $Al_2O_3$ level on the surface acidity of $Si_xAl_yNi_z$ catalysts, where $Al_2O_3$ varying from 0 to 90 wt.%.

The $Si_{93}Al_0Ni_7$ sample has the lowest acidity and has no medium and strong acid sites, unlike all other compositions. The density of acidic sites and the strength of the acidic sites are greater for the samples having a percentage of alumina of between 10 and 90% (when the percentage of NiO remains constant at around 10 wt.%). By way of comparison, a catalyst prepared by impregnation and containing 7 wt.% of NiO on a Al-SBA-15 support (with 13 wt.% of alumina) was analyzed under the same conditions as the NHSG catalysts (on the same apparatus and with the same experimental protocol). This sample has an acidity of 0.48 mol. of $NH_3$ per g of catalyst, at least four times lower than $Si_{80}Al_{10}Ni_{10}$ (1.9 mol $NH_3$ $g^{-1}$ ).[350] Synthesis by NHSG therefore leads to densities of acid sites larger than the conventional impregnation process.

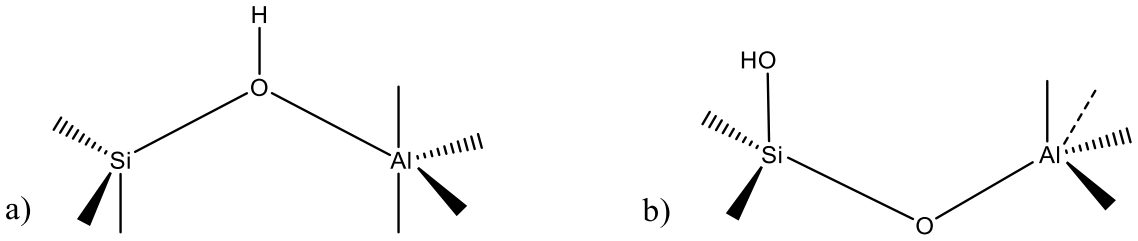


Figure 45: Brönsted acid site structures on the surface of an amorphous aluminosilicate, determined by theoretical calculations: (a) bridging Si- (OH) -Al, (b) Silanol-Al.[349]

## IV.2.5. Composition of surface: XPS

XPS brings additional information on the nature of Ni species. In all cases, the Ni2p3/2 spectra (Figure 48) displayed a main broad peak around 856-857 eV (with a satellite at 862-863 eV) ascribed to tetrahedral $Ni^{2+}$ species in nickel silicate/aluminate domains or to $Ni^{2+}$ species strongly interacting with the aluminosilicate support.[351-353] The higher binding energy (857.2 eV vs. 856.4 eV) observed for the silica-rich samples suggests a stronger interaction with the support. The silica-rich samples showed an additional peak at 855.3 eV ascribed to octahedral $Ni^{2+}$ species in NiO domains interacting with the support.[351-353] Furthermore, the spectrum of $Si_{80}Al_{12}Ni_8$ showed a signal at ≈853.3 eV corresponding to multiplet splitting characteristic of unsupported NiO, indicating the presence of some bulk NiO at the near surface of this sample.[326] The simple spectra observed for the alumina-rich samples are similar to those reported for Ni-based catalysts prepared by different methods, such as Ni-exchanged montmorillonite clays[326], which

displayed a peak at 856.9 eV [326], or NiO-$SiO_2$-$Al_2O_3$ catalysts with a 11 wt.% Ni content prepared by a hydrolytic sol-gel method with a peak at 856.8 eV.[353]

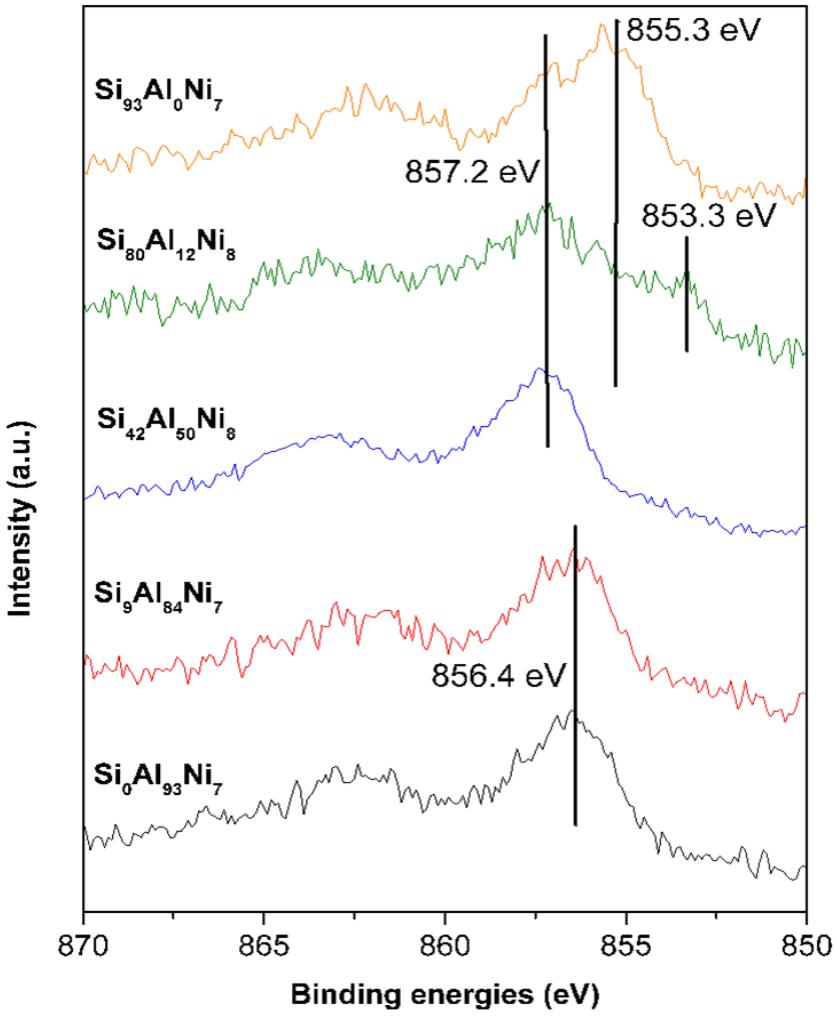


Figure 46: Ni2p3/2 XPS spectra of $Si_xAl_yNi_z$ samples.

XPS analysis was also used to estimate the concentration of the surface Ni species. In previous works, it was found that when the Tammann temperature of the active phase was sufficiently low (as in the case of $V_2O_5$, $MoO_3$, $Re_2O_7$), calcination led to the migration of the active phase toward the surface.[22, 354] The Tammann temperature is the temperature at which ionic diffusion becomes significant in a given material; this temperature roughly corresponds to 0.5 $T_f$, where $T_f$ is the melting temperature in Kelvin. However, NiO has a very high melting point (1955 °C, 2228 K),

which corresponds to a Tammann temperature of 1114 K (841 °C). Accordingly, migration is not expected to occur during calcination at 500 °C. The surface composition obtained from XPS and EDX characterizations is compared in Figure 49. The Ni content detected by XPS was actually lower than by EDX, indicating that the Ni surface concentration was lower than the bulk concentration. A possibility could be that the Ni precursors react faster than Al and Si precursors. This difference in the kinetics of the precursors could lead to a gradient of Ni in the particles building the gel: NiO crystallites formed first and were then embedded in the aluminosilicate matrix. This trend is less pronounced for alumina-rich samples, in agreement with the better dispersion of Ni attested by the smaller size of NiO particles found by XRD.

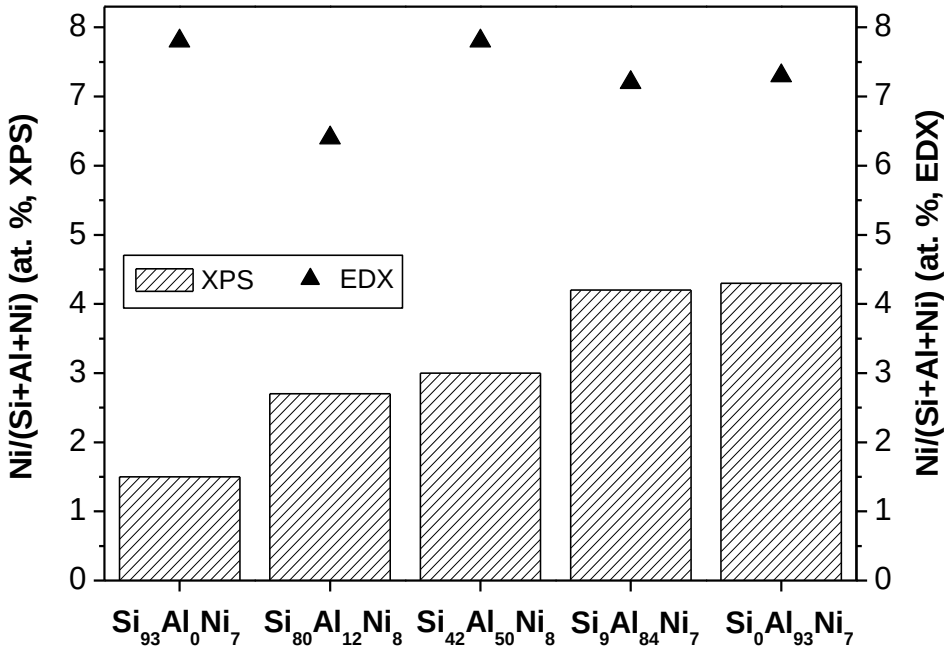


Figure 47: XPS (left axis, striped bars) and EDX (right axis, filled triangles) Ni/(Ni + Si + Al) atomic ratios for catalysts as a function of the $Al_2O_3$ weight loading.

## IV.2.6. Reducibility of surface NiO species: TPR Analysis

The reducibility of the nickel species present in each catalyst was examined by TPR reduction with hydrogen up to 900 °C (Figure 50).This technique is classically used to identify the active phases in Ni-based catalysts.[123, 351, 355, 356] Unsupported NiO is reduced at $T_{max}$ ≈350-400 °C (peak

maximum), while unsupported $NiAl_2O_4$ is reduced at much higher temperatures, at ≈800-900 °C .[351] In Ni catalysts supported on aluminosilicates, reduction peaks at $T_{max}$ ≈450-600 °C have been ascribed to NiO species strongly interacting with the support or amorphous Ni silicate/aluminate species [340, 351, 353]; reduction peaks at $T_{max}$ ≈700-800 °C have been attributed to $Ni^{2+}$ charge-compensating cations in aluminosilicates structures [123, 356] or to $NiAl_2O_4$ species.[340]

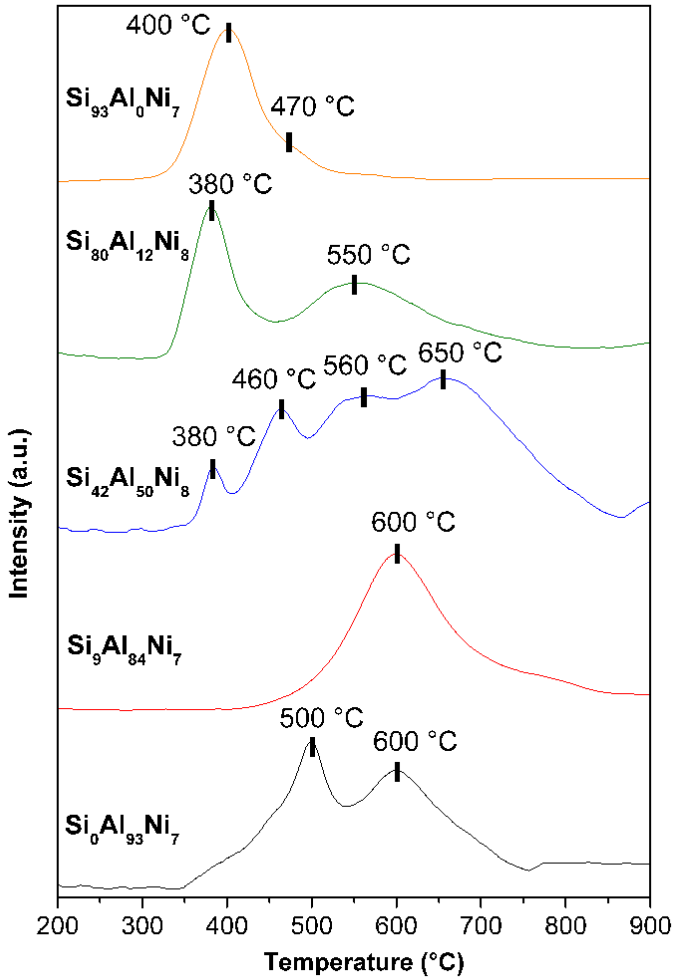


Figure 48: $H_2$-TPR profiles of $Si_xAl_yNi_z$ samples.

The $H_2$-TPR reduction profiles of $Si_xAl_yNi_z$ catalysts (Figure 50) strongly depend on their composition. The $H_2$-TPR thermogram of the Al-free $Si_{93}Al_0Ni_7$ sample exhibited a major reduction peak at 400 °C and a shoulder at 470 °C, suggesting that this catalyst contained mainly NiO species with weak interaction with the $SiO_2$ support. The TPR profiles of all other samples

displayed peaks at 500-600 °C implying a significantly stronger interaction of Ni species with the Al-containing matrices. In the case of $Si_{42}Al_{50}Ni_8$ sample, the TPR profile was particularly broad, with a major peak at 650 °C up to 800 °C suggesting the presence of a large amount of $NiAl_2O_4$ species or $Ni^{2+}$ charge-compensating cations in aluminosilicates structures.

# IV.2.7. Catalysts results

The conversion of ethylene into higher olefins by oligomerization reactions is of considerable interest, and significant research efforts have been directed to the development of heterogeneous catalysts for these processes. Among them, the mixed oxides catalysts prepared by non-hydrolytic sol-gel ($Si_xAl_yNi_z$). For these materials both the nature of the Ni sites and the texture of the catalyst are crucial variables affecting the catalytic activity and the stability. For example, the most active sites in this reaction are the nickel and acid sites. In these catalysts it was shown that the pore size is an important variable affecting their activity and stability.[357] For example, the Ni-exchanged zeolites suffered severe deactivation (due to the blocking of their micro pores with heavy products),[119, 358] while the catalysts with larger pores, i.e. Ni-Al-mesoporous materials, exhibited very high productivity in the ethylene conversion to oligomers.[115, 359]
The activity is calculated on the basis of the oligomerization products of ethylene (trans and cis-2-butene, hexane, heptane and octane), it was expressed in equation (1):

$$\text{Conversion (\%)} = \frac{nC_2\ \text{in} \ - \ nC_2\ \text{out}}{nC_2\ \text{in}} \times 100 \qquad (1)$$

Where $C_2$ is Ethylene

$$\text{Activity (mmol g}^{-1}\text{.h}^{-1}\text{)} = \frac{\text{No. of mmol of Ethylene converted}}{\text{M cat.(g)} \times \text{Time (h)}} \qquad (2)$$

Where M cat. is the weight of the catalyst.

In our case, the WHSV (weight hourly space velocity) is 10 $h^{-1}$ (i.e. 10 g ethylene per g catalyst per hour), 350 mmol ethylene per g catalyst per hour. Thus the activity is given in equation (3):

$$\text{Activity (mmol g}^{-1}\text{.h}^{-1}\text{)} = 350 \times \text{Conversion (\%)}/100 \qquad (3)$$

The catalytic performance measurements were performed in a fixed-bed dynamic reactor, at 150, 200, 250, 300 and 350 °C. Pure ethylene was supplied at 3 MPa with a mass hourly space velocity (WHSV) of 10 $h^{-1}$. A blank test was performed in the presence of a Ni-free Al-Si mixed oxide (Si/Al = 15) prepared by the non-hydrolytic method; at 150, 200 and 250 °C, the ethylene conversion was only 1, 2 and 5% respectively. In contrast, all $Si_xAl_yNi_z$ samples showed much higher activity (Table 14). This clearly underlines the crucial role played by Ni species in the activation of the ethylene.

Table 14: Effect of reaction temperature on the catalytic performance of $Si_xAl_yNi_z$ catalysts.[a]

| Catalyst | T (°C) | C2 conversion (%) | Product distribution (wt.%) | | | | Activity[c] (mmol $g^{-1}$ $h^{-1}$) |
|---|---|---|---|---|---|---|---|
| | | | C4 | C6 | C8 | Other[b] | |
| $Si_{93}Al_0Ni_7$ | 150 | 15 | 90 | 8 | 1 | 1 | 54 |
| | 200 | 30 | 85 | 11 | 2 | 2 | 107 |
| | 250 | 43 | 78 | 15 | 4 | 3 | 154 |
| | 300 | 48 | 73 | 14 | 4 | 9 | 171 |
| | 350 | 55 | 57 | 10 | 3 | 30 | 196 |
| $Si_{80}Al_{12}Ni_7$ | 150 | 40 | 83 | 11 | 3 | 3 | 143 |
| | 200 | 56 | 74 | 13 | 6 | 7 | 200 |
| | 250 | 76 | 54 | 19 | 12 | 15 | 271 |
| | 300 | 85 | 38 | 21 | 18 | 23 | 304 |
| | 350 | 95 | 21 | 18 | 15 | 46 | 339 |
| $Si_{42}Al_{50}Ni_8$ | 150 | 66 | 75 | 15 | 13 | 2 | 236 |
| | 200 | 80 | 63 | 17 | 16 | 4 | 286 |
| | 250 | 85 | 50 | 20 | 22 | 8 | 304 |
| | 300 | 90 | 39 | 28 | 24 | 9 | 321 |
| | 350 | 95 | 34 | 23 | 19 | 22 | 339 |
| $Si_9Al_{84}Ni_7$ | 150 | 76 | 71 | 18 | 8 | 3 | 271 |
| | 200 | 88 | 66 | 22 | 8 | 4 | 314 |
| | 250 | 92 | 63 | 24 | 9 | 4 | 329 |
| | 300 | 95 | 61 | 23 | 9 | 7 | 339 |
| | 350 | 96 | 27 | 5 | 1 | 67 | 343 |
| $Si_0Al_{93}Ni_7$ | 150 | 77 | 69 | 10 | 6 | 15 | 275 |
| | 200 | 78 | 65 | 12 | 6 | 17 | 279 |

| | | | | | | |
|---|---|---|---|---|---|---|
| 250 | 80 | 60 | 14 | 7 | 19 | 286 |
| 300 | 85 | 55 | 20 | 6 | 18 | 304 |
| 350 | 92 | 27 | 3 | 1 | 69 | 329 |

[a] Reaction conditions: P = 3 MPa, WHSV = 10 $h^{-1}$, reaction time 1 h.
[b] Alkanes and uneven olefins.
[c] Average specific activity (mmol of $C_2H_4$ converted per gram of catalyst per hour).

The ethylene conversion and the product distribution were highly dependent on the reaction temperature and the composition of the catalyst. As expected, regardless of the composition of the catalyst, the ethylene conversion increased with increasing temperature. Except at the highest temperature (350 °C), the products were typical of an ethylene oligomerization process catalyzed by Ni-based catalysts. Thus, the main products were C4, C6 and C8 olefins, in which butenes were the major compounds. Small amounts of C1- C3 alkanes and C3, C5, C7 olefins were also obtained, especially at 300 and 350 °C. Figure 63 (in Annex) shows typical chromatograms of the reaction products obtained at different temperatures over the $Si_9Al_{84}Ni_7$ catalyst. For all of the catalysts, the percentage of C4 olefins decreased when the temperature increased from 150 to 350 °C and the amount of butenes among the products decreased when the Al content in the catalyst increased (Table 14).

This indicates the occurrence of further reactions involving the primary compounds (*vide infra*). In the C4 fraction, the only detected molecules are the three *n*-butene isomers: 1-C4, *trans*-, and *cis*-2-C4. Typically, the distribution of butenes consisted of 17 ± 2% 1-C4, 50 ± 2% *trans*-2-C4, and 33 ± 2% *cis*-2-C4. An exception is the Al-free catalyst, which exhibited the lowest acidity among the catalysts (Table 14). In this case, at 150 °C, the distribution consisted of 40% 1-C4, 31% *trans*-2-C4, and 29% *cis*-2-C4.

The oligomerization results obtained in this study are in agreement with those produced by most of Ni-containing solid catalysts, and confirm the existence of several reactions, as shown in Scheme 13. Ethylene dimerization leading to 1-butene is the primary reaction which occurs on nickel sites. Further oligomerization reactions also occur on nickel sites, leading to 1-hexene then 1-octene. The initial 1-olefins are easily involved in double-bond isomerization reactions. These reactions are favored by the acid properties of the catalyst. The third series of chemical transformations involve the butenes and the hexenes. Known as co-oligomerization reactions, they are also acid-catalyzed reactions. Through an ionic mechanism, the C4 and C6 olefins are converted into branched octenes and higher branched olefins. These reactions are favored by a higher concentration of acid sites as

well as a high temperature. Under severe conditions (i.e. high temperature), the acid sites can also activate cracking and H transfer reactions. The higher selectivity to butenes, as well as the higher 1-butene yield over the $Si_{93}Al_0Ni_7$ catalyst are thus likely related to the lower acidity of this sample.

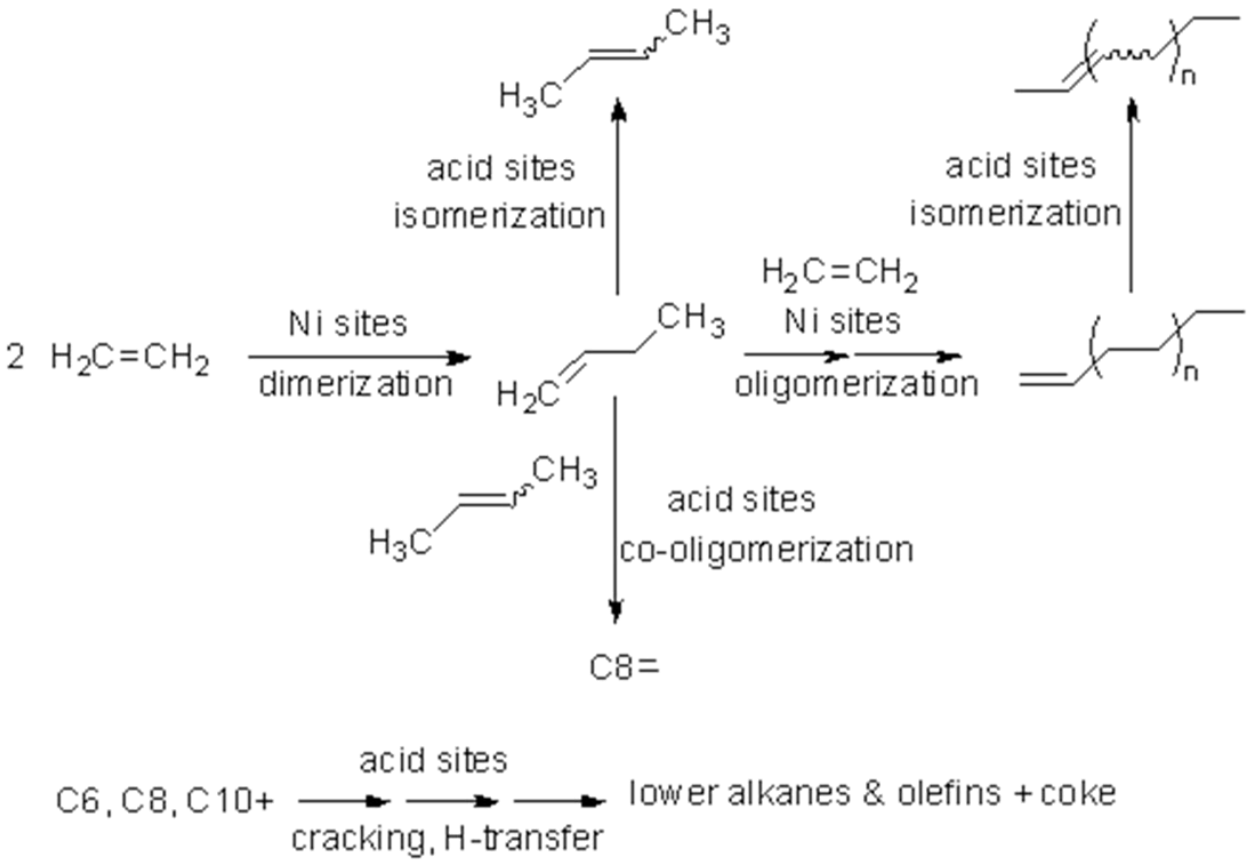


Scheme 13: Simplified scheme of the main reactions involved in ethylene oligomerization.

The results in Table 14 also show the prominent effect of the catalyst composition on ethylene conversion. At 150 °C, the ethylene conversion increased when the amount of aluminum in the catalyst increased, although the specific surface area of the catalysts strongly decreased. At higher reaction temperatures, the most active catalyst was $Si_9Al_{84}Ni_7$ (Figure 51).

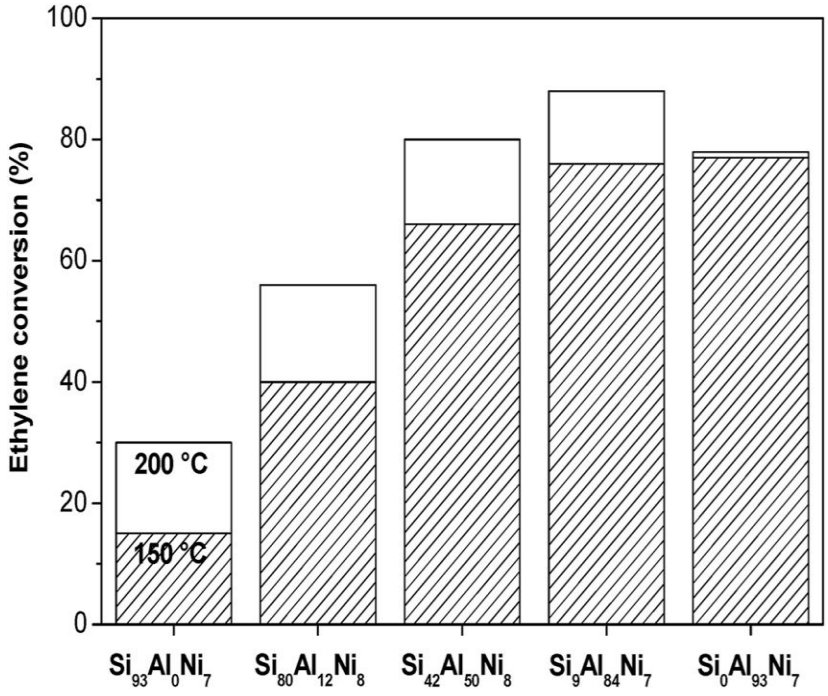


Figure 49: Ethylene conversion at 150 °C (striped bars) and 200 °C (empty bars) over the $Si_xAl_yNi_z$ catalysts.

The high activity of the alumina-rich catalysts, $Si_0Al_{83}Ni_7$ and $Si_9Al_{84}Ni_7$, cannot be accounted for by a textural effect as these two samples have significantly lower specific surface area than the other samples. XRD indicated the presence in these samples of NiO crystallites of ≈25 nm in size, but XPS suggested that these nanocrystals were not located at the extreme surface of the catalysts. $H_2$-TPR showed that both catalysts contained a high proportion of Ni sites that reduced at 600 °C, which is quite high for NiO species interacting with a support, and significantly lower than the temperature reported for $Ni^{2+}$ charge-compensating cations in aluminosilicates structures or bulk $NiAl_2O_4$ (> 700 °C). Accordingly, the high activity of $Si_0Al_{83}Ni_7$ and $Si_9Al_{84}Ni_7$ might be due to the presence in these catalysts of $Ni^{2+}$ species with a very strong interaction with the alumina/aluminosilicate matrix. These results are consistent with those previously obtained with other Ni-based catalysts.[102, 123] It has been shown that the catalytic sites of oligomerization are nickel cations in exchange position and that the oxide species are much less active in this reaction. To evaluate its stability, $Si_9Al_{84}Ni_8$ was tested over 6 h at 200 °C (Figure 52). Despite its relatively low pore diameter (3.5 nm) this catalyst appeared fairly stable. After 1 h on stream, it deactivated slowly, with a specific activity decreasing from 324 mmol $g^{-1}$ $h^{-1}$ after 1 h to

275 mmol $g^{-1}$ $h^{-1}$ after 6 h. In addition, the selectivity to butenes and hexenes remained practically constant.

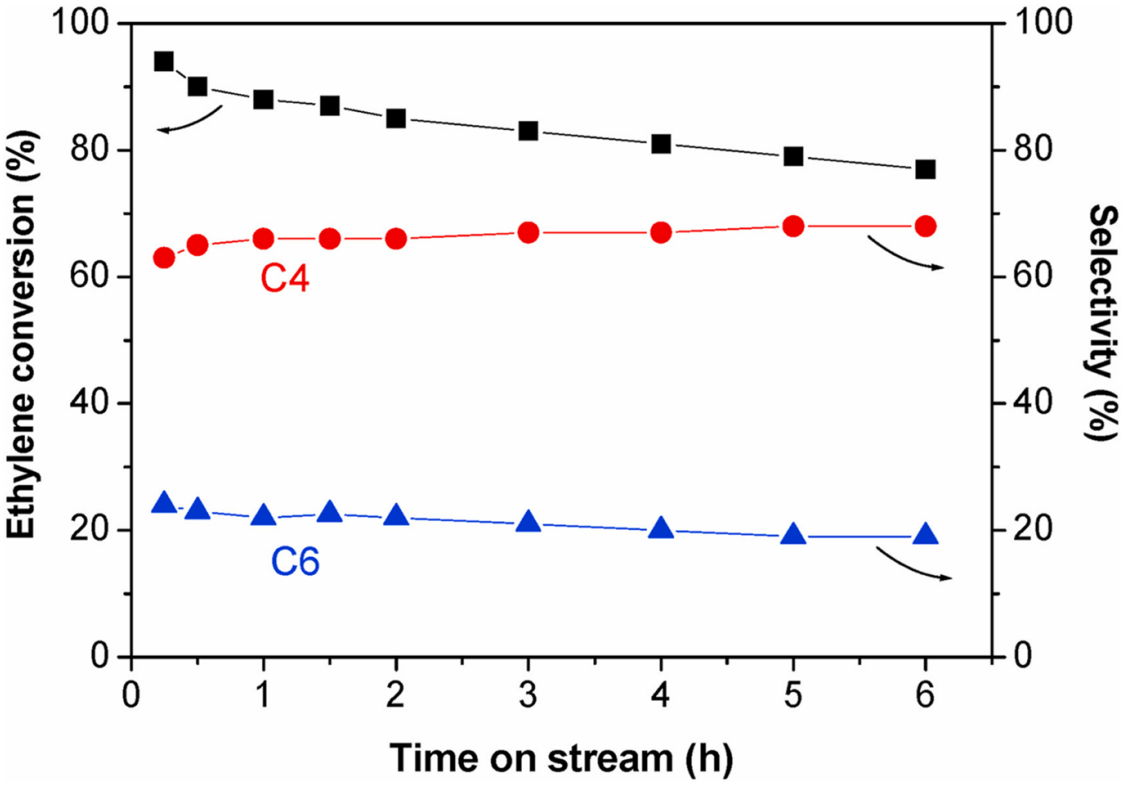


Figure 50: Ethylene conversion and C4/C6 selectivity vs. time on stream at 200 °C over the catalyst $Si_9Al_{84}Ni_7$ .

With a specific activity of 271 mmol $g^{-1}$ $h^{-1}$ at 150 °C, 314 mmol $g^{-1}$ $h^{-1}$ at 200 °C, and a selectivity to butenes of 71% at 150 °C, 66% at 200 °C, our best catalyst, $Si_9Al_{84}Ni_7$, compares well even with Ni catalysts supported on aluminated ordered mesoporous silicas which are considered the most active heterogeneous oligomerization catalysts. Thus, a Ni/Al-SBA-15 catalyst (Si/Al = 7, 2.6 wt.% of Ni) tested in flow mode under the exact same conditions exhibited a slightly higher activity: 325 mmol $g^{-1}$ $h^{-1}$at 150 °C, 343 mmol $g^{-1}$ $h^{-1}$at 200 °C, but a significantly lower selectivity to butenes: 45% at 150 °C, 38% at 200 °C.[99]

These experimental results are consistent with those previously obtained with other Ni-based catalysts.[360] The catalytic behavior of $Si_xAl_yNi_z$ materials is compared in Table 18 to that exhibited by post-synthesis alumination of SBA-15 silica with sodium aluminate, followed by ion exchange with nickel.[359] We can see that our best catalysts ($Si_0Al_{93}N_7$ and $Si_9Al_{84}Ni_7$) which

were obtained by one step reaction show slightly lower activity but significantly higher C4 selectivity than Ni-SBA-15 which was obtained in multi steps and more complicated method (Table 15).

Table 15: Catalysts behavior of Ni-SBA-15 catalysts for ethylene oligomerization.[359] Compared to that of our best catalysts. Temp. = 150 °C, P = 3.5 MPa, and WHSV =10 $h^{-1}$.

| Catalyst | Pressure (MPa) | WHSV | Conv.% | Activity ($mmol^1$ $h^{-1}$) | Selectivity to wt.% | | |
|---|---|---|---|---|---|---|---|
| | | | | | C4 | C6 | C8 |
| Ni-SBA-15 | 3 | 10 | 91 | 325 | 45 | 31 | 19 |

In order to show the effect of nickel in the ethylene oligomerization, the activity of different nickel loading catalysts at 150 °C was ploted against nickel content (Figure 53). It is clear that catalyst without nickel has no activity, the activity increases with the increasing of nickel loading and showing maximum activity at Ni (wt.% ~10). These results indicate that the nickel sites play a big role in the ethylene oligomerization.

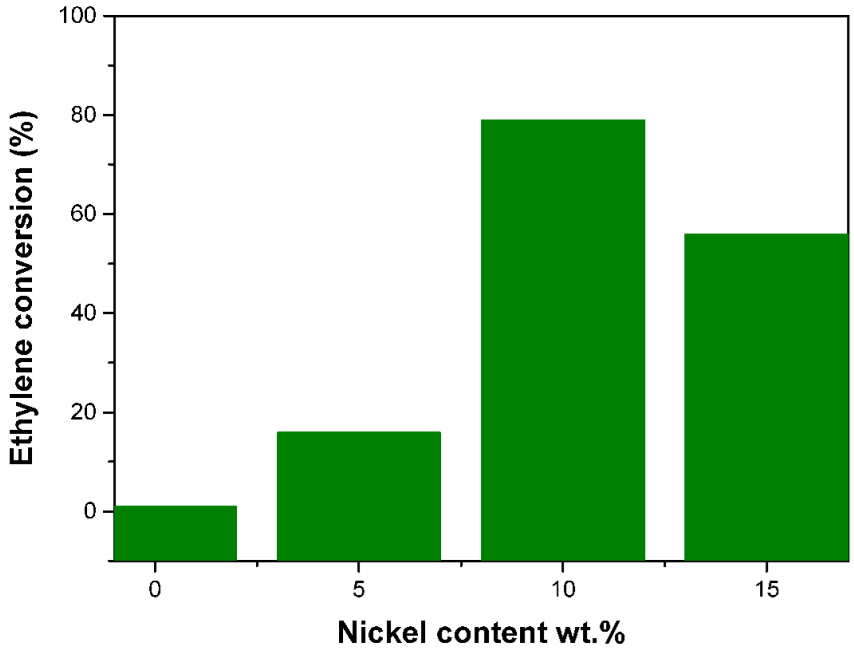


Figure 51: Effect of nickel content variation on Ethylene conversion at 150 °C.

## IV.2.7.1. Preparation of catalysts using alcohol route

Tow samples with expected compositions: $Si_0Al_{90}Ni_{10}$ and $Si_{10}Al_{80}Ni_{10}$ were prepared by alcohol route using Ethanol as a solvent and oxygen donor at the same time. We studied the texture and catalyst properties and compared them with the same composition catalysts prepared by ether route. For the texture, the results showed that specific surface area of samples prepared with ethanol is higher than those prepared with ether (Table 16).

Table 16: Texture of two $Si_xAl_yNi_z$ samples prepared by alcohol and ether routes measured by $N_2$-physisorption.

| Samples | Si/Al | Texture | | | Oxygen donor |
|---|---|---|---|---|---|
| | | S ($m^2 g^{-1}$) | $V_P$ ($cm^3 g^{-1}$) | $D_P$ (nm) | |
| $Si_0Al_{90}Ni_{10}$ a | 0.0 | 334 | 0.3 | 3.4 | EtOH |
| $Si_0Al_{90}Ni_{10}$ b | 0.0 | 368 | 0.3 | 3.1 | EtOH |
| $Si_{10}Al_{80}Ni_{10}$ a | 1.2 | 464 | 0.4 | 3.0 | EtOH |
| $Si_{10}Al_{80}Ni_{10}$ b | 1.2 | 486 | 0.3 | 2.7 | EtOH |
| $Si_0Al_{90}Ni_{10}$ a | 0.0 | 248 | 0.4 | 6.5 | $^iPr_2O$ |
| $Si_{10}Al_{80}Ni_{10}$ b | 1.2 | 395 | 0.3 | 3.5 | $^iPr_2O$ |

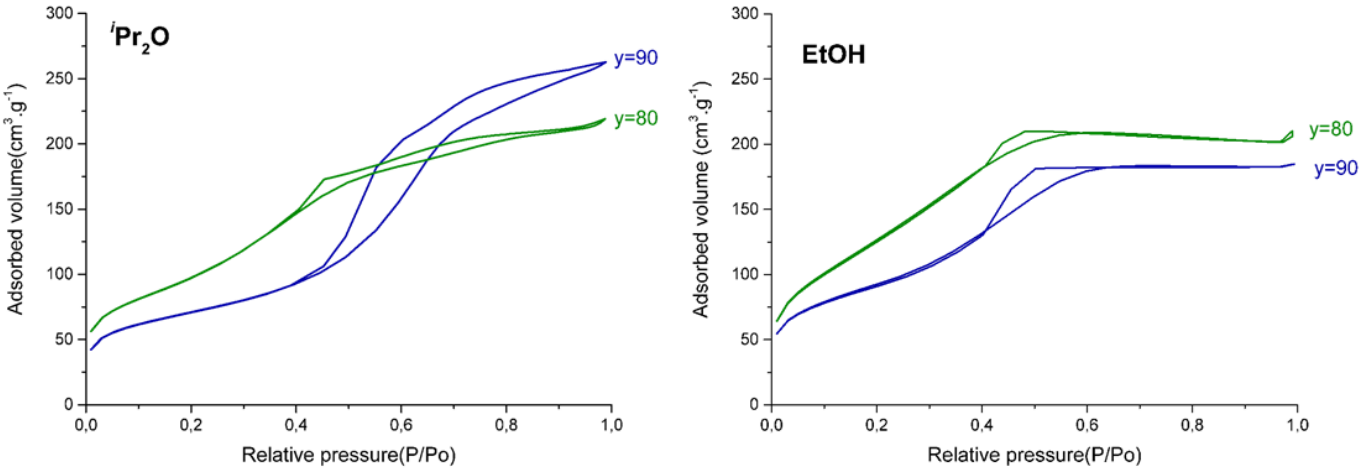


Figure 52: $N_2$ adsorption-desorption isotherms for $Si_0Al_{90}Ni_{10}$ and $Si_{10}Al_{80}Ni_{10}$ materials prepared by NHSG ($^{i}Pr_2O$ and EtOH) routes (y is the expected wt. % of $Al_2O_3$).

In order to evaluate the catalytic behavior under different reaction conditions and measure the activity of $Si_0Al_{90}Ni_{10}$ and $Si_0Al_{90}Ni_{10}$ prepared with alcohol and compared to the catalysts prepared with ether. The reaction was conducted at various conditions: T= 150-350 °C, P= 3.5 MPa and mass hourly space velocity (WHSV) =10 $h^{-1}$. Under these conditions, butenes, hexenes, and octenes are the major products and only small amounts of olefins having ≥ 10 carbon atoms are formed. In the C4 fraction, three n-butene isomers were detected: 1- C4, *trans*-2-C4, and *cis*-2-C4. The catalysts prepared with alcohol shows less ethylene conversion than these prepared with ether (Table 17).

Table 17: Catalysts behavior of Ni-based catalysts for ethylene oligomerization.

| Catalyst | Si/Al | Conv. | Activity | Selectivity to wt.% | | | Comment |
|---|---|---|---|---|---|---|---|
| | | | | C4 | C6 | C8 | |
| $Si_0Al_{90}Ni_{10}$ | 0.0 | 49 | 175 | 82 | 13 | 3 | EtOH |
| $Si_{10}Al_{80}Ni_{10}$ | 0.1 | 44 | 157 | 78 | 15 | 4 | EtOH |
| $Si_0Al_{90}Ni_{10}$ | 0.0 | 73 | 261 | 69 | 15 | 3 | $^{i}Pr_2O$ |
| $Si_{10}Al_{80}Ni_{10}$ | 0.1 | 79 | 282 | 72 | 20 | 5 | $^{i}Pr_2O$ |

Conditions: Temp. = 150 °C, P = 3.5 MPa, Reaction time = 65 min. and WHSV =10 $h^{-1}$.

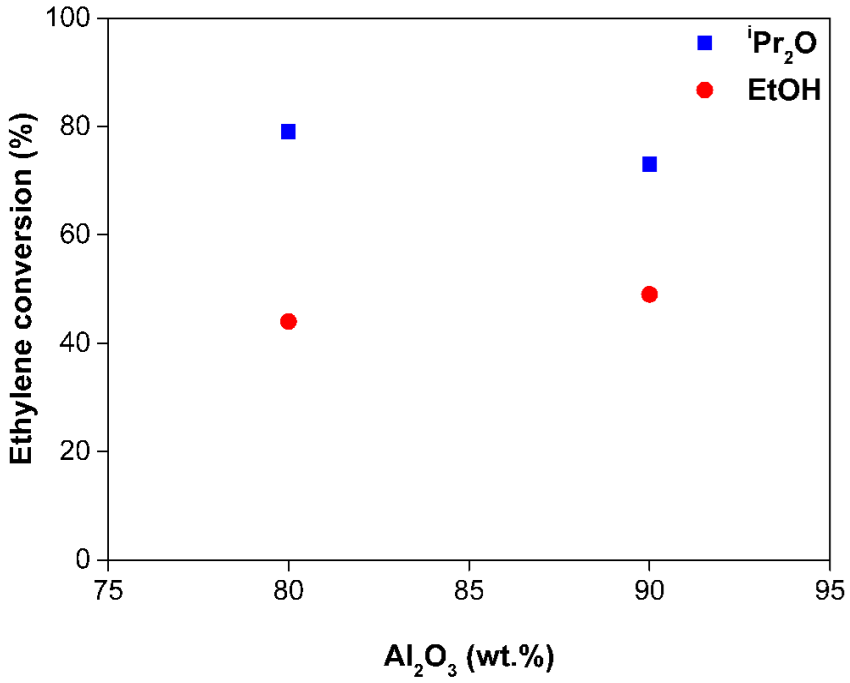


Figure 53: Comparison between the ethylene conversion for the catalysts prepared by NHSG (ether and alcohol routes).

# IV.3.Conclusion

In this study, we showed that $Si_xAl_yNi_z$ catalysts could be successfully prepared by a one-step NHSG route. Two parameters of the preparation were screened: the $Al_2O_3$ (or Si/Al ratio) and the NiO contents. The physico-chemical properties of the solids produced were studied and correlated with the catalytic performance. Particular attention was devoted to the description of the effect of $Al_2O_3$ content on the texture and on the acidity of the solids. NHSG provides a simple one-step route to mesoporous materials with a good control of the composition and relatively high surface areas and pore volumes. The specific surface area is maximum for the silica-NiO catalysts, and then it decreases markedly upon introduction of 20 and 45 wt.% alumina, and remains roughly constant for higher alumina contents. This effect seems to be intrinsic to silica-alumina based systems, regardless of the preparation method. Thus, the samples without alumina and with a low alumina content (ca. 5 wt.%) presented the best textures, with the specific surface area around (800 $m^2\ g^{-1}$) and very high pore volumes (1.1-1.7 $cm^3\ g^{-1}$). Conversely, the alumina-rich samples offered less interesting textures, with lower pore volume. According to XRD, independently of $Al_2O_3$ and

NiO contents, NiO crystals were detected. In the present study, the composition of the samples has a marked influence on the acidity of the samples. The Al-free catalyst is the least acidic in terms of absolute amount of acidic sites. As Al is introduced in silica-rich formulations, the density of both weak and medium/strong acidic sites increases and reaches a maximum for alumina contents of 80-90 wt.%. Furthermore, the alumina content affects the reduction temperature of the NiO species. The results of XPS demonstrate that Ni species are almost in the bulk than to the surface. The samples with high alumina content were highly active in the ethylene oligomerization of ethylene at 150 or 200 °C, and showed a high selectivity towards butenes and a good stability. Despite their very simple synthesis (one-step, no surfactant, one calcination) these catalysts compared well with the best model oligomerization catalysts reported, Ni-exchanged post-aluminated ordered mesoporous silicas, prepared by time-consuming and energy intensive multistep procedures. To reach higher catalytic activity, perspectives in the improvement of these materials properties could be the dispersal control of Ni species on the mesoporous aluminosilicate matrix. Two types of catalysts with compositions ($Si_0Al_{90}Ni_{10}$ and $Si_{10}Al_{80}Ni_{10}$) were prepared by alcohol route and the catalyst tests showed less activity than the catalysts with the same compositions prepared by ether route. The results obtained in this study confirm that oxygen donor plays an important role on the catalyst activity.

# GENERAL CONCLUSION-PERSPECTIVES

The main objective of this thesis was to show that Sol-Gel offered an interesting for the preparation of mixed oxides. Two different approaches were explored in this work, first one we showed that $Si_xAl_yNi_z$ catalysts can be successfully prepared by a one-step NHSG route. Two parameters of the preparation were screened: the $Al_2O_3$ (or Si/Al ratio) and the NiO contents. The physico-chemical properties of the solids produced were studied and correlated with the catalytic performance. Particular attention was devoted to the description of the effect of $Al_2O_3$ content on the texture and on the acidity of the solids. NHSG provides a simple one-step route to mesoporous materials with a good control of the composition and relatively high surface areas and pore volumes. The specific surface area is maximum for the silica-NiO catalysts, and then it decreases markedly upon introduction of 20 and 45 wt.% alumina, and remains roughly constant for higher alumina contents. This effect seems to be intrinsic to silica-alumina based systems, regardless of the preparation method. Thus, the samples without alumina and with a low alumina content (ca. 5 wt.%) presented the best textures, with specific surface area around 800 $m^2\ g^{-1}$ and very high pore volumes (1.1-1.7 $cm^3\ g^{-1}$). Conversely, the alumina-rich samples offered less interesting textures, with lower pore volume. According to XRD, independently of $Al_2O_3$ and NiO contents, NiO crystals were detected. In the present study, the composition of the samples has a marked influence on the acidity of the samples. The Al-free catalyst is the least acidic in terms of absolute amount of acidic sites. As Al is introduced in silica-rich formulations, the density of both weak and medium/strong acidic sites increases and reaches a maximum for alumina contents of 80-90 wt.%. Futhermore, the alumina content affects the reduction temperature of the NiO species. All silica-alumina and alumina supported catalysts were significantly active in ethylene oligomerization while the activity of the silica-based catalyst was very low. The catalysts with the higher $Al_2O_3$ contents $Si_0Al_{90}Ni_{10}$ and $Si_{10}Al_{80}Ni_{10}$ exhibit the highest catalytic activity for NiO loadings equal to 10 wt.%. The marked acidic character of Al-containing materials as compared to Al-free samples seems to be decisive. The nature of the support strongly determines the acidic properties of the catalyst. Furthermore, we showed that the specific activity in oligomerization decreases when the NiO loading increases.

Second part is another one-step NHSG (alcohol route) were successfully used to prepare ($Si_x$-$Al_y$) mixed oxides from non-expensive precursors. Two types of alcohol, ethanol and $^t$BuOH were used as a solvent and oxygen donor in the same time. The $Si_xAl_y$ mixed oxides were also prepared by

NHSG (ether route) and compared with the same composition samples prepared by alcohol route The Si/Al ratio can be easily controlled, knowing that it plays an important role in the structure, texture, acidity of the samples. Calcination in air largely eliminates chlorine and carbon from essentially non-condensed groups and the solvent. The composition of all samples prepared by both alcohol and ether routes show good control on composition. The texture is strongly depend on the Si/Al and on type of solvent, the $N_2$-adsorption desorption presented that samples prepared with EtOH and ether show high specific surface area and it decreases with Si loading decreases in the samples, in the same time ether route provides higher pore volume than alcohol route. The structure of all samples were studied by XRD and NMR, the results obtained showed that all the mixed oxides are amorphous. Two types of catalysts with compositions $Si_0Al_{90}Ni_{10}$ and $Si_{10}Al_{80}Ni_{10}$ were prepared by alcohol route (ethanol) and the catalyst tests showed less activity than the catalysts with the same compositions prepared by ether route.

Much remains to be done to explore all the possibilities offered by the NHSG process in catalysis and especially in acid catalysis.

(1) $SiO_2$-$Al_2O_3$-NiO mixed oxides prepared by NHSG route could be calcined under various range of temperature for example (500, 700, 800, 900°C) to investigate the effect of temperature on texture, structure, surface and catalyst activity.

(2) Furthermore, Mo-Ni, W-Ni supported on silica-alumina can be widely investigated via modification of the wt.% of active sites or/and Si/Al ratio in order to improve nickel catalytic activity for metathesis.

(3) Besides, a wide range of silica-alumina mixed oxides based on (Mo, Pd, Pt, W, Ni-Mo, Ni-W *etc.*) could be synthesized by using different types of alcohols (Ethanol, Tertiary butanol, Benzyl alcohol) .

(4) Sulfating of $SiO_2$-$Al_2O_3$-NiO is another interesting study in order to improve the acidity of catalysts. On sulfating, the nickel metal is converted to nickel sulfide, and the $H_2S$ reacts with the silica-alumina-nickel salts to regenerate the original strong acid sites of the silica-alumina support.

(5) To the best of our knowledge, there is no example of using NHSG to elaborate carriers with original textures, structures or surface chemistry. The use of multi-step synthetic procedures would undoubtedly make it possible to further increase the activity of mixed oxide catalysts.

# CHAPTER V

# EXPERIMENTAL PART

The first part of this chapter deals with the preparation of mixed oxides: the $SiO_2$-$Al_2O_3$ supports prepared by HSG in acidic and basic media, by NHSG process using alcohol and ether routes and the $SiO_2$-$Al_2O_3$-NiO catalysts synthetized using NHSG route. The second part focuses on the principles of the main characterizations used to correlate the physico-chemical properties of the materials and their application in heterogeneous catalysis.

# V.1. Preparation of mixed oxides

## V.1.1. Si-Al supports prepared by HSG route

The $SiO_2$-$Al_2O_3$ mixed oxides with different Si/Al ratios (0, 0.1, 0.3, 1, 2.9, 8.7 and∞) were synthesized in both acidic and basic medium (Tables 18,19).**In acidic medium**, $SiO_2$ sol was prepared by introducing (1:1:2) volume ratios TEOS, ethanol and water (which was adjusted to a pH of 1.5 with HCl), in 100ml conical flask. The solution was stirred for 1h using a magnetic stirrer at room temperature to get a transparent sol. $Al_2O_3$ sol was prepared by introducing Aluminum isopropoxide $Al(OC_3H_7)_3$ and $H_2O$ (pH 1.5) that had been preheated to about 90 °C in 250 ml conical flask. In addition, the solution was stirred for 1h to obtain homogenous sol. By mixing and stirring $SiO_2$ and $Al_2O_3$ sols, the $SiO_2$-$Al_2O_3$ sol was prepared. The sol was heated to 50 °C for 3 days (aging), the gel was washed under air atmosphere with ethanol, acetone and diethyl ether respectively and dried at 25 °C under vacuum (10 Pa) for 1 h and then for 4 h at 120 °C. The resulting xerogel was crushed in a mortar and calcined in air at 500 °C for 5h (heating rate 10 °C $min^{-1}$). **In Basic medium**, $SiO_2$ sol was prepared by mixing one part (by volume) of TEOS with two parts of distilled water, which was adjusted to a pH of 1.5 with nitric acid 100ml conical flask. The TEOS was then allowed to hydrolyze overnight at room temperature under continuous stirring to give a homogeneous sol. $Al_2O_3$ sol was prepared by introducing Aluminum nitrate $Al(NO_3)_3$ and $H_2O$ in 250 ml conical flask, the solution was stirred all the night. Next, the $SiO_2$-$Al_2O_3$ sol was prepared by mixing $SiO_2$ and $Al_2O_3$ sols and stirring was continued for 1 h. Finally, ammonium hydroxide solution (2 M) was added drop wisely to form a hydrogel at a pH of 8.5. The gel was washed with distilled water and vacuum filtered three times to remove the ammonium nitrate from the gel. In the final washing and filtering step, ethanol was used in same proportion. Dried at 25 °C under vacuum (10 Pa) for 1 h and then for 4 h at 120 °C. The resulting xerogel was crushed in a mortar and calcined in air at 500 °C for 5h (heating rate 10 °C $min^{-1}$).

Table 18: Mass weighting of starting materials used in HSG process in acidic medium.

| Sample | TEOS | Al-$(OiPr)_3$ | pH |
|---|---|---|---|
| | g (mol)/$H_2O$(mL) | g (mol)/$H_2O$(mL) | |
| $Si_{100}Al_0$ | 7.0(0.033)/ 15 | ---- | 1.6 |
| $Si_{90}Al_{10}$ | 6.3(0.03)/ 13.4 | 0.82(0.004)/11 | 1.6 |
| $Si_{75}Al_{25}$ | 5.2(0.025)/ 11.2 | 2.04(0.01)/27 | 1.6 |
| $Si_{50}Al_{50}$ | 3.54(0.017)/ 7.4 | 4.0(0.02)/54 | 1.6 |
| $Si_{25}Al_{75}$ | 1.73(0.008)/ 3.7 | 6.1(0.03)/81 | 1.6 |
| $Si_{10}Al_{90}$ | 0.7(0.003)/ 1.5 | 7.2(0.035)/95 | 1.6 |
| $Si_0A_{100}$ | ---- | 8.2(0.04)/ 108 | 1.6 |

Table 19: Mass weighting of starting materials used in HSG in basic medium.

| Sample | TEOS | $Al(NO_3)_3$ | $H_2O$ (mL) | pH |
|---|---|---|---|---|
| | g(mol) | g(mol) | | |
| $Si_{100}Al_0$ | 7.0(0.033) | ----- | 15 | 8.5 |
| $Si_{90}Al_{10}$ | 6.3(0.03) | 0.85(0.004) | 15 | 8.5 |
| $Si_{75}Al_{25}$ | 5.2(0.025) | 2.13(0.01) | 15 | 8.5 |
| $Si_{50}Al_{50}$ | 3.54(0.017) | 4.3(0.02) | 15 | 8.5 |
| $Si_{25}Al_{75}$ | 1.73(0.008) | 6.4(0.03) | 15 | 8.5 |
| $Si_{10}Al_{90}$ | 0.7(0.003) | 7.5(0.035) | 15 | 8.5 |
| $Si_0A_{100}$ | ----- | 8.5(0.04) | 15 | 8.5 |

## V.1.2. Si-Al supports prepared by NHSG route

### V.1.2.1 synthesis of the catalysts

In alcohol route, all $SiO_2$-$Al_2O_3$ samples were synthesized by NHSG process through using two different types of alcohols (ethanol and tertiary butanol) (Tables 20,21). The mixed oxides were synthesized by adding precursors ($SiCl_4$, $AlCl_3$) in schlenk under argon atmosphere inside the glove box (non-aqueous medium). An excess amount of alcohol (25 ml) of EtOH or $^tBuOH$ were added to the schlenk (outside the glove box) by using the syringe technique. Next, the reactant were transferred into an autoclave under Argon. The reaction takes place at 110 °C under autogenous pressure for 4 days, after being cooled to room temperature, gel was produced. The product was isolated by filtration and purified by successive washing with $CH_2Cl_2$. Powders were manually grinded by using mortar after drying 1h at room temperature and 4h at 100 °C. Finally, the samples were calcined under air at 500 °C for 5h.

For all the samples prepared by NHSG (ether route) (Table 22), the mixed oxides with formula $SiO_2$-$Al_2O_3$ were synthesized under argon atmosphere inside the glove box (non-aqueous medium), by using dried $SiCl_4$, $AlCl_3$. Dry diisopropyl ether was used as oxygen donor. All reactants were dissolved in 10 ml of dry $CH_2Cl_2$ inside the autoclave under stirring. The reaction was performed at 110 °C under autogenous pressure for 4 days. Colorless or white gel products were obtained. The gels were isolated by filtration and purified by washing with $CH_2Cl_2$ to remove unreacted species and bi-products. The final products were dried at 25 °C for 1h and then dried at 100 °C for 4h. Powders were grinded manually by using mortar to obtain fine powders.

Table 20: Mass weighting of starting materials used in NHSG using t-BuOH as solvent and oxygen donor.

| Sample | $SiCl_4$ | $AlCl_3$ | t-BuOH (mL) |
|---|---|---|---|
| | g (mol) | g (mol) | |
| $Si_{100}Al_0$ | 2.8 (0.016) | ----- | 25 |
| $Si_{90}Al_{10}$ | 2.6 (0.015) | 0.26 (0.002) | 25 |
| $Si_{75}Al_{25}$ | 2.1 (0.012) | 0.65 (0.005) | 25 |
| $Si_{50}Al_{50}$ | 1.42 (0.008) | 1.3 (0.01) | 25 |
| $Si_{25}Al_{75}$ | 0.42 (0.004) | 0.66 (0.015) | 25 |
| $Si_{10}Al_{90}$ | 0.28 (0.002) | 2.35 (0.018) | 25 |
| $Si_0A_{100}$ | ----- | 2.6 (0.02) | 25 |

Table 21: Mass weighting of starting materials used in NHSG using EtOH as solvent and oxygen donor.

| Sample | $SiCl_4$ | $AlCl_3$ | EtOH (mL) |
|---|---|---|---|
| | g (mol) | g (mol) | |
| $Si_{100}Al_0$ | 2.8 (0.016) | ----- | 25 |
| $Si_{90}Al_{10}$ | 2.6 (0.015) | 0.26 (0.002) | 25 |
| $Si_{75}Al_{25}$ | 2.1 (0.012) | 0.65 (0.005) | 25 |
| $Si_{50}Al_{50}$ | 1.42 (0.008) | 1.3 (0.01) | 25 |
| $Si_{25}Al_{75}$ | 0.42 (0.004) | 0.66 (0.015) | 25 |
| $Si_{10}Al_{90}$ | 0.28 (0.002) | 2.35 (0.018) | 25 |
| $Si_0A_{100}$ | ----- | 2.6 (0.02) | 25 |

Table 22: Mass weighting of starting materials used in NHSG using $CH_2Cl_2$ as solvent and $^{i}Pr_2O$ as oxygen donor.

| Sample | $SiCl_4$ | $AlCl_3$ | $iPr_2O$ g (mol) | $CH_2Cl_2$ (mL) |
|---|---|---|---|---|
| | g (mol) | g (mol) | | |
| $Si_{100}Al_0$ | 2.8 (0.016) | ----- | 3.4 (0.033) | 10 |
| $Si_{90}Al_{10}$ | 2.6 (0.015) | 0.26 - 0.002) | 3.36 (0.033) | 10 |
| $Si_{75}Al_{25}$ | 2.1 (0.012) | 0.65 - 0.005) | 3.3 (0.032) | 10 |
| $Si_{50}Al_{50}$ | 1.42 (0.008) | 1.3 - 0.01) | 3.2 (0.031) | 10 |
| $Si_{25}Al_{75}$ | 0.42 (0.004) | 0.66 - 0.015) | 3.1 (0.03) | 10 |
| $Si_{10}Al_{90}$ | 0.28 (0.002) | 2.35 - 0.018) | 3.04 (0.03) | 10 |
| $Si_0A_{100}$ | ----- | 2.6 - 0.02) | 3.0 (0.029) | 10 |

## V.1.3. Si-Al-Ni mixed oxides prepared by NHSG route

### V.1.3.1 Synthesis of the catalysts

All the samples were prepared by the non-hydrolytic sol-gel process (ether route) (Table 23).The $SiO_2$-$Al_2O_3$-NiO mixed oxides with different Si/Al ratios were prepared in 1 g quantities in 48 mL PTFE lined autoclaves (Parr Instruments). All manipulations were performed under argon using a glovebox to avoid hydrolysis. $SiCl_4$, $AlCl_3$ and $Ni(acac)_2$ were introduced first in the autoclave, then $iPr_2O$ and $CH_2Cl_2$ (10 mL) were added. The sealed autoclave was heated at 110 °C for 4 days under autogenous pressure. In this synthesis, the reactions around Si are catalyzed by $AlCl_3$. In the preparation of the Al-free mixed oxide (Si/Al = ∞), $FeCl_3$ (0.015 mmol) had to be used as a catalyst to obtain a gel. After cooling down to room temperature, the gel was washed (under air atmosphere) with $CH_2Cl_2$, dried at 20 °C under vacuum (10 Pa) for 1 h and then for 4 h at 120 °C. The resulting xerogel was crushed in a mortar and calcined in air at 500 °C for 5 h (heating rate 10 °C $min^{-1}$). The overall oxide yield was better than 90% in all cases. The as-prepared materials appeared either as fine powders (more than 45 wt% of $Al_2O_3$) or as coarse powders with larger particle sizes (less than 45 wt% of $Al_2O_3$).

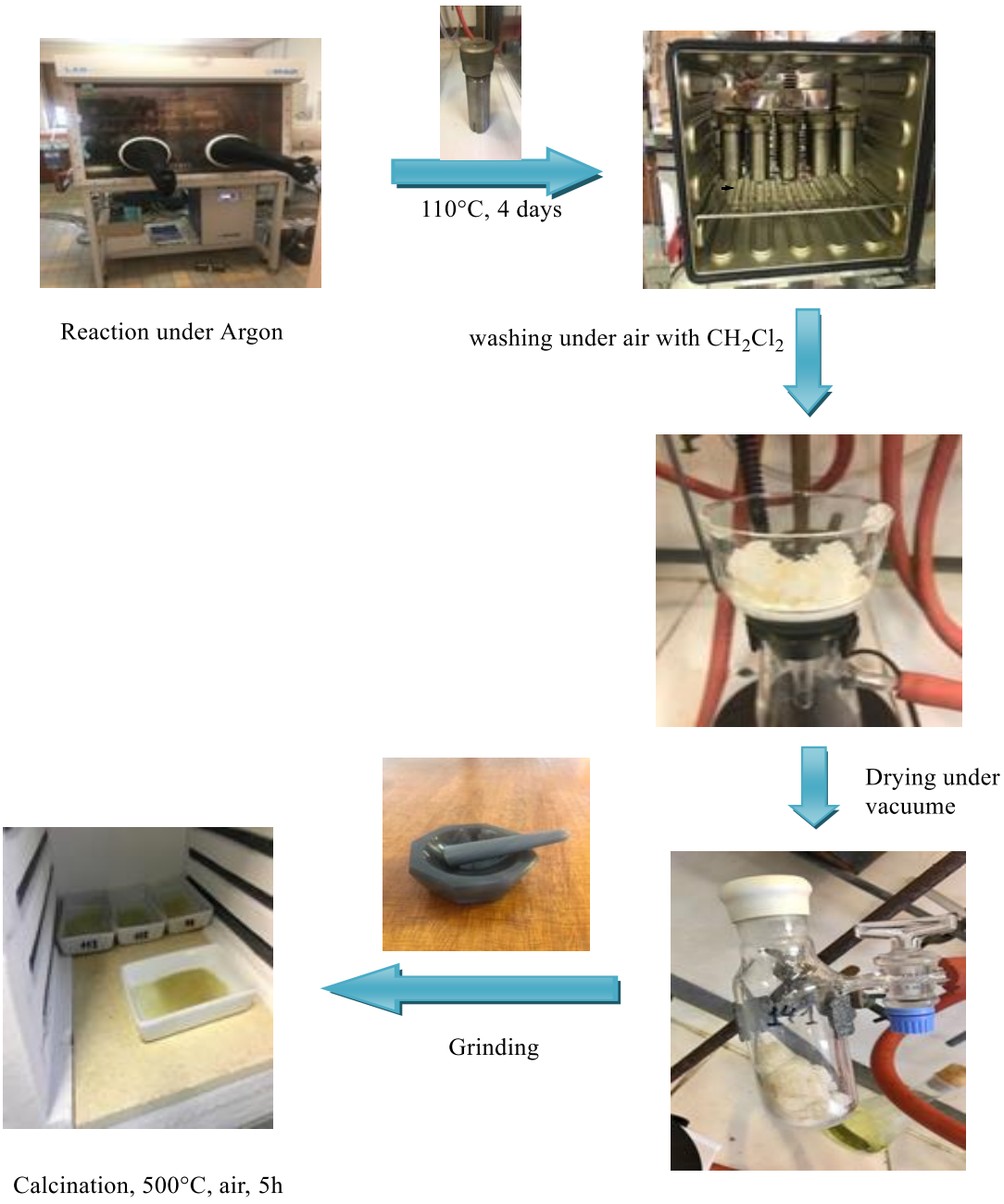


Figure 54: Synthesis of $Si_x$ $Al_y$ $Ni_z$ mixed oxides prepared by NHSG route.

Table 23: Mass weighting of starting materials used in the synthesis of $SiO_2$-$Al_2O_3$-NiO samples

| Samples | $SiCl_4$ | $AlCl_3$ | $Ni(acac)_2$ | $^{i}Pr_2O$ |
|---|---|---|---|---|
| | g (mol) | g (mol) | g (mol) | g (mol) |
| $Si_0Al_{95}Ni_5$ | ---- | 2.5 (0.019) | 0.17(0.0007) | 2.9(0.028) |
| $Si_{10.5}Al_{84.5}Ni_5$ | 0.3(0.0018) | 2.2(0.016) | 0.17(0.0007) | 3.0(0.029) |
| $Si_{75}Al_{20}Ni_5$ | 2.1(0.013) | 0.52(0.004) | 0.17(0.0007) | 3.2(0.031) |
| $Si_{85}Al_{10}Ni_5$ | 2.4(0.015) | 0.26(0.002) | 0.17(0.0007) | 3.3(0.032) |
| $Si_{80}Al_{15}Ni_5$ | 2.3(0.013) | 0.4(0.003) | 0.17(0.0007) | 3.2(0.031) |
| $Si_{90}Al_5Ni_5$ | 2.5(0.015) | 0.13(0.001) | 0.17(0.0007) | 3.3(0.032) |
| $Si_0Al_{90}Ni_{10}$ | ---- | 2.35(0.002) | 0.34(0.001) | 2.8(0.028) |
| $Si_{10}Al_{80}Ni_{10}$ | 0.28(0.002) | 2.1(0.016) | 0.34(0.001) | 2.9(0.028) |
| $Si_{45}Al_{45}Ni_{10}$ | 1.27(0.007) | 1.17(0.009) | 0.34(0.001) | 3.0(0.029) |
| $Si_{80}Al_{10}Ni_{10}$ | 2.3(0.013) | 0.26(0.002) | 0.34(0.001) | 3.1(0.03) |
| $Si_{85}Al_5Ni_{10}$ | 2.4(0.014) | 0.13(0.001) | 0.34(0.001) | 3.2(0.031) |
| $Si_{89}Al_1Ni_{10}$ | 2.5(0.015) | 0.03(0.0002) | 0.34(0.001) | 3.2(0.031) |
| $Si_{90}Al_0Ni_{10}$ * | 2.5(0.015) | ---- | 0.34(0.001) | 3.2(0.031) |
| $Si_0Al_{85}Ni_{15}$ | ---- | 2.2(0.016) | 0.51(0.002) | 2.8(0.028) |
| $Si_{85}Al_0Ni_{15}$ | 2.4(0.015) | ---- | 0.51(0.002) | 3.1(0.03) |
| $Si_{9.4}Al_{75.6}Ni_{15}$ | 0.26(0.0016) | 1.97(0.015) | 0.51(0.002) | 2.8(0.028) |
| $Si_{80}Al_5Ni_{15}$ | 2.3(0.013) | 0.13(0.0001) | 0.51(0.002) | 3.1(0.03) |
| $Si_{75}Al_5Ni_{20}$ | 2.12(0.012) | 0.13(0.001) | 0.68(0.003) | 2.9(0.029) |

*:0.015 mmol of $FeCl_3$.

# V.2. Instrumentation

Some techniques were widely explored during this PhD thesis based on the main properties of the materials in which this project was focused on: composition, crystallinity, porosity, acidity, structure and morphology.

## V.2.1. Energy Dispersive X-ray diffraction (EDX)

The atomic percentages of Ni, Si and Al were obtained by energy dispersive X-ray spectroscopy (EDX). Measurements were carried out using an X-Max Silicon Drift detector mounted on an FEI Quanta FEG 200 scanning electron microscope. To obtain reliable results in the analyses, the data for each sample is the average of three separate measurements. The use of a piece of Scotch® to fix the powder and the partial vacuum (0.3 Torr) in the measuring chamber does not allow having a correct analysis of the concentrations in C and O.

## V.2.2. Brunaruer-Emmett-Teller (BET)

Pores can be defined as cavities or channels that appear inside materials (called porous materials). Their surface give part of the specific surface area of materials and they can be opened or closed (*i.e.* inaccessible for fluids). Aside from their shape, pores can be classified according to their width, assuming spherical or cilindrical shape: Ø>50 nm pores are called macropores; Ø<2 nm pores are known as micropores and 2<Ø<50 pores are mesopores. To measure this parameter, adsorption of molecules on the surface of the solid is the mostly used technique. This phenomenon can be described as the retention of atoms of a gas or liquid on the surface of a solid by physical or chemical interactions between the solid (*i.e.* adsorbent) and the fluid. However, only physisorption is used for textural characterization because it does not modify the properties of the solid. The opposite process, desorption, consist in the release of the adsorbed molecules. It is noteworthy that adsorption methods used for materials characterization only take into account the opened pores because they are the only accessible ones[361]. In the same idea, accessibility of a particular molecule will always depend of the pore size; this is why small molecules of chemically inert gas such as $N_2$ or Ar are generally used.

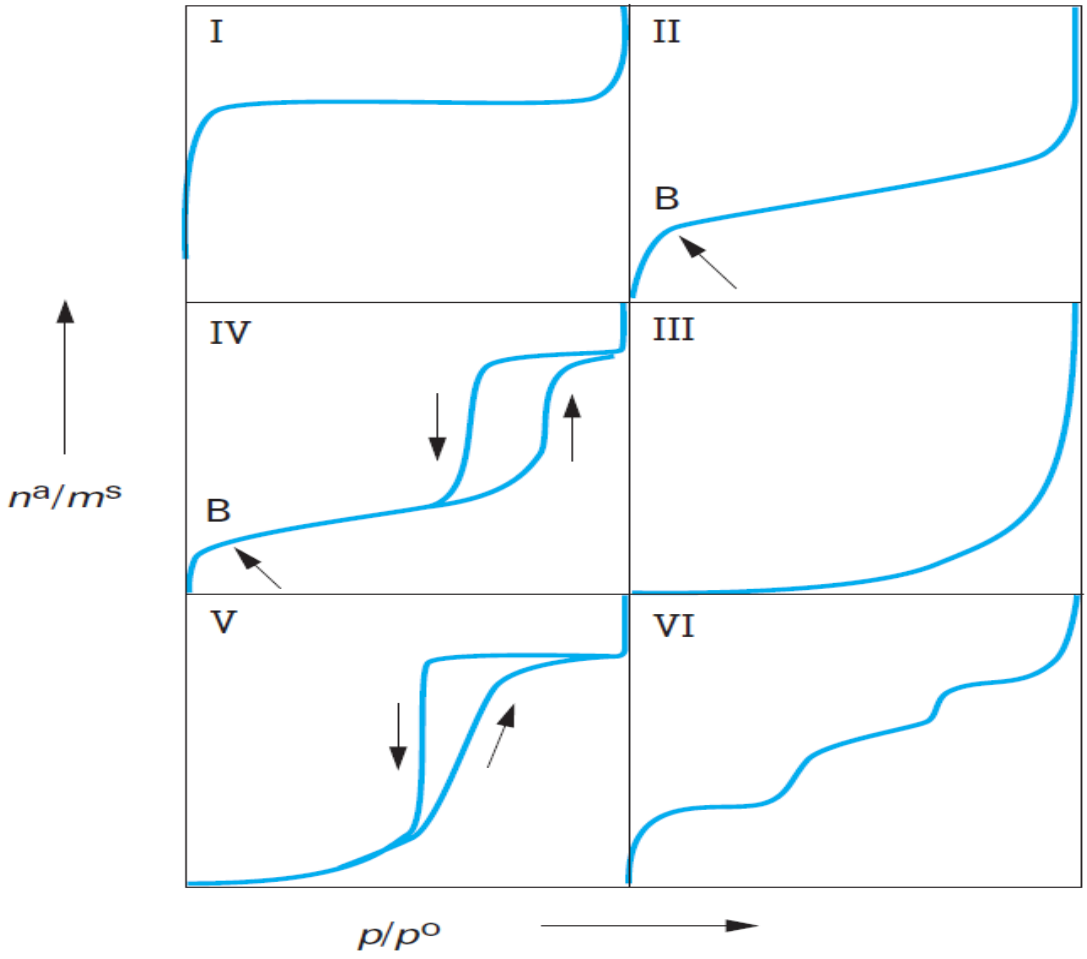


Figure 55: Classification of isotherms according to IUPAC.

Physisorption isotherms classification, represented in (Figure 58), was firstly used by Brunauer *et al* in 1940 and then taken in by the IUPAC (International Union of Pure and Applied Chemistry) in 1985. Isotherms shapes give valuable information about textural characteristics of materials. Type I corresponds to strictly microporous compounds; they present an adsorbent saturation at low relative pressures. Type II is characteristic of non-porous or macroporous compounds and corresponds to a multimolecular adsorption. Type IV corresponds to mesoporous materials; this isotherm is characterized by a similar shape of isotherm of type II at low relative pressures

(*P/P0*<0.42 for molecular nitrogen) and saturation for higher relative pressures. Another feature of type IV is the presence of hysteresis due to the irreversible process of desorption of nitrogen condensed by capillarity into the mesopores. Shape, at low relative pressures, of type III and V isotherms evidences low interaction between the adsorbent and the fluid. The last isotherm (type VI) is characteristic of materials having homogenous surfaces forming adsorbing layers one after another. There are different adsorption theories; nevertheless, the Brunauer-Emmett-Teller (BET) one is the most widely used for textural characterization of porous materials. This theory is based on the formation of a monomolecular layer covering the whole surface of the adsorbent. In brief, it stats that multimolecular adsorption takes place on the basis of the Langmuir theory and takes into account that the surface may be represented as a set of superficies (SN, N=0, 1, 2, etc.). In this set of superficies, *N* correspond to the number of layers of adsorbed molecules and those molecules may serve themselves as adsorbent sites for further ones, with no interaction between adsorbed molecules. So, they established a relationship between the relative pressure (*x=P/P0*) and the adsorbed amount of fluid (na) for a limited number of layers N eq. 1.

$$\frac{na}{n^a{}_m} = \left(\frac{Cx}{1-x}\right)\left(\frac{1-(N+1)x^N + Nx^{N+1}}{1+(C-1)x-Cx^{N+1}}\right) \qquad \text{Eq. 1}$$

where $n^a m$ is the amount of fluid needed for covering the surface with a single molecular layer and *C* a constant linked to the adsorption energy for the first layer *E1*, the liquefaction energy of the adsorbable fluid *EL*, the adsorption temperature *T* and the gas constant *R* eq. 2.

$$C = \exp\left(\frac{E_1 - E_L}{RT}\right) \qquad \text{Eq. 2}$$

When the number of layers *N* tends to infinity, Equation 1 can be simplified in eq. 3.

$$\frac{na}{n^a{}_m} = \frac{Cx}{1-x\ (1-x+Cx)} \qquad \text{Eq. 3}$$

This equation is only valid for low relative pressures (*P/P0*<0.35) and is more often used in its linear form eq. 4 also named transformed BET equation where the only unknown values are *C* and $n^a m$.

$$\frac{P/P_0}{n^a\,(1-P/P_0)} = \frac{1}{n^a{}_m C} + \left(\frac{C-1}{n^a{}_m C}\right)\left(\frac{P}{P_0}\right) \qquad \text{Eq. 4}$$

The specific surface area, *SBET*, can be determined knowing the surface *A* of the adsorbent following eq. 5. Surface *A*, in turn, can be calculated once it is completely covered by a single layer of adsorbable fluid and also knowing the occupied surface by an adsorbed molecule *σm* (*σm* =0.162 nm2 for the case of molecular nitrogen adsorbed at 77.4 K according to IUPAC).

$$S_{BET} = \frac{A}{m_a} = \left(\frac{n^a m}{m_a}\right) N_A \sigma_m \qquad \text{Eq. 5}$$

with *ma* being the adsorbent mass and *NA* the Avogadro constant (*NA*=6.023·1023 mol-1). Besides, *nam* can be determined graphically using experimental data into the isotherm linear region (*i.e.* calculating the slope and the ordinate at the origin values with the transformed BET equation (eq.4). The hysteresis shape, commonly observed in mesoporous materials, gives relevant information about the pores characteristics. For instance, Figure 62 shows the different hysteresis shapes according to IUPAC, H1 and H2 correspond to mesoporous compounds (*i.e.* type IV isotherms); H1 is usually observed in materials with a narrow pore distribution; while $H_2$ evidences intercommunication amongst mesopores. H3 appears in materials forming aggregates and H4 is often correlated to laminar microporous materials; the two last shapes correspond to type II isotherms .

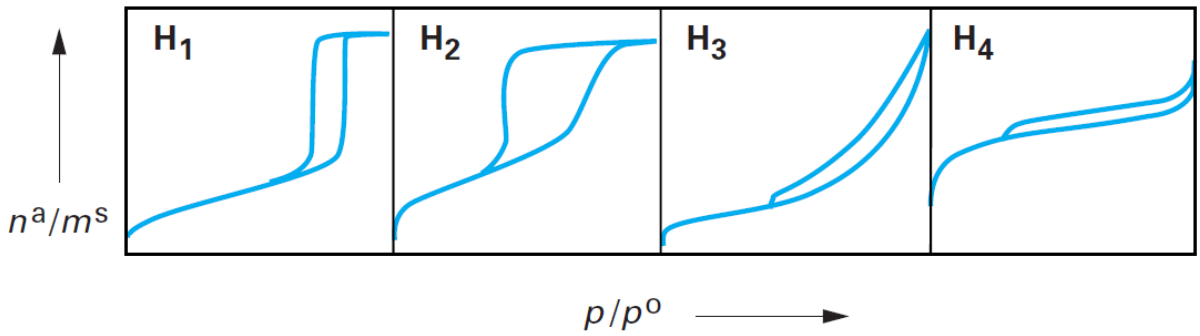


Figure 56: Hysteresis classification according to IUPAC.

Finally, the molecular nitrogen physisorption technique also allows the determination of pore size. As seen for the adsorption theories, it also exists different methods to determine the pore size distribution; however, the Barret-Joyner-Halenda (BJH) method is the most widely used. It take several assumptions such as porosity is constituted by independent, indeformable and well defined (*i.e.* cylinder) mesopores; multilayer adsorption in mesopores follow same rules as adsorption over a plane surface; Kelvin's law for capillary condensation is valid for mesopores (this law brings the Kelvin radius *rK*) and capillary condensation starts in pores already presenting a multi-molecular layer of thickness *t* which varies as function of the relative pressure (e.g. Harkins and Jura method -eq.6). Moreover, it generally uses the desorption branch as it is considered more representative for the capillary condensation phenomenon.

$$t = \left( \frac{0.1399}{0.034 - \lg(P/P)} \right)^{0.5} \qquad \text{Eq. 6}$$

The $N_2$ sorption analyzes were made on a Micrometrics Tristar. The samples are degassed overnight at 150°C under vacuum (2 Pa). The specific surface area is determined by the BET method in the range P/Po of 0.05 to 0.30. The pore size distribution is derived from the desorption branch using the BJH method. The average pore diameter is calculated as (4 × pore volume / BET surface area). The total volume of the micropores of the samples is estimated by the t-plot analysis.

## V.2.3. X-ray diffraction (XRD)

The X-ray diffraction technique is a powerful tool to determine the crystal structure of materials, their particle size and even the orientation of a single crystal into a polycrystalline framework. The

X-rays were discovered in 1895 and their wavelengths are included into the 0.5-2.5 °A range; however, it was not until 1912 that a crystal was used for the first time as diffraction network and one year later W.H. and W.L. Bragg determined the first crystalline structure. X-rays are generated for the fast deceleration of an electrically charged particle with enough kinetic energy. In practice, X-ray tubes contains an electron source and two metallic electrodes; when a high voltage is applied between them, electrons are thrown towards the anode striking the target at high speed. Thus, X-ray are the result of this impact and they radiate in all directions. This process may generate two different kind of spectrum: the continuous and the characteristic spectrum. The first one appears as a result of the process previously described; while the characteristic one, only appears above a certain high voltage value. The characteristic spectrum evidences new maxima over the continuous spectrum and they are dependent of the electron source (*i.e.* they do not depend from the electron deceleration as continuous spectrum); this characteristic lines, notably *Kα* line, have allowed the development of the X-ray diffraction technique. Crystals are composed by periodic arrays of atoms along the three dimensions of a plane. The X-ray diffraction phenomena is closely linked to the fact that the interatomic distances, in crystals, are in the same range than the X-rays wavelength. The direction of the diffracted beam follows the Bragg's law eq. 7.

$$n\lambda=2d\sin\theta \qquad \text{Eq. 7}$$

where $\lambda$ correspond to the wavelength of the diffracted X-ray; $d$ is the distance between atomic planes; $\theta$ is the angle formed by the incident beam and the scattering plane and *n*, an integer, gives the reflection order. Bragg's law can be demonstrated geometrically by analogy to the reflection phenomenon as observed in Figure 66 [362, 363]. Briefly; eq.8 and eq.10 can be geometrically obtained; then, as segments AB and BC are equals, eq.9 is determined. Finally, mixing eq.9 and eq. 10, Bragg's law is obtained.

$$\sin\theta=AB/d=BC/d \qquad \text{Eq. 8}$$

$$AB+BC=2d\sin\theta \qquad \text{Eq. 9}$$

$$2\text{dsin}\,\theta=n\lambda \qquad \text{Eq. 10}$$

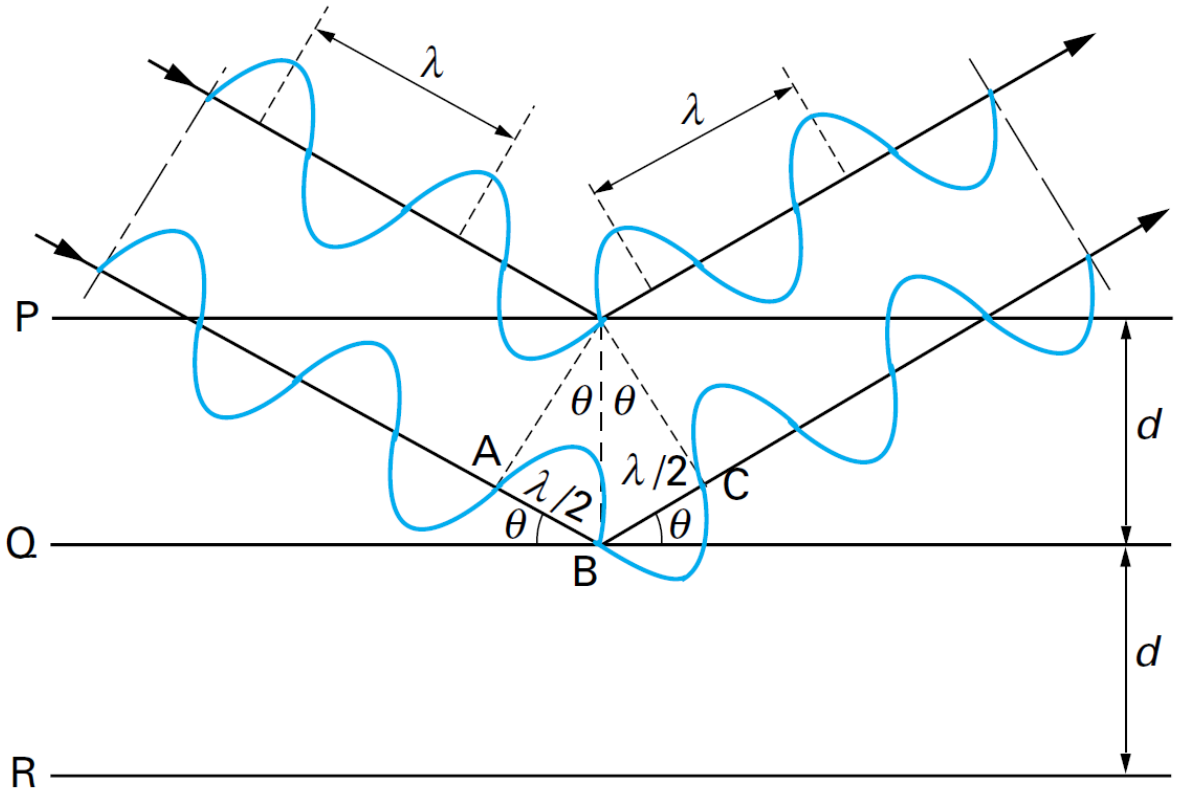


Figure 57: Figure corresponding to Bragg's law, taken from[363].

An easy method to determine crystallite size ($L$) was proposed by Scherrer as follows in eq. 11.

$$L=K\lambda/\beta\cos\theta \qquad \text{Eq. 11}$$

where $K$ is a geometry factor which value is close to 1 (usually 0.9); $\beta$ is full width at half maximum (FWHM); $\lambda$ correspond to the X-ray wavelength and $\theta$ is the Bragg's angle[363].

X-ray powder diffractograms were obtained on a Philips X-pert Pro II diffractometer using Kα copper Cu radiation (λ = 1.5418 Å) as a radiation source. The diffractograms were obtained in the range 2θ from 10 to 80 ° with a speed of 0.02 ° $s^{-1}$.

## V.2.4. Nuclear magnetic resonance (NMR)

### $^{29}$Si NMR

The $^{29}$Si spectra were made on a 59.6 MHz VARIAN VNMRS300 spectrometer with a MAS (magic angle rotation) probe using 3.2 mm zirconia rotors. The results were obtained using a single pulse sequence with decoupling 1H, pulses of 2 μs (corresponding to a pulse angle π / 6), a recycling time D1 = 60 s and a rotation frequency of 6 kHz. Chemical shifts are referenced by $Si(CH_3)_4$ tetramethylsilane ratio using the octa (dimethylsiloxy) silsesquioxane solid sample Q8M8H as a secondary reference.

### $^{27}$Al NMR

The $^{27}$Al spectra were made on a 104.26 MHz VARIAN VNMRS 400 spectrometer with a MAS (magic angle rotation) probe using 3.2 mm zirconia rotors. The results were obtained using a single pulse sequence with 1H decoupling, pulses of 1 μs (corresponding to a pulse angle π / 12), a recycling time D1 = 1 s and a rotation frequency of 20 kHz. The chemical shifts are referenced with respect to an aqueous solution of aluminum nitrate.

## V.2.5. Hydrogen-Thermal programmed reduction ($H_2$-TPR)

Temperature-programmed reduction (commonly abbreviated to TPR) is a technique used for the chemical characterization of solids. The essence of the technique is the reduction of a solid by a gas at the same time that the temperature of the system is changed in a predetermined way. Chemical information is derived from a record of the analysis of the gaseous products. In the most commonly encountered apparatus, the solid is reduced by hydrogen, the concentration of which is monitored downstream of the reactor. If reduction has taken place over the temperature excursion of the reactor, the analysis record is simply the hydrogen consumption and is usually displayed as a function of the temperature of the reactor. A typical reduction profile consists of a series of peaks. Each peak represents a distinct reduction process involving a particular chemical component of the solid. The position of a peak in the profile is determined by the chemical nature and environment of the chemical component, and the area of the peak reflects the concentration of that component present in the solid. It is highly sensitive and does not depend on any specific property of the solid under investigation other than its reducibility. $H_2$-Temperature-programmed reduction ($H_2$-TPR)

is a technique for the characterization of solid materials and is often used in the field of heterogeneous catalysis to find the most efficient reduction conditions. An oxidized catalyst precursor is submitted to a programmed temperature rise while a reducing gas mixture is flowed over it. The characterization of catalysts were obtained by using a Micrometrics Auto Chem 2910 apparatus. Prior to TPR, 140 mg of sample placed in a quartz tube reactor was treated at 500 °C in air for 1h. The TPR was carried out using $H_2$/He (25/75, v/v) at a flow rate of 13 $cm^3$/min. The temperature was increased linearly from 50 to 600 °C at a heating rate of 10 °C/min. The hydrogen consumption was monitored with a thermal conductivity detector.

## V.2.6. Ammoniac-Temperature programmed desorption ($NH_3$-TPD)

The samples acidity was measured by temperature programmed desorption (TPD) using ammonia as probe. Before TPD experiments, the solids were pretreated in helium flow at 200 °C for 1h. Ammonia was adsorbed for 30 min at 100 °C and rate flow 30 ml/min. The physisorbed ammonia was removed by evacuation of sample at 100°C for 1 h, in a dry helium stream. The ammonia desorption was carried out in helium stream at a heating rate of 10 °C/min up to 650 °C. The amount of desorbed ammonia was monitored with a TCD.

Figure 58: Temperature-programmed desorption analyzer

## V.2.7. X-ray photoelectron spectroscopy (XPS)

X-ray photoelectron spectroscopy (XPS) analyses were performed on Electron ESCALAB 250 instrument using the monochromatic source, line Al Kα (1486.6 e V) as excitation source, which was operated in the constant-pass energy mode. The samples powders pressed in small stainless steel troughs of 4 mm diameter were placed on a ceramic carousel. The pressure in the analysis chamber was around $10^{-6}$ Pa. The angle between the surface normal and the axis of the analyzer lens was 55◦. The analyzed area was approximately 1.4 $mm^2$ and the pass energy was set at 150 eV. In these conditions, the resolution determined by the full width at half maximum (FWHM) of the Au 4f7/2 peak was around 1.6 eV. A flood gun set at 10 eV and a Ni grid placed 3 mm above the sample surface were used for charge stabilization. Following sequence of spectra were recorded: survey spectrum, C1s, O1s together with Ni2p and C1s again to check the stability of charge compensation in function of time and the absence of degradation of the sample during the analyses. The binding energies were calculated with respect to the C-(C, H) component of the C 1s peak fixed at 284.8 eV. Data treatment was performed with the Casa XPS program (Casa Software Ltd., UK). Molar fractions were calculated using peak areas normalized based on acquisition parameters and sensitivity factors provided by the manufacturer. Scanning Electron Micrographs were obtained with a HITACHIS4800 electron microscope.

## V.2.8. Gas chromatography (GC-FID)

The products of the reaction were analyzed using a gas chromatograph with flame-ionization detection GC-FID (Agilent 6850). The chromatographic separation was performed on a HP-1 capillary column (30m x 0.25 mm x 8 µm). Hydrogen carrier gas was set a linear velocity of 24 cm $s^{-1}$. The temperature injector and detector were set at 250 °C with a split ratio of 30 for the injector. The oven temperature program was at an initial temperature of 40 °C for 4 min, and then it was increased to 100°C at 8°C/min for 1 min; the final temperature was 110 °C at 20 °C/min. 0.2 µL of that mixture was injected.

# V.3.Esterification catalyst test

The catalyst activity in the esterification reaction (acetic acid with *n*-butanol) was studied in a 50 mL centrifuge tube plastic at 80 °C for 1h. The esterification reaction was carried out by adding 5 mL of a mother solution to the mixed oxide catalysts. The mixed oxides were first activated by heating under vacuum at 150 °C for 5h. The mother solution was prepared by adding acetic acid (11.4 ml, 12.01 g, 0.1 mmol.) (VWR chemicals 99 - 100%), 1-butanol (18.6 ml, 14.80 g, 0.01 mmol.) (Acros organics 99.5%). The solvent, toluene (Fisher chemical 99.8%) was added to obtain a 100 mL total volume. Two types of test were realized: a fixed mass of catalyst (100 mg) and a fixed mole percentage of Al (20 mol.%). A volume of 5 ml of the mother solution was added to 100 mg of each catalyst. A reference reaction was also carried out in the absence of catalyst. A volume of 5 ml of the mother solution was added to a varied mass of catalyst depending on the Al composition. The mass weighting of the catalyst was calculated to obtain 20 mol. of Al related to the number of mole of *n*-butanol (0.01 of *n*-BuOH in each tube). After 1 h. heating at 80 °C, the tubes were cooled down at room temperature. The tubes were centrifuged at 20 000 rpm for 20 minutes. The supernatants were analysed by GC. All catalysts were employed under similar reaction conditions. The ester yield (butyl acetate) was defined as the number of moles of ester produced per moles of acetic acid introduced. By-products were not detected.

# ANNEX

Table 24: Composition obtained by EDX measurements on $SiO_2$-$Al_2O_3$-NiO samples prepared by NHSG ether route.

| Sample | Atomic % (expected) | | | | Atomic % (experimental) | | | |
|---|---|---|---|---|---|---|---|---|
| | Si/Al | Si | Al | Ni | Si/Al | Si | Al | Ni |
| $Si_{94}Al_6Ni_0$ | 13.3 | 93 | 7 | 0.0 | 10.6 | 91.4±0.3 | 8.6±0.2 | 0.0 |
| $Si_{100}Al_0Ni_0$ * | ∞ | 100 | 0.0 | 0.0 | ∞ | 99 .8±0.2 | 0.0 | 0.0 |
| $Si_0Al_{95}Ni_5$ | 0.0 | 0.0 | 96.6 | 3.4 | 0.0 | 0.0 | 98.2±0.7 | 1.8±0.1 |
| $Si_{85}Al_{10}Ni_5$ | 8.0 | 85.7 | 10.7 | 3.6 | 6.6 | 84.3±1.1 | 12.7±0.8 | 3.0±0.2 |
| $Si_{10.5}Al_{84.5}Ni_5$ | 0.1 | 9.3 | 87.2 | 3.5 | 0.12 | 9.9±0.01 | 84.3±0.5 | 5.8±0.03 |
| $Si_{85}Al_5Ni_{10}$ | 14.3 | 86 | 6.0 | 8.0 | 14 | 87.3±0.02 | 6.2±0.3 | 6.5±0.05 |
| $Si_{89}Al_1Ni_{10}$ | 75.5 | 90.6 | 1.2 | 8.2 | 83 | 91.6±0.04 | 1.1±0.2 | 7.3±0.08 |
| $Si_0Al_{85}Ni_{15}$ | 0.0 | 0.0 | 89.4 | 10.6 | 0.0 | 0.0 | 91.6±0.9 | 8.4±0.3 |
| $Si_{9.4}Al_{75.6}Ni_{15}$ | 0.13 | 8.5 | 80.7 | 10.9 | 0.1 | 7.6±0.1 | 80.6± 0.2 | 11.8±0.1 |
| $Si_{85}Al_0Ni_{15}$ * | ∞ | 87.8 | 0.0 | 12.2 | ∞ | 90.5±0.9 | 0.0 | 9.5±0.06 |
| $Si_{75}Al_5Ni_{20}$ | 12.7 | 77.3 | 6.1 | 16.6 | 10.9 | 75.8±0.2 | 6.9±0.5 | 17.3±0.2 |

* 0.015 mmol of $FeCl_3$.

Table 25: Texture of the samples measured by $N_2$ sorption $SiO_2$-$Al_2O_3$-NiO samples prepared by NHSG ether route.

| Sample | Texture | | | |
|---|---|---|---|---|
| | Si/Al | S ($m^2 g^{-1}$) | Vp ($cm^3 g^{-1}$) | Dp (nm) |
| $Si_{94}Al_6Ni_0$ | 16 | 465 | 1.4 | 12.5 |
| $Si_0Al_{95}Ni_5$ | 0 | 471 | 0.6 | 5.2 |
| $Si_{10.5}Al_{84.5}Ni_5$ | 0.1 | 449 | 0.5 | 4.4 |
| $Si_{75}Al_{20}Ni_5$ | 3.7 | 217 | 0.4 | 7.5 |
| $Si_{80}Al_{15}Ni_5$ | 5.3 | 368 | 0.9 | 9.9 |
| $Si_{85}Al_{10}Ni_5$ | 8.5 | 680 | 1.7 | 10.1 |
| $Si_{90}Al_5Ni_5$ | 18 | 781 | 1.1 | 6.0 |
| $Si_{85}Al_5Ni_{10}$ | 17 | 675 | 1.7 | 10.1 |
| $Si_{89}Al_1Ni_{10}$ | 89 | 691 | 1.6 | 8.5 |
| $Si_0Al_{85}Ni_{15}$ | 0 | 334 | 0.3 | 5.7 |
| $Si_{9.4}Al_{75.6}Ni_{15}$ | 0.13 | 353 | 0.2 | 3.0 |
| $Si_{80}Al_5Ni_{15}$ | 16 | 382 | 0.2 | 2.4 |
| $Si_{85}Al_0Ni_{15}$ | ∞ | 468 | 0.5 | 4.2 |
| $Si_{75}Al_5Ni_{20}$ | 15 | 155 | 0.2 | 4.7 |

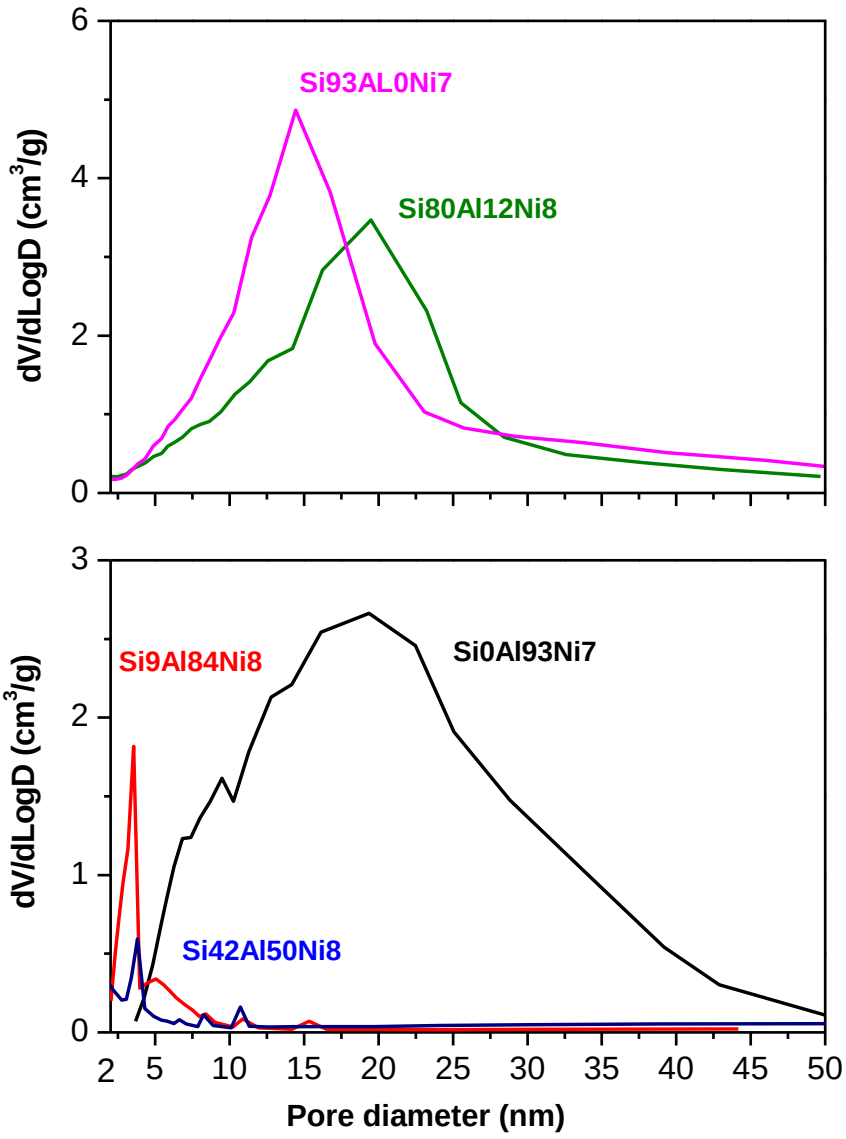


Figure 59: Pore size distribution (from the desorption branch using the BJH method) of SixAlyNiz samples with low $Al_2O_3$ content (top) and high $Al_2O_3$ content (bottom).

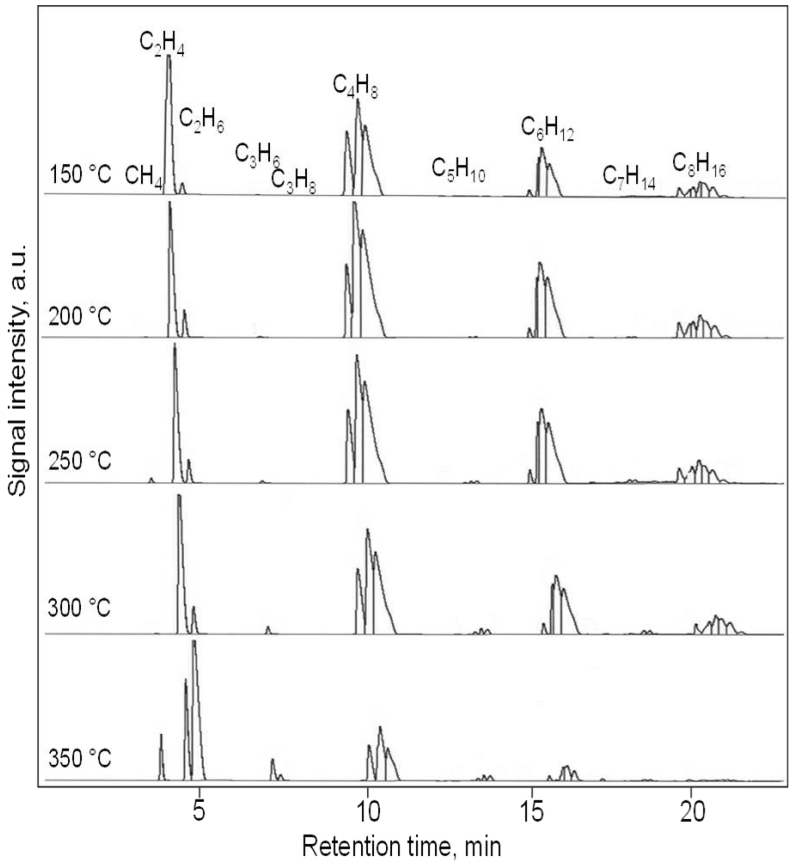


Figure 60: Typical chromatograms of the products obtained over the $Si_9Al_{84}Ni_8$ catalyst at different temperatures.

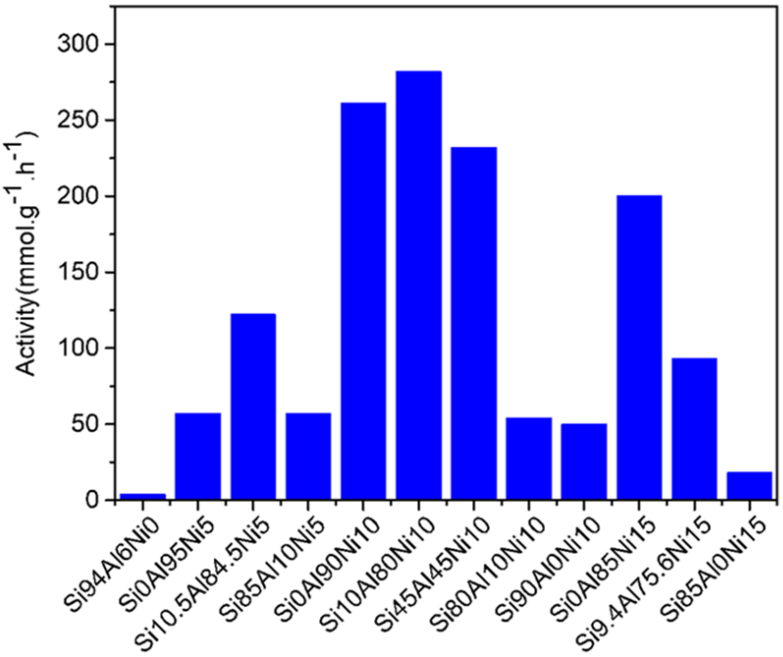


Figure 61: Activity of SixAlyNiz catalysts prepared by NHSG route for ethylene oligomerization.

Table 26: Ester yield and acid convertion.

| $SiO_2$ (wt.%) | $Al_2O_3$ (wt.%) | Ester yield (%) | | Acid conversion (%) | |
|---|---|---|---|---|---|
| | | 100 mg | 20%Al | 100 mg | 20%Al |
| 100 | 0 | 17 | 17 | 13 | 14 |
| | | 17 | 17 | 12 | 12 |
| | | ---- | ---- | ---- | ---- |
| 90 | 10 | 17 | 18 | 16 | 13 |
| | | 17 | 19 | 12 | 14 |
| | | n.a | n.a | n.a | n.a |
| 75 | 25 | 18 | 17 | 13 | 13 |
| | | 17 | 17 | 12 | 14 |
| | | 44 | 44 | 6 | 5 |
| 50 | 50 | 17 | 17 | 13 | 13 |
| | | 17 | 17 | 11 | 12 |
| | | 53 | 36 | 7 | 4 |
| 25 | 75 | 17 | 17 | 14 | 14 |
| | | 17 | 17 | 13 | 12 |
| | | 34 | 34 | 4 | 3 |
| 10 | 90 | 17 | 17 | 13 | 14 |
| | | 17 | 17 | 12 | 11 |
| | | n.a | n.a | n.a | n.a |
| 0 | 100 | 17 | 17 | 14 | 14 |
| | | 17 | 17 | 12 | 11 |
| | | 36 | 36 | 3 | 4 |
| Blank | | 17 | 17 | 13 | 13 |
| | | 16 | 16 | 14 | 14 |
| | | 38 | 38 | 4 | 4 |

Red: HSG (acidic medium).
Blue: HSG (basic medium).
Black: NHSG

# References

[1] J. Wisniak, The chemical educator, 5 (2000) 343-350.
[2] A. D. McNaught and A. D. McNaught, *Compendium of chemical terminology*, ed., Blackwell Science Oxford, 1997.
[3] M. Muhler, Berichte der Bunsengesellschaft für physikalische Chemie, 101 (1997) 1560-1560.
[4] I. Chorkendorff and J. W. Niemantsverdriet, *Concepts of modern catalysis and kinetics*, ed., John Wiley & Sons, 2017.
[5] F. Zaera, Catalysis letters, 142 (2012) 501-516.
[6] G. J. Hutchings, Journal of materials chemistry, 19 (2009) 1222-1235.
[7] Y. Liu, G. Zhao, D. Wang and Y. Li, National Science Review, 2 (2015) 150-166.
[8] S. Özkar, Applied surface science, 256 (2009) 1272-1277.
[9] H. Knözinger and K. Kochloefl, Ullmann's Encyclopedia of Industrial Chemistry, (2000).
[10] J. Liu, ChemCatChem, 3 (2011) 934-948.
[11] M. Fernández-Garcia and J. RODGRIGUEZ, *Metal oxide nanoparticles*, in: Secondary author (Ed.)^(Eds.) Secondary title, Brookhaven National Lab.(BNL), Upton, NY (United States), 2007.
[12] X. Carrier, S. Royer and E. Marceau, in: (Ed.)^(Eds.), Metal oxides in heterogeneous catalysis, Elsevier, 2018, pp. 43-103.
[13] E. D. Goodman, J. A. Schwalbe and M. Cargnello, ACS Catalysis, 7 (2017) 7156-7173.
[14] J. C. Matsubu, S. Zhang, L. DeRita, N. S. Marinkovic, J. G. Chen, G. W. Graham, X. Pan and P. Christopher, Nature chemistry, 9 (2017) 120-127.
[15] A. J. van Dillen, R. J. A. M. Terörde, D. J. Lensveld, J. W. Geus and K. P. de Jong, Journal of Catalysis, 216 (2003) 257-264. https://doi.org/10.1016/S0021-9517(02)00130-6
[16] J. Sun, X. Li, A. Taguchi, T. Abe, W. Niu, P. Lu, Y. Yoneyama and N. Tsubaki, ACS Catalysis, 4 (2014) 1-8.
[17] B. M. Reddy, B. Chowdhury, E. P. Reddy and A. Fernández, Applied Catalysis A: General, 213 (2001) 279-288.
[18] I. Bretos, R. Jiménez, J. Ricote and M. L. Calzada, Chemical Society Reviews, 47 (2018) 291-308. 10.1039/C6CS00917D
[19] M. Campanati, G. Fornasari and A. Vaccari, Catalysis Today, 77 (2003) 299-314.
[20] P. Kast, *Structure-function relationship of Strong Metal-Support Interaction studied on supported Pd reference catalysts*, ed., Technische Universitaet Berlin (Germany), 2015.
[21] M. C. Tucker, Journal of Power Sources, 195 (2010) 4570-4582.
[22] D. P. Debecker, K. Bouchmella, R. Delaigle, P. Eloy, C. Poleunis, P. Bertrand, E. M. Gaigneaux and P. H. Mutin, Applied Catalysis B: Environmental, 94 (2010) 38-45. https://doi.org/10.1016/j.apcatb.2009.10.018
[23] L. S. Lobo and S. A. C. Carabineiro, C, 6 (2020) 18.
[24] K. Bouchmella, P. Hubert Mutin, M. Stoyanova, C. Poleunis, P. Eloy, U. Rodemerck, E. M. Gaigneaux and D. P. Debecker, Journal of Catalysis, 301 (2013) 233-241. https://doi.org/10.1016/j.jcat.2013.02.016
[25] A. M. Venezia, V. La Parola and L. F. Liotta, Catalysis Today, 285 (2017) 114-124.
[26] A. Wang, J. Li and T. Zhang, Nature Reviews Chemistry, 2 (2018) 65-81.
[27] J. A. Rodríguez, J. C. Hanson and P. J. Chupas, *In-situ characterization of heterogeneous catalysts*, ed., John Wiley & Sons, 2013.
[28] J. C. Vedrine, Applied Catalysis A: General, 474 (2014) 40-50.
[29] T. Ressler, R. E. Jentoft, J. Wienold, F. Girgsdies, T. Neisius and O. Timpe, Nuclear Instruments and Methods in Physics Research Section B: Beam Interactions with Materials and Atoms, 200 (2003) 165-170. https://doi.org/10.1016/S0168-583X(02)01714-7
[30] J. H. Clark, Accounts of chemical research, 35 (2002) 791-797.
[31] Y. M. Sani, W. M. A. W. Daud and A. A. Aziz, Applied Catalysis A: General, 470 (2014) 140-161.

[32] I. S. Pieta, M. Ishaq, R. P. K. Wells and J. A. Anderson, Applied Catalysis A: General, 390 (2010) 127-134. https://doi.org/10.1016/j.apcata.2010.10.001
[33] G. Busca, Catalysis Today, 357 (2020) 621-629.
[34] M. K. Mardkhe, B. Huang, C. H. Bartholomew, T. M. Alam and B. F. Woodfield, Journal of Porous Materials, 23 (2016) 475-487.
[35] E. Hensen, D. Poduval, P. Magusin, A. Coumans and J. Van Veen, Journal of Catalysis, 269 (2010) 201-218.
[36] G. Crépeau, V. Montouillout, A. Vimont, L. Mariey, T. Cseri and F. Maugé, The Journal of Physical Chemistry B, 110 (2006) 15172-15185. 10.1021/jp062252d
[37] C. Chizallet, ACS Catalysis, 10 (2020) 5579-5601.
[38] X. Zhu, Technische Universiteit Eindhoven, Eindhoven, (2015).
[39] J. M. Campos, J. P. Lourenço, H. Cramail and M. R. Ribeiro, Progress in polymer science, 37 (2012) 1764-1804.
[40] K. Tanabe, *Solid acids and bases: their catalytic properties*, ed., Elsevier, 2012.
[41] M. S. Chen and D. W. Goodman, Science, 306 (2004) 252-255. doi:10.1126/science.1102420
[42] N. Lopez, T. V. W. Janssens, B. S. Clausen, Y. Xu, M. Mavrikakis, T. Bligaard and J. K. Nørskov, Journal of Catalysis, 223 (2004) 232-235. https://doi.org/10.1016/j.jcat.2004.01.001
[43] G. Zhao, H. Liu and J. Ye, Nano Today, 19 (2018) 108-125.
[44] E. S. Beach, Z. Cui and P. T. Anastas, Energy & Environmental Science, 2 (2009) 1038-1049.
[45] P. T. Anastas, M. M. Kirchhoff and T. C. Williamson, Applied Catalysis A: General, 221 (2001) 3-13.
[46] M. C. Lubinu, L. De Luca, G. Giacomelli and A. Porcheddu, Chemistry–A European Journal, 17 (2011) 82-85.
[47] M. R. Buchmeiser, Journal of Molecular Catalysis A: Chemical, 190 (2002) 145-158.
[48] A. F. Lee, J. A. Bennett, J. C. Manayil and K. Wilson, Chemical Society Reviews, 43 (2014) 7887-7916.
[49] D. W. Lee and B. R. Yoo, Journal of Industrial and Engineering Chemistry, 20 (2014) 3947-3959.
[50] T. Yalçinyuva, H. Deligöz, İ. Boz and M. Ali Gürkaynak, International Journal of Chemical Kinetics, 40 (2008) 136-144. https://doi.org/10.1002/kin.20293
[51] N. Fattahi, M. Ayubi and A. Ramazani, Tetrahedron, 74 (2018) 4351-4356. https://doi.org/10.1016/j.tet.2018.06.064
[52] S. A. Fernandes, R. Natalino, P. A. R. Gazolla, M. J. da Silva and G. N. Jham, Tetrahedron Letters, 53 (2012) 1630-1633. https://doi.org/10.1016/j.tetlet.2012.01.078
[53] S. Cebrián-García, A. M. Balu, A. García and R. Luque, Molecules, 23 (2018) 2283. https://doi.org/10.3390/molecules23092283
[54] B. R. Jermy and A. Pandurangan, Journal of Molecular Catalysis A: Chemical, 237 (2005) 146-154. https://doi.org/10.1016/j.molcata.2005.04.034
[55] G. Liu, S. Guo, B. He, J. Li and X. Qian, International Journal of Chemical Reactor Engineering, 14 (2016) 579-585. https://doi.org/10.1515/ijcre-2015-0198
[56] S. G. Cull, J. D. Holbrey, V. Vargas-Mora, K. R. Seddon and G. J. Lye, Biotechnology and Bioengineering, 69 (2000) 227-233. https://doi.org/10.1002/(SICI)1097-0290(20000720)69:2<227::AID-BIT12>3.0.CO;2-0
[57] K.-H. Chung, D.-R. Chang and B.-G. Park, Bioresource Technology, 99 (2008) 7438-7443. https://doi.org/10.1016/j.biortech.2008.02.031
[58] A. Engin, H. Haluk and K. Gurkan, Green Chemistry, 5 (2003) 460-466. https://doi.org/10.1039/B303327A
[59] K. Y. Nandiwale and V. V. Bokade, Chemical Engineering & Technology, 38 (2015) 246-252. https://doi.org/10.1002/ceat.201400326
[60] C. D. Prates, F. C. Ballotin, H. Limborço, J. D. Ardisson, R. M. Lago and A. P. d. C. Teixeira, Applied Catalysis A: General, 600 (2020) 117624. https://doi.org/10.1016/j.apcata.2020.117624

[61] L. H. O. Pires, A. N. de Oliveira, O. V. M. Jr, R. S. Angélica, C. E. F. d. Costa, J. R. Zamian, L. A. S. d. Nascimento and G. N. R. Filho, Applied Catalysis B: Environmental, 160-161 (2014) 122-128. https://doi.org/10.1016/j.apcatb.2014.04.039
[62] S. R. Kirumakki, N. Nagaraju and K. V. R. Chary, Applied Catalysis A: General, 299 (2006) 185-192. https://doi.org/10.1016/j.apcata.2005.10.033
[63] R. J. Baxter and P. Hu, The Journal of Chemical Physics, 116 (2002) 4379-4381. https://doi.org/10.1063/1.1458938
[64] N. Jurtz, M. Kraume and G. D. Wehinger, Reviews in Chemical Engineering, 35 (2019) 139-190.
[65] Y. Wang, G. Wu, M. Yang and J. Wang, The Journal of Physical Chemistry C, 117 (2013) 8767-8773. https://doi.org/10.1021/jp3122775
[66] Y. Liu, E. Lotero and J. G. Goodwin Jr, Journal of Catalysis, 242 (2006) 278-286.
[67] K. Suwannakarn, E. Lotero and J. G. Goodwin, Catalysis letters, 114 (2007) 122-128.
[68] T. A. Peters, N. E. Benes, A. Holmen and J. T. Keurentjes, Applied Catalysis A: General, 297 (2006) 182-188.
[69] W. Chu, X. Yang, X. Ye and Y. Wu, Applied Catalysis A: General, 145 (1996) 125-140.
[70] D. E. Lopez, K. Suwannakarn, J. G. Goodwin and D. A. Bruce, Industrial & engineering chemistry research, 47 (2008) 2221-2230.
[71] F. Bamoharram, M. Heravi, P. Ardalan and T. Ardalan, Reaction Kinetics, Mechanisms and Catalysis, 100 (2010) 71-78.
[72] S. R. Kirumakki, N. Nagaraju and K. V. Chary, Applied Catalysis A: General, 299 (2006) 185-192.
[73] J. Bedard, H. Chiang and A. Bhan, Journal of catalysis, 290 (2012) 210-219.
[74] R. Koster, B. van der Linden, E. Poels and A. Bliek, Journal of Catalysis, 204 (2001) 333-338.
[75] M. R. Altıokka and A. Çıtak, Applied Catalysis A: General, 239 (2003) 141-148.
[76] H. Teo and B. Saha, Journal of Catalysis, 228 (2004) 174-182.
[77] W.-T. Liu and C.-S. Tan, Industrial & engineering chemistry research, 40 (2001) 3281-3286.
[78] S. R. Kirumakki, N. Nagaraju and S. Narayanan, Applied Catalysis A: General, 273 (2004) 1-9.
[79] I. Pieta, M. Ishaq, R. Wells and J. Anderson, Applied Catalysis A: General, 390 (2010) 127-134.
[80] F. C. de Mattos, E. N. de Carvalho, E. F. d. Freitas, M. F. Paiva, G. F. Ghesti, J. L. d. Macedo, S. C. Dias and J. A. Dias, Journal of the Brazilian Chemical Society, 28 (2017) 336-347.
[81] A. N. Chermahini and M. Nazeri, Fuel Processing Technology, 167 (2017) 442-450.
[82] P. Shah, A. V. Ramaswamy, K. Lazar and V. Ramaswamy, Applied Catalysis A: General, 273 (2004) 239-248.
[83] S. Abate, K. Barbera, G. Centi, P. Lanzafame and S. Perathoner, Catalysis Science & Technology, 6 (2016) 2485-2501.
[84] A. Corma and A. Martinez, Advanced Materials, 7 (1995) 137-144.
[85] E. Schulman, W. Wu and D. Liu, Materials, 13 (2020) 1822. 10.3390/ma13081822
[86] J. Čejka and S. Mintova, Catalysis Reviews, 49 (2007) 457-509.
[87] L. Tosheva and V. P. Valtchev, Chemistry of materials, 17 (2005) 2494-2513.
[88] Y. Tao, H. Kanoh, L. Abrams and K. Kaneko, Chemical reviews, 106 (2006) 896-910.
[89] P. Lanzafame, K. Barbera, G. Papanikolaou, S. Perathoner, G. Centi, M. Migliori, E. Catizzone and G. Giordano, Catalysis Today, 304 (2018) 97-102.
[90] A. Zukal, M. Thommes and J. Čejka, Microporous and mesoporous materials, 104 (2007) 52-58.
[91] S. Shylesh, P. P. Samuel and A. Singh, Microporous and mesoporous materials, 100 (2007) 250-258.
[92] M. Caillot, A. Chaumonnot, M. Digne and J. A. Van Bokhoven, ChemCatChem, 6 (2014) 832-841.
[93] S. Ajaikumar and A. Pandurangan, Journal of Molecular Catalysis A: Chemical, 266 (2007) 1-10. https://doi.org/10.1016/j.molcata.2006.10.010
[94] W. Xie, L. Hu and X. Yang, Industrial & Engineering Chemistry Research, 54 (2015) 1505-1512.
[95] W. Xie, C. Qi, H. Wang and Y. Liu, Fuel processing technology, 119 (2014) 98-104.

[96] G. Muthu Kumaran, S. Garg, K. Soni, M. Kumar, J. K. Gupta, L. D. Sharma, K. S. Rama Rao and G. Murali Dhar, Microporous and Mesoporous Materials, 114 (2008) 103-109. https://doi.org/10.1016/j.micromeso.2007.12.021
[97] C. Gonzalez-Arellano, R. A. D. Arancon and R. Luque, Green Chemistry, 16 (2014) 4985-4993. 10.1039/C4GC01105H
[98] M. Crucianelli, B. M. Bizzarri and R. Saladino, Catalysts, 9 (2019) 984. https://doi.org/10.3390/catal9120984
[99] R. D. Andrei, M. I. Popa, F. Fajula and V. Hulea, Journal of Catalysis, 323 (2015) 76-84. https://doi.org/10.1016/j.jcat.2014.12.027
[100] S. Seifzadeh Haghighi, M. R. Rahimpour, S. Raeissi and O. Dehghani, Chemical Engineering Journal, 228 (2013) 1158-1167. https://doi.org/10.1016/j.cej.2013.05.048
[101] M. Yang, D. Fan, Y. Wei, P. Tian and Z. Liu, Advanced Materials, 31 (2019) 1902181. https://doi.org/10.1002/adma.201902181
[102] A. Finiels, F. Fajula and V. Hulea, Catalysis Science & Technology, 4 (2014) 2412-2426. 10.1039/C4CY00305E
[103] C. P. Nicholas, Applied Catalysis A: General, 543 (2017) 82-97. https://doi.org/10.1016/j.apcata.2017.06.011
[104] C. Janiak, Coordination Chemistry Reviews, 250 (2006) 66-94. https://doi.org/10.1016/j.ccr.2005.02.016
[105] M. Yamamura, K. Chaki, T. Wakatsuki, H. Okado and K. Fujimoto, Zeolites, 14 (1994) 643-649. https://doi.org/10.1016/0144-2449(94)90121-X
[106] A. Al-Jarallah, J. Anabtawi, M. Siddiqui, A. Aitani and A. Al-Sa'doun, Catalysis Today, 14 (1992) 1-121.
[107] H. Horie and K. Morikawa, Kogyo Kagaku Zasshi, 41 (1938) Medium: X; Size: Pages: 401-403 2009-2012-2016. https://www.osti.gov/biblio/5218554
[108] R. B. Seymour, *History of Polyolefins*, in: Secondary author (Ed.)^(Eds.) Secondary title, Springer US, Boston, MA, 1987, pp. 3-14.
[109] T. Shiba and A. Ozaki, Nippon Kagaku Zasshi, 74 (1953) 295-297.
[110] T. Matsuda, H. Miura, K. Sugiyama, N. Ohno, S. Keino and A. Kaise, Journal of the Chemical Society, Faraday Transactions 1: Physical Chemistry in Condensed Phases, 75 (1979) 1513-1520. https://doi.org/10.1039/F19797501513
[111] H. Fogler, Elements of chemical reaction engineering, (2006) 813-852.
[112] G. W. Huber, S. Iborra and A. Corma, Chemical Reviews, 106 (2006) 4044-4098. https://doi.org/10.1021/cr068360d
[113] G. W. Huber, S. Iborra and A. Corma, Chemical reviews, 106 (2006) 4044-4098.
[114] M. Lallemand, O. A. Rusu, E. Dumitriu, A. Finiels, F. Fajula and V. Hulea, Applied Catalysis A: General, 338 (2008) 37-43. https://doi.org/10.1016/j.apcata.2007.12.024
[115] V. Hulea and F. Fajula, Journal of Catalysis, 225 (2004) 213-222.
[116] A. L. Lapidus, A. A. Slinkin, L. N. Rudakova, T. N. Myshenkova, M. I. Loktev, T. S. Papko and Y. T. Éidus, Bulletin of the Academy of Sciences of the USSR, Division of chemical science, 23 (1974) 1880-1884. https://doi.org/10.1007/BF00922780
[117] J. R. Sohn and J. S. Han, Studies in surface science and catalysis, (2006) 269-272. https://doi.org/10.1016/S0167-2991(06)81585-5
[118] A. A. Davydov, M. Kantcheva and M. L. Chepotko, Catalysis Letters, 83 (2002) 97-108. https://doi.org/10.1023/A:1020669818242
[119] M. Lallemand, A. Finiels, F. Fajula and V. Hulea, Applied Catalysis A: General, 301 (2006) 196-201. https://doi.org/10.1016/j.apcata.2005.12.019

[120] A. Lapidus, Y. I. Isakov, A. Slinkin, R. Avetisyan, K. M. Minachev and Y. T. Éidus, Russian Chemical Bulletin, 20 (1971) 1797-1801.
[121] C. P. Nicolaides, M. S. Scurrell and P. M. Semano, Applied Catalysis A: General, 245 (2003) 43-53. https://doi.org/10.1016/S0926-860X(02)00615-4
[122] J. Heveling, C. P. Nicolaides and M. S. Scurrell, Applied Catalysis A: General, 248 (2003) 239-248. https://doi.org/10.1016/S0926-860X(03)00160-1
[123] A. Lacarriere, J. Robin, D. Świerczyński, A. Finiels, F. Fajula, F. Luck and V. Hulea, ChemSusChem, 5 (2012) 1787-1792. https://doi.org/10.1002/cssc.201200092
[124] A. Martínez, M. A. Arribas, P. Concepción and S. Moussa, Applied Catalysis A: General, 467 (2013) 509-518.
[125] J. Heveling, C. P. Nicolaides and M. S. Scurrell, Applied Catalysis A: General, 173 (1998) 1-9. https://doi.org/10.1016/S0926-860X(98)00147-1
[126] F. T. T. Ng and D. C. Creaser, Applied Catalysis A: General, 119 (1994) 327-339. https://doi.org/10.1016/0926-860X(94)85200-6
[127] J. Joseph, K. C. Potter, M. J. Wulfers, E. Schwerdtfeger, M. P. McDaniel and F. C. Jentoft, Journal of Catalysis, 377 (2019) 550-564. https://doi.org/10.1016/j.jcat.2019.07.057
[128] E. Koninckx, P. S. F. Mendes, J. W. Thybaut and L. J. Broadbelt, Applied Catalysis A: General, 624 (2021) 118296. https://doi.org/10.1016/j.apcata.2021.118296
[129] R. L. Espinoza, C. J. Korf, C. P. Nicolaides and R. Snel, Applied Catalysis, 29 (1987) 175-184. https://doi.org/10.1016/S0166-9834(00)82615-9
[130] Q. Zhang, M. Kantcheva and I. G. Dalla Lana, Industrial & Engineering Chemistry Research, 36 (1997) 3433-3438. https://doi.org/10.1021/ie9701480
[131] M. D. Heydenrych, C. P. Nicolaides and M. S. Scurrell, Journal of Catalysis, 197 (2001) 49-57. https://doi.org/10.1006/jcat.2000.3035
[132] M. Lallemand, A. Finiels, F. Fajula and V. Hulea, Chemical Engineering Journal, 172 (2011) 1078-1082. https://doi.org/10.1016/j.cej.2011.06.064
[133] Ebelmen, *Recherches sur les combinaisons des acides borique et silicique avec les éthers*, ed., 1846.
[134] M. Ebelmen, *On the synthesis of silica gels from alkoxides*, in: Secondary author (Ed.)^(Eds.) Secondary title, 1846, pp. 318-327.
[135] A. C. Pierre, *Introduction to sol-gel processing*, ed., Springer Nature, 2020.
[136] W. Geffcken and E. Berger, *German Patent 736,411*, in: Secondary author (Ed.)^(Eds.) Secondary title, May, 1939.
[137] Y. Dimitriev, Y. Ivanova and R. Iordanova, Journal of the University of Chemical technology and Metallurgy, 43 (2008) 181-192.
[138] H. Schroeder, G. Hass and R. Thun, Advances in Research and Development, 5 (1969) 87.
[139] H. Dislich and P. Hinz, Journal of Non-Crystalline Solids, 48 (1982) 11-16. https://doi.org/10.1016/0022-3093(82)90242-3
[140] L. Levene and I. Thomas, Inc., USA.
[141] G. J. Owens, R. K. Singh, F. Foroutan, M. Alqaysi, C.-M. Han, C. Mahapatra, H.-W. Kim and J. C. Knowles, Progress in Materials Science, 77 (2016) 1-79. https://doi.org/10.1016/j.pmatsci.2015.12.001
[142] M. Niederberger and N. Pinna, *Metal oxide nanoparticles in organic solvents: synthesis, formation, assembly and application*, ed., Springer Science & Business Media, 2009.
[143] J. Livage, Le monde, 26 (1977).
[144] P. C. Hiemenz and R. Rajagopalan, Chemistry, 3 (1977).
[145] C. J. Brinker and G. W. Scherer, *Sol-gel science: the physics and chemistry of sol-gel processing*, ed., Academic press, 2013.
[146] J. Livage and C. Sanchez, Journal of Non-Crystalline Solids, 145 (1992) 11-19.
[147] Z. Zelča, S. Kukle and J. Kajaks, Materials Science. Textile and Clothing Technology, 11 (2016) 6-11.

[148] C. Milea, C. Bogatu and A. Duta, Bulletin of the Transilvania University of Brasov. Engineering Sciences. Series I, 4 (2011) 59.
[149] D. P. Debecker and P. H. Mutin, Chemical Society Reviews, 41 (2012) 3624-3650. https://doi.org/10.1039/C2CS15330K
[150] S. Esposito, Materials, 12 (2019) 668.
[151] E. D. Gaspera and A. Martucci, Sensors, 15 (2015) 16910-16928.
[152] C. Anderson and A. J. Bard, The Journal of Physical Chemistry, 99 (1995) 9882-9885.
[153] M. Yabuki, R. Takahashi, S. Sato, T. Sodesawa and K. Ogura, Physical Chemistry Chemical Physics, 4 (2002) 4830-4837.
[154] Q. Lei, J. Guo, A. Noureddine, A. Wang, S. Wuttke, C. J. Brinker and W. Zhu, Advanced Functional Materials, 30 (2020) 1909539.
[155] J. Livage, M. Henry and C. Sanchez, Progress in solid state chemistry, 18 (1988) 259-341.
[156] K. Keefer, C. Brinker, D. Clark and D. Ulrich, *Better ceramics through chemistry*, in: Secondary author (Ed.)^(Eds.) Secondary title, North-Holland New York, 1984, pp. 15-24.
[157] S. Okumoto, N. Fujita and S. Yamabe, The Journal of Physical Chemistry A, 102 (1998) 3991-3998. 10.1021/jp980705b
[158] M. Elanany, P. Selvam, T. Yokosuka, S. Takami, M. Kubo, A. Imamura and A. Miyamoto, The Journal of Physical Chemistry B, 107 (2003) 1518-1524. 10.1021/jp026816z
[159] H. K. Schmidt, E. Geiter, M. Mennig, H. Krug, C. Becker and R.-P. Winkler, Journal of sol-gel science and technology, 13 (1998) 397-404.
[160] D. Wang and G. P. Bierwagen, Progress in organic coatings, 64 (2009) 327-338.
[161] E. Pope and J. Mackenzie, Journal of non-crystalline solids, 87 (1986) 185-198.
[162] K. A. Yasakau, J. Carneiro, M. L. Zheludkevich and M. G. S. Ferreira, Surface and Coatings Technology, 246 (2014) 6-16. https://doi.org/10.1016/j.surfcoat.2014.02.038
[163] R. Aelion, A. Loebel and F. Eirich, Journal of the American chemical society, 72 (1950) 5705-5712.
[164] L. Klein, Annual Review of Materials Science, 15 (1985) 227-248.
[165] F. Brunet, J. Virlet and P. Lux, New Journal of Chemistry, 18 (1994) 1059-1064.
[166] P. H. Mutin and A. Vioux, Chemistry of Materials, 21 (2009) 582-596.
[167] D. P. Debecker, V. Hulea and P. H. Mutin, Applied Catalysis A: General, 451 192-206.
[168] W. Gerrard and A. Woodhead, Journal of the Chemical Society (Resumed), (1951) 519-522.
[169] R. J. P. Corriu, D. Leclercq, P. Lefèvre, P. H. Mutin and A. Vioux, Journal of Non-Crystalline Solids, 146 (1992) 301-303. https://doi.org/10.1016/S0022-3093(05)80505-8
[170] L. Bourget, R. Corriu, D. Leclercq, P. Mutin and A. Vioux, Journal of Non-Crystalline Solids, 242 (1998) 81-91.
[171] R. Mehrotra, Journal of Non-Crystalline Solids, 100 (1988) 1-15.
[172] C. Le Roux, H. Yang, S. Wenzel, S. Grigoras and M. A. Brook, Organometallics, 17 (1998) 556-564.
[173] M. Niederberger and G. Garnweitner, Chemistry–A European Journal, 12 (2006) 7282-7302.
[174] T. J. Trentler, T. E. Denler, J. F. Bertone, A. Agrawal and V. L. Colvin, Journal of the American Chemical Society, 121 (1999) 1613-1614.
[175] K. W. Terry and T. D. Tilley, Chemistry of materials, 3 (1991) 1001-1003.
[176] J. Jarupatrakorn and T. D. Tilley, Journal of the American Chemical Society, 124 (2002) 8380-8388.
[177] J. Caruso and M. Hampden-Smith, Journal of Sol-Gel Science and Technology, 8 (1997) 35-39.
[178] K. G. Sharp, Advanced Materials, 10 (1998) 1243-1248.
[179] E. Stathatos, P. Lianos, U. Lavrencic-Stangar and B. Orel, Advanced Materials, 14 (2002) 354-357.
[180] J. Joo, S. G. Kwon, T. Yu, M. Cho, J. Lee, J. Yoon and T. Hyeon, The Journal of Physical Chemistry B, 109 (2005) 15297-15302.
[181] S. Dai, Y. Ju, H. Gao, J. Lin, S. Pennycook and C. Barnes, Chemical Communications, (2000) 243-244.

[182] R. Sui, A. S. Rizkalla and P. A. Charpentier, The Journal of Physical Chemistry B, 108 (2004) 11886-11892.
[183] P. Arnal, R. J. Corriu, D. Leclercq, P. H. Mutin and A. Vioux, Journal of Materials Chemistry, 6 (1996) 1925-1932.
[184] M. Fujiwara, H. Wessel, H. S. Park and H. W. Roesky, Chemistry of materials, 14 (2002) 4975-4981.
[185] G. Guo, J. K. Whitesell and M. A. Fox, The Journal of Physical Chemistry B, 109 (2005) 18781-18785.
[186] A. Aboulaich, O. Lorret, B. Boury and P. H. Mutin, Chemistry of Materials, 21 (2009) 2577-2579.
[187] S. Yuh, E. Bescher, F. Babonneau and J. Mackenzie, *Better Ceramics Through Chemistry VI*, in: Secondary author (Ed.)^(Eds.) Secondary title, 1994, pp. 803.
[188] G. Garnweitner and M. Niederberger, Journal of the American Ceramic Society, 89 (2006) 1801-1808.
[189] A. Vioux, Chemistry of Materials, 9 (1997) 2292-2299.
[190] M. Andrianainarivelo, R. J. Corriu, D. Leclercq, P. H. Mutin and A. Vioux, Chemistry of materials, 9 (1997) 1098-1102.
[191] A. de la Hoz, A. Diaz-Ortiz and A. Moreno, Chemical Society Reviews, 34 (2005) 164-178.
[192] K. Rao, B. Vaidhyanathan, M. Ganguli and P. Ramakrishnan, Chemistry of Materials, 11 (1999) 882-895.
[193] J. D. Moseley and C. O. Kappe, Green Chemistry, 13 (2011) 794-806.
[194] I. Bilecka and M. Niederberger, Nanoscale, 2 (2010) 1358-1374.
[195] J. A. Schwarz, C. Contescu and A. Contescu, Chemical Reviews, 95 (1995) 477-510.
[196] A. P. Wilkinson, C. Lind and S. Pattanaik, Chemistry of materials, 11 (1999) 101-108.
[197] S. D. Gates, J. A. Colin and C. Lind, Journal of Materials Chemistry, 16 (2006) 4214-4219.
[198] D. Portehault, C. Giordano, C. Sanchez and M. Antonietti, Chemistry of Materials, 22 (2010) 2125-2131.
[199] M. Niederberger, M. H. Bartl and G. D. Stucky, Journal of the American Chemical Society, 124 (2002) 13642-13643. 10.1021/ja027115i
[200] Y. w. Jun, J. s. Choi and J. Cheon, Angewandte Chemie International Edition, 45 (2006) 3414-3439.
[201] R. Corriu, D. Leclercq, P. LefÃ¨vre, P. H. Mutin and A. Vioux, Chemistry of materials, 4 (1992) 961-963.
[202] M. Andrianainarivelo, R. J. Corriu, D. Leclercq, P. H. Mutin and A. Vioux, Chemistry of materials, 9 (1997) 1098-1102.
[203] S. Acosta, R. Corriu, D. Leclercq, P. Mutin and A. Vioux, Journal of Sol-Gel Science and Technology, 2 (1994) 25-28.
[204] A. Vioux, Chemistry of materials, 9 (1997) 2292-2299.
[205] P. Arnal, R. J. Corriu, D. Leclercq, P. H. Mutin and A. Vioux, Journal of Materials Chemistry, 6 (1996) 1925-1932.
[206] P. Yang, D. Zhao, D. I. Margolese, B. F. Chmelka and G. D. Stucky, Chemistry of Materials, 11 (1999) 2813-2826. 10.1021/cm990185c
[207] V. Lafond, P. H. Mutin and A. Vioux, Chemistry of Materials, 16 (2004) 5380-5386. 10.1021/cm0490569
[208] V. Lafond, P. Mutin and A. Vioux, Chemistry of materials, 16 (2004) 5380-5386.
[209] C. J. Brinker and G. W. Scherer, *Sol-gel science: the physics and chemistry of sol-gel processing*, ed., Academic press.
[210] A. M. Cojocariu, P. H. Mutin, E. Dumitriu, F. Fajula, A. Vioux and V. Hulea, Applied Catalysis B: Environmental, 97 (2010) 407-413. https://doi.org/10.1016/j.apcatb.2010.04.027
[211] D. Dutoit, M. Schneider and A. Baiker, Journal of Catalysis, 153 (1995) 165-176.
[212] M. Niederberger and G. Garnweitner, Chemistryâ€“A European Journal, 12 (2006) 7282-7302.

[213] G. Orsini and V. Tricoli, Journal of Materials Chemistry, 21 (2011) 14530-14542. 10.1039/C1JM10777A
[214] M. Andrianainarivelo, R. J. P. Corriu, D. Leclercq, P. Hubert Mutin and A. Vioux, Journal of Materials Chemistry, 7 (1997) 279-284. 10.1039/A605168E
[215] R. Deshmukh and M. Niederberger, The Sol-Gel Handbook, (2015).
[216] R. Corriu, D. Leclercq, P. Lefevre, P. H. Mutin and A. Vioux, Chemistry of Materials, 4 (1992) 961-963. 10.1021/cm00023a001
[217] A. Aboulaich, O. Lorret, B. Boury and P. H. Mutin, Chemistry of Materials, 21 (2009) 2577-2579. 10.1021/cm900291p
[218] M. Niederberger, G. Garnweitner, N. Pinna and M. Antonietti, Journal of the American Chemical Society, 126 (2004) 9120-9126. 10.1021/ja0494959
[219] M. Niederberger, Accounts of chemical research, 40 (2007) 793-800.
[220] P. Kitschke, S. Schulze, M. Hietschold and M. Mehring, Main Group Metal Chemistry, 36 (2013) 209-214.
[221] M. Niederberger, G. Garnweitner, N. Pinna and M. Antonietti, Journal of the American Chemical Society, 126 (2004) 9120-9126.
[222] N. Pinna, M. Antonietti and M. Niederberger, Colloids and Surfaces A: Physicochemical and Engineering Aspects, 250 (2004) 211-213.
[223] N. Pinna, G. Garnweitner, P. Beato, M. Niederberger and M. Antonietti, Small, 1 (2005) 112-121.
[224] I. Bilecka and M. Niederberger, Electrochimica Acta, 55 (2010) 7717-7725. https://doi.org/10.1016/j.electacta.2009.12.066
[225] I. Bilecka, P. Elser and M. Niederberger, ACS nano, 3 (2009) 467-477.
[226] I. Bilecka, L. Luo, I. Djerdj, M. D. Rossell, M. Jagodic, Z. Jaglicic, Y. Masubuchi, S. Kikkawa and M. Niederberger, The Journal of Physical Chemistry C, 115 (2011) 1484-1495.
[227] L. Luo, D. Bozyigit, V. Wood and M. Niederberger, Chemistry of Materials, 25 (2013) 4901-4907.
[228] I. Bilecka, A. Hintennach, I. Djerdj, P. Novák and M. Niederberger, Journal of Materials Chemistry, 19 (2009) 5125-5128.
[229] I. Bilecka, A. Hintennach, M. D. Rossell, D. Xie, P. Novák and M. Niederberger, Journal of Materials Chemistry, 21 (2011) 5881-5890.
[230] D. Morselli, M. Niederberger, I. Bilecka and F. Bondioli, Journal of nanoparticle research, 16 (2014) 2645.
[231] D. Ito, S. Yokoyama, T. Zaikova, K. Masuko and J. E. Hutchison, ACS nano, 8 (2014) 64-75.
[232] K. G. Sharp, Journal of Sol-Gel Science and Technology, 2 (1994) 35-41. 10.1007/BF00486210
[233] S. Khurana and A. Chandra, Solid State Ionics, 340 (2019) 115027. https://doi.org/10.1016/j.ssi.2019.115027
[234] R. Sahrash, A. Siddiqa, H. Razzaq, T. Iqbal and S. Qaisar, Heliyon, 4 (2018) e00847. https://doi.org/10.1016/j.heliyon.2018.e00847
[235] J. Caruso and M. J. Hampden-Smith, Journal of Sol-Gel Science and Technology, 8 (1997) 35-39. 10.1007/BF02436814
[236] E. Stathatos, P. Lianos, U. Lavrencic-Stangar and B. Orel, Advanced Materials, 14 (2002) 354.
[237] C. Wang, Z.-X. Deng and Y. Li, Inorganic chemistry, 40 (2001) 5210-5214.
[238] E. Rauwel, G. Clavel, M. G. Willinger, P. Rauwel and N. Pinna, Angewandte Chemie International Edition, 47 (2008) 3592-3595.
[239] P. Yang, D. Zhao, D. I. Margolese, B. F. Chmelka and G. D. Stucky, Nature, 396 (1998) 152-155.
[240] D. P. Debecker, V. Hulea and P. H. Mutin, Applied Catalysis A: General, 451 (2013) 192-206.
[241] K. Bouchmella, P. H. Mutin, M. Stoyanova, C. Poleunis, P. Eloy, U. Rodemerck, E. M. Gaigneaux and D. P. Debecker, Journal of catalysis, 301 (2013) 233-241.

[242] D. P. Debecker, K. Bouchmella, R. Delaigle, P. Eloy, C. Poleunis, P. Bertrand, E. M. Gaigneaux and P. H. Mutin, Applied Catalysis B: Environmental, 94 (2010) 38-45.
[243] D. P. Debecker, K. Bouchmella, M. Stoyanova, U. Rodemerck, E. M. Gaigneaux and P. H. Mutin, Catalysis Science & Technology, 2 (2012) 1157-1164.
[244] D. P. Debecker, R. Delaigle, K. Bouchmella, P. Eloy, E. M. Gaigneaux and P. H. Mutin, Catalysis Today, 157 (2010) 125-130.
[245] S. Maksasithorn, P. Praserthdam, K. Suriye, M. Devillers and D. P. Debecker, Applied Catalysis A: General, 488 (2014) 200-207.
[246] A. Styskalik, D. Skoda, C. E. Barnes and J. Pinkas, Catalysts, 7 (2017) 168.
[247] D. Skoda, A. Styskalik, Z. Moravec, P. Bezdicka, M. Babiak, M. Klementova, C. E. Barnes and J. Pinkas, RSC Advances, 6 (2016) 24273-24284.
[248] F. Bertinchamps, C. Grégoire and E. M. Gaigneaux, Applied Catalysis B: Environmental, 66 (2006) 10-22.
[249] J. R. Caresani, R. M. Lattuada, C. Radtke and J. H. dos Santos, Powder Technology, 252 (2014) 56-64.
[250] A. G. Fisch, N. S. Cardozo, A. R. Secchi, F. C. Stedile, N. P. da Silveira and J. H. dos Santos, Journal of Non-Crystalline Solids, 354 (2008) 3973-3979.
[251] L. B. Capeletti, J. H. Z. Dos Santos, E. Moncada, Z. N. Da Rocha and I. M. Pepe, Powder technology, 237 (2013) 117-124.
[252] A. Styskalik, D. Skoda, Z. Moravec, C. E. Barnes and J. Pinkas, New Journal of Chemistry, 40 (2016) 3705-3715.
[253] M. Kejik, Z. Moravec, C. E. Barnes and J. Pinkas, Microporous and Mesoporous Materials, 240 (2017) 205-215. https://doi.org/10.1016/j.micromeso.2016.11.012
[254] X. Cattoën, A. Noureddine, J. Croissant, N. Moitra, K. Bürglová, J. Hodačová, O. de los Cobos, M. Lejeune, F. Rossignol, D. Toulemon, S. Bégin-Colin, B. P. Pichon, L. Raehm, J.-O. Durand and M. Wong Chi Man, Journal of Sol-Gel Science and Technology, 70 (2014) 245-253. 10.1007/s10971-013-3155-x
[255] K. Čebular, B. Đ. Božić and S. Stavber, Molecules, 23 (2018) 2235.
[256] A. Sáenz-Galindo, L. I. López-López, N. Fabiola, A. O. Castañeda-Facio, L. A. Rámirez-Mendoza, K. C. Córdova-Cisneros and D. de Loera-Carrera, Carboxylic acid: Key role in life sciences, 35 (2018).
[257] B. R. Jermy and A. Pandurangan, Journal of Molecular Catalysis A: Chemical, 237 (2005) 146-154.
[258] W. Wang, Y. Xu, X. Wang, B. Zhang, W. Tian and J. Zhang, Bioresource technology, 250 (2018) 474-480.
[259] C. Liu, L. Kong, Y. Wang and L. Dai, Algal research, 33 (2018) 156-164.
[260] A. A. Kiss, A. C. Dimian and G. Rothenberg, Advanced Synthesis & Catalysis, 348 (2006) 75-81.
[261] C. Sanchez, P. Belleville, M. Popall and L. Nicole, Chemical Society Reviews, 40 (2011) 696-753.
[262] M. Catauro, E. Tranquillo, A. Salzillo, L. Capasso, M. Illiano, L. Sapio and S. Naviglio, Molecules, 23 (2018) 2447.
[263] E. P. Gelves, S. M. B. Ordóñez, J. O. Loza and A. R. Vélez, Revista EIA, 10 (2013) 123-132.
[264] H. Pérez, R. Miranda, Z. Saavedra-Leos, R. Zarraga, P. Alonso, E. Moctezuma and J. Martínez, RSC Advances, 10 (2020) 39580-39588.
[265] M. Ebelmen, Comptes rendus de l'académie des Sciences, 25 (1847) 854-856.
[266] T. Graham, Journal of the Chemical Society, 17 (1864) 318-327.
[267] T. Montheil, C. Echalier, J. Martinez, G. Subra and A. Mehdi, Journal of Materials Chemistry B, 6 (2018) 3434-3448.
[268] S. Alias, A. Ismail and A. Mohamad, Journal of Alloys and Compounds, 499 (2010) 231-237.
[269] C. Brinker, K. Keefer, D. Schaefer and C. Ashley, Journal of Non-Crystalline Solids, 48 (1982) 47-64.
[270] S. Clément and A. Mehdi, *Sol-Gel Chemistry: From Molecule to Functional Materials*, in: Secondary author (Ed.)^(Eds.) Secondary title, Multidisciplinary Digital Publishing Institute, 2020.

[271] C. Hernandez and A. Pierre, Journal of sol-gel science and technology, 20 (2001) 227-243.
[272] W. J. Li, E. W. Shi and T. Fukuda, Crystal Research and Technology: Journal of Experimental and Industrial Crystallography, 38 (2003) 847-858.
[273] P. R. Aravind, P. Shajesh, S. Smitha, P. Mukundan and K. G. Warrier, Journal of the American Ceramic Society, 91 (2008) 1326-1328.
[274] J. Livage, C. Sanchez, M. Henry and S. Doeuff, Solid state ionics, 32 (1989) 633-638.
[275] S. Zhang and W. Lee, Journal of the European Ceramic Society, 23 (2003) 1215-1221.
[276] B. E. Yoldas and Y. BE, (1975).
[277] C. Lin, J. A. Ritter and M. D. Amiridis, Journal of non-crystalline solids, 215 (1997) 146-154.
[278] T. SHINDO, Y. Nagai, T. Ikeuchi and S. Ozawa, International Journal of the Society of Materials Engineering for Resources, 18 (2011) 1-6.
[279] T. Li, L. Zhang, Z. Tao, C. Hu, C. Zhao, F. Yi, X. Gao, X. Wen, Y. Yang and Y. Li, Fuel, 279 (2020) 118487.
[280] H. Yoshida, N. Matsushita, Y. Kato and T. Hattori, Physical Chemistry Chemical Physics, 4 (2002) 2459-2465.
[281] Y.-F. Huang, H.-L. Zhang, Z.-Z. Yang, M. Zhao, M.-L. Huang, Y.-L. Liang, J.-L. Wang and Y.-Q. Chen, Acta Physico-Chimica Sinica, 33 (2017) 1242-1252.
[282] M. May, M. Asomoza, T. Lopez and R. Gomez, Chemistry of materials, 9 (1997) 2395-2399.
[283] G. Engelhardt, TrAC Trends in Analytical Chemistry, 8 (1989) 343-347. https://doi.org/10.1016/0165-9936(89)87043-8
[284] W. Lutz, D. Täschner, R. Kurzhals, D. Heidemann and C. Hübert, Zeitschrift für anorganische und allgemeine Chemie, 635 (2009) 2191-2196. https://doi.org/10.1002/zaac.200900237
[285] X. S. Zhao, G. Q. Lu, A. K. Whittaker, G. J. Millar and H. Y. Zhu, The Journal of Physical Chemistry B, 101 (1997) 6525-6531. https://doi.org/10.1021/jp971366+
[286] W. Hu, Q. Luo, Y. Su, L. Chen, Y. Yue, C. Ye and F. Deng, Microporous and Mesoporous Materials, 92 (2006) 22-30. https://doi.org/10.1016/j.micromeso.2005.12.013
[287] E. Lippmaa, A. Samoson and M. Magi, Journal of the American Chemical Society, 108 (1986) 1730-1735. https://doi.org/10.1021/ja00268a002
[288] D. Müller, W. Gessner, H. Behrens and G. Scheler, Chemical Physics Letters, 79 (1981) 59-62.
[289] A. Leonard, S. Suzuki, J. Fripiat and C. D. Kimpe, The Journal of Physical Chemistry, 68 (1964) 2608-2617.
[290] A. Al Khudhair, K. Bouchmella, R. D. Andrei, A. Mehdi, P. H. Mutin and V. Hulea, Microporous and Mesoporous Materials, (2021) 111165.
[291] P. Innocenzi, Journal of non-crystalline solids, 316 (2003) 309-319.
[292] H. Aguiar, J. Serra, P. González and B. León, Journal of Non-Crystalline Solids, 355 (2009) 475-480.
[293] M. Klevenz, S. Wetzel, M. Möller and A. Pucci, Applied spectroscopy, 64 (2010) 298-303.
[294] M. Gómez-Cazalilla, J. Mérida-Robles, A. Gurbani, E. Rodríguez-Castellón and A. Jiménez-López, Journal of Solid State Chemistry, 180 (2007) 1130-1140.
[295] M. R. Agliullin, I. G. Danilova, A. V. Faizullin, S. V. Amarantov, S. V. Bubennov, T. R. Prosochkina, N. G. Grigor'eva, E. A. Paukshtis and B. I. Kutepov, Microporous and Mesoporous Materials, 230 (2016) 118-127.
[296] P. Aravind, P. Mukundan, P. K. Pillai and K. Warrier, Microporous and mesoporous materials, 96 (2006) 14-20.
[297] L. Rodríguez-González, F. Hermes, M. Bertmer, E. Rodríguez-Castellón, A. Jiménez-López and U. Simon, Applied Catalysis A: General, 328 (2007) 174-182.
[298] N. Katada, H. Igi and J.-H. Kim, The Journal of Physical Chemistry B, 101 (1997) 5969-5977. 10.1021/jp9639152

[299] L. Bourget, R. J. P. Corriu, D. Leclercq, P. H. Mutin and A. Vioux, Journal of Non-Crystalline Solids, 242 (1998) 81-91. https://doi.org/10.1016/S0022-3093(98)00789-3
[300] R. J. P. Corriu, D. Leclercq, P. Lefèvre, P. H. Mutin and A. Vioux, Journal of Non-Crystalline Solids, 146 (1992) 301-303. https://doi.org/10.1016/S0022-3093(05)80505-8
[301] R. J. Corriu and D. Leclercq, Angewandte Chemie International Edition in English, 35 (1996) 1420-1436.
[302] M. Niederberger, M. H. Bartl and G. D. Stucky, Chemistry of Materials, 14 (2002) 4364-4370.
[303] I. Djerdj, D. Arčon, Z. Jagličić and M. Niederberger, Journal of Solid State Chemistry, 181 (2008) 1571-1581.
[304] N. Pinna and M. Niederberger, Angewandte Chemie International Edition, 47 (2008) 5292-5304. 10.1002/anie.200704541
[305] J. M. Szeifert, J. M. Feckl, D. Fattakhova-Rohlfing, Y. Liu, V. Kalousek, J. Rathousky and T. Bein, Journal of the American Chemical Society, 132 (2010) 12605-12611.
[306] E. J. Nassar, P. F. dos Santos Pereira, E. C. de Oliveira Nassor, L. R. Ávila, K. J. Ciuffi and P. S. Calefi, Journal of Materials Science, 42 (2007) 2244-2249. 10.1007/s10853-006-0077-9
[307] D. Santilli and S. Zones, Catalysis Letters, 7 (1990) 383-387.
[308] O. Saber and H. M. Gobara, Egyptian Journal of Petroleum, 23 (2014) 445-454. https://doi.org/10.1016/j.ejpe.2014.11.001
[309] V. La Parola, G. Deganello, S. Scirè and A. M. Venezia, Journal of Solid State Chemistry, 174 (2003) 482-488. https://doi.org/10.1016/S0022-4596(03)00321-9
[310] J. G. Chęcmanowski and B. Szczygieł, Corrosion Science, 50 (2008) 3581-3589. https://doi.org/10.1016/j.corsci.2008.09.012
[311] R. Sato, P. McMillan, P. Dennison and R. Dupree, The Journal of Physical Chemistry, 95 (1991) 4483-4489.
[312] D. Müller, W. Gessner, H. J. Behrens and G. Scheler, Chemical Physics Letters, 79 (1981) 59-62. https://doi.org/10.1016/0009-2614(81)85288-8
[313] J. McManus, S. E. Ashbrook, K. J. MacKenzie and S. Wimperis, Journal of Non-Crystalline Solids, 282 (2001) 278-290. https://doi.org/10.1016/S0022-3093(01)00313-1
[314] N. Katada, H. Igi, J.-H. Kim and M. Niwa, The Journal of Physical Chemistry B, 101 (1997) 5969-5977.
[315] J. Handzlik, J. Ogonowski, J. Stoch, M. Mikołajczyk and P. Michorczyk, Applied Catalysis A: General, 312 (2006) 213-219. https://doi.org/10.1016/j.apcata.2006.07.002
[316] J. Shi, L. Zhang and Z. Cheng, Catalysis Surveys from Asia, 25 (2021) 279-300. 10.1007/s10563-021-09334-8
[317] Y. Yue, H. Liu, Y. Zhou, Z. Bai and X. Bao, Applied Clay Science, 126 (2016) 1-6. https://doi.org/10.1016/j.clay.2016.02.024
[318] J. Kuljiraseth, A. Wangriya, J. M. C. Malones, W. Klysubun and S. Jitkarnka, Applied Catalysis B: Environmental, 243 (2019) 415-427. https://doi.org/10.1016/j.apcatb.2018.10.073
[319] S. M. Opalka and T. Zhu, Microporous and Mesoporous Materials, 222 (2016) 256-270. https://doi.org/10.1016/j.micromeso.2015.10.030
[320] M. Di Serio, R. Tesser, L. Pengmei and E. Santacesaria, Energy & Fuels, 22 (2008) 207-217. 10.1021/ef700250g
[321] V. C. dos Santos, K. Wilson, A. F. Lee and S. Nakagaki, Applied Catalysis B: Environmental, 162 (2015) 75-84. https://doi.org/10.1016/j.apcatb.2014.06.036
[322] C. Bianchini, G. Giambastiani, I. G. Rios, G. Mantovani, A. Meli and A. M. Segarra, Coordination Chemistry Reviews, 250 (2006) 1391-1418. https://doi.org/10.1016/j.ccr.2005.12.018
[323] D. S. McGuinness, Chemical Reviews, 111 (2011) 2321-2341. 10.1021/cr100217q
[324] H. Olivier-Bourbigou, P. A. R. Breuil, L. Magna, T. Michel, M. F. Espada Pastor and D. Delcroix, Chemical Reviews, 120 (2020) 7919-7983. 10.1021/acs.chemrev.0c00076

[325] V. Hulea, ACS Catalysis, 8 (2018) 3263-3279.
[326] A. Aid, R. D. Andrei, S. Amokrane, C. Cammarano, D. Nibou and V. Hulea, Applied Clay Science, 146 (2017) 432-438. https://doi.org/10.1016/j.clay.2017.06.034
[327] S. Moussa, P. Concepción, M. A. Arribas and A. Martínez, ACS Catalysis, 8 (2018) 3903-3912. 10.1021/acscatal.7b03970
[328] R. D. Andrei, E. Borodina, D. Minoux, N. Nesterenko, J.-P. Dath, C. Cammarano and V. Hulea, Industrial & Engineering Chemistry Research, 59 (2020) 1746-1752. 10.1021/acs.iecr.9b05576
[329] M. Lallemand, A. Finiels, F. Fajula and V. Hulea, Chemical Engineering Journal, 172 (2011) 1078-1082. 10.1016/j.cej.2011.06.064
[330] M. Lallemand, A. Finiels, F. Fajula and V. Hulea, in: R. Xu, Z. Gao, J. Chen and W. Yan (Ed.)^(Eds.), Studies in Surface Science and Catalysis, Elsevier, 2007, pp. 1863-1869.
[331] P. H. Mutin and A. Vioux, Chem. Mater., 21 (2009) 582-596.
[332] D. P. Debecker, V. Hulea and P. H. Mutin, Applied Catalysis A: General, 451 (2013) 192-206. http://dx.doi.org/10.1016/j.apcata.2012.11.002
[333] P. H. Mutin, A. F. Popa, A. Vioux, G. Delahay and B. Coq, Appl. Catal., B, 69 (2006) 49-57.
[334] D. P. Debecker, K. Bouchmella, R. Delaigle, P. Eloy, C. Poleunis, P. Bertrand, E. M. Gaigneaux and P. H. Mutin, Appl. Catal., B, 94 (2010) 38-45.
[335] O. Lorret, V. Lafond, P. H. Mutin and A. Vioux, Chemistry of Materials, 18 (2006) 4707-4709. 10.1021/cm061478q
[336] D. P. Debecker, K. Bouchmella, C. Poleunis, P. Eloy, P. Bertrand, E. M. Gaigneaux and P. H. Mutin, Chem. Mater., 21 (2009) 2817-2824.
[337] K. Bouchmella, P. Hubert Mutin, M. Stoyanova, C. Poleunis, P. Eloy, U. Rodemerck, E. M. Gaigneaux and D. P. Debecker, Journal of Catalysis, 301 (2013) 233-241. http://dx.doi.org/10.1016/j.jcat.2013.02.016
[338] D. P. Debecker, K. Bouchmella, M. Stoyanova, U. Rodemerck, E. M. Gaigneaux and P. Hubert Mutin, Catal. Sci. Technol., 2 (2012) 1157-1164.
[339] K. Bouchmella, M. Stoyanova, U. Rodemerck, D. P. Debecker and P. Hubert Mutin, Catalysis Communications, 58 (2015) 183-186. http://dx.doi.org/10.1016/j.catcom.2014.09.024
[340] T. Huang, Q. Peng, W. Shi, J. Xu and Y. Fan, Applied Catalysis B: Environmental, 230 (2018) 154-164. https://doi.org/10.1016/j.apcatb.2018.02.053
[341] C. Jiménez-González, Z. Boukha, B. de Rivas, J. J. Delgado, M. Á. Cauqui, J. R. González-Velasco, J. I. Gutiérrez-Ortiz and R. López-Fonseca, Applied Catalysis A: General, 466 (2013) 9-20. https://doi.org/10.1016/j.apcata.2013.06.017
[342] M. Gil-Calvo, C. Jiménez-González, B. de Rivas, J. I. Gutiérrez-Ortiz and R. López-Fonseca, Applied Catalysis B: Environmental, 209 (2017) 128-138. https://doi.org/10.1016/j.apcatb.2017.02.063
[343] P. Burattin, M. Che and C. Louis, The Journal of Physical Chemistry B, 101 (1997) 7060-7074. 10.1021/jp970194d
[344] K. Bouchmella, *Synthèse par procédé sol-gel non-hydrolytique de catalyseurs oxydes mixtes pour la métathèse d'oléfines*, in: Secondary author (Ed.)^(Eds.) Secondary title, Montpellier 2, 2013.
[345] M. F. Williams, B. Fonfé, C. Sievers, A. Abraham, J. A. van Bokhoven, A. Jentys, J. A. R. van Veen and J. A. Lercher, Journal of Catalysis, 251 (2007) 485-496. https://doi.org/10.1016/j.jcat.2007.06.009
[346] E. J. M. Hensen, D. G. Poduval, P. C. M. M. Magusin, A. E. Coumans and J. A. R. v. Veen, Journal of Catalysis, 269 (2010) 201-218. https://doi.org/10.1016/j.jcat.2009.11.008
[347] M. May, M. Asomoza, T. Lopez and R. Gomez, Chemistry of Materials, 9 (1997) 2395-2399. 10.1021/cm970320q
[348] S. Rajagopal, J. A. Marzari and R. Miranda, Journal of Catalysis, 151 (1995) 192-203. https://doi.org/10.1006/jcat.1995.1021
[349] C. Chizallet and P. Raybaud, ChemPhysChem, 11 (2010) 105-108. 10.1002/cphc.200900797

[350] M. Lindo, A. Vizcaíno, J. Calles and A. Carrero, international journal of hydrogen energy, 35 (2010) 5895-5901.
[351] E. Heracleous, A. F. Lee, K. Wilson and A. A. Lemonidou, Journal of Catalysis, 231 (2005) 159-171. https://doi.org/10.1016/j.jcat.2005.01.015
[352] R. Hernández-Huesca, J. Mérida-Robles, P. Maireles-Torres, E. Rodríguez-Castellón and A. Jiménez-López, Journal of Catalysis, 203 (2001) 122-132. https://doi.org/10.1006/jcat.2001.3321
[353] S. R. Kirumakki, B. G. Shpeizer, G. V. Sagar, K. V. R. Chary and A. Clearfield, Journal of Catalysis, 242 (2006) 319-331. https://doi.org/10.1016/j.jcat.2006.06.014
[354] D. P. Debecker, K. Bouchmella, C. Poleunis, P. Eloy, P. Bertrand, E. M. Gaigneaux and P. H. Mutin, Chemistry of Materials, 21 (2009) 2817-2824. https://doi.org/10.1021/cm900490t
[355] R. López-Fonseca, C. Jiménez-González, B. de Rivas and J. I. Gutiérrez-Ortiz, Applied Catalysis A: General, 437-438 (2012) 53-62. https://doi.org/10.1016/j.apcata.2012.06.014
[356] A. N. Mlinar, G. B. Baur, G. G. Bong, A. B. Getsoian and A. T. Bell, Journal of Catalysis, 296 (2012) 156-164. https://doi.org/10.1016/j.jcat.2012.09.010
[357] A. Finiels, F. Fajula and V. Hulea, Catalysis Science & Technology, 4 (2014) 2412-2426.
[358] M. Lallemand, O. A. Rusu, E. Dumitriu, A. Finiels, F. Fajula and V. Hulea, Applied Catalysis A: General, 338 (2008) 37-43.
[359] R. D. Andrei, M. I. Popa, F. Fajula and V. Hulea, Journal of Catalysis, 323 (2015) 76-84. https://doi.org/10.1016/j.jcat.2014.12.027
[360] A. Finiels, F. Fajula and V. Hulea, Catalysis Science & Technology, 4 2412-2426. 10.1039/c4cy00305e
[361] P. LLEWELLYN, J. ROUQUEROL, L. LUCIANI, R. DENOYEL and F. ROUQUEROL, *Texture des Materiaux Pulverulents ou Poreux*, ed., Ed. Techniques Ingénieur, 2003.
[362] S. Stock, J. Barss, T. Dahl, A. Veis and J. Almer, Journal of structural biology, 139 (2002) 1-12.
[363] N. Broll, *Caractérisation de solides cristallisés par diffraction X*, ed., Ed. Techniques Ingénieur, 1996.

## RESUME:

The sol-gel route offered an interesting way for the preparation of mixed oxides. Two processes were explored in this work: hydrolytic sol-gel (HSG) and non-hydrolytic sol-gel (NHSG). We showed that $Si_xAl_y$ supports can be successfully prepared and used as heterogeneous catalysts in esterification reaction. Using HSG process, two parameters of the preparation were screened: the $Al_2O_3$ content (or Si/Al ratio) and pH medium. The $Si_xAl_y$ mixed oxides were also prepared by NHSG. The NHSG synthesis used in this work is based on the one pot reaction of commercially available chloride precursors ($SiCl_4$, $AlCl_3$) with an ether at 110 °C in dichloromethane. Ethanol and $^t$BuOH were also used as solvent and oxygen donor. The simplicity of NHSG makes it attractive: multi-step procedures, expensive precursors, reactivity modifiers or supercritical drying are not needed. The $Si_xAl_y$ mixed oxides exhibited well-controlled compositions and mesoporous textures, with high acidity. In this way, the Si/Al ratio can be easily controlled, knowing that it plays an important role in the structure, texture and acidity of the samples. We showed that the texture strongly depends on the Si/Al ratio and on synthesis conditions. The structures were studied by XRD and NMR showing that all the mixed oxides are amorphous. Ternary $Si_xAl_yNi_z$ mixed oxides catalysts were successfully prepared by a one-step NHSG ether route for ethylene oligomerization. Particular attention was devoted to the study of the influence of the composition (Si/Al ratio and Ni loading) on texture, structure, acidity and surface properties, which were correlated with the catalytic performances. According to XRD, part of the Ni formed NiO crystallites, but according to XPS, no bulky NiO was detected at the surface of the catalysts. XPS spectra and TPR experiments are consistent with the formation of dispersed $Ni^{2+}$ species strongly interacting with the surface. The samples with high Al content displayed excellent performances with very high specific activity up to 270 mmol ethylene converted per g of catalyst per hour at 150 °C, and a percentage of butenes in the products of ~70%. These catalysts compare well with model catalysts prepared by time-consuming multistep procedures from expensive ordered mesoporous silica supports.



**KEYWORDS:** SG ; silica-alumina ; nickel ; oligomerization ; esterification


---


## RESUME :

Le sol-gel offre une voie intéressante pour la préparation d'oxydes mixtes. Dans cette thèse, deux procédés ont été explorés: le sol-gel hydrolytique (HSG) et le sol-gel non hydrolytique (NHSG). Nous avons montré que les supports SixAly peuvent être préparés et utilisés avec succès comme catalyseurs hétérogènes dans la réaction d'estérification. A partir du procédé HSG, deux paramètres ont été étudiés : la teneur en $Al_2O_3$ (ou le rapport Si/Al) et le pH du milieu réactionnel. Les oxydes mixtes SixAly ont également été préparés par NHSG. La synthèse NHSG utilisée dans cette thèse est basée sur la réaction en une étape de précurseurs chlorures métalliques disponibles dans le commerce ($SiCl_4$, $AlCl_3$) en présence d'un éther à 110 °C dans le dichlorométhane. L'éthanol et le $_t$BuOH ont également été utilisés comme solvant et donneur d'oxygène. La simplicité du NHSG le rend attrayant : des procédures en plusieurs étapes, des précurseurs coûteux, des modificateurs de réactivité ou un séchage supercritique ne sont pas nécessaires. Les oxydes mixtes SixAly présentent des compositions bien contrôlées et des textures mésoporeuses, avec une acidité élevée. De cette façon, le rapport Si/Al peut être facilement contrôlé, sachant qu'il joue un rôle important dans la structure, la texture et l'acidité des échantillons. Nous avons montré que la texture dépend fortement du rapport Si/Al et des conditions de synthèse. Les structures ont été étudiées par DRX et RMN montrant que tous les oxydes mixtes sont amorphes. Des catalyseurs d'oxydes mixtes ternaires SixAlyNiz ont été préparés avec succès en une étape à partir de la voie éther NHSG, pour l'oligomérisation de l'éthylène. Une attention particulière a été dédiée à l'étude de l'influence de la composition (rapport Si/Al et teneur en Ni) sur la texture, la structure, l'acidité et les propriétés de surface, qui sont corrélées avec les performances catalytiques. D'après la DRX, une partie du Ni forme des cristallites de NiO, mais selon l'XPS, aucun NiO massique n'a été détecté à la surface des catalyseurs. Les spectres XPS et les expériences TPR sont cohérents avec la formation d'espèces $Ni^{2+}$ dispersées et interagissant fortement avec la surface. Les échantillons à haute teneur en Al ont montré d'excellentes performances catalytiques avec une activité spécifique très élevée jusqu'à 270 mmol

d'éthylène converti par gramme de catalyseur par heure à 150 °C et un taux de butènes formés d'environ 70 %. Ces catalyseurs se comparent bien aux catalyseurs modèles préparés par des procédures multi-étapes chronophages à partir de supports de silice mésoporeux ordonnés coûteux.

**MOTS CLÉS:** SG ; silice-alumine ; nickel ; oligomérisation ; estérification